KOVINE ZLITINE TEHNOLOGIJE

METALS ALLOYS TECHNOLOGIES

LETO 1997 / 6

Izdajatelji / Publishers: Inštitut za kovinske materiale in tehnologije Ljubljana, ACRONI Jesenice, Institut Jožef Stefan Ljubljana, IMPOL Slovenska Bistrica, Kemijski inštitut Ljubljana, Koncern Slovenske železarne, Metal Ravne, Talum Kidričevo, Fakulteta za strojništvo Ljubljana, Slovensko društvo za tribologijo Ljubljana

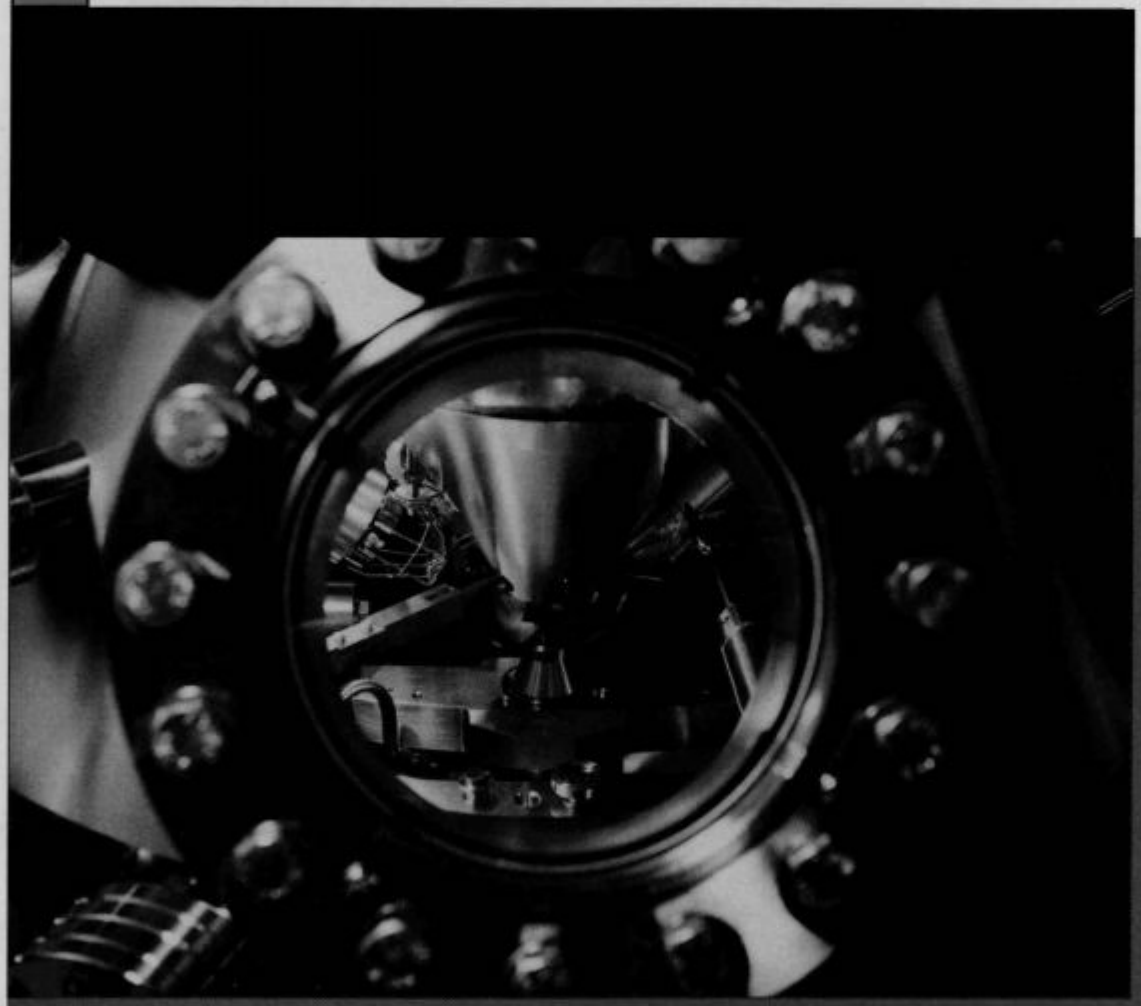

KOVINE ZLITINE TEHNOLOGIJE	LETNIK 31	ŠTEV. 6	STR. 465-608	LJUBLJANA SLOVENIJA	NOV.-DEC. 1997

ISSN 1318-0010
CODEN: KZLTET

Navodilo avtorjem

Prosimo avtorje, da pri pripravi rokopisa za objavo članka dosledno upoštevajo naslednja navodila:
- Članek mora biti izvirno delo, ki ni bilo v dani obliki še nikjer objavljeno. Deli članka so lahko že bili podani kot referat.
- Avtor naj odda članek oz. besedilo napisano na računalnik z urejevalniki besedil:
- WORDSTAR, verzija 4, 5, 6, 7 za DOS
- WORD za DOS ali WINDOWS.

Če avtor besedila ne more dostaviti v prej naštetih oblikah, naj pošlje besedilo urejeno v ASCII formatu.
Prosimo avtorje, da pošljejo disketo z oznako datoteke in računalniškim izpisom te datoteke na papirju. Formule so lahko v datoteki samo naznačene, na izpisu pa ročno izpisane.

Celoten rokopis članka obsega:
- naslov članka (v slovenskem in angleškem jeziku),
- podatke o avtorju,
- povzetek (v slovenskem in angleškem jeziku),
- ključne besede (v slovenskem in angleškem jeziku),
- besedilo članka,
- preglednice, tabele,
- slike (risbe ali fotografije),
- podpise k slikam (v slovenskem in angleškem jeziku),
- pregled literature.

Članek naj bi bil čim krajši in naj ne bi presegal 5–7 tiskanih strani, pregledni članek 12 strani, prispevek s posvetovanj pa 3–5 tiskanih strani.

Obvezna je raba merskih enot, ki jih določa zakon o merskih enotah in merilih, tj. enot mednarodnega sistema SI.

Enačbe se označujejo ob desni strani besedila s tekočo številko v okroglih oklepajih.

Preglednice (tabele) je treba napisati na posebnih listih in ne med besedilom.
V preglednicah naj se – kjer je le mogoče – ne uporabljajo izpisana imena veličin, ampak ustrezni simboli.

Slike (risbe ali fotografije) morajo biti priložene posebej in ne vstavljene (ali nalepljene) med besedilom. Risbe naj bodo izdelane praviloma povečane v merilu 2:1.
Za vse slike po fotografskih posnetkih je potrebno priložiti izvirne fotografije, ki so ostre, kontrastne in primerno velike.

Vsi podpisi k slikam (v slovenskem in angleškem jeziku) naj bodo zbrani na posebnem listu in ne med besedilom.

V pregledu literature naj bo vsak vir oštevilčen s tekočo številko v oglatih oklepajih (ki jih uporabljamo tudi med besedilom, kadar se želimo sklicevati na določeni literarni vir).

Vsak vir mora biti opremljen s podatki, ki omogočajo bralcu, da ga lahko poišče:
knjige: – avtor, naslov knjige, ime založbe in kraj ter leto izdaje (po potrebi tudi določene strani):
H. Ibach and H. Luth, Solid State Physics, Springer, Berlin 1991, p. 245
članki: – avtor, naslov članka, ime revije in kraj izhajanja, letnik, leto, številka ter strani:
H. J. Grabke, Kovine zlitine tehnologije, 27, 1993 , 1–2, 9

Avtorji naj rokopisu članka priložijo povzetek v omejenem obsegu do 10 vrstic v slovenskem in angleškem jeziku.

Rokopisu morajo biti dodani tudi podatki o avtorju:
- ime in priimek, akademski naslov in poklic, ime delovne organizacije v kateri dela, naslov stanovanja, telefonska številka, E-mail in številka fax-a.

Uredništvo KZT
- odloča o sprejemu članka za objavo,
- poskrbi za strokovne ocene in morebitne predloge za krajšanje ali izpopolnitev,
- poskrbi za jezikovne korekture.

Rokopisi člankov ostanejo v arhivu uredništva Kovine zlitine tehnologije.

Instructions to Authors

Authors are kindly requested to prepare the manuscripts according to the following instructions:
- The paper must be original, unpublished and properly prepared for printing.
- Manuscripts should be typed with double spacing and wide margins on numbered pages and should be submitted on floppy disk in form of:
- WORDSTAR, version 4, 5, 6, 7 for DOS,
- WORD for DOS or WINDOWS,
- ASCII text without formulae, in which case formulae should be clearly written by hand in the printed copy.

Preparation of Manuscript:
- the paper title (in English and Slovenian Language)*
- author(s) name(s) and affiliation(s)
- the text of the Abstract (in English and Slovenian Language)*
- key words (in English and Slovenian Language)*
- the text of the paper (in English and Slovenian Language)*
- tables (in English Language)
- figures (drawings or photographs)
- captions to figures (in English and Slovenian Language)*
- captions to tables (in English)
- acknowledgement
- references

* The Editorial Board will provide for the translation in Slovenian Language for foreign authors.

The length of published papers should not exceed 5–7 journal pages, of review papers 12 journal pages and of contributed papers 3–5 journal pages.

The international system units (SI) should be used.
Equations should be numbered sequentially on the right-hand side in round brackets.

Tables should be typed on separate sheets at the end of manuscript. They should have a descriptive caption explaining displayed data.

Figures (drawings or photographs) should be numbered and their captions listed together at the end of the manuscript. The drawings for the line figures should be twice the size than in the print. Figures have to be original, sharp and well contrasted, enclosed separately to the text.

References must be typed in a separate reference section at the end of the manuscript, with items refereed too in the text by numerals in square brackets.

References must be presented as follows:
- books: author(s), title, the publisher, location, year, page numbers
  H. Ibach and H. Luth, Solid State Physics, Springer, Berlin 1991, p. 245
- articles: author(s), a journal name, volume, a year, issue number, page
  H. J. Grabke, Kovine zlitine thenologije, 27, 1993 , 1–2, 9

The abstract (both in English and in Slovenian Language) should not exceed 200 words.

The title page should contain each author(s) full names, affiliation with full address, E-mail number, telephone and fax number if available.

The Editor
- will decide if the paper is accepted for publication,
- will take care of the refereeing process,
- language corrections.

The manuscripts of papers accepted for publication are not returned.

KOVINE ZLITINE TEHNOLOGIJE

METALS ALLOYS TECHNOLOGIES

KOVINE ZLITINE TEHNOLOGIJE

Izdajatelj (Published for):
Inštitut za kovinske materiale in tehnologije Ljubljana
Soizdajatelji (Associated Publishers):
SŽ ŽJ ACRONI Jesenice, IMPOL Slovenska Bistrica, Institut Jožef Stefan Ljubljana, Kemijski inštitut Ljubljana, Koncern Slovenske Železarne, Metal Ravne, Talum Kidričevo, Fakulteta za strojništvo Ljubljana, Slovensko društvo za tribologijo Ljubljana

Izdajanje **KOVINE ZLITINE TEHNOLOGIJE** sofinancira: Ministrstvo za znanost in tehnologijo Republike Slovenije
(Journal **METALS ALLOYS TECHNOLOGIES** is financially supported by Ministrstvo za znanost in tehnologijo, Republika Slovenija)

Glavni in odgovorni urednik (Editor-in-chief):
prof. Franc Vodopivec, Inštitut za kovinske materiale in tehnologije Ljubljana, 1000 Ljubljana, Lepi pot 11, Slovenija

Pomočnik glavnega urednika:
doc. dr. Monika Jenko

Področni uredniki:
kovinski materiali (prof. dr. Franc Vodopivec), polimeri (dr. Majda Žigon), keramika (dr. Marija Kosec), vakuumska tehnika (dr. Jože Gasperič)

Urednik (Editor):
mag. Aleš Lagoja

Tehnični urednik (Technical Editor):
Jana Jamar

Lektorji (Linguistic Advisers):
dr. Jože Gasperič in Jana Jamar (slovenski jezik), prof. dr. Andrej Paulin (angleški jezik)

Uredniški odbor (Editorial Board):
doc. dr. Monika Jenko, prof. Jakob Lamut, prof. Vasilij Prešeren, prof. Drago Kolar, prof. Stane Pejovnik, prof. Jože Vižintin, dipl. ing. Sudradjat Dai, Jana Jamar

Mednarodni pridruženi člani uredniškega odbora (International Advisory Board):
prof. Hans Jürgen Grabke, Max-Planck-Institut für Eisenforschung, Düsseldorf, Deutschland
prof. Thomas Bell, Faculty of Engineering School of Metallurgy and Materials, The University of Birmingham, Birmingham, UK
prof. Jozef Zrník, Technicka Univerzita, Hutnicka fakulteta, Košice, Slovakia
prof. Ilija Mamuzić, Sveučilište u Zagrebu, Hrvatska
prof. V. Lupinc, Istituto per la Technologia dei Materiali Metalici non Tradizionali, Milano, Italia
prof. Günther Petzov, Max-Planck-Institut für Metallforschung, Stuttgart, Deutschland
prof. Hans-Eckart Oechsner, Universität Darmstadt, Deutschland

Izdajateljski svet (Editorial Advisory Board):
prof. Marin Gabrovšek, prof. Blaženko Koroušić, prof. Ladislav Kosec, prof. Alojz Križman, prof. Tatjana Malavašič, dr. Tomaž Kosmač, prof. Leopold Vehovar, prof. Anton Smolej, dr. Boris Ule, doc. dr. Tomaž Kolenko, dr. Jelena Vojvodič-Gvardjančič

Članki objavljeni v periodični publikaciji KOVINE ZLITINE TEHNOLOGIJE so indeksirani v mednarodnih sekundarnih virih:
(Articles published in journal are indexed in international secondary periodicals and databases):
- METALS ABSTRACTS
- ENGINEERED MATERIALS ABSTRACTS
- BUSINESS ALERT ABSTRACTS (STEELS, NONFERROUS, POLYMERS, CERAMICS, COMPOSITES)
- CHEMICAL ABSTRACTS
- ALUMINIUM INDUSTRY ABSTRACTS
- REFERATIVNYJ ŽURNAL: METALLURGIJA

Naslov uredništva (Editorial Address):
KOVINE ZLITINE TEHNOLOGIJE
IMT Ljubljana
Lepi pot 11
1000 Ljubljana, Slovenija
Telefon: +386 61 125 11 61
Telefax: +386 61 213 780
Žiro račun: 50101-603-50316 IMT pri Agenciji Ljubljana

Na INTERNET-u je revija KOVINE ZLITINE TEHNOLOGIJE dosegljiva na naslovu: http : // www. ctk. si /kovine/
(INTERNET: http://www.ctk.si/kovine/)

Elektronska pošta (E-mail):
cobissimtlj @ ctklj.ctk.si

Slika na ovitku: Pogled skozi opazovalno okno v ultra visokovakuumsko analizno posodo na vzorec, elektronsko in ionsko puško ter rentgenski izvir visokoločljivega Augerjevega spektrometra na poljsko emisijo

Oblikovanje ovitka: Ignac Kofol
Tisk (Print): Tiskarna PLANPRINT, Ljubljana

Po mnenju Ministrstva za znanost in tehnologijo Republike Slovenije št. 23-335-92 z dne 09. 06. 1992 šteje KOVINE ZLITINE TEHNOLOGIJE med proizvode, za katere se plačuje 5-odstotni davek od prometa proizvodov.

BESEDA GLAVNEGA UREDNIKA

Za vsako revijo, še posebej za revije, ki delajo v majhnem okolju, imajo jubilejne številke poseben pomen. To velja tudi za revijo Kovine Zlitine Tehnologije. Poseben pomen jubilejnih številk pove najmanj dvoje: da v okolju, v katerem revija vrši svoje poslanstvo, seznanja javnost z raziskovalnimi, razvojnimi in tehnološko tehničnimi dosežki posameznikov, ki s kakovostjo in obsegom dovolj izstopajo iz poprečja. Posebne številke so tudi dokaz, da posamezniki z dosežki presegajo lokalni nivo, zato se med govornike, ki pred javnostjo nastopajo v njihovo počastitev, vključijo tudi priznani znanstveniki iz tujine. Organizatorji Konference o materialih in tehnologijah ter uredništvo revije Kovine Zlitine Tehnologije so veseli in ponosni, da sta jubilanta leta 1997 dva eminentna raziskovalca iz področij keramike in vakuuma, ki sodita v delovno področje konference in revije.

Prof. dr. Dragu Kolarju lahko brez pretiravanja pripišemo očetovstvo resnega znanstveno raziskovalnega dela na področju elektro in elektronske keramike v Sloveniji. Njegovo ime najdemo med avtorji mnogih publikacij v Sloveniji in tujini, pa tudi med pobudniki in izvajalci razvojnih projektov za industrijska podjetja. Enako pomembno je tudi delo, ki ga je opravil pri vzgoji naslednikov, od katerih mnogi nadaljujejo delo na institutu, drugi pa kariero nadaljujejo v industrijskih podjetjih.

Manj opaženo v raziskovalni sferi in javnosti, zato pa nič manj uspešno in koristno, je delo na področju vakuuma opravljal dr. Jože Gasperič, eden od utemeljiteljev vakuuma kot vede, stroke in tehnologije v Sloveniji in bivši Jugoslaviji. Kot pionir se je moral soočati z vrsto problemov, od pridobivanja začetnih znanj, preko visokega vakuuma kot bistvene komponente sodobne elektronike, humanih aplikacij vakuuma, do načrtovanja difuzijskih črpalk. Nekako logično ga najdemo zato tudi med razvijalci elektronskih komponent in tehnologij. V reviji Kovine Zlitine Tehnologije smo še posebej veseli, da zelo uspešno opravlja zahtevno nalogo lektorja slovenskih tekstov.

Uredništvo revije in organizatorji Konference o materialih in tehnologijah obema slavljencema čestitajo, jima želijo še vnaprej dobrega zdravja in uspešnega dela, tudi mnogo uspeha pri prenosu znanja in izkušenj na mlade sodelavce.

Glavni in odgovorni urednik:
Prof. dr. Franc Vodopivec

Jubilee numbers are of special importance for scientific journals, especially those operating in small environments. Also for the journal Metals Alloys Technologies the editor sees at least two arguments supporting this view. The printing of a jubilee number demonstrates that also in the small environment, where the journal fulfils its role of information and education, individuals are found who are above the average by the quality and quantity of research and development performances to a level justifing the celebration.

And, what is probably even more important, it is evident, that their work as scientists and engineers meets sufficient interest in the foreign research community and eminent scientists from abroad are ready to speak on the jubilants work or on their honour.

The organisers of the Conference on Materials and Technologies and the editors of the journal Metals Alloys Technologies are glad and honoured to celebrate in 1997 the jubilee of Drago Kolar and Jože Gasperič, two eminent scientists and engineers active in the fields of ceramics and vacuum, two research and engineer domains of interest for both, the conference and the journal.

It is possible, without exaggeration, to attribute to Drago Kolar the fatherhood of modern research in the field of electronic and electric ceramics in Slovenia. His name is found as author and coauthor in a a great number of scientific paper in domestic and foreign publications, and also between the proposers and performers of research and development projects for industrial companies. At least of equal importance is the work of Drago Kolar by the education of young scientists and engineers, which are continuing and spreading his scientific and engineer activity.

Less in public eyes, however with equal success and benefit, was the activity of Jože Gasperič, one of the pioneers of vacuum, as science and technology in Slovenia. As pioneer, he had to deal with many problems, from the acquisition of basic knowledge, over vacuum as vital component of the modern electronics and human vacuum applications, till the development and construction of diffusion vacuum pumps. It seems logical to find him also between the developers of electronic components and technology. The journal Metals Alloys Technologies is honoured to have Jože Gasperič as appreciated assistance as lecturer of manuscripts submitted in slovenian language.

The editors of the journal and the organisers of the Conference on Materials and Technologies felicitate both jubilants and wish to both of them good health, productive work continuation, and successful transfer of knowledge and experience to younger colloborators.

The editor
Prof. dr. Franc Vodopivec

5. KONFERENCA O MATERIALIH IN TEHNOLOGIJAH

1.–3. oktober 1997, Kongresni center Grand hotel Emona, Portorož, Slovenija

50. POSVETOVANJE O METALURGIJI IN KOVINSKIH GRADIVIH
5. POSVETOVANJE O MATERIALIH
17. SLOVENSKO VAKUUMSKO POSVETOVANJE

ZBORNIK – 1. DEL

Posvetovanje so organizirali:

INŠTITUT ZA KOVINSKE MATERIALE IN TEHNOLOGIJE, LJUBLJANA
ODDELEK ZA MATERIALE IN METALURGIJO, NTF, UNIVERZA V LJUBLJANI
KEMIJSKI INŠTITUT, LJUBLJANA; INŠTITUT JOŽEF STEFAN, LJUBLJANA;
SLOVENSKO DRUŠTVO ZA MATERIALE; SLOVENSKO KEMIJSKO DRUŠTVO:
SEKCIJI ZA POLIMERE IN KERAMIKO; DRUŠTVO ZA VAKUUMSKO TEHNIKO SLOVENIJE

Posvetovanje je finančno podprlo Ministrstvo za znanost in tehnologijo Republike Slovenije

Uredila: M. Jenko in F. Vodopivec, IMT Ljubljana

5th CONFERENCE ON MATERIALS AND TECHNOLOGY

October 1–3, 1997 Convention Centre Grand Hotel Emona, Portorož, Slovenia

50th SYMPOSIUM ON METALLURGY AND METALLIC MATERIALS
5th SYMPOSIUM ON MATERIALS
17th SLOVENIAN VACUUM SYMPOSIUM

SELECTED PAPERS – PART 1

The Conference is organized by:

INSTITUTE OF METALS AND TECHNOLOGY, LJUBLJANA
DEPARTMENT OF MATERIALS AND METALLURGY, NTF, UNIVERSITY OF LJUBLJANA; NATIONAL INSTITUTE OF CHEMISTRY, LJUBLJANA; JOŽEF STEFAN INSTITUTE, LJUBLJANA; SLOVENIAN SOCIETY OF MATERIALS SLOVENIAN CHEMICAL SOCIETY: DIVISIONS OF POLYMERS AND CERAMICS; SLOVENIAN VACUUM SOCIETY

The Conference is financially supported by Ministrstvo za znanost in tehnologijo, Republika Slovenija.

Edited by M. Jenko and F. Vodopivec, IMT Ljubljana

Vsebina - Contents

IZBRANI PRISPEVKI, predstavljeni na 5. Konferenci o materialih in tehnologijah, Portorož, 1997 - SELECTED PAPERS presented at 5th Conference on Materials and Technology, Portorož 1997

ZNANSTVENI PRISPEVKI - SCIENTIFIC PAPERS

I. KOLARJEV DAN - KOLAR'S DAY

Anorganski materiali - Inorganic Materials

II. GASPERIČEV DAN - GASPERIČ'S DAY

Vakuumska tehnika - Vacuum Technique

III. Kovine - Metals

Anorganski materiali - Inorganic Materials

Polimeri - Polymers

Kovine - Metals

ISSN 1318-0010
KZLTET 31(6)473(1997)

CONTEMPORARY CERAMIC RESEARCH - A CASE STUDY

GÜNTHER PETZOW

Max-Planck-Institut, Institut für Metalforschung, Heissenbergstrasse 5, 70569 Stuttgart

Mr. Chairman,
Ladies and Gentlemen,

it is my great pleasure to be here today and to look at many faces so familiar to me. And this is especially true with Drago Kolar, the bright centre of our Kolar' s Day.

When I was asked by the organisers of Kolar's Day for the title of my speech I suggested: "Drago Kolar - A Pioneer and Ambassador of Science of Ceramics". But as you can realise from the program the title is printed as "Contemporary Ceramic Research - A Case Study " since I do not know the reason for the change, I assume it is a printing error.

May it be as it is: It does not matter! I simply take as my Case Study: "Drago Kolar" a short circuit. Because it is evident that "Contemporary Ceramic Research " and Drago Kolar are synonymous.

Ladies and Gentlemen, dear Drago,

"It is an obvious privilege of age to be able to relieve worldly things of their material focus and gravity and illuminate them with the inner light of the mind, where they can be seen in a panoramic view".

These words were written by Baron Wilhelm von Humboldt, the elder brother of the famous scholar Alexander von Humboldt as he turned sixty-five (230 years ago).

I should like to preface my laudatory remarks with these words. They convincingly impact a sense of the maturity that results from a full life, whichever turns it may have taken. Experience and calmness are expressed with these words and, if you will, an independence of spirit, a piece of self -actualisation. Humbaldt's words are eminently suitable for the present occasion.

Drago Kolar has been a mover and has achieved much. This was not always accomplished at first blush and things may not always have gone according to plan. But setbacks are the spice which brings flavour to success. And in the ups and downs in Drago's life dealt by fate he has remained ever true to his own self, and that alone matters.

The inner light of his ideas - to pick up Humbaldt's thought, the inner light, shines and is reflected in his actions.

Today I am honoured to report on them. I shall do so by following the chronological progress of his career, but take some liberties in the selection of events because the limitations of this programme do not permit full coverage of his remarkably multifaceted life.

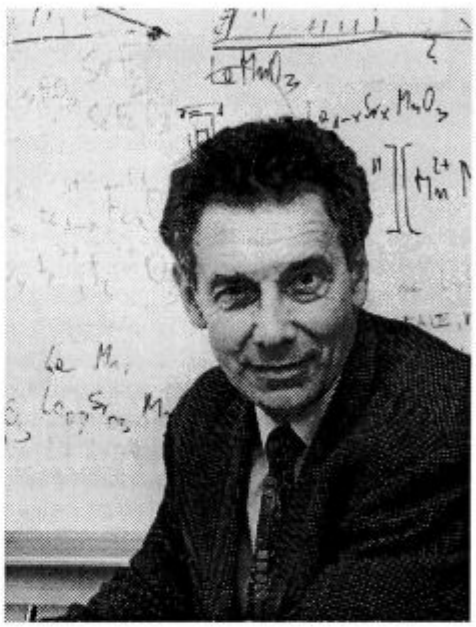

Prof. dr. Drago Kolar

"Omnium euim reum..." we were taught in school. All things begin small - so also little Drago when he entered the stage of life on the fifteenth of September, 1932, that is exactly sixty-five years and fifteen days ago.

On this platform, he considered a calling in the arts or perhaps in literature - such were the career goals of the growing boy, whose broad spectrum of talents indicated a specific inclination for chemistry, but certainly none in the direction of materials science and engineering. However, it appears that Saint Barbara, the patron of the foundryman and metallurgists and more recently of materials scientists too, had an eye on him. All things begin small, but if time is used, they grow! And little Drago grew up. He went to school and he was an excellent schoolboy and then at the University of Ljubljana a very good student, who passed his final examination with great success in 1957.

Thereafter he began to work on his Ph.D. thesis. The experimental work he did at the highly respectable Jožef Stefan Institute and graduated at the University of Ljubljana. It was in 1964, when the doctor's degree of science in chemistry was confirmed upon him. This is 7 to 8 years after he has received his master certificate. 7 to 8 years are really an unusual time spent for a gradu-

ation. And at first sight one could have the impression of a lazy candidate of poor dynamic, living an unconventional life like a bohemian devoted to all kinds of fun and pleasure.

But as we know: the reverse is true! He has made optimum use of his time besides his Ph.D. activities. From 1957 to 1959 he has been a Research Assistant at the Jožef Stefan Institute. This occupation was interrupted by a one year's military service, which he has completed in the rank of a non-commissioned officer. Obviously he has not had great interest in a military career. At that time it was a must for a young and ambitious scientist to go for a research stay in a top laboratory in USA. Drago Kolar became a research participant at the International Institute for Nuclear Science and Engineering of Argonne National Laboratory, Illinois. He was in the age of 28 then and really enjoyed the stimulating atmosphere in a famous and renowned laboratory in which well experienced, well-known scientists co-operated with highly motivated young colleagues from all over the world.

Drago Kolar became involved in investigations on kinetic processes in solid materials. A topic of great fascination to him and which he took up again and again during his further research work; of course always with improved methods and on the basis of an advanced knowledge. His special interest was preferably directed to high performance ceramics which at that time became a research topic of highest actuality. Remember, it was the time of beginning of the so called ceramic fever. Today it is obvious with this work he has established himself in the elite of the Contemporary Ceramic Research.

It was in 1961, when Drago Kolar came back home to the Jožef Stefan Institute, where he then ran through a brilliant career form a Research Assistant to a Senior Research Associate and finally, already in 1965 to the Head of the new founded Ceramic Department, which under his leadership has grown up to be among the top ceramic research facilities in the world.

Beside his busy professional career he found enough time to court a lovely lady student named Majda, who he married in 1960. In 1964 - the year of his graduation - he also became father of the wonderful twins Jana and Aleš. Good timing! So, again, I would like to repeat: The guess, Drago has been a lazy Ph.D. candidate is completely disproved. Also in his spare private hours he was active and successful.

In addition he wrote during this time five papers, which have been published in recognised scientific journals. It is really remarkable!

His very first article was published 1962 in the March issue of the Journal of the American Ceramic Society, the leading Journal in the field.

In his first paper entitled: " Influence of Gas Flow on DTA curves of UO_2.", he described the use of Differential Thermal Analysis to study the oxidation behaviour of UO_2. The resultant conclusions he gave in regard to the oxidation kinetics are still relevant today.

Numerous other publications followed the first ones. Meanwhile more than 200 papers are on his list of publications and another more than 200 are published in proceedings, monographs and encyclopaedias. He holds 8 patents, has written two fine textbooks on ceramics and is editor of 5 Proceeding Volumes of International Conferences. To underline Dr. Kolar's great scientific potential, one should also mention the high number of invited and introductory lectures on conferences, universities and institutes abroad. I have had the pleasure to hear many of his lectures and I have always been impressed by theirs precision and lucidity.

Drago Kolar's first scientific actions have fallen in a prosperous time for the field of materials science, which flourished, and consequently had a strong influx of students and scientists from traditional disciplines, mainly from physics. It has been a wonderful stimulating period, full of new and exciting possibilities.

The electron microscopy, for instance, became introduced to materials investigations and brought a deeper insight into the microstructure. The metal physicists examined the structure of real crystals and established the basic understanding of the influence of structural failures on properties. With the upcoming modern computers, simulations and calculations of complex processes and multicomponent materials of higher order could be handled much easier than ever before.

In those days generous support to all fields of science was the rule but the outstanding contributions were given to nuclear research and development. Accordingly, nuclear materials have been investigated with preference. This has also influenced Drago Kolar's work. Synthesis, processing and properties of Uranium containing materials have been mainly his study objects. However, the period of nuclear euphoria was short and even changed to serious non-acceptance by many people, as we know. Many of the reactor research centres, which have had grown up very fast had to take into account the changing situation and to look for other research topics.

No doubt Drago Kolar was among those, who have easily foreseen this development. As a consequence he fixed another aim for the research activities in his department and himself. He decided for advanced materials, and more specifically for functional ceramics. $BaTiO_3$ based materials became his personal favourite - one can say "his great love". And indeed these substances are multifunctional with many facets and suitable for several applications; as disks and multilayer capacitors for instance and microwave ceramics and others. $BaTiO_3$ can really be compared with a coquettish, charming, but mysterious and sometimes even a tricky lady who never fully opens her heart. Comparable with Mona Lisa whose mysterious smile has inspired men's fantasy since long. But Drago Kolar took away many secrets from the difficult and brittle lady $BaTiO_3$ and clarified utmost complex phase relations of $BaTiO_3$ based multicomponent systems. He discovered several ternary compounds with perovskite like structures which exhibit good dielectric properties and high temperature stabilities. And he is among those who gave the most solid results in this field. With same exactness he studied the exaggerated

grain growth, twins formation, processing, and sintering of $BaTiO_3$ based materials with the aim of dense materials of excellent quality.

But of course, $BaTiO_3$ was not the only substance investigated by him. More or less all oxide - nitride and carbide based advanced ceramics have been object of his sophisticated studies. His main scientific interest was always directed to the interrelation between processing, microstructure and properties. Processing mechanism determine the microstructural formation. And the microstructure affects many technically important properties and is therefore given considerable attention in science, development and testing of materials. The higher the demands on a material, the more sophisticated the microstructural insight becomes, i.e. the more exacting the requirements on the microstructural parameters will be. "Microstructural engineering" or "microstructural design" are the key words that characterise these problems. This scientific strategy is in full accordance with the intentions of the Max-Planck Institute for Metals Research at Stuttgart. And this conformity is the basis for our long-lasting fruitful and pleasant co-operation with professor Kolar and his wonderful team. For that co-operation I would like to express my sincere thanks to you and your co-workers. And I am doing this also on behalf of the board of directors of our institute. I have to bring the greetings and the message: " Dear Drago, you are welcome in Stuttgart at any time!"

It is an extraordinary merit of Drago Kolar that he in all his scientific efforts has never lost the view for the requirements of application. Drago Kolar took a scientific curiosity and turned it into an engineering material, whose economic utilisation he significantly influenced.

Best in all these activities he never deviated from his high scientific standards.

Doubtless he belongs to those pioneers who build bridges from basic research to application, seeking close co-operation with industrial partners.

This underlines again his foresight, for today transfer of science and innovation are required more than ever before. It is a precondition for all support from governments, business and industry. Here I would like to quote some remarks of Gottfried Wilhelm Leibniz, the great philosopher and mathematician who lived three hundreds years ago. He stated in that time already: "The work of science should be application-oriented from the outset. Otherwise government will withdraw its hands for, the ministries will soon tire of useless curiosities and not recommend the prices to put much stock in them."

Teaching and research were always an inseparable unity to Drago Kolar and it is his ongoing concern that his knowledge and research skills will pass on to future generations.

Numerous diploma and doctoral candidates have contributed to his scientific work. Here, it is Drago Kolar, who must be credited for defining the problems, setting quality standards and providing critical guidance to his co-workers. Many of them are present today and will testify to his positive influence on their work.

It is indeed impressive how engaged Drago Kolar took over all the pleasure and burden of an academic teacher beside his extensive duties as head of the Ceramics Department of the Jožef Stefan Institute. Since 1972 he is teaching at the Faculty of Chemistry and Chemical Technology at the University of Ljubljana. The same place where he had done his first steps into science. What a nicely closed circle! After being assistant professor first, he became a full professor of ceramics and materials science in 1977. He thereby entered a circle of individuals of whom Johann Wolfgang Goethe stood in awe and admiration when he wrote to his father in October of 1765: You will not believe what a splendid affair a professor is: I was delighted to observe several of these fellows in their glory."

Beyond research and teaching he maintained contacts with many universities and research laboratories and succeeded in bridging research and applications in a most impressive manner. Some of this will become evident in the presentations by several of his road companions, which are to follow. In acknowledgement of his extraordinary merits in broadening the foundations of materials science and applying this knowledge to the development of advanced materials he received several honourable invitations as a guest professor or a member of advisory boards. I can not mention all of them. As an example for many others I would like to mention the Keating Crawford distinguished visiting professorship of Metallurgical Engineering and Materials Science of the University of Notre Dame, Indiana. During this period from 1982 to 1983 he had the opportunity to stay in close exchange of ideas and theories with the famous George Kuczynski, one of the bright brains in the science of sintering.

The high reputation of Drago Kolar creative power is also underlined by the many awards he has won. I have counted about 25, but would like to mention only one, which I think is the one which represents Drago Kolar's life - work best. That is the distinction as an ambassador of science of the Republic of Slovenia. And I would like to go beyond that and add: he is in addition an impressive ambassador of contemporary ceramics and of science of sintering!

Ladies and Gentlemen, there is a saying among children in our country which is often quoted: "The uncle, who brings a present is much better than the aunt, who plays the piano." And I think since I have not played the laudation piano plentifully, I have to deliver a present. It is a very special one: This sculpture is known as the "Two Particle Man" or "Sinterman". It is the highest distinction that the P/M Committee of the German Materials Society can bestow. It is only conferred for exceptional contributions to the field of sintering whereby the recipient is not only critical of his own performance, but also has a sense of humour. The Two-Particle Man consists of spherical powder particles of a particular size distribution, so that in the first sintering stage they form a neck, just as how we understand the two particle sintering theory. The body which represents the particle, and the head which embodies the theory, are equally large.

Of course, that is a big compliment to the theoreticians. Drago knows very well: Theory and practice in sintering are like the hare and the tortoise in a race. Whenever the theory - hare breathlessly reaches the next check point he finds the Practice - tortoise already there. The tortoise smiles and explains: I don't know how, but I am already here!"

This trophy, a high distinction in a humorous form, is in significance comparable to an Oscar. Up to now it has only been awarded five times to excellent scientists and practitioners in the field of sintering. And now Drago Kolar; the award of this trophy is in recognition of your extraordinary contribution in densification ceramic powders which has brought many advantages. Here symbolised by an alumina ball of full density for bioimplantation. The recognition of your theoretical contribution is symbolised by the 3 particles in your hands, which stand for the 3 particle theory, on which we already had endless discussions. May you, Drago Kolar, as the youngest prize holder, stay in freshness of your colleagues and friends of the German Powder Metallurgy Committee. And I may add, it is the desire of all of us.

Ladies and Gentlemen,

Drago Kolar is a scientist for whom mental image and practical implementation are not opposites but form a fertile contribution. This I have attempted to demonstrate with an account of his professional career.

His recognition among peers had led to his engagement in numerous extra curricular activities which he took on and continues to take on cheerfully. By the latest count there have been 16 membership in workshops, topical committees, advisory boards, executive councils, review committees, editorial boards, and others. In all of these bodies he is never just a member but an active participant in word and deed who gets noticed by his crisp language and his spirited involvement in discussions. Again, I will mention only one example, which involves all fun and trouble of the preparation and realisation in connection with committee activities. That is the Yugoslav - German co-operation on Engineering Materials Science and Technology. This co-operation started in 1972 with good financial support of German government and is now continued by bilateral Slovene-German activities. From the beginning this scientific partnership was characterised by a stimulating exchange of scientists in different fields of research. I think it is not exaggerated to claim, Drago Kolar was a main driving force behind the co-operation and pushing the realisation of the regular meetings. He was the first who has contacted us after the disintegration of former Yugoslavia to start with the Slovene-German co-operation again. In June 1992, he wrote to me: "In the meantime, we are trying here to keep our activities on decent level. It is not easy in changing political situation. We are trying to escape the pitfalls of separation. However, the price in economical terms is high. But prospects are great and with a little help we may catch the prosperity again. My letter concerns possible co-operation ...". And now, five years after independence, Slovenia is a completely accepted candidate for the European Union.

Now, of course, Ladies and Gentlemen, no honest human being would want to stand up and praise his fellow colleague unless he can claim some affinity with him. In this sense, I had no difficulty answering in the affirmative when Prof. Stane Pejovnik asked me to present this laudation.

However, the more I dug into Drago Kolar's background the more obvious it became that I had missed a few things and that, perhaps, someone else would have been better qualified to give the talk. He might have put a different spin on events in his life and surely would have illustrated other facts than I did. What I can say is that: with the study of his life history, my admiration of Drago Kolar has grown greatly. The performance of Drago Kolar can only be explained by personal effort beyond the call of duty, a sovereign command of the scientific field and the joy of creative work. It goes without saying that one's work environment must be supportive, providing outstanding co-workers, good infrastructure and a peaceful home.

A word about Drago's hobbies: First his work on $BaTiO_3$, second his work on exaggerated grain growth, third condensor ceramic and then some gardening in the garden of his weekend house, bicycle riding and slow walking together with his male cat David.

Now Drago Kolar leaves his position as Head of the Ceramics Department. But he will not disappear and will be present in the department and his partners at the university and, of course, in the minds and heads of his coworkers and colleagues. And it would be wise to trust furthermore in his experience and advice.

In closing, I should like to add a personal note of friendship that brings us full circle to the words of Wilhelm von Humboldt with which I began. The words are borrowed from inscriptions in St. Paul's Cathedral at Baltimore: "Cheerful and calmly accept the council of age. Take leave of things of youth with grace. Whatever your work and your yearnings may be, maintain peace within your soul, in the noisy bustle of life".

Dear Drago, your colleagues and the present assembly thank you for your many contributions to our field. We wish you, your family and your institute the very best for a happy future.

Please accept our congratulations and best wishes on your 65th birthday.

ISSN 1318-0010
KZLTET 31(6)477(1997)

CHEMICALLY CONTROLLED SINTERING AND MICROSTRUCTURAL DEVELOPMENT IN CERAMICS

KEMIJSKO NADZOROVANO SINTRANJE IN RAZVOJ MIKROSTRUKTURE V KERAMIKI

DRAGO KOLAR

Fakulteta za kemijo in kemijsko tehnologijo, Murnikova 5a, 1000 Ljubljana in Institut J. Stefan, Ljubljana
Faculty of Chemistry & Chemical Engineering, University of Ljubljana, and J. Stefan Institute, Ljubljana

Prejem rokopisa - received: 1997-10-01; sprejem za objavo - accepted for publication: 1997-10-21

The sintering step in manufacturing most ceramic articles is dominated by the chemical reactions which occur during firing. Such chemical reactions may be caused by chemical heterogeneity of the constituents of the ceramic body, small amounts of additives or impurities. Even in chemically equilibrated multicomponent systems the capillary forces may cause dehomogenisation and influence the sintering mechanism. Reaction sintering in the $BaTiO_3$-$CaZrO_3$-TiO_2 system is described as an example of a system where controlled chemical heterogeneity may optimise the electrical properties. Sintering of $PbZr_{1-x}Ti_xO_3$ ceramic is described as an example of chemical dehomogenisation due to capillary forces.

Key words: reaction sintering, ceramic microstructure, barium titanate, lead zirconate-titanate, sintering mechanisms

Proces sintranja v proizvodnji večine keramičnih izdelkov določajo kemijske reakcije, ki potekajo med žganjem. Kemijske reakcije lahko povzročajo heterogenost sestavin keramike, majhne količine dodatkov ali nečistoče. Celo v kemijsko uravnoteženih večkomponentnih sistemih lahko kapilarne sile povzročijo dehomogenizacijo in vplivajo na mehanizem sintranja. Delo obravnava reakcijsko sintranje v sistemu $BaTiO_3$-TiO_2-$CaZrO_3$ kot primer procesa, pri katerem lahko z nadzorovano kemijsko heterogenostjo optimiziramo električne lastnosti keramike. Sintranje $PbZr_{1-x}Ti_xO_3$ keramike obravnavamo kot primer sistema, pri katerem se kemijsko homogena trdna raztopina med sintranjem prehodno dehomogenizira. Fenomen vpliva na mehanizem sintranja in električne lastnosti piezokeramike.

Ključne besede: reakcijsko sintranje, keramična mikrostruktura, barijev titanat, svinčev cirkonat-titanat, mehanizmi sintranja

1 INTRODUCTION

1.1 SWOT analysis of advanced technical ceramics

SWOT analysis (S = strength, W = weakness, O = opportunities, T = threat) is a frequently used method for evaluation of the potential of a particular activity. Such analysis applied to the manufacture of ceramic articles may give the following answers: (Many other arguments may be added).

S: Ceramics are the oldest artificial materials invented by mankind. In last 50 or 60 years the applicability of ceramics increased enormously. As a result, the market growth in many segments in recent decades maintained a level of 8-10 % per year, which is far above many other industrial activities.

W: The weaknesses of ceramics are well known: The producers and consumers complain of insufficient reproducibility, insufficient reliability and insufficient cost effectiveness of ceramic products.

O: Experts agree on the great yet unexploited technical potential of ceramics.

T: There are several obstacles which limit opportunities in the ceramic field. To be competitive and assure high performance products, high investments in knowledge and manufacturing equipment are necessary.

In the following, we examine reasons for shortcomings of ceramics, listed in "W". In this article, we concentrate on sintering.

Sintering is the final step in the ceramic fabrication process. It decisively influences the properties of products made from powders by sintering and represents the last chance of optimising the product.

Sintering theories are based on physical arguments such as the tendency for reduction in free surface energy and on simplified assumptions such as simple particle shapes (spheres) and simple particle arrangements (two or a limited number of spheres).

The general validity of sintering theories developed in pioneering works by Frenkel[1], Ivensen[2], Kucyznski[3], Kingery[4], Coble[5], Johnson[6] and others was proven by numerous experiments. Sintering theories are primarily concerned with material transport mechanisms and the kinetics of the sintering process. Knowledge of both are of fundamental importance for designing a cost effective manufacturing process for ceramic and powder metal articles with optimal properties.

However, the value of sintering theories in the manufacturing practice of specific ceramic products is limited due to the fact that theoretical assumptions about sintering processes are not valid in practice[7]. Fundamental studies assume (I) a pure, a homogeneous, single component starting powder, (II) uniform, small, spherical grains, (III) homogeneous body before sintering, and (IV) sintering at constant temperature. In contrast, practitioners in industrial production deal with (I) impure powders, usually inhomogeneous mixtures, (II) powders with a wide distribution of particle sizes, agglomerated to various degree, (III) with non-uniform density distri-

bution, and (IV) sintering at practically non-isothermal conditions.

Among serious inconsistencies between the assumptions underlying theoretical and basic experimental research on sintering phenomenon, chemical reactions at sintering temperature among constituents in the sintered body play an important role.

Chemical reactions in many ceramic systems occur among the constituents which are not in equilibrium at high temperatures and form new compounds or solid solutions. When the sintering process involves purposely chemically heterogeneous mixtures which are supposed to react during the sintering operation, one uses the term "reaction sintering". Examples are $BaTiO_3$ capacitor ceramics or ZnO based varistor ceramics. Most ceramic products are made of a basic compound with a small amount of additives which are intended to accelerate densification, suppress grain growth or modify the physical properties of the fired ceramics. The role of additives was frequently analysed, for example in [8] and [9]. In general, the additives may accelerate sintering by forming a liquid phase or control the microstructure by forming solid second phases which pin grain boundaries and impede grain growth. More subtle effects, which, however, profoundly influence the sintering process, are segregation at the grain boundaries, change of lattice defect concentration and diffusion constants when additives form a solid solution with the major component and a change in the ratio of grain boundary energy to free surface energy.

It is clear that the design of the sintering process, based on theoretical physical arguments only, must be modified by taking into account the possible chemical reactions.

In the following section, we report the results of research conducted in our laboratory on the effects of various aspects of chemical reactions on sintering. Specifically, we report effects of chemical heterogeneity on the sintering process in multicomponent systems. We demonstrate that even in single phase systems chemical dehomogenisation/homogenisation takes place. The aim of the review is to stress the importance of knowledge of chemical phenomena which occur during sintering of ceramics in designing and controlling the sintering process.

2 REACTION SINTERING IN THE $BaTiO_3$-$CaZrO_3$-TiO_2 SYSTEM

The term "reaction sintering" or "reactive sintering" is used to describe a sintering process in which a chemical reaction in the starting powder mixture and the densification of the ceramic body occur in the same heating operation. Depending on the material system and processing variables (particle size, temperature, pressure, etc.) the two processes, reaction and densification, can occur simultaneously, in sequence or as some mixture of these.

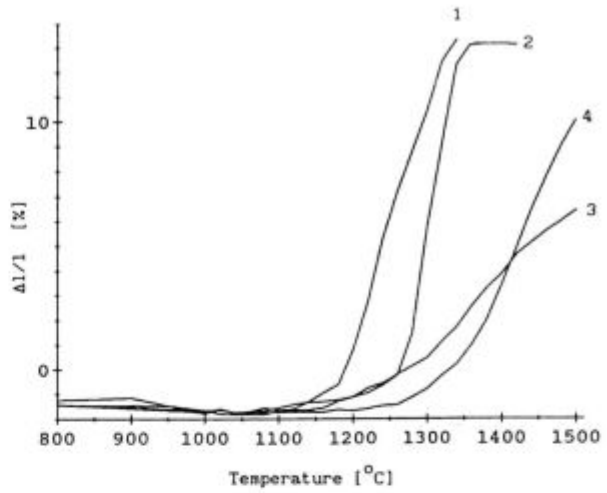

Figure 1: Dilatometric curves for $BaTiO_3$ - 2 mol % TiO_2 (1), $BaTiO_3$ - 2 mol % TiO_2 - 8 mol % $CaZrO_3$ (2), $BaTiO_3$ - 8 mol % $CaZrO_3$ (3) and $CaZrO_3$ (4).

Slika 1: Krivulje krčenja za mešanice $BaTiO_3$ - 2 mol % TiO_2 (1), $BaTiO_3$ - 2 mol % TiO_2 - 8 mol % $CaZrO_3$ (2), $BaTiO_3$ - 8 mol % $CaZrO_3$ (3) in $CaZrO_3$ (4).

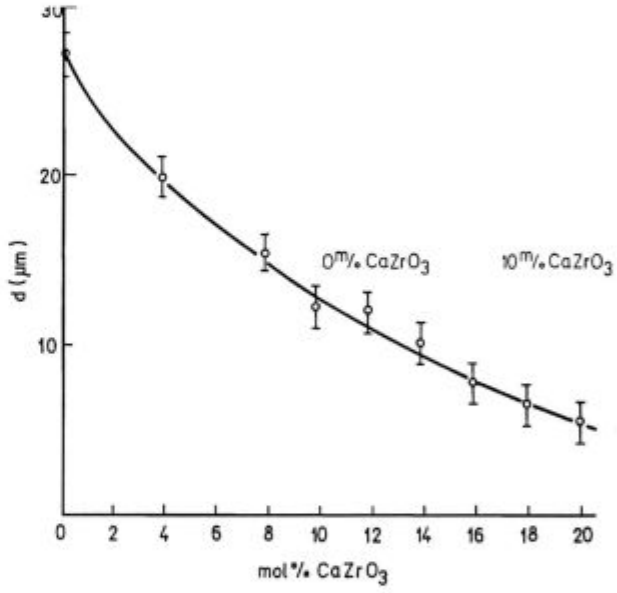

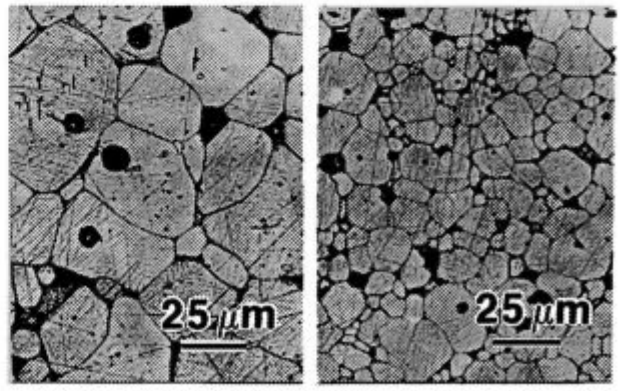

Figure 2: Average grain size vs. composition in $BaTiO_3$ - 2 mol % TiO_2 - $CaZrO_3$ ceramics sintered 1 hour at 1360°C.

Slika 2: Poprečna velikost zrn v odvisnosti od sestave keramike $BaTiO_3$ - 2 mol % TiO_2 - $CaZrO_3$, sintrane 1 uro pri 1360°C.

In ceramic fabrication practice, reaction sintering is usually avoided. The complexity of the processes caused by the chemical potential on one hand and the tendency to decrease the surface energy on the other renders the process difficult to control reproducibly. So, for example, in the manufacturing of soft Mn-Zn ferrites, the oxides are first calcined to form spinel solid solutions and then sintered. On the other hand, reactive sintering offers the possibility to optimise the properties of sintered products which are intentionally not in chemical equilibrium. Such is the case with several types of functional ceramics, for example varistors or high permittivity ceramic capacitors.

Frequently used compositions for ceramic capacitors are based on the solid solutions $(Ba_{1-x}Ca_x)(Ti_{1-y}Zr_y)O_3$. If Zr is incorporated into $BaTiO_3$ the maximum of the permittivity curve (at the Curie point) is shifted from 130°C to room temperature, whereas the non-ferroelectric $CaTiO_3$ broadens this maximum. $CaTiO_3$ has only limited solubility in $BaTiO_3$ and small undissolved particles of $CaTiO_3$ act as grain-growth inhibitors in the ferroelectric matrix[10].

$(Ba_{1-x}Ca_x)(Ti_{1-y}Zr_y)O_3$ capacitor ceramic is usually prepared by reaction sintering of $BaTiO_3$ - $CaZrO_3$ mixed powders. $BaTiO_3$ and $CaZrO_3$ are not compatible at high temperatures. During sintering, chemical reaction takes place resulting in formation of $(Ba,Ca)(Ti,Zr)O_3$ and $(Ca,Ba)TiO_3$ solid solutions[11]. The sintering kinetics and microstructural development of $BaTiO_3$-$CaZrO_3$ formulations are influenced by the kinetics of the chemical reaction, particularly at lower temperatures, i.e. in the initial sintering stage.

Research in our laboratory[12,13] showed that the particular batch of $BaTiO_3$ used started to shrink at around 1100°C and sintered considerably in the temperature region 1300-1350°C (Fig. 1). $CaZrO_3$, being more refractory, started to shrink at around 1250°C and sintered to high density in the temperature region 1450-1500°C. A $BaTiO_3$ - 8 mol % $CaZrO_3$ mixture started to shrink at approximately the same temperature as $BaTiO_3$. However, after a few % shrinkage the kinetics slowed down and temperatures higher than 1500°C were needed for densification. The sinterability of the $BaTiO_3$-$CaZrO_3$ mixture was improved by avoiding solid state diffusion. A small addition of TiO_2 (2 mol %), causing the formation of a low melting $BaTiO_3$-$Ba_6Ti_{17}O_{40}$ eutectic at around 1310°C, strongly improved the sinterability of the mixture. Temperatures between 1300-1350°C were sufficient to achieve high density. The microstructures of dense $BaTiO_3$ - 2 mol % TiO_2 and $BaTiO_3$ - 10 mol % $CaZrO_3$-2 mol % TiO_2 ceramics sintered at 1360°C are shown in Fig. 2. The microstructures also show that $CaZrO_3$ strongly reduces the exaggerated grain growth which is common phenomenon in $BaTiO_3$ - TiO_2 ceramics.

Comparison of the relative linear shrinkage of $BaTiO_3$ - 2 mol % TiO_2 and $BaTiO_3$ - 2 mol % TiO_2 - 8 mol % $CaZrO_3$ compacts as a function of time for isothermal sintering at 1260°C (Fig. 3) clearly indicated the differences in the sintering mechanism. $BaTiO_3$ - 2 mol % TiO_2 sintering kinetics in the initial stage can be described by an equation for first order kinetics $\Delta l/l = kt^n$ in which n is constant over the whole temperature range of sintering. In contrast, for $BaTiO_3$ - 2 mol % TiO_2 - 8 mol % $CaZrO_3$ the graphical representation of $\ln(\Delta l/l_0)$ vs. ln t shows a change in slope, indicating two different densification regions with different n - values. The densification process is especially disturbed in the first stage of sintering at lower temperatures (Fig. 4) due to the chemical reaction between $BaTiO_3$ and $CaZrO_3$. When heated, $BaTiO_3$ and $CaZrO_3$ react to form a $(Ba,Ca)(Ti,Zr)O_3$ solid solution. The equilibrium solid solution limit is

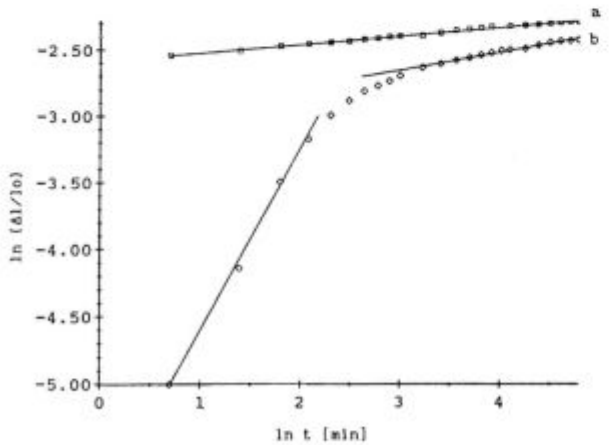

Figure 3: Comparison of the relative linear shrinkage of $BaTiO_3$ - 2 mol % TiO_2 (a) and $BaTiO_3$ - 2 mol % TiO_2 - 8 mol % $CaZrO_3$ (b) compacts as a function of time for the isothermal sintering at 1260°C.

Slika 3: Primerjava med relativnim skrčkom oblikovancev iz $BaTiO_3$ - 2 mol % TiO_2 (a) in $BaTiO_3$ - 2 mol % TiO_2 - 8 mol % $CaZrO_3$ (b) v odvisnosti od časa izotermnega sintranja pri 1260°C.

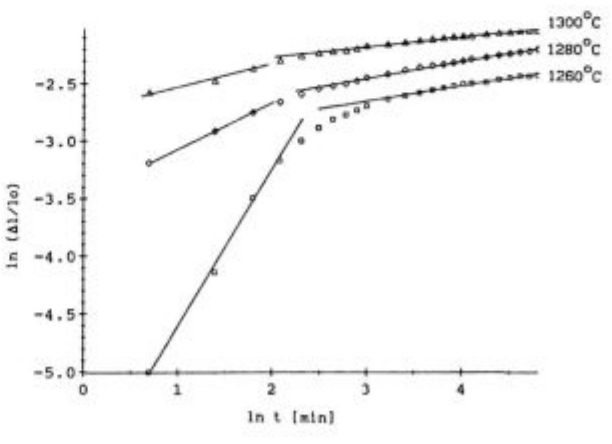

Figure 4: The relative linear shrinkage of $BaTiO_3$ - 2 mol % TiO_2 - 8 mol % $CaZrO_3$ samples as a function of time for the isothermal sintering temperatures of 1260°C, 1280°C and 1300°C.

Slika 4: Relativni linearni skrček oblikovancev iz $BaTiO_3$ - 2 mol % TiO_2 - 8 mol % $CaZrO_3$ v odvisnosti od časa pri izotermnem sintranju pri 1260°C, 1280°C in 1300°C.

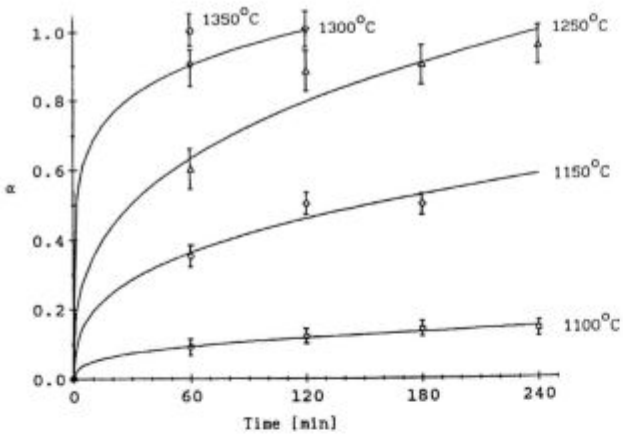

Figure 5: Degree of reaction (α) as a function of time for $BaTiO_3$ + $CaZrO_3$ → $BaZrO_3$ + $CaTiO_3$ at various temperatures.

Slika 5: Stopnja reakcije (α) v odvisnosti od časa za reakcijo $BaTiO_3$ + $CaZrO_3$ → $BaZrO_3$ + $CaTiO_3$ pri različnih temperaturah.

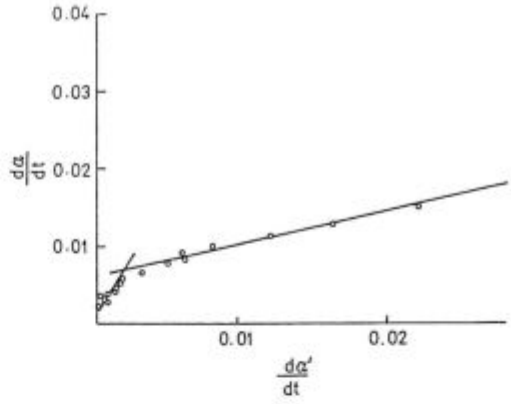

Figure 6: Comparison of the reaction rate dα/dt and densification rate dα'/dt ($\alpha=\rho'-\rho_o/\rho_{th}-\rho_o$) for $BaTiO_3$ - 2 mol % TiO_2 - 8 mol % $CaZrO_3$ samples at 1260°C.

Slika 6: Primerjava med reakcijsko hitrostjo dα/dt in hitrostjo zgoščevanja dα'/dt ($\alpha'=\rho'-\rho_o/\rho_{th}-\rho_o$) oblikovancev iz $BaTiO_3$ - 2 mol % TiO_2 - 8 mol % $CaZrO_3$ pri 1260°C.

around 16 mol % $CaZrO_3$. Larger amounts of $CaZrO_3$ cause formation of barium zirconate phase with some Ca and Ti in solid solution and a calcium titanate phase with some dissolved $BaTiO_3$[10,14]. In a 1:1 mole ratio $BaTiO_3$ - $CaZrO_3$ mixture the reaction was detectable by XRD analysis after only 1 hour's heating at 1100°C. The two characteristic X-ray reflections of $CaTiO_3$ at 2 θ = 59.052 (d = 1.563) and 2 θ = 47.401 (d = 1.918) were used for identification of $CaTiO_3$ and to determine the amount of $CaTiO_3$ formed during the reaction.

The degree of reaction α as a function of time for the reaction $BaTiO_3$ + $CaZrO_3$ → $BaZrO_3$ + $CaTiO_3$ at various temperatures is shown in Fig. 5. At lower temperatures (1100°C) α remains under 20 % even after prolonged heating. A considerably higher degree of reaction was achieved by heating the mixture of $BaTiO_3$ and $CaZrO_3$ at 1250°C and higher. The relationship α = f(t) at various temperatures has been evaluated using different mathematical expressions, theoretically derived for various models. The best fit was achieved with Jander's equation[15]:

$$[1 - (1 - \alpha)^{1/3}]^2 = kt,$$

which describes three dimensional diffusion[16]. It may be concluded that the diffusion mechanism is rate controlling.

The reaction kinetics dα/dt were compared with the sintering kinetics dα'/dt. The densification parameter α' ($\alpha'= \rho-\rho_o/\rho_{th}-\rho_o$) was calculated from dilatometric measurements in the temperature region 1200-1300°C (Fig. 6).

Comparison of the reaction rates with the densification rates at various temperatures confirmed the priority of chemical reaction in the first stage of sintering, and densification in the second stage (at higher temperatures). Sintering conditions have a strong influence on the microstructural development. A slower heating rate (1°/min) leads to the development of a coarse microstructure with a broad grain size distribution, whereas more rapid heating (5° or 10°C/min.) results in a finer microstructure with a narrower grain size distribution. The results may be explained on the basis of the kinetic studies. A fast heating rate favours reaction sintering with hindered grain growth, whereas a slow heating rate favours chemical reaction which takes place at lower temperatures than densification. The heterogeneous structure with phase separations in the initial sintering stage favours discontinuous grain growth and a broad grain size distribution.

Microstructural development also depends on the solid state diffusion rate during heating. A small excess of TiO_2, causing a liquid phase eutectic at sintering temperature, promotes grain growth, especially at slow heating rates. When $BaTiO_3$ with a small excess of BaO was used, grain growth during sintering was considerably hindered, especially when a slow heating rate was used.

Coarsening of the microstructure as a result of prolonged firing is accompanied by dielectric property changes. Different compositions of $BaTiO_3$ - $CaZrO_3$ based ceramics were fired at 1360°C for 15, 60, 480 minutes and the resulting dielectric properties were measured (Table 1). Whereas an ε value below the Curie temperature decreases with increasing firing time, the peak at the Curie temperature increases in value and broadens. Changes in the intensity and broadness of the peak are accompanied by coarsening of the microstructure. The coarse microstructure shows a more pronounced T_C shift and higher permittivity, while the room temperature permittivity is lowered. Maximum values of permittivity were obtained with the composition 84 mol % $BaTiO_3$ - 16 mol % $CaZrO_3$ near to the limit of solid solubility in the system.

Table 1: Dielectric properties of $BaZrO_3$ based ceramics with 2 mol % TiO_2 addition vs. soaking rime at 1360°C (at 1 kHz)

Composition	90 m/o $BaTiO_3$-10 m/o CZ			84 m/o $BaTiO_3$-16 m/o CZ			80 m/o $BaTiO_3$-20 m/o CZ		
time (min)	15	60	480	15	60	480	15	60	480
$\varepsilon_{25°C}$	4753	4270	2030	4045	7200	10694	2780	3105	5210
$tg\delta.10^4$	107	105	200	79	92	130	45	74	105
Tc(°C)	60	60	70	20	25	35	-20	-15	-10
ε_{max}	6350	7820	8960	4600	7200	10767	3820	4650	6619
$\Delta C/C$ (%)	/	/	/	-31,0 +14,0	-48,20	-71,2 +0,7	/	/	/

Chemically inhomogeneous ceramics in metastable ceramic equilibrium make it possible to make, by careful control of firing conditions, the temperature stable dielectric materials. This is ascribed to specific core-shell grain structure[17]. The relatively flat temperature characteristic of dielectric constant of $BaTiO_3$-$CaZrO_3$ based ceramics is determined by the superposition of the two permittivity/temperature maxima, those of $BaTiO_3$ core at – 120°C and (Ca,Zr) doped $BaTiO_3$ shell with maximum at lower temperature. Core-shell structure is discernible in TEM micrograph in Fig. 7. In the formation of the shell, reactive liquid phase plays important role, since the shell is formed by precipitation of dissolved matter on $BaTiO_3$ nuclei. Prolonged sintering provokes chemical homogenisation by solid state diffusion giving rise to increased permittivity and increased temperature dependence of permittivity.

3 SINTERING OF MONOPHASE COMPLEX CERAMICS: SINTERING OF $Pb(Zr_{0.5}Ti_{0.5})O_3$ (PZT)

In analysing sintering phenomena, it is important to realise that chemical reactions may influence the densification mechanism even in chemically homogenous compounds.

In recent years, considerable progress in the processing of ceramics has been achieved by improving the quality of powders. Attention is paid to wet-chemical methods of powder preparation, which assure fine particle size, controlled morphology, high purity and high homogeneity. Improved homogeneity is particularly desirable in complex multicomponent ceramics.

It is frequently stressed that wet chemical methods, such as coprecipitation or sol-gel methods, assure chemical homogeneity "on a molecular" level. However, this homogeneity may be temporarily lost during the sintering operation due to the very nature of the sintering process.

Kuczynski et al[18] pointed out that the vacancy gradient set up between sintered particles by the sharp curvature of the neck between particles can, under favourable conditions, produce considerable segregation in a completely homogenised solid solution. When the diffusion coefficients of constituent atoms in solid solution are different (which is frequently the case), the neck area becomes enriched in the faster diffusing atoms, at least in the early stage of sintering when the vacancy gradient due to the smallness of the radius of neck curvature is large. Such segregation must be a transient phenomenon, since segregation gives rise to a chemical potential gradient arising from the concentration gradient between the neck and regions adjacent to the neck, and acts in a direction opposite to the chemical potential gradient due to the neck curvature. When the radius of curvature of the neck increases, the chemical potential which causes the dehomogenization decreases. With accumulation of faster diffusing atoms in the neck, the concentration gradient also increases and the maximum segregation is reached. After this, the chemical potential gradient due to the concentration gradient predominates and back diffusion from the neck to other regions occurs. As a result, homogeneity is re-established.

Kuczynski et al[18] demonstrated segregation in Cu-In and Cu-Ag alloys. Mishra et al[19] demonstrated dehomogenization of Au-Ag alloy and concluded that the initial neck growth as well as segregation take place by surface

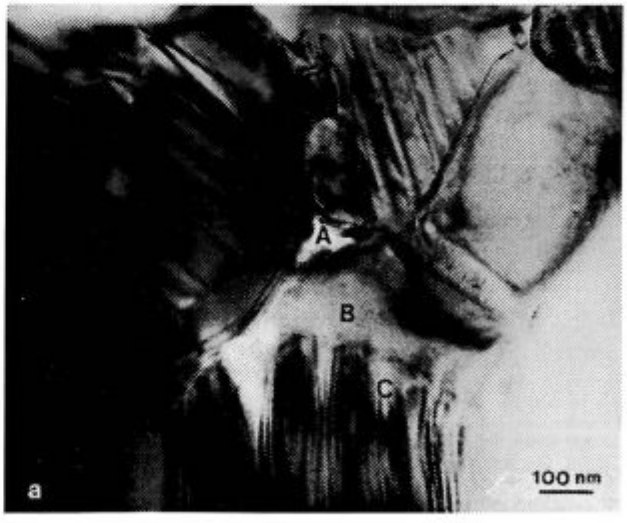

Figure 7: TEM photomicrograph of $BaTiO_3$ - 2 mol % TiO_2 - 8 mol % $CaZrO_3$ ceramic, sintered 2 hours at 1260°C showing (A) solidified TiO_2 - rich phase at grain corners and along grain boundaries, (B) Ca- and Zr- modified domain free region and (C) ferroelectric $BaTiO_3$ grain core.

Slika 7: TEM posnetek keramike iz $BaTiO_3$ - 2 mol % TiO_2 - 8 mol % $CaZrO_3$ keramike, sintrane 2 uri pri 1260°C. Posnetek kaže (A) strjeno talino, bogato na TiO_2 med zrni in vzdolž zrn, (B) s Ca in Zr bogat rob zrn brez domen in (C) ferroelektrično $BaTiO_3$ jedro z domenami.

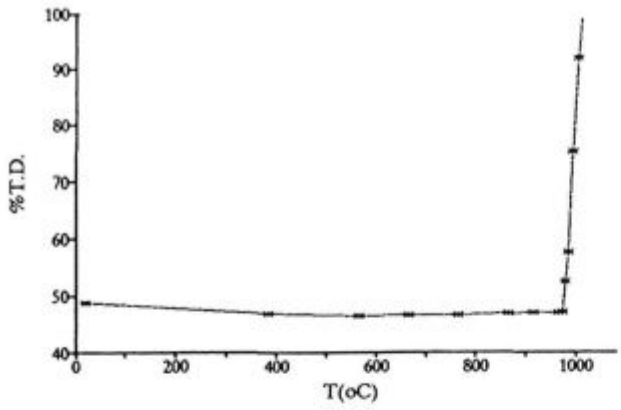

Figure 8: Sintering curve of $Pb(Zr_{0.5}Ti_{0.5})O_3$ compact in air, pressed at 100 MPa. Heating rate: 10°C/minute.
Slika 8: Krivulja zgoščevanja oblikovanca iz $Pb(Zr_{0.5}Ti_{0.5})O_3$, stisnjenega s tlakom 100 MPa. Hitrost segrevanja 10°C/min.

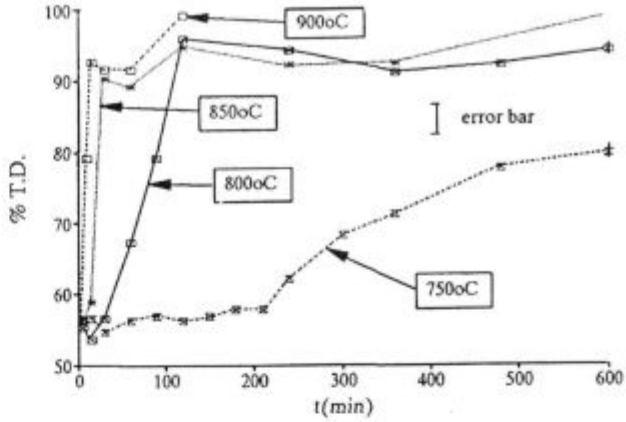

Figure 9: Density of $Pb(Zr_{0.5}Ti_{0.5})O_3$ ceramics as a function of temperature and time of isothermal heating runs in an air atmosphere.
Slika 9: Gostota $Pb(Zr_{0.5}Ti_{0.5})O_3$ keramike v odvisnosti od temperature in časa pri izotermnem segrevanju v atmosferi zraka.

diffusion, whereas back diffusion occurs by a combination of surface and volume diffusion.

It may be expected, due to capillary forces in the early sintering stage, that the dehomogenization effect occurs in complex ceramic systems as well. It should be particularly pronounced in sintering of nanosized powders, where surface diffusion plays an important role. The segregation-homogenisation phenomenon should be reflected in densification curves.

To demonstrate the effect, we examined the sintering of fine sol-gel prepared powders of lead zirconate - lead titanate solid solution, $Pb(Zr_{0.5}Ti_{0.5})O_3$ (PZT)[20].

Fig. 8 shows the densification curve of a $Pb(Zr_{0.5}Ti_{0.5})O_3$ compact, made of fine powder prepared by alkoxide sol-gel synthesis. The very rapid densification above ~950°C does not support the expected solid state sintering mechanism. Instead, the sudden and steep increase in sintering rate and the well crystallised grains are indicative of liquid phase sintering. The liquid phase may be the PbO-PZT eutectic above ~840°C; however, the presence of PbO could not be detected by XRD or TEM in the starting powder.

The isothermal densification curves, presented in Fig. 9, show anomalous behaviour in the temperature region 750-800°C. The anomaly is an extended "induction" period in the densification curves at 750 and 800°C. Anomalous densification of PZT in the initial sintering stage may be explained by preferential diffusion of PZT constituents.

Accumulation of faster diffusing species in the necks between the particles, triggered by surface curvature, causes an increased tendency for backward diffusion, sustained by the concentration gradient. Formation of the thermodynamically nonequilibrium phase and its subsequent annihilation interferes with the normal densification process, being reflected as an induction period. Further densification commences only after neck curvature decreases and the material homogenises again.

At low sintering temperatures, material transport takes place predominantly by surface diffusion and, when possible, by vapour transport. PZT is known for the high vapour pressure of PbO[21]. To the author's knowledge, surface diffusivities of Pb, Zr and Ti ions in PZT have not been reported. Slinkina and Doncov[22], using radioactive tracers, measured the effective self-diffusion coefficients in polycrystalline 99 % dense $Pb(Zr_{0.5}Ti_{0.5})O_3$ ceramics. The effective diffusion coefficient of Pb^{2+} was 5 - 40 times higher than that of O^{2-} and almost two orders of magnitude higher than D_{Ti} and D_{Zr},

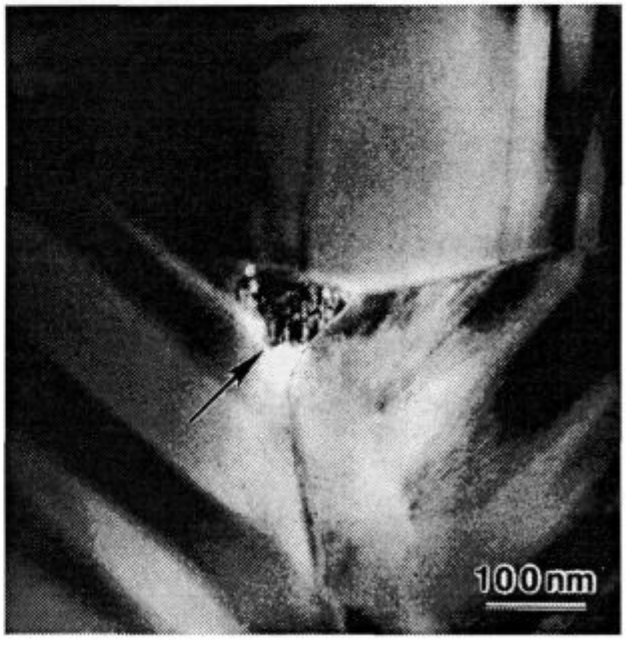

Figure 10: TEM micrograph of $Pb(Zr_{0.5}Ti_{0.5})O_3$ ceramic, sintered at 900°C for 1 hour. Arrow points to Pb-rich inclusion among 3 perovskite grains (Courtesy G. Dražič).
Slika 10: TEM posnetek $Pb(Zr_{0.5}Ti_{0.5})O_3$ keramike, sintrane pri 900°C 1 uro. Puščica kaže vključek, bogat s Pb, med 3 perovskitnimi zrni (posnetek G. Dražič).

which were close to each other. Nakamura, Chandratreya and Fulrath[23] and Kosec and Kolar[24] reported that during the formation of PZT from $PbTiO_3$ and $PbZrO_3$, titanium ions diffuse much faster than zirconium ions. The vapour pressure transport of PbO into the necks is also possible. To maintain electrical neutrality, diffusion of cations is accompanied by a simultaneous flow of oxygen ions, or through gas-phase transport. Faster diffusion of Pb and Ti, caused by high neck curvature in the initial sintering stage of fine-grained PZT compacts, causes accumulation of Pb and Ti or Zr in the necks, and corresponding depletion of both species in other regions of PZT grains. According to the phase diagram[25], PZT may be Pb deficient up to 2 mol % PbO; however, PbO does not dissolve in PZT. The simplified equation derived by Kuczynski et al[18], makes it possible to estimate the maximal excess concentration of the faster diffusing species in the neck area.

In simplified form, Kuczynski's equation reads:

$$\rho_c = \frac{2\gamma\Omega C}{\Delta C k T}$$

where

ρ_c critical neck radius necessary to reverse the neck curvature driven atoms outward flow to concentration gradient driven inward flow

γ surface energy

Ω mean atomic volume

$\Delta C/C$ relative concentration gradient between neck area and grain interior

k Baltzman's constant

T temperature

Neck radius is related to particle diameter (2a) and neck diameter (2x) by expression

$$\rho_c = \frac{x^2}{4a}$$

Assuming surface energy ≅1 J/m^2, mean atomic volume 10^{-29} m^3, and kT (at 1000 K) $1{,}4.10^{-20}$ J, one can estimate the maximal excess concentration of the faster diffusing specie in the neck area. With 200 nm size particles and neck diameter 140 nm, the calculated excess concentration is 8 mol %. In view of crudity of assumptions, the result seems reasonable.

The proposed explanation of the PZT sintering anomaly was supported by the following experimental observations:

(1) XRD patterns of PZT after the early sintering stage confirmed the presence of tetragonal and rhombohedral phases, whereas in the starting PZT powder only reflections of the tetragonal phase were present. $Pb(Zr_xTi_{1-x})O_3$ solid solution exhibits a phase transformation from the tetragonal to rhombohedral structure at x ~ 0.53. The appearance of rhombohedral phase indicates the shift in PZT composition. After prolonged sintering, the rhombohedral phase disappeared, confirming homogenisation to the initial composition with x = 0.5.

(2) After the early sintering stage, PbO inclusions in the microstructure were observed by SEM and TEM examinations (Fig. 10). Enrichment of PbO in the necks as compared with the grain interior was confirmed by quantitative EDX analysis in the transmission electron microscope. On further heating, PbO inclusions redissolved.

The findings of the work presented disprove the correctness of solid state sintering models assumed for PZT by several researchers. The transient presence of PbO, which forms a eutectic in the early sintering stage, provokes liquid phase sintering. This has several important consequences, for example that microstructural development in PZT must be sensitive to the heating schedule. Probably the most important result from this investigation is that the dehomogenization phenomenon with the transient existence of metastable phases is likely to be a frequent occurrence in the initial stage of sintering of multicomponent ceramics. It is particularly to be expected in sintering of fine powders with a high driving force for sintering.

4 SUMMARY

The critical issues in mastering ceramic processing to assure the reliability and reproducibility of ceramic bodies are well known. These are (a) appropriate raw materials (purity, finess, grain size distribution), (b) correct shaping of homogenous bodies without macro defects and (c) suitable sintering parameters (T, t, dT/dt, etc.) But of particular importance for the reliable manufacturing process is a knowledge and control of chemical reactions at high temperatures. This in turn demands knowledge of high temperature phase relations, knowledge of reaction kinetics and availability of data such as (1) systematic trends in the periodic system, (2) the nature and strength of chemical bonds, (3) thermodynamics ($\Delta G,\gamma$) and (4) kinetic parameters (diffusion coefficients). In short, to achieve optimal properties of ceramic products and to assure competitiveness demands a high professional knowledge and appropriate equipment.

5 REFERENCES

[1] J. Frenkel, *J. Phys.*, 9 (1945) 5, 385-91

[2] B. Ya. Pines, *J. of Techn. Phys.*, 16 (1946), 737

[3] G. C. Kuczynski, *Trans. Am. Inst. Mining Met. Eng.*, 185, (1949), 169-78

[4] W. D. Kingery and M. Berg, *J. Appl. Phys.*, 26 (1955), 1205-12

[5] (a) R. L. Coble, *J. Appl. Phys.*, 32 (1961), 787-92
(b) *J. Appl. Phys.*, 36 (1965), 2327

[6] D. L. Johnson, *J. Appl. Phys.*, 40 (1969) 1, 192-200

[7] D. Kolar, *Mat. Sci. Res.*, 13 (1980), 335

[8] M. F. Yan, *Materials Science and Engineering*, 48 (1981), 53

[9] R. J. Brook, S. P. Howlet, and S. X. Wu, *Mat. Sci. Monographs*, 14 (1982), 135

[10] M. McQuarrie and F. Behke, *J. Am. Ceram. Soc.*, 37 (1954), 539-543

[11] H. J. Hagemann, D. Hennings, and R. Wernicke, *Philips Tech. Rev.*, 41 (1983/84), 89-98

[12] D. Suvorov and D. Kolar, Sintering and Dielectric Properties in The $BaTiO_3$-$CaZrO_3$ System, pp 2.314-2.318 in *Euro-Ceramics*, Vol. 2, ed. by G. de With, R. A. Tepstra and R. Metselaar, Elsevier, Amsterdam 1989

[13] D. Suvorov and D. Kolar, *Silicates Industriels*, 5-6 (1993), 109-113

[14] G. H. Jonker, *Philips Tech. Rundschau*, 17 (1955), 127-135

[15] W. Jander, *Z. Anorg. Allg. Chem*, 163 (1927), 1-52

[16] J. Beretka, *J. Amer. Ceram. Soc.*, 76 (1984), 615-620

[17] B. S. Rawal, M. Kahn, and W. R. Buessem, Grain Core - Grain Shell Structure in Barium Titanate-Based Dielectrics, pp 172-88 in *Advances in Ceramics*, Vol. 1, The American Ceramic Society, Columbus, Ohio, 1981

[18] G. C. Kuczynski, G. Matsumura, and B. D. Cullity, *Acta Metallurgica*, 8 (1960), 209-15

[19] A. Mishra, F. V. Lenel, and G. S. Ansell, *Mat. Sci. Research*, 10, Plenum, New York, 1975, 339-347

[20] B. Malič, D. Kolar, and M. Kosec, Anomalous Densification of Complex Ceramics in the Initial Sintering Stage, pp 69-76 in Sintering Technology, ed. by R. M. German, G. L. Messing and R. G. Cornwall, Marcel Dekker Inc., New York, 1996

[21] K. H. Härdtl and H. Rau, *Solid State Comm.*, 7 (1969), 41-45

[22] M. V. Slinkina and G. L. Doncov, *Izv. Akad. Nauk SSSR Neorgan. Mat.*, 28 (1992), 567-570

[23] Y. Nakamura, S. S. Chandratreya, and R. M. Fulrath, *Ceramurgia Int.*, 6 (1980), 57-60

[24] M. Kosec and D. Kolar, PZT solid solution formation from $PbZrO_3$ and $PbTiO_3$, *Mater. Sci. Monographs* 16: *Ceramic Powders*, ed. by P. Vinzenzini, Elsevier, Amsterdam, pp. 421-427, 1983

ISSN 1318-0010
KZLTET 31(6)485(1997)

GROWTH OF III-NITRIDES VIA SUBLIMATION AND METALORGANIC VAPOR PHASE EPITAXY

RAST III-NITRIDOV S SUBLIMACIJO IN METALORGANSKO PARNO FAZNO EPITAKSIJO

ROBERT F. DAVIS[1], C. M. BALKAS[1], M. D. BREMSER[1], O. H. NAM[1], W. G. PERRY[1], B. L. WARD[2], Z. SITAR[1], T. ZHELEVA[1], L. BERGMAN[2], I. K. SHMAGIN[3], J. F. MUTH[3], R. M. KOLBAS[3], R. J. NEMANICH[2]

[1]Department of Materials Science and Engineering, North Carolina State University, Box 7907 Raleigh, NC, 27695-7907
[2]Department of Physics, North Carolina State University, Box 8202, Raleigh, NC 27695-8202
[3]Department of Electrical and Computer Engineering, North Carolina State University, Box 7911, Raleigh, NC 27695-7911

Prejem rokopisa - received: 1997-10-01; sprejem za objavo - accepted for publication: 1997-10-21

Single crystals of GaN ≤ 3 mm in length were grown by sublimation/recondensation of GaN in 760 Torr NH_3 at 1100°C. Platelets of AlN ≤ 1 mm thick were similarly grown between 1950 and 2250°C using an Al source. Monocrystalline GaN and $Al_xGa_{1-x}N$(0001) ($0.05 \leq x \leq 0.96$) films were grown via MOVPE on α(6H)-SiC(0001) wafers with and without, respectively, a 1000 Å AlN buffer layer. Photoluminescence (PL) spectra of GaN showed bound and free excitonic recombinations. Selective growth of hexagonal pyramid arrays of undoped GaN and Si-doped GaN was achieved on 6H-SiC(0001)/AlN/GaN multilayer substrates using a patterned SiO_2 mask. Field emission of these arrays exhibited a turn-on field of 25 V/μm for an emission current of 10.8 nA at an anode-to-sample distance of 27 μm. Lateral growth and coalescence of GaN have been achieved using stripes oriented along <1$\bar{1}$00> at 1100°C and a triethylgallium flow rate of 26 mmol/min. Approximately 10^9 cm^{-2} dislocations, originating from the underlying GaN/AlN interface, were contained in the GaN grown in the window regions. The overgrowth regions contained a very low density of dislocations.

Key words: gallium nitride, aluminum nitride, single crystals, thin films, photoluminescence, Raman spectroscopy, cathodoluminescence, selective growth, lateral overgrowth

Kristali GaN ≤ 3 mm dolžine so bili izdelani s sublimacijo/rekondenzacijo GaN pri 760 tor. NH_3 in 1100°C. Ploščice AlN ≤ 1 mm debeline so bile na podoben način izdelane pri 1950 do 2250°C z uporabo Al kot izvora. Monokristalini filmi GaN in Al_xGa_{1-x} N(001) z ($0.05 \leq x \leq 0.96$) so bili izdelani z MOVPE na α(6H)-SiC(0001) vaferjih z in brez 1000 Å AlN bufer sloja. Fotoluminiscentni (PL) spektri GaN so pokazali vezi in proste excitonske rekombinacije. Selektivna rast združb heksagonalnih piramid nedopiranega GaN in GaN dopiranega s silicijem je bila dosežena na 6H - Si(0001)/AlN/GaN večslojnih substratih z uporabo vzorčastih SiO_2 mask. Prag polja emisije teh združb je imel jakost 25 V/μm za emisijski tok 10.8 nA pri razdalji 27 μm med anodo in preizkušancem. Lateralna rast in koalescenca GaN je bila dosežena z uporabo lamel orientiranih vzdolž <1$\bar{1}$00> pri 1100°C in pretoku trietilgalija 26 mmol/min. V GaN, ki je nastal v področju oken je bilo približno 10^9 cm^{-2} dislokacij, ki so izvirale iz mejne površine GaN/AlN. Področja večje rasti so imela majhno gostoto dislokacij.

Ključne besede: galijev nitrid, aluminijev nitrid, posamični kristali, tanki filmi, fotoluminiscenca, Raman spektroskopija, katodoluminiscenca, selektivna rast, pospešena lateralna rast

1 INTRODUCTION

The realization of blue and green light emitting diodes and blue lasers as well as prototypes of several microelectronic devices produced from GaN-based materials containing copious line and planar defects has been most fortunate. These achievements also indicate that the employment of substrates on which homoepitaxial films can be grown would result in marked improvements in the properties of the devices fabricated in these films. At present, very thin films of GaN, AlN and $Al_XGa_{1-X}N$ are deposited on foreign substrates as buffer layers on which the device-related III-V nitrides films are grown. Aluminum nitride is also a candidate material for selected piezoelectric applications and surface acoustic wave (SAW) devices. However, the potential of AlN in these and other applications has been hampered by the lack of bulk single crystals, as discussed in several review articles[1-4]. Gallium nitride is a promising material for field emission because of its low electron affinity (2.7-3.3eV)[5,6], reasonable thermal, chemical and mechanical stability and the ability for controlled n-type doping. Recently, it has been reported[6,7] that AlN and Al-rich $Al_XGa_{1-X}N$ ($x \geq 0.75$) films exhibit a negative electron affinity which suggests that these materials belong to a special class of field emitters.

Recent research conducted by the authors and described in the following sections represent important advances in the determination of the process parameters necessary to achieve growth of GaN and AlN bulk single crystals via seeded sublimation/recondensation. Additionally, we discuss the employment of a 1000 Å, monocrystalline, high-temperature (HT) (1100°C) AlN buffer layer for metalorganic vapor phase epitaxy (MOVPE) thin film deposition which has resulted in subsequently deposited GaN films void of oriented domain structures and associated low-angle grain boundaries[8,9]. Monocrystalline films of $Al_xGa_{1-x}N$ ($0.05 \leq x \leq 0.96$) of the same quality as GaN with a HT-AlN buffer layer have also been achieved directly on 6H-SiC(0001) wafers at 1100°C. We also report the selective growth of GaN and Si-doped GaN hexagonal pyramid arrays on

circular patterns etched in SiO_2 masks deposited on GaN/AlN/6H-SiC(0001) multilayer substrates and the field emission results from these arrays, as well as the deposition, the lateral overgrowth and subsequent coalescence of the GaN stripes selectively grown in the same manner.

2 EXPERIMENTAL PROCEDURES

A. GaN Bulk Growth

Growth of individual GaN crystals was achieved by evaporating 0.5" diameter and 0.25" high GaN pellets cold pressed from high purity GaN powders produced in our laboratory[10] in a stream of 99.9999% pure NH_3 gas. Experiments were conducted in a system that was specifically designed for GaN growth. The growth system consisted of: (1) an outer vacuum chamber that contained the heat shields and electrical feed-throughs and (2) a reaction tube containing the source and seed materials. Two independently controlled heaters were used to achieve the necessary temperature gradients for sublimation growth. Heater temperatures were monitored and controlled via the use of thermocouples placed adjacent to each heater. Source and substrate temperatures were monitored independently from within the reaction tube. Experiments were performed within the source temperature range of 1100-1450°C. The seed heater was maintained at 1100°C throughout each deposition. Growth pressures of 50-760 torr were investigated; however, most experiments were conducted at 760 torr. An NH_3 flow rate of 50 sccm was used for all growth experiments. Blank BN seed holders were used as substrates and placed at a distance from the source wherein the crystals with low aspect ratios could be obtained.

B. AlN Bulk Growth

Aluminum nitride sublimation/recondensation experiments were also conducted in a resistively heated graphite furnace. Bulk AlN (99% dense) blocks produced via sintering without additives were used as the source material. The source was positioned in the isothermal section of the furnace to ensure an essentially constant evaporation rate. Single crystal, 6H-SiC (0001) squares (10 mm x 10 mm) were used as seeds in all experiments due to the relatively small lattice mismatch to AlN (0.9%) and high temperature stability. The seed crystals were heated in vacuum at ≈1150°C prior to crystal growth to desorb the surface oxide, hydrocarbons and any other contaminants.

All AlN experiments were performed under a 100 sccm flow of ultra-high purity N_2. The background pressure was maintained at 500 Torr by an automatic throttle valve. The temperature ranges of 2100-2250°C and 1950-2050°C were investigated consecutively. The lower temperature range was employed primarily because of the degradation of the furnace and the seed crystals at the higher temperatures. In both cases, a temperature difference of 80-150°C was employed, depending on the separation distance (1-40 mm) between the source and the seed. The growth rate at a separation of 3 mm was ≈30 times higher than at a 15 mm separation. The AlN source was repositioned to the desired source height before each experiment.

C. Metalorganic Vapor Phase E pitaxy and Selective Area Growth

As-received vicinal 6H-SiC(0001) wafers[11] oriented 3°-4° off-axis toward <11$\bar{2}$0> were cut into 7 mm squares. These pieces were degreased in sequential ultrasonic baths of trichloroethylene, acetone and methanol and rinsed in deionized water. The substrates were subsequently dipped into a 10% HF solution for 10 minutes to remove the thermally grown oxide layer and blown dry with N_2 before being loaded onto the SiC-coated graphite susceptor contained in a cold-wall, vertical, pancake-style, MOVPE deposition system. The system was evacuated to $\leq 3 \times 10^{-5}$ Torr prior to initiating growth. The continuously rotating susceptor was RF inductively heated to the GaN ($Al_xGa_{1-x}N$) deposition temperature of 1050°C (1100°C) (optically measured on the susceptor) in 3 SLM of flowing H_2 diluent. Hydrogen was also used as the carrier gas for the various metalorganic precursors. Deposition of $Al_xGa_{1-x}N$ was initiated by flowing various ratios of triethylaluminum (TEA) and triethylgallium (TEG) in combination with ammonia (NH_3).

Selective growths of GaN and $Al_{0.2}Ga_{0.8}N$ were achieved at 1000-1050°C with TEG flow rates = 26.1-70.0 μm/min. on stripe (window width = 3-80 μm) and circular (diameter = 5 μm) patterned GaN/AlN/6H-SiC(0001) multilayer substrates. To produce these patterned substrates, a SiO_2 mask layer (thickness = 1000Å) was subsequently deposited on each GaN film via RF sputtering or low pressure chemical vapor deposition. Patterning of the mask layer was achieved using standard photolithography techniques and etching with a buffered HF solution. The edges of the stripe patterned samples were parallel to <11$\bar{2}$0>. Prior to selective growth, the patterned samples were dipped in a buffered HCl solution to remove the surface oxide of the underlying GaN layer. Incorporation of the n-type Si dopant into the GaN pyramids during growth was achieved using SiH_4 at a flow rate of 5.5 nmol/min.

Field emission measurements (FEM) were performed on the Si-doped GaN hexagonal pyramid arrays in a UHV-FEM system having a working pressure of 2×10^{-8} Torr. Each array was placed beneath a five mm diameter movable Mo anode having a flat tip. The anode was controlled by a stepping motor such that one step yielded a translation of 0.44 μm. The current-voltage (I-V) measurements were taken from 2 to 40 μm for anode voltages in the range of 0 to 1100 V.

The lateral overgrowth of GaN was achieved in a manner similar to that of the films[12]. The GaN grew vertically to the top of the mask and then both laterally and vertically over the mask until the lateral growth fronts from many different windows coalesced and formed a continuous layer. The samples were characterized by scanning electron microscopy (SEM-JEOL 6400 FE), atomic force microscopy (AFM-Digital Instrument NanoScope III) and transmission electron microscopy (TEM-TOPCON 002B, 200KV).

3 RESULTS AND DISCUSSION

A. Bulk GaN Growth

Colorless wurtzitic GaN crystals ≤ 3 mm in size were achieved by sublimation of the pressed GaN pellets in a stream of ammonia. **Figure 1** shows an optical micrograph of ≈1 mm long, well faceted, transparent GaN crystals with low aspect ratios which are in contrast to the commonly observed[13] needle-shaped crystals grown via vapor phase reaction. The GaN crystals primarily grew by spontaneous nucleation on the BN seed holders. The use of temperatures above 1200°C resulted in the rapid conversion of the GaN source into Ga metal. Crystals were grown at source temperatures in the range of 1100-1200°C; however, the majority of experiments were conducted at 1200°C to achieve higher growth rates. The temperature of the BN surface where crystals nucleated was ≈1000°C. The growth time and pressure for the growth of the crystals shown in **Figure 1** were 2.5 hrs and 760 Torr, respectively.

The direction of fastest growth and thus the crystal shape were observed to change with the changing Ga/NH_3 flux ratio and the growth temperature. These observations are in contrast to all previous reports which indicate that growth of bulk GaN from the vapor phase results primarily in long needles.

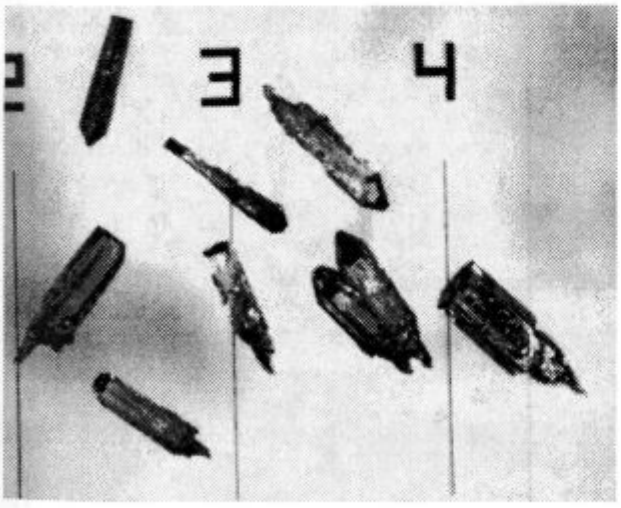

Figure 1: GaN crystals grown by sublimation/recondensation on BN. Lines are spaced 1 mm
Slika 1: GaN kristali zrastli s sublimacijo/rekombinacijo na BN. Črte so oddaljene 1 mm

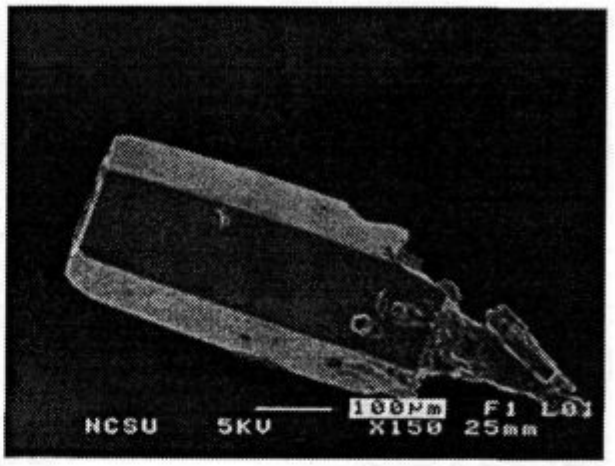

Figure 2: Secondary electron microscopy of a GaN crystal showing well developed {1010} and {0001} crystallographic facets
Slika 2: SEM posnetek GaN kristalov, ki kaže dobro razvite {1010} in {0001} kristalne ploskve

Figures 2 and 3 show SEM images of the same crystal. This crystal grew from a single isolated nucleation site and developed into a well faceted hexagonal shape terminated by flat {1010} and {0001} planes. **Figure 3** shows a higher magnification image in which the (0001) and (1010) facets are observed.

A spectral mass scan via SIMS indicated that all impurities with the exception of oxygen were at background levels. Quantitative analysis revealed an oxygen concentration of $3x10^{18}$ atoms/cm^3 which is similar to that present in high quality GaN thin films.

A representative room temperature PL spectrum for bulk GaN taken at 300K is shown in **Figure 4**. Strong near band edge (bound exciton) emission with a peak position at 365.0 nm (3.4 eV) and a FWHM of 9.0 nm (83 meV) was observed. The visible portion of the PL

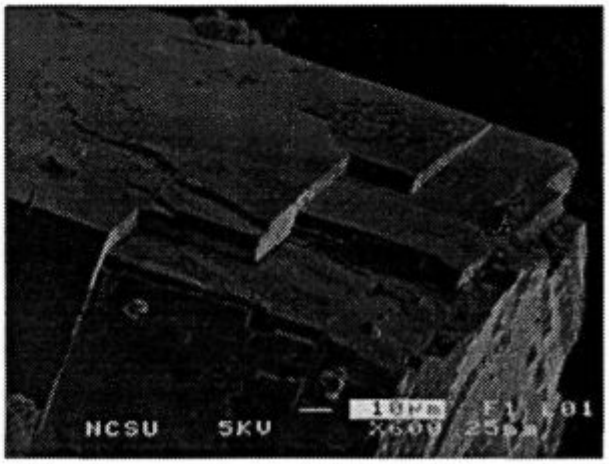

Figure 3: Higher magnification of the crystal in **Figure 2**
Slika 3: Kristal na **sliki 2** pri večji povečavi

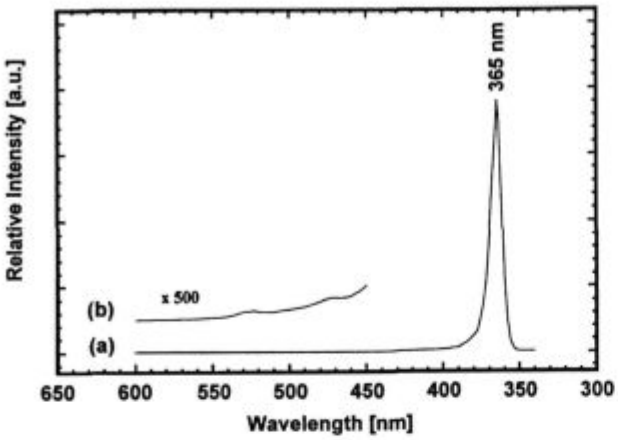

Figure 4: Photoluminescence spectrum of GaN taken at 300 K
Slika 4: Fotoluminiscentni spekter GaN pri 300 K

spectrum is expanded 500 times in the inset in **Figure 4**. No yellow emission usually attributed to deep level transitions was detected on this scale or to the naked eye. A peak position of 359.0 nm with a FWHM of 54 meV was detected for a PL spectrum obtained at 77 K.

The allowed Raman modes of the wurtzite structure are presented in **Figure 5**. The inset in this figure shows that the $E2^{(2)}$ mode is at 567 cm^{-1} and has a FWHM ≈ 3.5 cm^{-1}. These values are indicative of a material of the highest quality reported to date[14].

The results of optical absorption studies are shown in **Figure 6**. The absorption band edge is distinct but is not as sharply defined as observed in thin epitaxial films. This is due to the absorption tail below the band edge. The absorption edge is expected to shift to wavelengths above the actual band gap (360 nm for GaN) as the material thickness increases. For example, in the absorption spectrum of a high quality 50 μm thick GaN film the absorption edge is observed at 369 nm, and 75% transmission is observed at 379 nm [15]. Since the GaN crystal

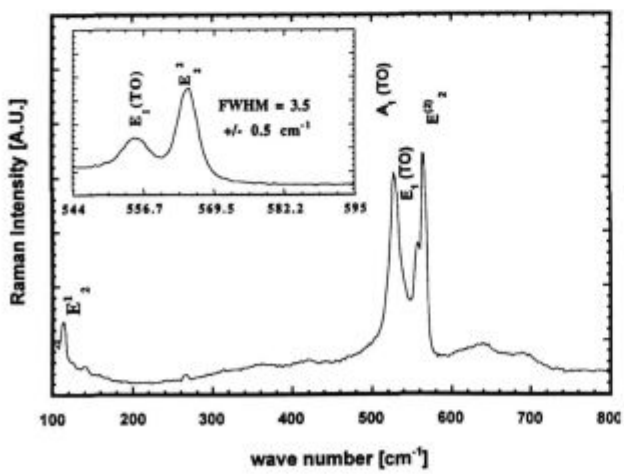

Figure 5: Raman spectrum of GaN
Slika 5: Raman spekter GaN

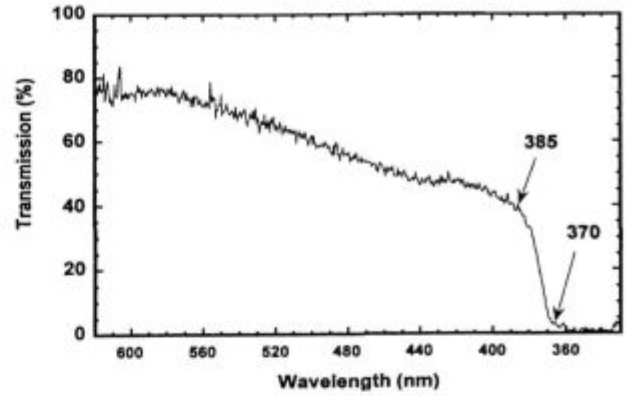

Figure 6: Optical absorption spectrum of GaN crystal
Slika 6: Optični absorpcijski spekter GaN kristala

from which the above spectrum taken was ≈ 300 μm thick, the absorption edge position of ≈ 370 nm and 75% transmission indicate these crystals to be of high optical quality.

B. AlN Bulk Growth

Growth in the 2100-2250°C range

Single crystal platelets of AlN having thicknesses to one millimeter and covering the whole seed crystal were obtained at a source temperature of 2150°C and a 4 mm source-to-seed separation. The growth rate was estimated to be 0.5 mm/hr. The results of XRD and Laue back reflection studies confirmed the monocrystallinity.

At higher growth temperatures between 2150-2250°C several ≈ 2 x 2 mm individual hexagonal crystals were obtained on the seeds, since at these temperatures, severe degradation of the SiC substrates resulted in isolated stable nucleation sites. These crystals and the aforementioned platelets ranged in color from green to blue. The coloration strongly indicated the incorporation of impurities which was confirmed via SIMS analysis to be C and Si from the SiC substrates.

Upon cooling, the AlN crystals frequently delaminated and cracked. This was most probably due to the mismatch in the coefficients of thermal expansion between the two materials; however, intrinsic stress in the deposited material and/or the extension of pre-existing cracks at the edges of the SiC substrates may also have contributed to these phenomena. Unfortunately, the thermal expansion coefficients data for these materials are not available for the entire temperature range of the experiments. Since AlN boules will ultimately be grown on obtained AlN crystals, this cracking problem should not be a significant barrier to the attainment of much larger crystals.

Growth in the 1950-2050°C range

Growth of AlN in the temperature range of 1950 to 2050°C was conducted because complete structural and chemical stability of the SiC seeds and a significant re-

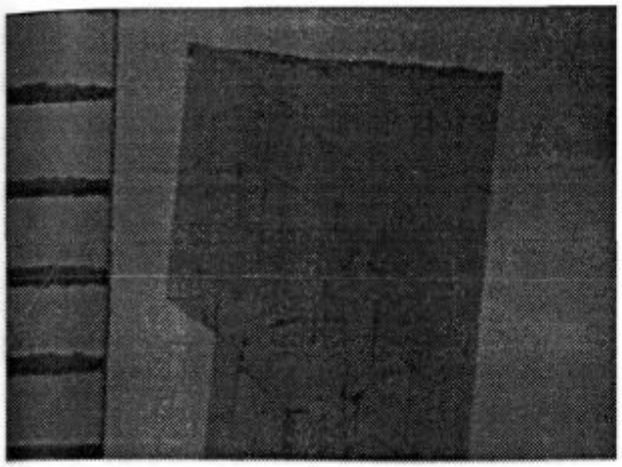

Figure 7: Optical micrograph of a single crystal of AlN grown at 1950°C and a 4 mm source-to-seed separation (Scale: mm)
Slika 7: Optični posnetek kristala AlN, ki je zrastel pri 1950°C in razdalji 4 mm med izvorom in kaljo (merilo: mm)

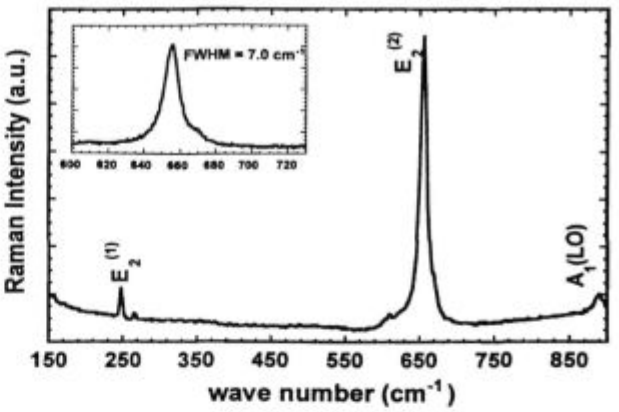

Figure 8: Raman spectrum of transparent bulk AlN grown at 1950°C
Slika 8: Raman spekter prosojnega AlN, ki je bil zraščen pri 1950°C

duction in the deterioration of the SiC coated crucibles were attained. Crystals grown in this temperature range were always colorless regardless of the morphology or growth site and contained almost two orders of magnitude less Si and C than the crystals deposited at >1950°C; whereas, the O levels were similar in all crystals. Typical growth rates were reduced to 30-50 μm/hr. Growth runs of 10-15 hrs yielded 0.3-0.5 mm thick crystals on 1 cm^2 SiC substrates. A 0.4 mm thick transparent AlN platelet grown at 1975°C can be seen in **Figure 7**. Unfortunately cracking occurred in these crystals as well and presumably for the same reasons stated in the previous subsection. Crystals grown in both temperature ranges had very smooth surfaces (– RMS = 6Å) as determined by atomic force microscopy (AFM).

All crystals showed strong and well defined single crystalline XRD patterns. Only the (002) reflection positioned at 36° was observed in symmetric È-2È scans for a crystal grown at 1950°C. This suggests that the residual stress level in these crystals was low. Bright field, plan view TEM micrographs and associated selected area diffraction (SAD) patterns taken along the [0001] direction showed uniform contrast density throughout the specimen and spot patterns without streaks or arcs, respectively, indicative of single-crystalline material without high angle boundaries, stacking faults, misoriented grains or twinned regions.

A Raman spectrum acquired using back scattering geometry from the (0001) face of an transparent AlN crystal grown at 1950°C is presented in **Figure 8**. The spectrum exhibits the allowed modes for this geometry, namely, $A_1(LO) \approx 893$ cm^{-1}, $E_2^{(1)} \approx 250$ cm^{-1}, $E_2^{(2)} \approx 660$ cm^{-1} with no detectable contribution from the forbidden modes. The results support the aforementioned crystallographic and microstructural results in that a well defined wurtzite structure exists without significant concentrations of structural defects or internal stress which could relax the selection rules. The inset shows the high resolution spectrum of the $E_2^{(2)}$ mode. The FWHM of this peak was 7.0±0.5 cm^{-1}; the same spectrum taken from a blue crystal grown at 2200°C had a FWHM value of 9.5±0.5 cm^{-1}. This marked difference complements the results of the SIMS analysis in which the colored crystals contained two orders of magnitude more Si.

C. Metalorganic Vapor Phase Epitaxial Growth of GaN and $Al_xGa_{1-x}N$ films

Previous research in our laboratories has shown that thin films of GaN deposited directly on 6H-SiC(0001) substrates at high and low temperatures had columnar-like grains, faceted surfaces and high net carrier concentrations (n_D-$n_A > 1 \times 10^{19}$ cm^{-3})[16]. In contrast, in the present research monocrystalline thin films of both the HT-AlN buffer layers and the subsequently grown GaN films deposited on similar SiC substrates have been deposited with no misorientation or low-angle grain boundaries, as determined by selective are diffraction and microstructural analysis via transmission electron microscopy. Similar results have been achieved for $Al_xGa_{1-x}N$ without the use of an AlN buffer layer. The stacking fault density was also very low. The dislocation density of the $Al_xGa_{1-x}N$ films at the SiC interface appeared similar to GaN films deposited on high temperature (HT) buffer layers[8,9]. The dislocation densities of the GaN and $Al_xGa_{1-x}N$ films decreased rapidly as a function of thickness; only threading dislocations which result from misfit dislocations at the interface persisted through the film.

The surfaces of the GaN and $Al_xGa_{1-x}N$ films exhibited a slightly mottled appearance as a result of the step and terrace features on the growth surface of the 6H-SiC(0001) substrates. Random pinholes, caused by incomplete coalescence of the two dimensional islands which occurred as an intermediate growth stage between the initial nucleation and the final layer-by-layer growth stage representative of the majority of the film, were also observed. An increasing number of pinholes appeared on

the surface of $Al_xGa_{1-x}N$ compositions where $x > 0.5$. The pinhole density was decreased by increasing the growth temperature to enhanced surface mobility of the adatoms. The DCXRC measurements taken on GaN and $Al_xGa_{1-x}N$ films revealed the FWHM of the (0002) reflections to be as low as 58 and 186 arcsec, respectively.

The low-temperature (8K) PL spectra of the undoped GaN films revealed an intense near band-edge emission at 3.466 eV, which has been attributed to an exciton bound to a neutral donor[17,18]. The FWHM value of this peak was 4 meV. Also, a less intense peak was observed at higher energies (3.472 eV) which is attributed to free excitonic recombination. The low-temperature (4.2K) CL spectra of the undoped $Al_xGa_{1-x}N$ films for compositions in the range of $0.05 \leq x \leq 0.96$ revealed an intense near band-edge emission which has been attributed to an exciton bound to a neutral donor (I_2-line emission)[17,18]. Broadening of this emission is attributed to both exciton scattering in the alloys as well as small variations in alloy composition in the film. The lowest FWHM value observed in the $Al_xGa_{1-x}N$ alloys was 31 meV. Strong defect peaks, previously ascribed to donor-acceptor pair recombination[19], were observed at midgap energies. The broad peak centered at 545 nm (2.2 eV) for GaN, commonly associated[20] with deep-levels (DL) in the bandgap, was also observed; however, these emissions shifted sublinearly with changing composition. The nature of this behavior is under investigation.

The compositions of the $Al_xGa_{1-x}N$ films were determined using EDX, AES and RBS. Standards of AlN and GaN grown in the same reactor under similar conditions were used for the EDX and AES analyses. After carefully consideration of the errors (±2 at.%) involved with each technique, compositions were assigned to each film. The data from EDX and AES measurements showed excellent agreement. The RBS data did not agree as well with the other two techniques due to small compositional variations through the thickness of the film. Simulation of the composition determined by RBS was conducted only on the surface composition.

These compositions were compared with their respective CL emission peaks and bandgap as determined by SE. Using a parabolic model, the functional relationships between I_2-line emission energy of the CL and the Al mole fraction for $0 \leq x \leq 0.96$ is shown in **Figure 9** and expressed analytically as

$$E_{I2}(x) = 3.47 + 0.64x + 1.78x^2 \qquad (1)$$

Clearly, this shows a negative deviation from a linear fit. This is in general agreement with earlier research over a smaller range of x by other investigators[16,17].

D. Selective Growth and Lateral Growth

The prismatic morphology of the GaN and $Al_{0.2}Ga_{0.8}N$ stripes deposited within the various window widths of the SiO_2 masks was observed using scanning electron microscopy. Micrographs of these results are

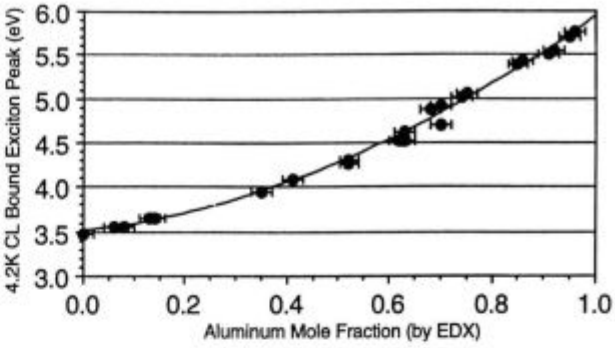

Figure 9: Low-temperature (4.2K) CL emissions of $Al_xGa_{1-x}N$ films as a function of aluminum mole fraction

Slika 9: Nizko temperaturni (4.2K) CL emisije $Al_xGa_{1-x}N$ filmov v odvisnosti od molarnega deleža AlN

shown in **Figure 10**. Both materials exhibited $(1\bar{1}00)$ side facets and ridge lines (i.e., no truncation) when deposited on the 3 µm-wide SiO_2 windows. Truncated prismatic growth with (0001) top facets and $(1\bar{1}01)$ side facets was observed on stripe patterns with widths ≥ 5 µm. Polycrystalline islands of $Al_XGa_{1-X}N$ nucleated on the SiO_2 mask because of the chemical interaction between Al and SiO_2 [20]. There was no significant difference in the final growth morphologies between the GaN and the $Al_{0.2}Ga_{0.8}N$ patterns, except for a slight roughening of the $(1\bar{1}01)$ facets of the latter. This roughening is believed due to the changes in the gas flow dynamics caused by the formation of the polycrystalline islands. No excessive growth was observed along the top edges of the truncated stripes, as shown in **Figure 11**; the (0001) top facets were very smooth and flat regardless of the width of these stripes. This suggests that the low growth pressure reduced the lateral vapor phase diffusion of the reactive species over the mask to the window region relative to that observed in related research conducted at one atmosphere[21]. The large ratio (=0.5) of the window-to-mask area may have also contributed to the perfection of the stripes, since lower values of this ratio were observed[22] to induce marked growth and rounding of the top edges at one atmosphere in GaAs, reportedly as a result of increased lateral vapor diffusion.

An increase in the flow rate of TEG resulted in a decrease in the area of the (0001) top facets and the development of $(1\bar{1}01)$ side facets. This behavior supports the model[23] that the resulting morphology of the selectively grown GaN depends on the balance between the incoming vapor flux on the (0001) top facets and the rate of diffusion on the (0001) surface to the $(1\bar{1}01)$ side facets. Increased exposure of the former to the TEG via an increase in the flow rate causes the growth rate of these facets to become faster than the latter.

The optimum conditions for the selective growth of the GaN pyramids on the circular patterns were based on the selective growth conditions on the stripe patterns. Each pyramid contained six $(1\bar{1}01)$ side facets. The growth rate of these pyramids was strongly dependent

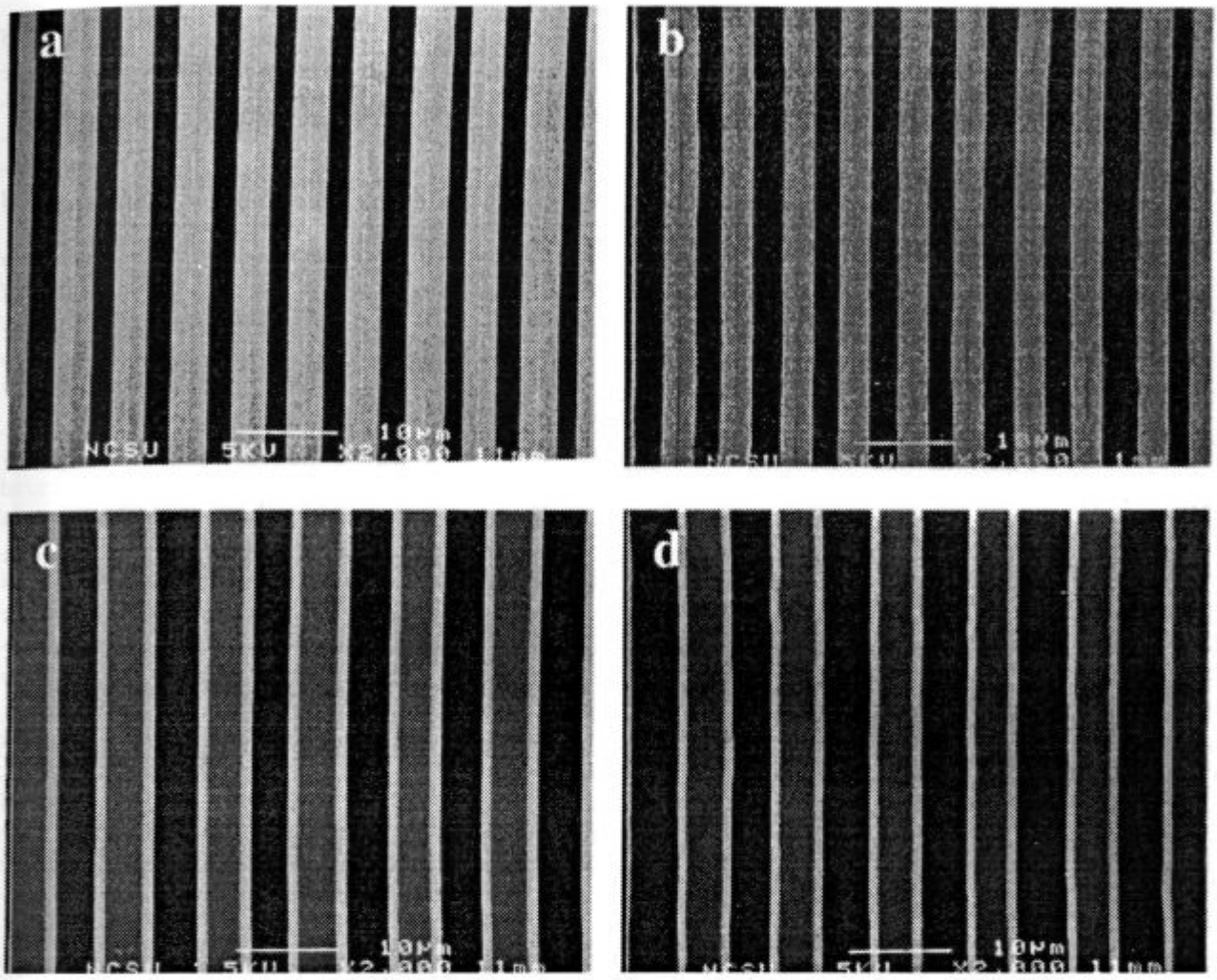

Figure 10: Secondary electron microscopy micrographs of GaN(left) and $Al_{0.2}Ga_{0.8}N$(right) stripes selectively grown at 1050°C and having initial SiO_2 widths of (a and b) 3 µm and (c and d) 5 µm

Slika 10: SEM posnetki GaN (levo) in $Al_{0.2}Ga_{0.8}N$ (desno) trakov selektivno zrastli pri 1050°C z začetno širino SiO_2 (a in b) 3 µm in (c in d) 5 µm

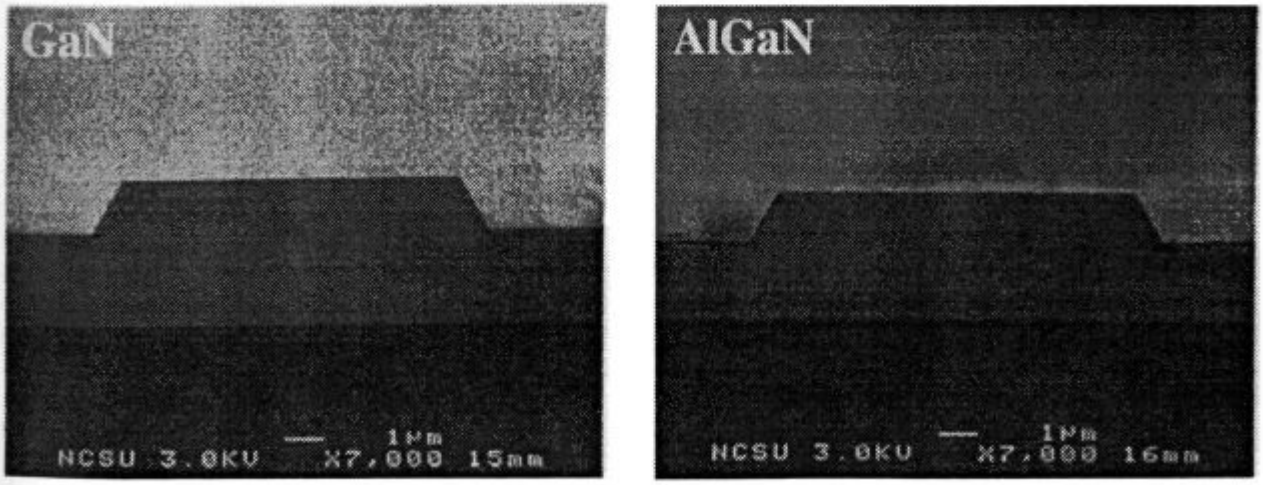

Figure 11: Secondary electron microscopy micrographs of 10 µm wide GaN and $Al_{0.2}Ga_{0.8}N$ stripes selectively grown at 1050°C with 10 µm wide SiO_2 windows

Slika 11: SEM posnetki 10 µm širokih GaN in $Al_{0.2}Ga_{0.8}N$ lamel selektivno zraščeni pri 1050°C z 10 µm širokimi SiO_2 okni

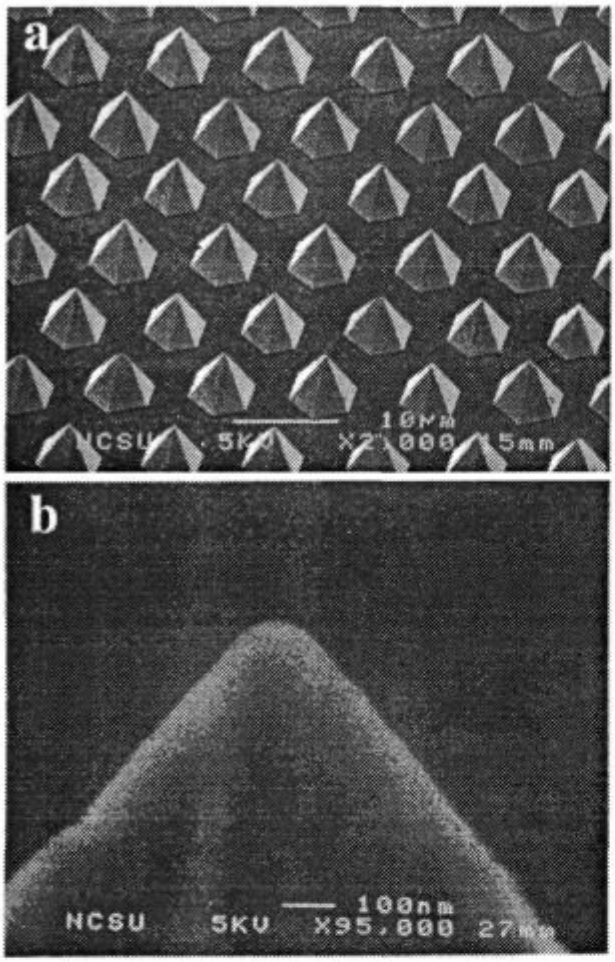

Figure 12: (a) SEM micrograph of a Si-doped GaN hexagonal pyramid array grown at 1000°C. (b) High magnification SEM image of the apex of a hexagonal pyramid having a tip radius of 100 nm
Slika 12: SEM posnetek heksagonalne združbe piramid GaN dopiranega s Si zrastlih pri 1000°C. (b) SEM posnetek vrha heksagonalne piramide z radijem konice 100 nm

upon the ratio of the window-to-mask area in the patterned region as well as the selective growth conditions. The average diagonal width of the pyramids was 7.7 μm using a ratio of 0.1. However, increasing the ratio to 0.23 resulted in an average diagonal width of 5.7 μm for the same growth conditions. These results indicate that the lateral diffusion of the reactive species from the mask to the window area is also an important factor for the successful fabrication of the GaN pyramids. As shown in **Figure 12(a)**, the growth of an uniform array of Si-doped GaN pyramids in a 0.5x0.5 mm^2 area was achieved. The high magnification SEM image shown in **Figure 12(b)** reveals that the tip radius of the pyramids was less than 100 nm.

The field emission current from the Si-doped GaN pyramid arrays was measured as a function of the anode voltage. The I-V curve in **Figure 13** shows a turn-on voltage of ≈680V for a current of 10.8 nA at a distance of 27 μm between the pyramid array and the anode. This turn-on voltage corresponds to a turn-on field of 25 V/μm. Using the same system, a polycrystalline p-type diamond film (p = 2.5E17cm^{-3}) grown on Si(100) exhibited a turn-on field intensity of 27 V/μm. The Fowler-Nordheim (F-N) plot obtained from the I-V data was linear and, therefore, indicates that the emission occurred via electron tunneling through the GaN.

The morphologies of the GaN layers selectively grown on the stripe openings were a strong function of the growth temperature, the flow rates of TEG and the stripe orientation. Continuous 2 μm thick GaN layers were obtained using 3 μm wide stripe openings spaced 7 μm apart and oriented along <1$\bar{1}$00> **(Figure 14 (a))**. The growth parameters were 1100°C and a TEG flow rate of 26 mmol/min. Plan view SEM of the coalesced GaN layer revealed a microscopically flat and pit-free surface, as shown in **Figure 14 (b)**. Atomic force microscopy showed the surfaces of the laterally grown GaN layers to possess a terrace structure having an average step height of 0.32 nm. The average RMS roughness values of the regrown and overgrown layers were 0.23 nm and 0.29 nm, respectively.

The cross-sectional TEM micrograph presented in **Figure 15** shows a typical laterally overgrown GaN. Threading dislocations, originating from the GaN/AlN buffer layer interface, propagate to the top surface of the regrown GaN layer within the window regions of the mask. The dislocation density within these regions, calculated from plan view TEM micrographs is approximately 10^9 cm^{-2}. By contrast, there were no observable threading dislocations in the overgrown layer. Additional microstructural studies of the areas of lateral growth obtained using various growth conditions have shown that the overgrown GaN layers contain only a few dislocations.

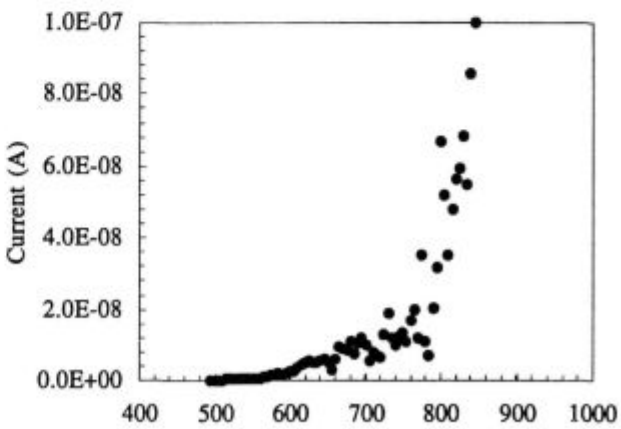

Figure 13: Emission current and anode voltage characteristics of Si-doped GaN hexagonal pyramid array shown in **Figure 12**
Slika 13: Karakteristike emisijskega toka in anodne napetosti heksagonalnih piramid s Si dopiranega GaN s **slike 12**

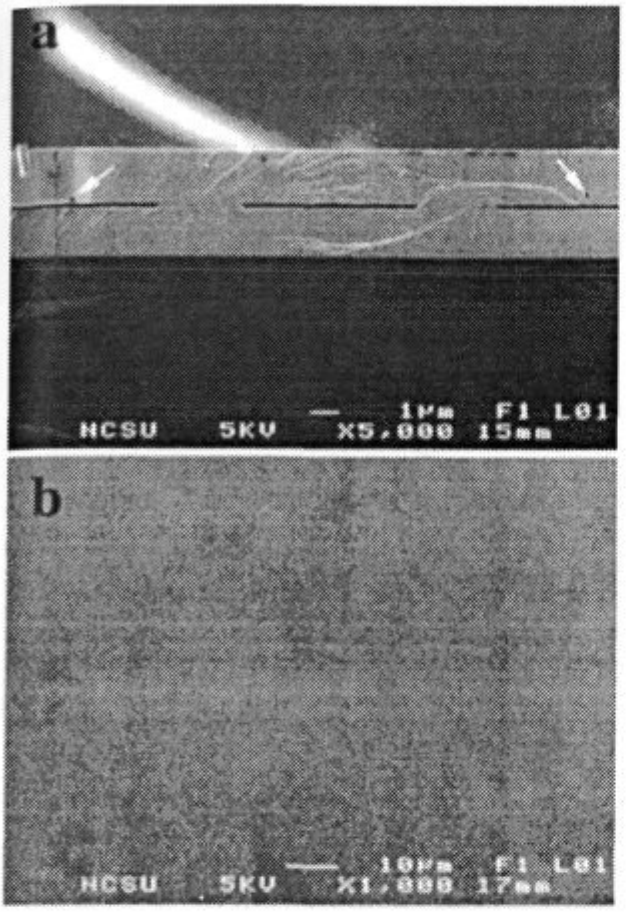

Figure 14: (a) Cross-section and (b) surface SEM micrographs of coalesced GaN layers grown on 3 μm wide and 7 μm spaced stripe openings, respectively, oriented along <1$\bar{1}$00>
Slika 14: Posnetki (a) prereza in (b) površina kolesciranih slojev GaN, ki so zrastli na 3 μm širokih 7 μm med seboj oddaljenih lamelnih odprtinah orientiranih vzdolž <1$\bar{1}$00>

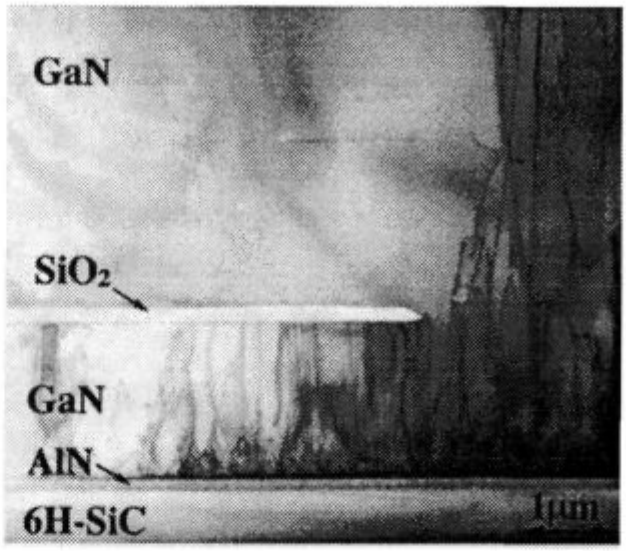

Figure 15: Cross-section TEM micrograph of a section of a laterally overgrown GaN layer on an SiO_2 mask region
Slika 15: TEM posnetek prereza lateralno zrastlega GaN sloja na področju SiO_2 maske

4 CONCLUSIONS

Growth of bulk, wurtistic GaN crystals to 3 mm length was achieved at a substrate temperature and pressure of 1100°C and 760 Torr, respectively, via sublimation of GaN pellets produced by uniaxial cold pressing of GaN powder. The concentrations of H, C and Si were ≤ 10^{16} atoms/cm^3 and the concentration of O was ≈ $3x10^{18}$ atoms/cm^3. Strong, sharp near band edge (bound exciton) emission was observed in the PL spectra of these crystals. No yellow emission was observed. An optical absorption edge of ≈ 370 nm and 75% transmission was determined. The Raman spectrum showed narrow and well positioned peaks.

Seeded bulk growth of single crystalline AlN (001) platelets was achieved on 6H-SiC (0001) substrates in the temperature range of 1950-2250°C at 500 torr of N_2. Color variations were observed above 2150°C and linked to the incorporation of Si and C from the substrate and the growth crucible. The results of TEM and XRD analyses revealed low densities of line and planar defects and the absence of residual stress in the grown crystals. No misoriented grains or twinned regions were observed. Very smooth surfaces (RMS≈6 Å) were observed via AFM.

Monocrystalline GaN and $Al_xGa_{1-x}N$(0001) ($0.05 \leq x \leq 0.96$) thin films, void of oriented domain structures and associated low-angle grain boundaries, were obtained via MOVPE on α(6H)-SiC(0001) wafers. A 1000Å high temperature (HT) AlN buffer layer was employed for the GaN deposition while $Al_xGa_{1-x}N$ was deposited directly on 6H-SiC. Double-crystal XRC measurements showed FWHM values as low as 58 and 186 arc sec for the GaN(0002) and $Al_xGa_{1-x}N$(0002) reflections. Photoluminescence spectra of GaN showed bound and free excitonic recombination. Spectra obtained via CL of $Al_xGa_{1-x}N$ showed strong near band-edge emissions with FWHM values as low as 31 meV.

The selective growth of GaN and $Al_{0.2}Ga_{0.8}N$ has been achieved on striped and circular patterned GaN/AlN/6H-SiC(0001) multilayer substrates. Prismatic morphology with well-defined (1$\bar{1}$01) side facets was observed on 3 μm wide stripes for both materials. Truncated prismatic growth with smooth, flat (0001) top facets and (1$\bar{1}$01) side facets were obtained on stripe patterns with widths ≥ 5 μm. Uniform hexagonal pyramid arrays of Si-doped GaN were successfully grown on circular patterns having diameters of 5 μm. Field emission measurements of these arrays showed a turn-on field of 25 V/μm and an associated emission current of 10.8 nA at an anode-to-pyramid array distance of 27 μm. Lateral growth and coalescence over the SiO_2 masks have been achieved using stripes oriented along <1$\bar{1}$00>. A density of ≈10^9 cm^{-2} threading dislocations, originating from the

underlying GaN/AlN interface, were contained in the GaN grown in the window regions. The overgrowth regions contained a very low density of dislocations.

ACKNOWLEDGEMENTS

The authors express their appreciation to Cree Research, Inc. for the SiC wafers. This work was supported by the Office of Naval Research under research contracts N00014-96-1-0765 and N00014-92-J-1477. R. Davis was supported in part by the Kobe Steel, Ltd. Professorship.

5 REFERENCES

[1] M. T. Duffy, in *Heteroepitaxial Semiconductors for Electronic Devices*, G. W. Cullen and C. C. Wang, Eds., Spinger Verlag, Berlin 1978 pp. 150-181

[2] R. F. Davis, *Proc. IEEE 79* (1991) 702

[3] S. Strite and H. Morkoç, *J. Vac. Sci. Technol. B*, 10, (1992) 1237

[4] J. H. Edgar, *J. Mater. Res.*, 7 (1992) 235

[5] J. L. Shaw, H. F. Gray, K. L. Jensen and J. M. Jung, *J. Vac. Sci. & Technol.*, B14 (1996) 2072

[6] R. J. Nemanich, M. C. Benjamin, S. P. Bozeman, M. D. Bremser, S. W. King, B. L. Ward, R. F. Davis, B. Chen, Z. Zhang and J. Bernholc, *Proc. Mat. Res. Soc.*, 395 (1996), 777

[7] M. C. Benjamin, C. Wang, R. F. Davis and R. J. Nemanich: *Appl. Phys. Lett.*, 64 (1994) 3288

[8] T. W. Weeks, Jr., M. D. Bremser, K. S. Ailey, E. P. Carlson, W. G. Perry, R. F. Davis, *Appl. Phys. Lett.*, 67 (1995) 401

[9] T. W. Weeks, Jr., M. D. Bremser, K. S. Ailey, W. G. Perry, E. P. Carlson, E. L. Piner, N. A. El-Masry, R. F. Davis, *J. Mat. Res.*, 4 (1996) 1011

[10] C. M. Balkas and R. F. Davis, *J. Am. Ceram. Soc.*, 79 (1996) 2309

[11] Cree Research, Inc., 2810 Meridian Parkway, Suite 176, Durham, NC 27713

[12] O. H. Nam, M. D. Bremser, T. S. Zheleva and R. F. Davis, to be published in *Appl. Phys. Lett.*, 71 (1997), 2638

[13] S. Sakai, S. Kurai, T. Abe and Y. Naoi, *Jpn. J. Apl. Phys.*, 35 (1996) L77

[14] L. Bergman and R. J. Nemanich, *Annu. Rev. Mater. Sci.*, 26 (1996) 551

[15] J. F. Muth, Private communication, North Carolina State University (1997)

[16] T. W. Weeks, Jr., D. W. Kum, E. Carlson, W. G. Perry, K. S. Ailey and R. F. Davis, *Second International High Temperature Electronics Conference*, Charlotte, NC, June 5-10 (1994)

[17] M. R. H. Khan, Y. Koide, H. Itoh, N. Sawaki, I. Akasaki, *Solid State Commun.*, 60 (1986) 753

[18] B. V. Baranov, V. B Gutan, U. Zhumakulev, *Sov. Phys.-Semicond.*, 16 (1982) 819

[19] R. Dingle and M. Ilegems, *Solid State Commun.*, 9 (1971) 175

[20] W. Götz, N. M. Johnson, R. A. Street, H. Amano and I. Akasaki, *Appl. Phys. Lett.*, 66 (1995) 1340

[21] Y. Kato, S. Kitamura, K. Hiramatsu and N. Sawaki, *J. Cryst. Growth*, 144 (1994) 133

[22] K. Yamaguchi and K. Okamoto: *Jpn. J. Appl. Phys.*, 32 (1993) 1523

[23] S. Kitamura, K. Hiramatsu and N. Sawaki, *Jpn. J. Appl. Phys.*, 34 (1995) 1184

ISSN 1318-0010
KZLTET 31(6)495(1997)

PIONEER YEARS OF ELECTRON PROBE MICROANALYSIS IN SLOVENIA

PIONIRSKO OBDOBJE ELEKTRONSKE MIKROANALIZE V SLOVENIJI

FRANC VODOPIVEC

Institute of Metals and Technology Lepi pot 11, 1000 Ljubljana, Slovenia

Prejem rokopisa - received: 1997-10-01; sprejem za objavo - accepted for publication: 1997-10-21

Two periods are found in the pioneer years of electrons probe microanalysis (EPMA) in Slovenia:

- a longer period up to 1969 when an electron probe microanalyser was put in operation in the Institute of Metallurgy in Ljubljana, and
- a shorter period after this date until the spreading of EPMA backed by sufficent research achievents demonstrating it wide field of use and the sufficient mastering of methodology.

The use of EPMA up to 1969 was of marginal extent but not of marginal scientific merit and centred to topics of selective oxydation of alloys of iron with arsenic, copper, tin and antimony. The interest for EPMA and the conviction that it will greatly improve the quality of the actual research as well as open new topics helped significantly were great. Prof. D. Kolar and his collaborators were among the best prepared and also among the must successfull. With the cooperation of some younger scientists he accomplished several projects which found significant interest in the international research community and were realised thanks to the fast governing of EPMA methodology. Let us quote only some achievements published up to some years after the putting in operation of EPMA in 1969:

- binary phase equilibria diagrams were established for niobium, titanium and circonium carbides with iron, nickel, chromium and cobalt;
- binary phase equilibria diagrams were established for uranium sulphide and sulphides of calcium, barium and strontium;
- several projects were accomplished with the aim to understand better the microstructure of ferrite ceramics, its sintering process and the effect of microstructure and sintering on magnetic and electrical properties.

In binary phase equilibria diagrams solid solubilities and eutectic compositions were determined. Also because of the contribution of prof. D. Kolar the pioneer period od EPMA in Slovenia was short and successful and helped to strengthen it as one of the base scientific facility for research of solid materials on microstructure level.

Key words: electron probe microanalysis, selective oxydation, binary phase diagrams Fe - NbC, TiC, ZrC, activated sintering of Ba titanate, binary phase diagrams US and CaS, SrS and BaS

Pionirsko obdobje elektronske mikroanalize (EMA) delimo na dva dela:

- daljše obdobje do postavitve elektronskega mikroanalizatorja na tedanjem Metalurškem inštitutu v Ljubljani leta 1969 in
- krajše obdobje po zagonu naprave in začetku njene široke uporabnosti kot dokaz zadostnega obvladovanja metodologije dela.

Uporaba elektronske mikroanalize je bila do začetka leta 1969 v Sloveniji po obsegu marginalna, vendar ne marginalna po vsebini. Raziskave so od leta 1962 posegale na področje selektivne oksidacije predvsem zlitin železa z elementi z majhno afiniteto do kisika, na pr. arzen, antimon, kositer in baker. Zanimanje za EMA in pričakovanje, da bo omogočila kvaliteten skok v raziskovalnih projektih je bilo veliko, okolje pa pripravljeno na intenzivno uporabo nove metodike. Prof. D. Kolar je bil s sodelavci pri tem gotovo nadpovprečno uspešen. Bil je snovalec in izvajalec vrste raziskav, ki so prinesle temeljne novosti na nekaj področjih raziskovanja. Omenjene bodo le tri, ker so bili izsledki objavljeni najkasneje nekaj let po postavitvi naprave tudi zaradi zelo hitrega osvajanja metodologije dela, še posebej kvantitativne analize:

- določeni so bili binarni ravnotežni fazni sistemi niobijevega, titanovega in cirkonijevega karbida s prehodnimi kovinami železo, krom, nikelj in kobalt;
- določeni so bili binarni ravnotežni fazni diagrami uranovega sulfida s kalcijevim, stroncijevim in barijevim sulfidom;
- izvršena je bila vrsta raziskav s ciljem, da se bolje razpozna mikrostruktura feritne keramike, proces njenega sintranja in vpliv sestavin in procesa sintranja na magnetne in električne lastnosti.

V binarnih faznih sistemih je bila določena topnost v trdnih fazah ter temperature in sestava evtektikov. Tudi zaradi velikega prispevka prof. D. Kolarja in sodelavcev je bilo pionirsko obdobje EMA kratko in uspešno ter je metodo utrdilo kot eno od temeljnih pri raziskovanju vseh vrst trdne snovi na nivoju mikrostrukture.

Ključne besede: elektronska mikroanaliza, selektivna oksidacija železa, binarni fazni diagrami železa NbC, TiC in ZrC, aktivirano sintranje Ba titanata, fazni diagrami US in CaS, SrS in BaS

1 INTRODUCTION

This paper was prepared in the frame of the celebration of the 65th jubilee of prof. dr. Drago Kolar, eminent scientists at the Institute J. Stefan and teacher of ceramic materials at the University of Ljubljana. I had the opportunity to meet prof. Kolar in major extent after april 1969, when the second electron probe microanalyser (EPMA) in the former Jugoslavia was put in operation in the former Institute of Metallurgy in Ljubljana. The EPMA was purchased by combining funding from the Institute of vacuum technique and electronics, Institute of automation, Institute for research of materials and structures, Institute of metallurgy, Metallurgy dpt of the University of Ljubljana, Slovenian Steelworks, and the Slovenian governement. The project was coordinated by the Institute of metallurgy and the EPMA installed in his premises.

2 EPMA IN THE WORK A SLOVENIAN RESEARCHERS UP TO 1969

From disponible data it seems that EPMA was first used in the work of a slovenian scientist in 1962 in the investigation of the selective surface oxydation of the alloy Fe - 0.075% As[1,2]. Arsenic free energy of oxydation is smaller than that of iron. Consequently, by surface oxydation only iron reacts with oxygen, while arsenic is segregated in the metal layer in contact with the oxyde. By EPMA the distribution of arsenic in the segregated layer obtained by electrolytic dissolution of μm layers of metal and microradiochemical analysis was verified. The distribution was different after surface oxydation above and below AC3 because of the limited solubility of arsenic in γ phase (**figure 1**). The results obtained by both methods did agree very good. In the same reference EPMA was used also to determine the composition of the eutectic FeO - $3FeOP_2O_5$ obtained at surface oxydation of an Fe - 0.092% P alloy.

In the following case EPMA was used also in the investigation of the selective oxydation of iron. In iron alloys with copper, arsenic, tin, and antimony by EPMA point, line and scanning analyses the sequence of formation of solid and liquid phases in binary, ternary and quaternary equilibria was established as consequence of selective oxydation, f.i.:

$$\gamma \rightarrow \gamma_1 + \alpha_1 \rightarrow \gamma_1 + \alpha_1 + lp_1$$

$$\gamma \rightarrow \gamma_1 + lp_2 \rightarrow \gamma_1 + \alpha_1 + lp_2 \rightarrow \gamma_1 + \alpha_1 + lp_1 + lp_2$$

with α, γ as solid and lp_1, lp_2 as liquid phases.

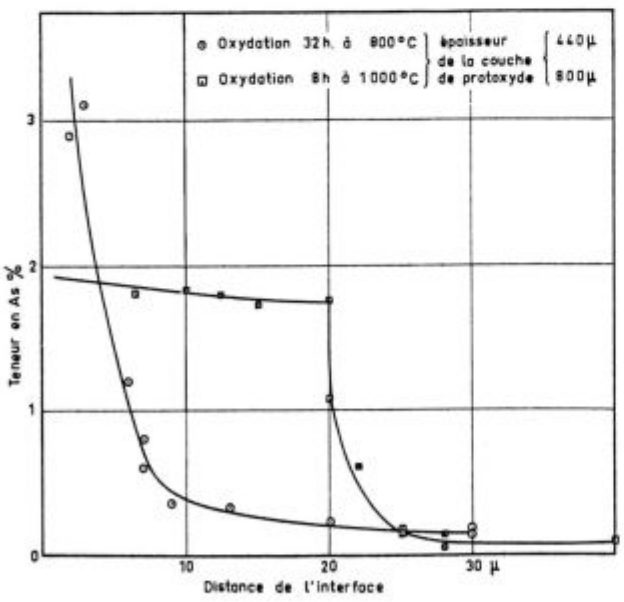

Figure 1: Distribution of arsenic in the segregated layer of an Fe-0.075% As alloy after surface oxydation at 800 and 1000°C determined by electron probe microanalysis (EMA). Ref. 1 and 2

Slika 1: Porazdelitev arzena v segregirani plasti zlitine Fe-0.075% As po oksidaciji pri 800 in 1000°C določena z elektronsko mikroanalizo (EMA). Po virih 1 in 2

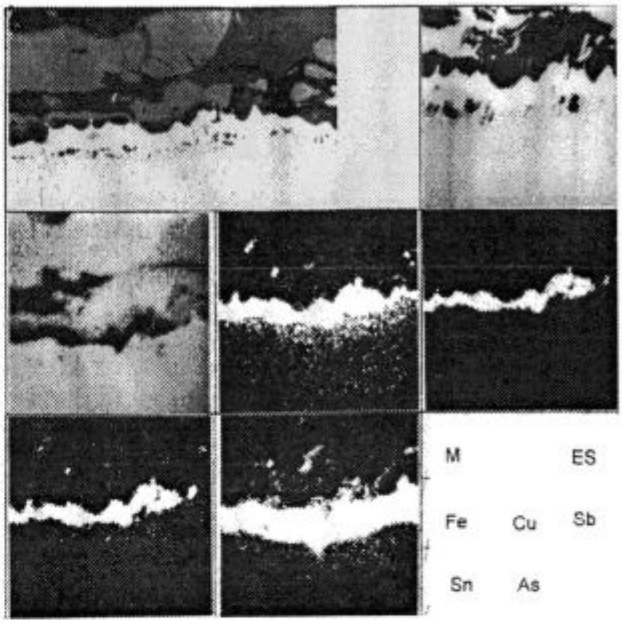

Figure 2: Optical, back scattered electrons and X rays scanning pictures of different elements in the segregated layer after air surface oxydation of an iron alloy at 1200°C. Ref.3 and 4

Slika 2: Optični, elektronski in specifični X posnetki za različne elemente v segregirani plasti na železovi zlitini po oksidaciji na zraku pri 1200°C. Ref. 3 in 4

For EPMA methodology it is of special importance the fact that the distribution of segregated elements was demonstrated also by scanning elemental pictures (**figure 2**). No use of EPMA was found in printed works of Slovenian scientists up to the start of the facility put in operation in 1969.

3 SOME DATA ON THE OPERATION OF EPMA FROM 1969 TO 1974

EPMA was ready for qualitative and semiquantitative work in april 1969. In **table 1** statistics on the work up to

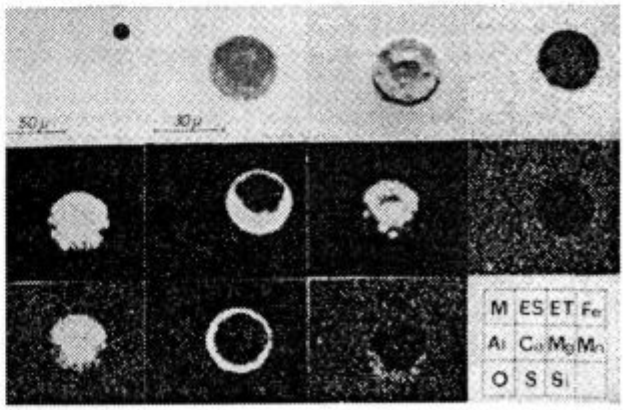

Figure 3: Optical, back scattered electrons and X rays scanning pictures of different elements. Spherical nonmetallic inclusion in steel. Ref. 9

Slika 3: Optični, elektronski in specifični X posnetki za različne elemente. Kroglasti nekovinski vključek v jeklu. Po viru 9

1974 are shown. Allready in the first year the work performed for users outside of the Institute of metallurgy reached a level which did not change significantly up to 1974. This level shows that EPMA was really needed and also satisfactorily exploited. Methods for qualitative and quantitative investigations for basic, applied, and development research as well as routine analysis for different institutions and industrial companies from geology, mineralogy, metallurgy, ceramic, building materials, electronics, and even forensic cases were developed fastly. The reader can have an idea on the level of quality and accuracy from the scanning picture in **figure 3** as well as the composition of carbides and nonmetallic inclusions in **table 2**.

Table 1: Clients for EPMA work

Year	Academic institutions	Companies	Payed working hours	Articles[1]
1969	10	14	1276	
1970	12	17	1330	6
1971	12	10	1335	8
1972	12	11	1330	5
1973	10	11	1301	2
1974	11	17	1241	10

In the year 1969 to 1974 54 different institutions and companies committed once or several times EPMA work, 29 ind. companies committed the investigation from 1 to 18 different specimens yearly.
[1] - Authors from the EPMA laboratory

Table 2: Composition of nonmetallic inclusions and carbides
F. Vodopivec und B. Ralić: Radex Rundschau (1975) 1, 289-294

Inclusion[1]	MnO	FeO	SiO_2 v ut.%	Al_2O_3	CaO	Vsota
1	28.0	8.3	-	63	-	99.3
2	16.4	2.3	37.8	7.5	36.0	100
3	55.5	6.3	31.1	5.9	-	99.8
4	50.3	6.3	32.4	9.7	-	98.6
5	21.4	4.6	30.4	2.4	41	99.8
Carbide[2]	W	V	Fe	Cr	Mo	C
M_6C[2]	56.0	3.1	28.6	4.75	2.25	1.93
$(W_{1.6}Fe_{3.3}V_{0.36}Cr_{0.56}C_1)$						
MC	14.2	57.2	3.3	7.65	1.6	16.95
$(V_{0.91}W_{0.06}Fe_{0.05}Cr_{0.11}Mo_{0.01}C_1)$						

[1] Correction calculation after Bence-Albee[7]
[2] Correction calculation after Philibert[6] and Reed[8]

In combination with optical microscopy it was possible to find reliable answers also for significant technological problems, f.i. inhomogenity and kinetics of homogenisation of steels as well as copper and aluminium alloys, composition of nonmetallic phases in steels and alloys. The allready mentioned **figure 3** shows a non metallic inclusion enriched at the surface by calcium and sulphur[9]. This was one of the first proofs for the reaction between calcium bounds to aluminate or alumosilicate inclusions with sulphur in the liquid steel. The homogenising times for aluminium and copper alloys were diminished on the base of investigations of segregation kinetics to less than half of the so far prescribed length[10]. It was established also that after homogenisation a virtually ideally homogeneus distribution was obtained in some cases, while in case of mutual interactivity also after long time homogenisation the average segregation was approaching a level significantly far from homogeneity.

4 EPMA IN THE RESEARCH OF D. KOLAR

D. Kolar and his research collaborators were frequent clients of the EPMA laboratory during the first year with different topics from ceramic magnets, hard metals and phase equilibria diagrams. Several papers based signifi-

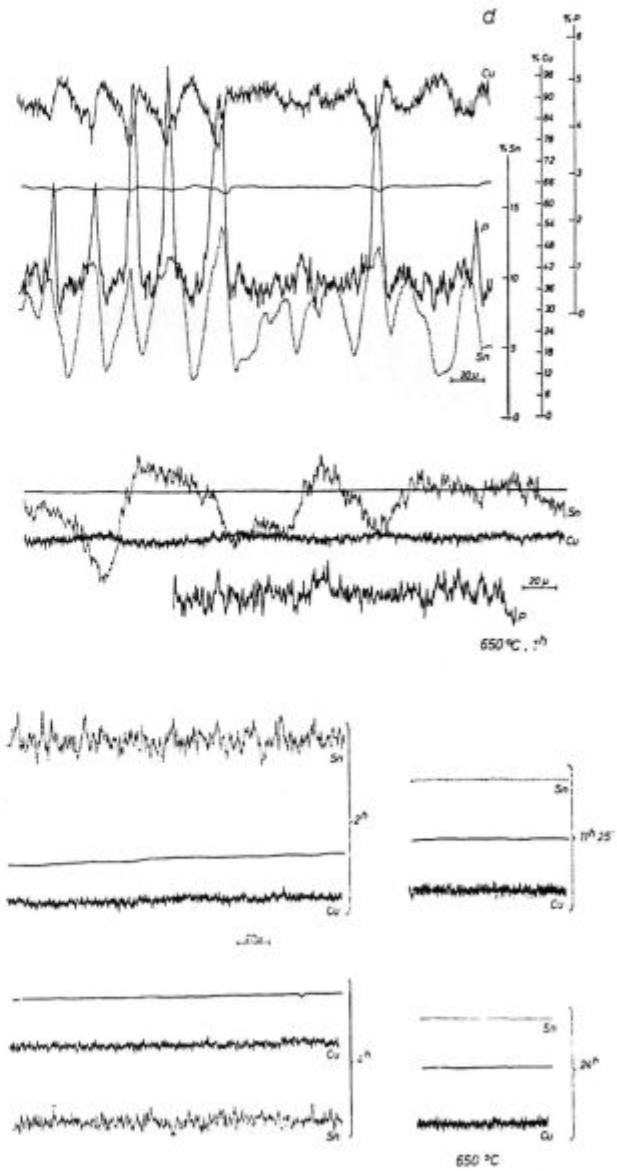

Figure 4: Distribution of alloying elements in an Cu 8% Sn 0,38% P alloy as cast and after homogenisation. Ref. 10
Slika 4: Porazdelitev legirnih elementov v zlitini Cu 8% Sn 0.38% P po litju in po homogenizaciji. Po viru 10

cantly on EPMA work were printed in international journals. The authors is avare of the possibility that some of the phase diagrams were later modified on the base of results of improved EPMA. Also if it happened, it could not change the type of phase diagrams which have therefore a permanent value.

The ambition of the author of the present survey is not to present all the work of D. Kolar in the quoted years, but to show that D. Kolar was prepared for EPMA and prepared to exploit optimally the new research facility in Slovenia due to the putting in operation of EPMA and was able in this way to improve considerably the scientific value of his investigations.

Figure 4 is taken from ref. 11, where Drofenik and Kolar reported on the effect of Bi_2O_3 addition on sintering process and properties of strontium ferrite. The attention of the reader is called on the quality of electron and scanning pictures in **figure 4**, where details near the size of μm are discernible. The morphology of bismuth oxyde containing phase shows that it fills as liquid spaces between polyhedric grains of ferrite with higher melting point. EPMA showed in this phase 50% Bi_2O_3, 31% Fe_2O_3 and 19% of SrO. It was concluded that the addition of bismuth oxyde lowered the sintering temperature and increased the volume density and energy product $(BH)_m$.

In the same year Komac, Golič, Kolar, and Brčič[12] established the crystal structure, phase composition and transformation temperatures in binary phase equilibria systems US-CaS, US-SrS and US-BaS. EPMA was used for the determination of solid solubilities and eutectic compositions shown in **table 3**, while **figure 5** presents the phase diagrams US-CaS and US-BaS. Jurca, Kolar and Trontelj investigated the effect of nickel on activated sintering of tungsten and established that nickel is not found in solid solution in tungsten in a detectable content and that also at grain boundaries nickel is not found in appreriable quantity[13,14]. 1.2 to 2.8% was found for the solid solubility of tungsten in silver, which is lower than the value found in published phase diagrams.

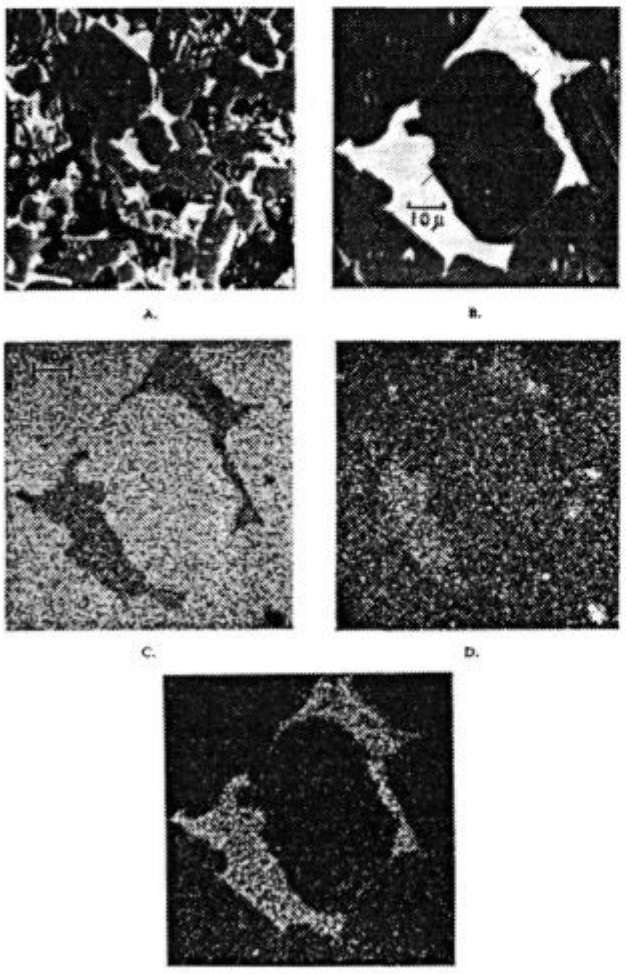

Figure 5: Back scattered electron and X rays scanning picture for different elements. Sintered strontium titanate with addition of Bi_2O_3. Ref. 11

Slika 5: Elektronski in specifični X posnetki za različne elemente. Sintran stroncijev titanat z dodatkom Bi_2O_3. Po viru 11

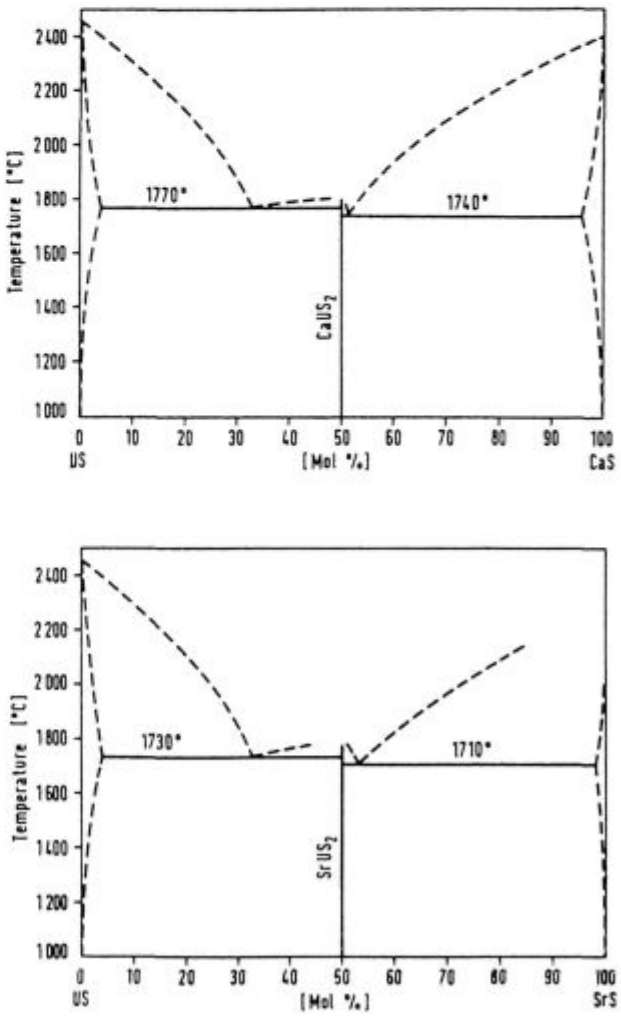

Figure 6: Phase diagrams US-CaS and US-BaS. Ref. 12

Slika 6: Fazna sistema US-CaS in US-BaS. Po viru 12

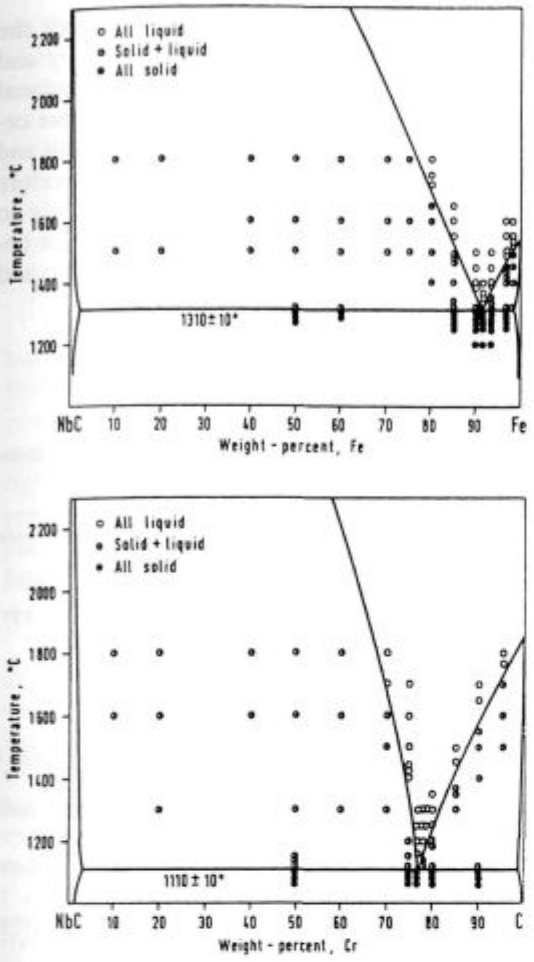

Figure 7: Phase diagrams NbC-Fe and NbC-Cr. Ref. 15
Slika 7: Fazna diagrama NbC-Fe in NbC-Cr. Po viru 15

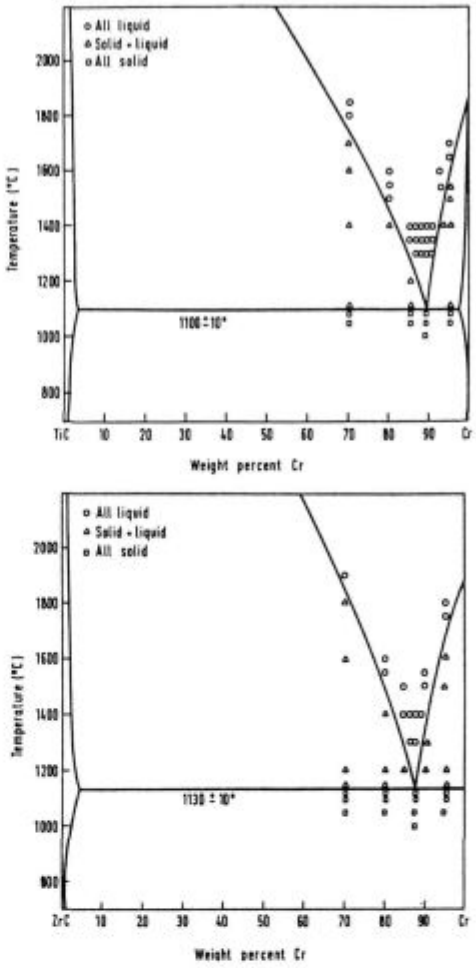

Figure 8: Phase diagrams TiC-Cr and ZrC-Cr. Ref. 16
Slika 8: Fazna diagrama TiC-Cr in ZrC-Cr. Po viru 16

Table 3: Phase composition in binary phase equilibria systems US-CaS, US-BaS in US-SrS
M. Komac, L. Golič, D. Kolar and B. S. Brčič: *J. Less-Common Metals*, 24 (1971) 121-128

System Phase	US-CaS	US-SrS	US-BaS
Solid solution US[1],%	3.5	3.5	3.0
Solid solution MS[1],%	4.0	n.d.	n.d.
Intermediate phase,%	50	50	50
	$CaUS_2$	$SrUS_2$	$BaUS_2$
Eutectic 1,%	33.0	33.0	38.0
Eutectic 2,%	50.5	53.0	n.d.

[1] - Maximal solubility by eutectic temperature

Guha and Kolar[15] investigated the phase equilibria diagrams niobium carbide with transition metals iron, chromium, nickel, and cobalt. Solid solubilities and eutectic compositions are shown in **table 4** and the phase systems NbC-Fe and NbC-Cr in **figure 6**. Eutectic points are deplaced near the metal side and the solid solubilities are in the range 1 to 4.3% Guha and Kolar[16] investigated also the phase diagrams TiC-Cr and ZrC-Cr in **figure 7**. EPMA results in **table 5** indicate small solid solubility and eutectic point deplaced on metal side.

Table 4: Phase composition in binary phase equilibria systems NbC-Fe, NbC-Cr, NbC-Ni, and NbC-Co
J. P. Guha and D. Kolar: *J. Less-Common Metals*, 29 (1972) 33-40

System	Eutectic	Solid solution[1],wght.%	
	wght.% metal	metal in NbC	NbC in metal
NbC-Fe	91.2	1.8	0.98
NbC-Cr	76.0	2.8	0.85
NbC-Ni	89.0	1.8	3.5
NbC-Co	88.0	1.2	4.3

[1] - Maximal solubility by eutectic temperature

Table 5: Phase composition in binary phase equilibria systems TiC-Cr and ZrC-Cr
J. P. Guha in D. Kolar: *J. Less-Common Metals*, 31 (1973) 331-343

System	Eutectic	Solid solution[1],wght.%	
	Metal,wght.%	Metal in carbide	Carbide in metal
TiC-Cr	89.0±0.5	3.5	3.5
ZrC-Cr	88.0±0.5	4.5	0.2

[1] - Maximal solid solubility at eutectic temperature

Finally Guha and Kolar[17] established also the phase diagram $BaTiO_3$-$BaGeO_3$ on **figure 8 and 9**, determined

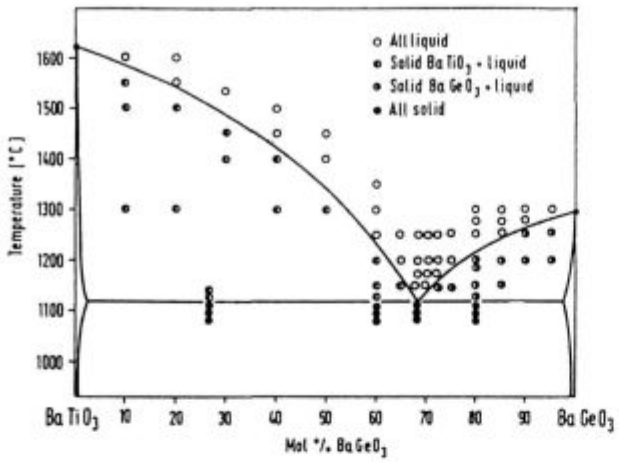

Figure 9: Phase diagram $BaTiO_3$-$BaGeO_3$. Ref. 17
Slika 9: Fazni diagram $BaTiO_3$ - $BaGeO_3$. Po viru 17

the liquidus and solidus temperature, the eutectic composition as well as the solid solubilities 1 of mol % $BaTiO_3$ in $BaGeO_3$ and 2.2 mol % of $BaGeO_3$ in $BaTiO_3$ at eutectic temperature.

5 CONCLUSION

The slovenian research community obtained relatively late the possibility to use EPMA at acceptable time and expense as standard research method for in situ quali and quantitative investigations of solid materials. Statistical data show that the community was well prepared for the use of the new facility. For that reason, the use expanded relatively fast in research academic and industrial laboratories in metallurgy, geology, mineralogy, ceramic, building materials and electronics. On average, in the first years more EPMA work was performed for industrial companies than academic institutions. D. Kolar was between the researchers which did profit the must from EPMA. Based on optical microscopy and EPMA he and his collaborators reported in international journals on significant findings on topics of magnet ceramics and binary phase equilibria systems of metals and carbides as well as sulfide compounds. It is therefore justifield to conclude that D. Kolar helped greatly to strengthen EPMA as rutine investigation method for basic, applied and development research of metallic and non metallic materials.

6 REFERENCES

[1] F. Vodopivec: Dr. thesis, University of Paris, 1962
[2] F. Vodopivec, A. Kohn, J. Philibert et J. Manenc: *Revue de Metallurgie*, 60 (1963) 801-818
[3] L. Kosec: Mag. thesis, University of Ljubljana, 1967
[4] L. Kosec, F. Vodopivec et R. Tixier: *Metaux-Corrosion-Industries*, (1969) No.525, 1-25
[5] F. Vodopivec und B. Ralić: *Radex-Rundschau*, (1975) 1, 289-294
[6] J. Philibert: *Metaux-Corrosion-Industries*, 40 (1964) no. 465, 157-176, no. 466, 216-240, no. 469, 325-342
[7] A. E. Bence and A. L. Albee: *J. of Geology*, 76 (1968) 382-403
[8] S. J. B. Reed: *Brit J. Applied Physics*, 16 (1965) 913-926
[9] F. Vodopivec in B. Ralić: *Železarski zbornik*, 6 (1972) 215-229
[10] L. Kosec, A. Podgornik in B. Ralić: *Rudarsko Metalurški Zbornik*, 4 (1972) 417-428
[11] D. Kolar and M. Drofenik: *Proceedings of the British Ceramic Society*, N 18 1970 125-138
[12] M. Komac, L. Golič, D. Kolar and B. S. Brčič: *Journal of Less-Common Metals*, 24 (1971) 121-128
[13] S. Jurca, D. Kolar and M. Trontelj: Activated sintering of Tungsten: *Proceedings of the Inf. Conf. on Powder Metallurgy*, Zakopane, 1971, 247-258
[14] D. Kolar, S. Jurca and M. Trontelj: *Rudarsko Metalurški zbornik*, (1970) 1, 35-41
[15] J. P. Guha and D. Kolar: *Journal of Less-Common Metals*, 29 (1972) 33-40
[16] J. P. Guha and D. Kolar: *Journal of Less-Common Metals*, 31 (1973) 331-343
[17] J. P. Guha and D. Kolar: *J. Materials Science*, 7 (1972) 1192-1196

ISSN 1318-0010
KZLTET 31(6)501(1997)

LAUDATION IN HONOUR OF PROFESSOR DR. JOŽE GASPERIČ ON THE OCCASION OF HIS 65th BIRTHDAY

MONIKA JENKO
Institute of Metals and Technology, Lepi pot 11, 1000 Ljubljana, Slovenia

Professor Dr. Jože Gasperič, scientific councillor, leading Slovenian vacuumologist is celebrating his 65th birthday. This event is the occasion to look at the background and the development of this well known scientist and at the influence which his research work has in the field of vacuum science, development, construction and production of vacuum diffusion, rotary and diaphragm pumps, valves, traps etc, measuring vacuum gauges like Pirani, Penning, ionization gauges, McLeods, vacustats, mercury manometers, vacuum metrology, etc.

Jože Gasperič was born in Ljubljana on March 7, 1932. After finishing the grammar school education, he studied Electrical Engineering at the University of Ljubljana. In 1958 he passed the final examinations and second degree thesis. In 1957 he joined as Research Associate the Institute for Electronics and Vacuum Techniques in Ljubljana directed by its founder Professor Dr. Dušan Lasič. He was also Assistant in Electronics at the University of Ljubljana from 1956 to 1958 and later from 1959 to 1964 the lecturer of vacuum technique at Electrical Technical High School, Ljubljana. He prepared his master thesis in the field of Electrooptics and Electrooptical devices at the University of Ljubljana and graduated in 1964. In 1972 he graduated at the University of Ljubljana for doctor of Science in the field of Microelectronics - thin films.

In 1970 he was senior researcher and the manager of Vacuum Department from 1980 to 1985 at the Institute for Electronics and Vacuum Technique (IEVT). In 1986 he accepted the position of a visiting professor at the Department of Physics, Thin Film Laboratory, at Sri Venkateswara University, Tirupati, India and at Indian Institute of Science in Bangalore, India as visiting scientist.

In 1988 he returned to Ljubljana and joined to Solid State Physics Department of Jožef Stefan Institute.

Jože Gasperič, as a senior researcher and manager of Vacuum Department at IEVT Ljubljana, originated many new research programs, which received founding from institutes, industry, Slovenian and former Yugoslav research communities. His work has included characterization of evaporated and sputtered materials, metals compounds and alloys, especially cermets, decorative thin layers, etc. Developing high stabilized cermet resistor films. He developed and simplified theory for calculation of jet system for oil diffusion pumps for production in the range from 100 to 15000 l/s.

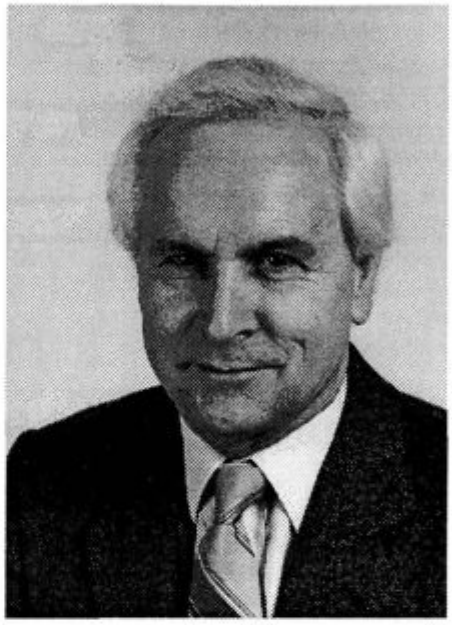

Dr. Jože Gasperič

He developed many vacuum pumping systems and equipment on the base of his own technologies, for industry and labs, for production of photo-sensitive and X-ray tubes, for degazation of insulating oils and other liquids for impregnation of electronic discrete circuits, condenser, power motor windings, wood, tools made by powder technologies, etc.

He developed also many types of medical inhalers and suction devices for surgical purposes, for suction of mother's milk for feeding prematurely born babies and he organized some centres in Slovenia for hiring such devices. He developed freeze-drying devices for pharmaceutical and biological labs.

He developed many special vacuum gauges as standards for calibration of other electronic vacuum gauges, baffles and traps, cooled with Peltier couples, complete portable equipment for service work on cooling devices (refrigerators, deep freezers, air conditioning devices).

At the IEVT he set up the universal calibration system for vacuum gauges, system for measuring all characteristics for rotary, diaphragm and diffusion pumps, monopol mass spectrometer, leak detection, various rough, high and ultra high vacuum systems for investigations, thin film evaporation systems.

He organized Leybold Heraeus and Jeol representative & service stations, both are now private.

Jože Gasperič is also an excellent organizer of conferences and congresses and he taught us how to organize the meetings in Slovenian Vacuum Society as well as in Union of Vacuum Societies of former Yugoslavia. He was the president of the Union and organizer of 4 Yugoslav vacuum congresses and Joined vacuum conference of Hungary-Austria-Yugoslavia and he was a member of organizing committee of the European Conference on Applications of Polar Dielectrics, FORUM BLED '97, and Solid State Protonic Conductors.

He succeeded with his project Vacuum impregnation of fossil bones of mammoth for Natural museum of Slovenia to save the prehistoric mammoth for our descendants.

He was editor of News of the Slovenian Society for Medical and Biological technique, co-editor of Slovenian journal Vakuumist - *Vacuumologist* and lector for Slovenian scientific journal Kovine zlitine tehnologije - Metals, Alloys, Technologies.

Our colleague and friend Jože is full of development spirit and creative ideas.

Jože Gasperič has published over 100 papers in international journals and conferences and 100 papers in Slovenian journals and conferences on the topics of science, technology, vacuum science and technique as well as vacuum metrology.

Professor Gasperič has been supervisor to several Ph.D. and Master Degree students at the Universities of Ljubljana, Maribor and India. He is also very active in the international academic field.

He is a member of executive council of Slovenian Vacuum Society, member of Slovenian Electronics and Micrelectronics Society, Slovenian Society of Biomedicine, member of Electronics Materials scientific division of International Union for Vacuum Science, Technique and Applications - IUVSTA.

His colleagues and friends hope very much that he will take part in discussions, lectures and publications also in the future and we would like to wish him and his family many years in good health.

ISSN 1318-0010
KZLTET 31(6)503(1997)

THE PROPER OPERATION OF THE HIGH VACUUM PUMPING SYSTEM

PRAVILNO DELOVANJE VISOKOVAKUUMSKEGA ČRPALNEGA SISTEMA

JOŽE GASPERIČ[1]

Jožef Stefan Institute, Jamova 39, 1001 Ljubljana, Slovenia

Prejem rokopisa - received: 1997-10-01; sprejem za objavo - accepted for publication: 1997-10-21

The proper operation of high vacuum pumping systems with oil diffusion pumps and backing rotary pumps is very important, otherwise the contamination of vacuum chambers by backstreaming oil vapours is extremely high as well as the oxidation and the loss of diffusion pump oil. The forepressure switching point, where the diffusion pump is put into the operation by opening the high vacuum and forepressure valves is discussed. There are three possible situations: the pumping throughput is just adapted, or it is to low, or to high. What is going on, when the pumping troughput is adapted, it is illustrated using the troughput-pressure diagrams. At the end some practical advices are done, how to recognize that the operation of the HV pumping system is correct.

Key words: high vacuum pumping system, contamination, loss of diffusion pump oil, tolerable forepressure, switching point

Pravilno upravljanje in delovanje visokovakuumskega črpalnega sistema z oljno difuzijsko črpalko in rotacijsko predčrpalko je zelo pomembno, kajti v nasprotnem primeru pride do močno povečanega povratnega toka oljnih par iz difuzijske črpalke v vakuumsko komoro in s tem do njene kontaminacije. Izguba olja v difuzijski črpalki in njegova pospešena oksidacija sta spremljajoča pojava. Pri ročnem ali avtomatiziranem upravljanju črpalnega sistema je zelo pomemben trenutek oz. točka preklopa, ko prenehamo črpati s predčrpalko po obtočnem vodu in odpremo visokovakuumski in predvakuumski ventil in začnemo črpati z difuzijsko črpalko. Možna so tri delovna stanja: delovanje obeh črpalk je usklajeno, predčrpalka ima premajhno ali preveliko črpalno hitrost. Usklajeno stanje smo ponazorili na diagramu. Podani so tudi praktični napotki, kako spoznamo, ali je črpalni sistem pravilno upravljan.

Ključne besede: visokovakuumski črpalni sistem, kontaminacija, izguba olja difuzijske črpalke, mejni predtlak, preklopna točka

1 INTRODUCTION

Most usual, the high vacuum pumping systems consist of diffusion pumps and corresponding rotary backing pumps. The basic sheme is shown on **Figure 1**. Normally, all producers of such high vacuum systems give the prescription how to work with them at the begining, when the vacuum chamber is pumped from atmospheric pressure, down to 10^{-4} and 10^{-5} mbar, respectively, when the technological process is started (e.g. evaporation). In practice this procedure is never exactly followed by users. Only in the case, when the high vacuum system is fully automatized, the users can avoid the mistakes in the pumping procedure. Usually it happens that not skilled persons change the programme by moving the pressure switching points of valves. The results of that action are:

- by backstreaming oil vapours from the diffusion pump the vacuum chamber as well as all material in it are contaminated
- the oxidation, deterioration and loss of the diffusion pump oil are very intensive.

The service and cleaning work of the system is required.

2 EXPERIMENTAL

The procedure of pumping from atmospheric pressure to the high vacuum is well known. The action of both pumps has to be adjusted to minimize the pumping time, which is very important in the industrial production. If shorter time is required ("The time is money!"), we have to know all effects which influence on it. One of them is the time switching programme of valves, which

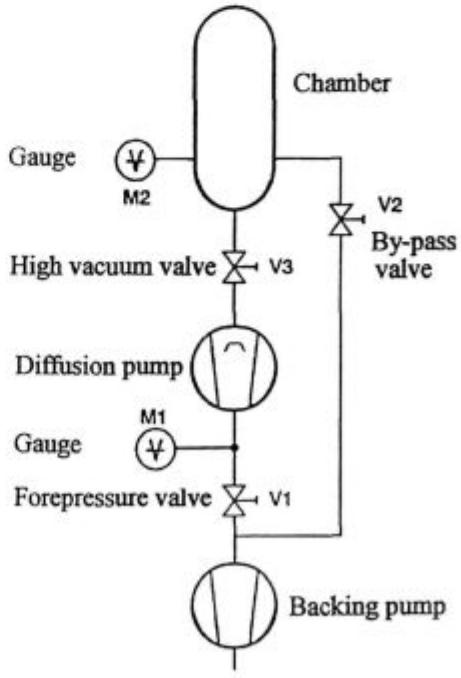

Figure 1: High vacuum pumping system
Slika 1: Visokovakuumski črpalni sistem

is also depended on the pumping characteristics of both pumps.

The most evident way, how to explain the interrelation between diffusion and backing pumps, are their throughput-pressure characteristics. As an example let us use the throughput characteristics of DI 12000 diffusion pump (Leybold) and corresponding backing pump (a combination of Roots pump WA 250 and the one stage rotary pump S 60A). From the diagram (**Figure 2**) it is evident that both throughput characteristics have the cross-section point M at the throughput Q_M and pressure p_t. The pumps are selected so that the end of the diffusion pump curve is just on the throughput curve of backing pump. The pressure p_t is called the tolerable forepressure. Practically, this forepressure is a limit of the diffusion pump operation. The total air flow from the vacuum chamber is now depended only on the backing pump and conductivities of connected lines, valves etc. When the tolerable forepressure takes place the oil vapours which are generated in the diffusion pump boiler and ejected through the jet system do not reach the water cooled walls of the pump, where the condensation of them is expected, but one part escapes in the direction of vacuum chamber, where it condenses (contamination!), the other part of oil vapours is pumped by the backing pump (the loss of the oil from diffusion pump). The oxidation and deterioration of the oil in the boiler of the pump and on the surface of jet system (temp. approx. 200°C) is accelerated.

Case 1: When pumping of the chamber is started through the by-pass valve V2 from the atmospheric pressure (V1 and V3 are closed) the air throughput Q and the pressure are slowly reducing (the direction from point A to M in diagram, **Figure 2**). When the point M on the throughput curve is reached, the theoretical possibility is done to pump with the diffusion pump. If in this moment the by-pass valve is closed, and V1 and V3 are open, from the point M we are "driving" the pumping action of the chamber in the direction of DI 12000 (upper curve) to the next point C, where the pressure is P_c (M2) and forepressure p_c (M1) at the throughput point C'. The pressure p_c is lower than tolerable one p_t, and the diffusion pump can normally operate. After a longer time of pumping we "come" to the point D, where the throughput is Q_D, pressure on high vacuum side P_d and forepressure p_d (point D'). We can continue the pumping procedure as long as the operating (or ultimate) pressure is achieved. The diagram on **Figure 2** is an example, how the diffusion and backing pumps are well adjusted.

Case 2: Supposing that the by-pass valve (V2) is closed and other valves (V1, V3) are open in the point A, where the pressure p_a is higher then the tolerable forepressure p_t. The pump capacity of the diffusion pump is totally lost. The diffusion pump is now like "a cooking pot" for oil. Bad results were described above, although the pumping action of backing pump is continued. The situation is normalized, when the point M is achieved and after that, as described above. This means that on such a way we can not shorten the total pumping time.

Case 3: If the by-pass valve (V2) is closed later, e.g. at the point E, and valves V1, V3 are open in next moment, the diffusion pump as well as backing pump throughput suddenly "jump" to the value at E' and the forepressure (M1) increases from p_e to p_e". If in our pumping procedure is such a case, we had lost the time, which is needed to pump the chamber from E" to E with backing pump.

We have described three characteristical situations in the operating procedure, and now we can ask ourselves, how to recognize that the high vacuum pumping system is operating correct or not. Normally, we have not the

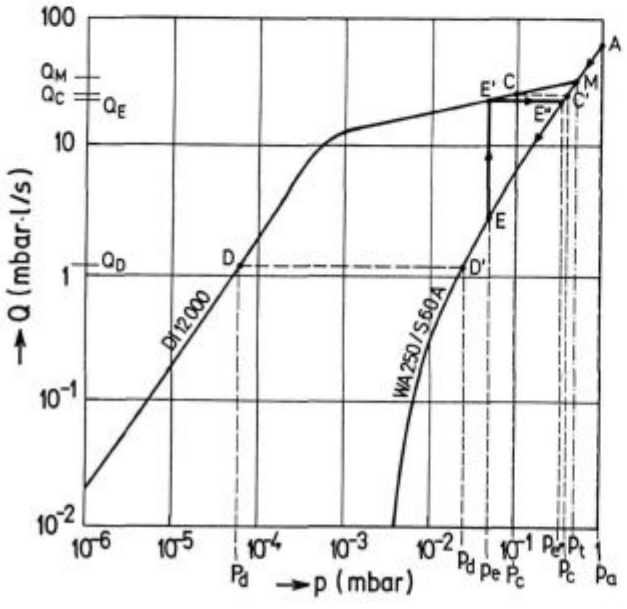

Figure 2: Throughput Q vs. pressure p
Slika 2: Pretok zraka Q v odvisnosti od tlaka p

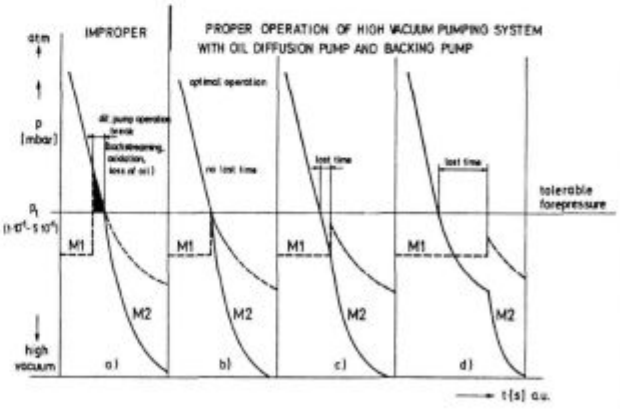

Figure 3: Pumping time characteristics of the adjusted high vacuum pumping system: a) inproper operation, b) proper and optimal operation, c), d) proper but not optimal operation
Slika 3: Črpalna karakteristika usklajenega visokovakuumskega sistema: a) nepravilno delovanje, b) pravilno in optimalno delovanje, c), d) pravilno, vendar ne optimalno delovanje

pumping diagram (like that shown on **Figure 2**) at the hand.

The best way is monitoring of the both pressures readings M1 and M2. If the forepressure (M1) increases to the values, which are higher than the torelable forepressure, when we close V2 and open V1 and V3, the operation of the diffusion pump is stopped (oil backstreaming and contamination of vacuum system, the oxidation and loss of the oil begin) (**Figure 3a**). The situation is normalized, when the pressure (M1) is lower then the tolerable forepressure.

The optimal case is, when after switching of the valves, as desribed above, the forepressure (M1) increases just to the value p_t (tolerable forepressure), **Figure 3b**. All other cases, as we can see on the pumping characteristics, **Figure 3c, d**, are also proper but not optimal, we are loosing time, which is very important, especialy in the production in the industry.

It is also very simply to practically identify the tolerable forepressure. For most types of oil diffusion pumps it is between 0,1 and 0,5 mbar. Many other cases exist, where the pump combinations are not adapted (e.g. the pumping speed of backing pump is to high or to low) which will be described later in a separate paper.

3 CONCLUSION

It is very simple to estimate that a high vacuum system is operating optimaly or not by observing the pressure changes in the vacuum chamber as well as the forepressure of diffusion pump during the switching period of values.

ISSN 1318-0010
KZLTET 31(6)507(1997)

ULTRA THIN DEPOSITED AND SEGREGATED FILMS

ULTRA TANKE NANESENE IN SEGREGIRANE PLASTI

MONIKA JENKO

Institute of Metals and Technology, Lepi pot 11, 1000 Ljubljana, Slovenia

Prejem rokopisa - received: 1997-10-01; sprejem za objavo - accepted for publication: 1997-10-21

Dedicated to Prof. Jože Gasperič at the occasion of his 65th birthday

Research, development and use of vacuum thin films started at the Institute for Electronics and Vacuum Techniques, IEVT, Ljubljana after its foundation around 1950. With the development of the miniature thin film potentiometers and thin films resistors of high stability at IEVT the first production of thin film electronic components in former Yugoslavia was established. The technology was successfully transferred to Slovenian foreign factory in Cormons Italy where Slovenian minority is living. At the same time the high tech research and development of the second and third generation image intensifier tubes was started. Prof. Dr. Jože Gasperič was one of the leading scientists investigating the sputtered cermet thin films in his BS and Ph.D. works. His findings are basic for understanding the mechanism of growth of thin sputtered cermet films. In the middle of eighties an experimental ultra high vacuum, UHV, system equipped with Auger spectrometer, was built at IEVT and the investigation of physical and chemical processes of ultra thin oxide film growth on the surface of liquid indium and indium alloys in situ was achieved for the first time. The experimental method based on Auger Electron Spectroscopy for in situ investigation of the initial phase of the ultra thin oxide film growth on liquid indium, was developed at the institute. The modified experimental method was also used for the study of ultra thin segregated Sb, Sn or Se films on the surface of FeSiC alloy, microalloyed by Sb, Sn or Se. The investigation of ultra thin Sn, Sb or Se films on well defined Fe surfaces is the topic of our present research which is close connected with the purchase of new AES/XPS instrument with the very high spatial resolution. The results of investigations of ultra thin oxide films on the liquid indium and InSn alloy as well as Sb and Sn ultra thin film growth on the surface of FeSiC alloy were presented.

Key words: ultra thin films, deposited films, segregated films, surface segregation, oxidation, dissociation

Prve raziskave, razvoj in uporaba vakuumskih tankih plasti so se začele na Inštitutu za elektroniko in vakuumsko tehniko v Ljubljani takoj po ustanovitvi, okrog leta 1950. Z razvojem miniaturnega tankoplastnega potenciometra MP in stabilnih tankoplastnih miniaturnih uporov se je pričela na IEVT tudi prva proizvodnja tankoplastnih elektronskih komponent v takratni Jugoslaviji. Tehnologija izdelave MP je bila uspešno prenesena v novo ustanovljeno slovensko zamejsko tovarno v Krminu v Italiji. Obenem pa so se vršile raziskave in razvoj specialnih fotoelektronk, Sb fotokatod druge in tretje generacije za slikovne ojačevalnike z bližinskim prenosom slike, ki je predstavljal "high-tech" v svetovnem merilu. Vakuumisti IEVT so s svojim znanjem sodelovali v svetovno znanih institucijah kot npr.: SAES Geters, Heimann, Leybold Heraeus. Skupne rezultate so že takrat objavili v tuji znanstveni periodiki. Z raziskavami vakuumskih tankih plasti se je na IEVT intenzivno ukvarjal tudi prof. dr. Jože Gasperič, ki je problematiko kermetnih napršenih plasti obdelal v svojem magistrskem in nato še v doktorskem delu. Njegova temeljna spoznanja so pomembeno prispevala k razumevanju mehanizma rasti tankih napršenih plasti. Z izgradnjo eksperimentalnega ultravisoko vakuumskega sistema, opremljenega s spektrometrom Augerjevih elektronov na IEVT v sredini osemdesetih let pa je bila dana možnost raziskav fizikalno kemijskih procesov pri nastanku ultra tankih oksidnih plasti na površini tekočih kovin in zlitin "in situ". Tovrstne raziskave so bile izvedene prvič. Načrtovana in osvojena je bila nova eksperimentalna metoda, ki je omogočila študij začetnih stopenj rasti oksidnih plasti na tekočem indiju, ki smo ga tudi naparili in situ v spektrometru Augerjevih elektronov. Metoda je bila uporabljena tudi za študij ultra tankih segregiranih plasti Sb, Sn in Se na površini zlitin Fe-Si-C, mikrolegiranih z Sb, Sn ali Se. Študij ultra tankih plasti Sb, Sn, Se na dobro definiranih površinah Fe in V pa je predmet naših sedanjih raziskav, ki so vezane na nabavo novega AES/XPS instrumenta z visoko lateralno ločljivostjo. Prikazani so rezultati raziskav ultra tankih oksidnih plasti na tekočem indiju in zlitini InSn ter ultra tankih segregiranih Sb in Sn plasti na zlitini FeSiC.

Ključne besede: ultra tanke plasti, oksidacija, disociacija, In_2O_3, In_2O, Sb, Sn, površinska segregacija, AES, XPS

INTRODUCTION

Advanced technologies are strongly dependent on products of electronic industries such as optoelectronics, sensors, high density integrated components, etc. Thin films of thicknesses from ten to several hundreds of nanometers are very important in the production of these products. Ultrathin films-UTF whose thickness is up to few monoatomic layers are very decesive in the segregation, corrosion, recrystallization and catalytic processes. UTF are influenced by their interaction with the substrate and open a completly new perspective in the development of new advanced materials with desired physical and chemical properties.

Research, development and use of thin films started at the Institute for Electronics and Vacuum Techniques, IEVT, Ljubljana Slovenia after its foundation in early fifties. With the development of the miniature thin film potentiometers and thin films resistors of high stability at IEVT the first production of thin film electronic components in the country was established. The technology was successfully transferred to Slovenian factory in Cormons-Italy where the Slovenian minority is living.

Prof. Jože Gasperič was one of the leading scientists investigating the sputtered cermet thin films in his BS and Ph.D. works. His findings are basic for understanding the mechanism of growth of thin sputtered cermet films.

In the middle eighties the "high tech" research and development of the second and third generation image intensifier tubes was started at IEVT. An experimental ultra high vacuum, UHV, system equipped with Auger spectrometer, was built and the author was the first to investigate in situ the physical and chemical processes of ultra thin oxide film growth on the surface of liquid indium and indium alloys.

The experimental method based on Auger Electron Spectroscopy for the in situ investigation of the initial phase of ultra thin oxide film growth on liquid indium, was developed at the IEVT institute. The simplified experimental method was used for the investigation of segregated Sb, Sn or Se UTF on the surface of FeSiC alloy, microalloyed with Sb, Sn or Se at the Institute of Metals and Technology Ljubljana, where the first studies of P segregation started already in 1962.

The investigation of Sn, Sb or Se UTF on well defined Fe surfaces is being the topic of our present research work which is close connected with the purchase of new AES/XPS device with the very high spatial resolution.

The results of investigations of ultra thin oxide films on liquid In and InSn alloy as well as Sb, Sn and Se ultra thin film growth on the surface of FeSiC alloy are presented.

1 AES INVESTIGATION OF INITIAL PHASE OF LIQUID In AND InSn ALLOY OXIDATION AND DISSOCIATION OF In_2O_3

1.1 Fluxless vacuum soldering

In the production of the third generation image intensifier tubes the fluxless vacuum soldering is the most important process for hermetic encapsulation. Extremely clean surfaces are indispensable for obtaining good wetting of liquid solder. In the first model experiments we found that the leakage of fluxless vacuum soldered seals may often be caused by thin oxide film, covering the liquid solder. The solder is low melting InBi or InSn alloy. For the basic investigation we used pure indium as a solder and we realized that only in situ surface characterization may give direct insight into these complex surface phenomena.

For this purpose a very sensitive experimental method based on AES was developed at IEVT Ljubljana. The initial phase of surface oxidation on high purity in situ deposited indium and the mechanism of cleaning process of oxidised indium surface In_2O_3 was the main goal of the investigation.

1.2 Experimental method for the investigation of surface phenomena at fluxless vacuum soldering

The experiments were performed in an adapted Scanning Auger Electron Microprobe, additionally equipped with addapted sample holder, heater and thermocouple, evaporation source for in situ deposition of high purity indium, quartz microbalance for determination of In thin film thickness, quadrupole mass spectrometer-QMS for residual gas analysis and precise metal valve for oxygen introduction. Especially designed connections enabled the movement of the sample, **figure 1**.

The sample high purity indium thin film was deposited in situ on a pure molybdenum substrate. The oxide In_2O_3 film was obtained by exposure of the indium surface to pure oxygen at constant pressure $5x10^{-5}$ mbar with oxygen time exposure up to 100 minutes in temperature range from 25 to 250°C.

The resistive heater for investigating In/In_2O_3 film was a Mo strip which could be heated up to 1000°C. A thermocouple Fe-CuNi was welded on the rear side of the Mo strip. The indium source for in situ deposition was prepared from indium metal of 6N purity.

1.3 AES studies of the initial phase of liquid indium oxidation

The surface oxidation of indium in bulk and thin film occurs as (1):

$$4\ In\ (l) + 3\ O_2\ (g) \leftrightarrow 2\ In_2O_3\ (c) \qquad (1)$$

where (c), (l) and (g) mean crystalline, liquid and gas state, respectively. The solubility of oxygen in pure liquid indium is extremely low, $1x10^{-6}$ atomic percent at 550°C and it is negligible in the temperature range of our investigation from 25 to 250°C. The diffusivity of

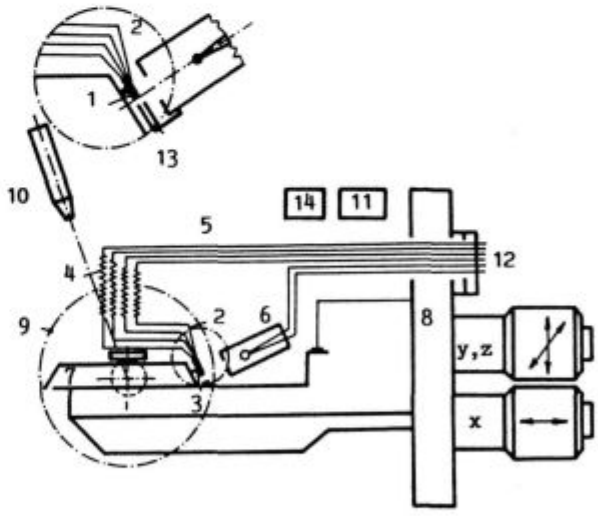

Figure 1: AES spectrometer adapted for liquid indium surface investigations: 1 - sample, 2 - Thermocouple, 3 - sample holder, 4 - flexible connections, 5 - rigid connections, 6 - In source for in situ evaporation, 8 - flange, 9 - CMA, 10 - ion gun, 11 - QMS, 12 - lead through, 13 - quartz microbalance, 14 - metal valve for oxygen introduction

Slika 1: Spektrometer Augerjevih elektronov prirejen za raziskave procesov na tekočem indiju: 1 - vzorec, 2 - termočlen, 3 - nosilec vzorca, 4 - gibljivi priključki, 5 fiksni priključki, 6 - In izvir za "in situ" naparevanje, 8 - prirobnica, 9 - CMA, 10 - ionska puška, 11 - QMS, 12 - prevodnice, 13 - kremenova mikrotehtnica, 14 - vpustni ventil za kisik

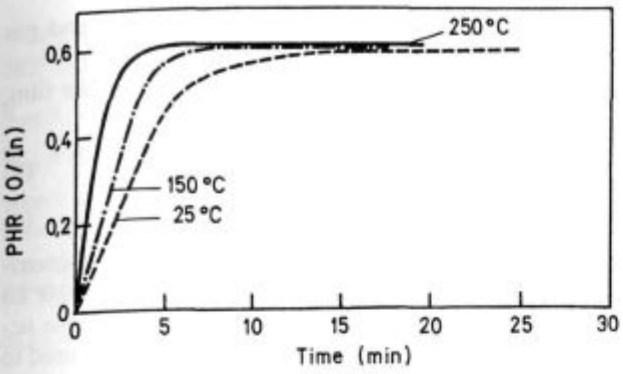

Figure 2: Surface oxidation rate of crystalline and liquid indium at temperatures 25, 150 in 250°C at a constant oxygen pressure of $5x10^{-5}$ mbar

Slika 2: površinska oksidacija trdnega in tekočega indija pri temperaturah 25, 150 in 250 °C in konstantnem tlaku kisika $5x10^{-5}$ mbar.

oxygen in liquid indium is very low, $3.7x10^{-7}$ cm^2 s^{-1} at 550°C.

It was concluded from these facts that the process of pure liquid indium oxidation occurs at the surface.

The kinetics of thin oxide film growth on crystalline and liquid indium was investigated by AES, following the peak height ratio-PHR of amplitudes between O(KLL) and In ($M_5N_{45}N_{45}$) Auger transition at kinetic electron energies of 512 eV and 402 eV (for In^0) and 405 eV (for In^{3+}) respectively. For a defined geometrical sample position in the AES spectrometer, the kinetics of the thin oxide film growth was followed up to the film thickness of 3.5 nm, which corresponds to an effective electron depth escape λ_{ef} for In_2O_3.

Surface indium oxidation was investigated at the temperatures of 25, 150, 250 in 550°C, **figure 2**.

Thin oxide film thickness of 3.5 nm on pure indium were obtained at conditions listed in **Table 1**.

Table 1: In_2O_3 films, 3.5 nm thick obtained at different temperatures and different oxygen exposures

Temperature (°C)	Oxygen exposure (L)
25	$6x10^4$
250	$3x10^4$
550	$1.5x10^4$

At higher temperatures T > 360°C, a volatile oxide was formed by the reaction:

$$In_2O_3\ (c) + 4\ In\ (l) \leftrightarrow 3\ In_2O\ (g) \qquad (2)$$

The reaction between the In_2O_3 thin film and the underlying liquid indium, corresponding to equation (2) was studied at the temperature of 360, 400, 450 and 550°C in vacuum of $1x10^{-9}$ mbar. The results are shown in **figure 3**.

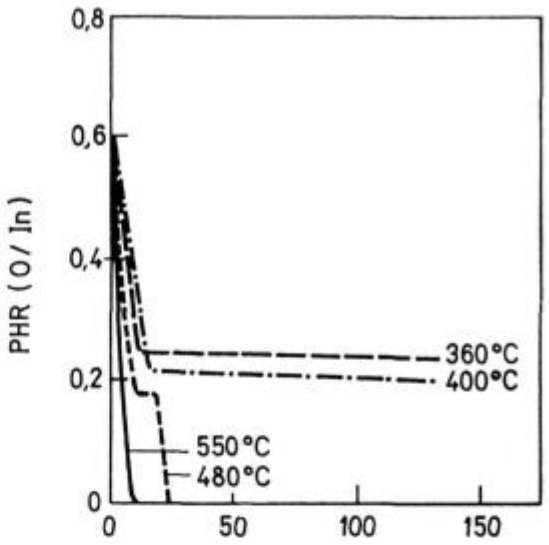

Figure 3: Isothermal dissociation of In_2O_3 ultra thin solid film on liquid indium at the temperatures 360, 400, 450 in 550°C in a vacuum below $1x10^{-9}$ mbar

Slika 3: Izotermna disociacija ultra tanke plasti In_2O_3 na tekočem indiju pri temperaturah 360, 400, 450 in 550 °C in vakuumu pri tlaku < $1x10^{-9}$ mbar.

1.4 Investigation of In_2O_3 dissociation in uhv by AES

At temperature T > 360°C the evaporation of volatile In_2O corresponding to equation (2) proceeded with perceivable velocity. At 550°C the process was so fast that AES studies of In_2O_3 to In were not possible.

The use of indium as a solder for vacuum fluxless soldering depends upon the fact that the thin In_2O_3 film spontaneously disappeared - dissociated at T > 360°C by In_2O evaporation following the equation (2) In_2O_3 (c) + 4 In (l) ↔ 3 In_2O (g).

1.5 AES investigation of initial phases oxidation of InSn liquid solder

In the second part of our investigation the knowledge of the initial phase of surface oxidation on pure liquid In to InSn solder (20 at.% In, 80 at% Sn) was applied. The samples high purity InSn film, 2.5 μm thick were prepared in Balzers Sputron plasma beam apparatus, **figure 4**.

On the oxidised InSn surface a difference between AES spectra of pure metal In (402, 408 eV) and In_2O_3 (399, 405 eV) was found. For tin (428, 435 eV) the characteristic chemical shift was not determined and only changes in the shape and intensity of Auger spectra were recognized.

Figure 5 shows the AES spectra of the liquid InSn alloy exposed to pure oxygen $1.5x10^4$ L, covered by thin oxide film, approximately 3.5 nm thick **(figure 6)**, corresponding to an effective electron depth escape λ_{ef} for In_2O_3.

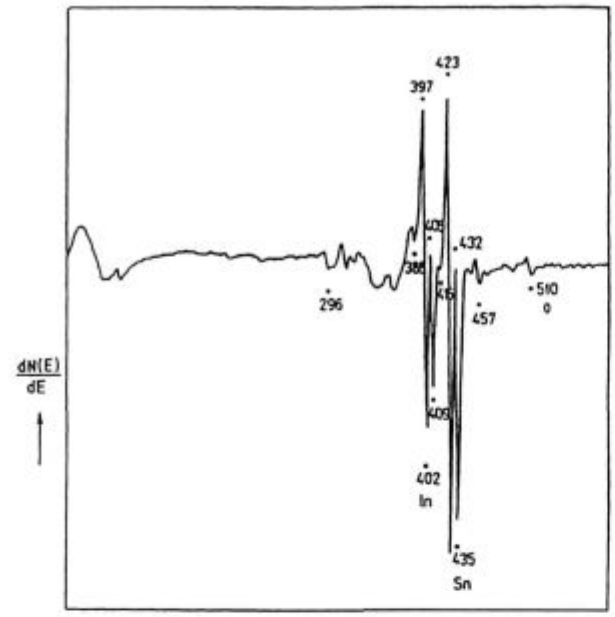

Figure 4: AES spectrum of InSn solder (20 at.% In and 80 at% Sn) after ion etching approximately 3 nm under surface

Slika 4: AES spekter InSn spajke(20 at.% In and 80 at% Sn) po ionskem jedkanju približno 3nm pod površino

The samples were oxidised in situ in Auger Spectrometer by exposure of a clean surface of liquid InSn alloy to pure oxygen (10^4 - 10^6 L) at 250°C.

The results indicate that all oxide films on the surface of liquid InSn solder were enriched in indium in varying amounts, depending on oxygen pressure, time exposure etc.

In the first part of the investigation it was found that the surface oxidation of In, in bulk or in the form of a thin film can be formulated by equation (1):

$$4\ In\ (l) + 3\ O_2\ (g) \leftrightarrow 2\ In_2O_3\ (c) \qquad (1)$$

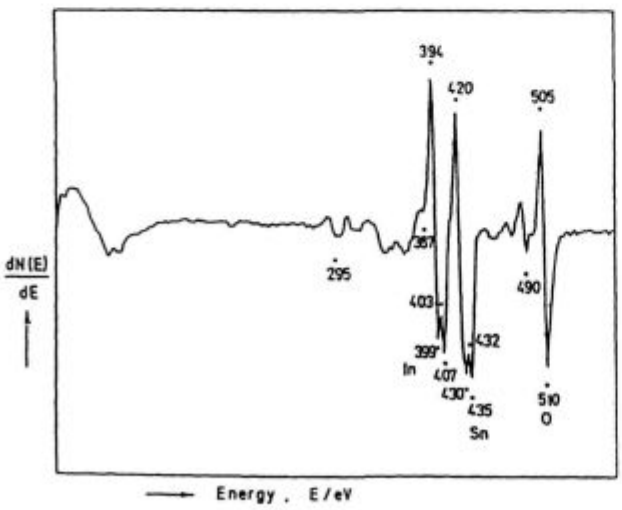

Figure 5: AES spectrum of 3.5 nm thick oxide UTF on the surface of liquid InSn alloy

Slika 5: AES spekter 3.5 nm debele oksidne plasti na površini tekoče spajke InSn.

where (c), (l) and (g) mean crystalline, liquid and gas state, respectively.

The surface oxidation of Sn, in bulk or in thin film, occurs by the reactions:

$$2\ Sn\ (l) + O_2\ (g) \leftrightarrow 2\ SnO\ (c) \qquad (3)$$

$$Sn\ (l) + O_2\ (g) \leftrightarrow SnO_2\ (c) \qquad (4)$$

AES chemical shifts of SnO and SnO_2 are approximately the same. On tin exposed to oxygen (10^4 - 10^6 L) both oxides SnO and SnO_2 were found. As the same occurs for SnO and SnO_2, chemical shift can not be used to identify the oxidized state of the tin film. It was proposed that a mixture of oxides SnO, SnO_2 and In_2O_3 was formed on InSn alloy at the exposure to oxygen (10^4 - 10^6 L). The mixture of oxides appeared to be thermodynamically unstable near the alloy-oxide interface; SnO and SnO_2 oxides were reduced to Sn with the tendence to the formation of additional In_2O_3

$$3SnO_{(oxide,c)} + 2In_{(alloy,l)} \leftrightarrow In_2O_{3(oxide,c)} + 3Sn_{(alloy,l)} \qquad (5)$$

$$3SnO_{2(oxide,c)} + 4In_{(alloy,l)} \leftrightarrow 2In_2O_{3(oxide,c)} + 3Sn_{(alloy,l)} \qquad (6)$$

Free energy ΔG^o of reactions (5) and (6) are obtained by using the data for free energy of formation SnO, SnO_2 and In_2O_3

$$\Delta G^o(SnO) = \\ = -69670 + 3.06\ T\log T - 1.5\times10^{-3}T^2 - 0. + 18.39T \qquad (7)$$

$$\Delta G^o(SnO_2) = -143080 - 7.37\ T\log T - \\ - 0.7\times10^{-3}T2 + 2.38\times10^5T^{-1} + 76.53T \qquad (8)$$

$$\Delta G^o(In_2O_3) = -220970 + 24.22T\log T - \\ 3\times10^{-3}T^2 - 0.3\times10^5T^{-1} + 41.36T \qquad (9)$$

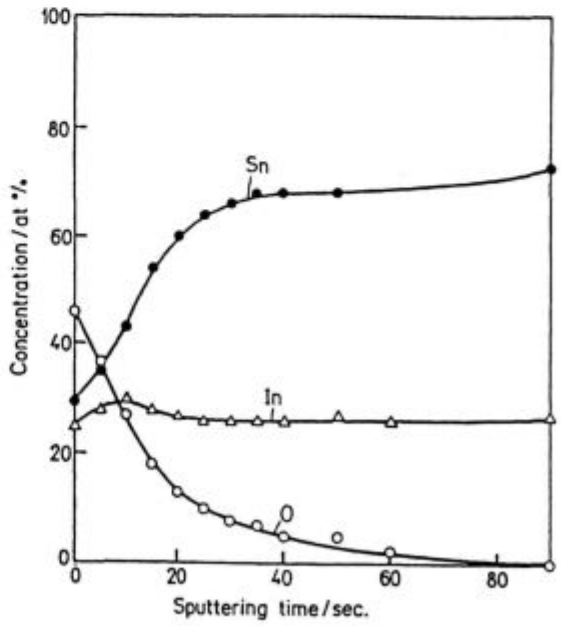

Figure 6: AES depth profile of oxide UTF on surface of liquid InSn solder. Oxide UTF was made in situ

Slika 6: AES profilni diagram ultra tanke oksidne plasti na tekoči spajki InSn; oksidna plast je bila narejena *in situ*

At the temperature 250°C ΔG° (5) = -525 kJmol^{-1} and ΔG° (6) = -285 kJmol^{-1} and the equilibrium constants:

$$K_{(5)} = (a_{Sn}^3 \times a_{In2O3})/(a_{SnO3} \times a_{In2}) = 2.2\times10^{52} \quad (10)$$

$$K_{(6)} = (a_{Sn}^3 \times a_{In2O3}^2)/(a_{SnO}^3 \times a_{In}^4) = 2.8\times10^{28} \quad (11)$$

where a_i s are the activities of the reactants and products. The mixed oxide thin film formed during oxidation would be a mixture of pure In_2O_3, SnO and SnO_2. The driving force for reactions (5) and (6) is therefore

$$\Delta G_{(5)} = \Delta G^{\circ} + RT \ln[(1 - N_{In})^3/N^2_{In}] \quad (12)$$

$$\Delta G_{(6)} = \Delta G^{\circ} + RT \ln[(1 - N_{In})^3/N^4_{In}] \quad (13)$$

N_{In} is the indium concentration in the SnIn alloy. At 250°C ΔG for N_{In} 10^{-6} (1ppm) is -108 kJmol^{-1} for reaction (5) and -351 kJmol^{-1} for reaction (6).

In other words, SnO and SnO_2 are thermodynamically unstable are in the mixed oxide even when in contact with extremely dilute In in Sn. The only stable oxide formed at InSn alloy should be In_2O_3 at 250°C. Since all oxidation processes are of the nonequilibrium type, the amounts of SnO and SnO_2 and the overall SnO, SnO_2/In_2O_3 ratio depend on O_2 pressure, temperature, diffusion coefficient, solubilities and other factors. Consequently the mixed oxides SnO and SnO_2 in the oxide-alloy interface tend to be converted into Sn and In_2O_3.

1.6 AES investigation of In_2O_3 dissociation on the surface of liquid InSn solder in UHV

The last part of fluxless vacuum soldering in UHV investigation dealt with the "cleaning process" by dissociation of thin In_2O_3 film from the surface of the liquid InSn solder. The reaction between the thin In_2O_3 film and the underlying liquid InSn solder correspond to equation

$$4\ In\ (l) + 3\ O_2\ (g) \leftrightarrow 2\ In_2O_3\ (c) \quad (1)$$

was investigated at 550°C and the results are shown in **figure 7**. It was found that at T>250°C in UHV the thin In_2O_3 film formed on the surface of liquid InSn alloy spontaneously disappeared by In_2O_3 dissociation according to equation (1). The oxides SnO and SnO_2 or In_2O_3 are unstable in very thin oxide films on the surface of a liquid InSn solder at T>250°C.

For fluxless vacuum vacuum soldering with liquid indium, previously cleaned at T > 360°C, recontamination is negligible in UHV in the temperature range:

Tm < T < 360°C

At fluxless vacuum soldering with liquid InSn solder, previously cleaned at T > 360°C, recontamination is negligible in UHV in the temperature range Tm < T < 360°C.

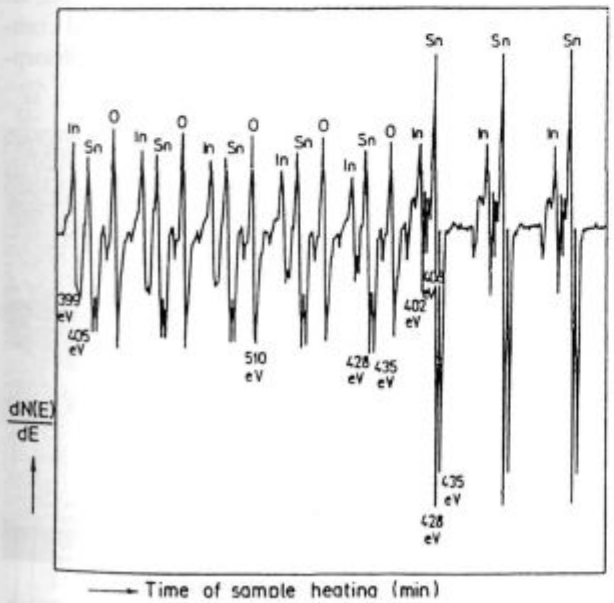

Figure 7: Changes in AES peaks of In, Sn and O between heating of oxidized InSn solder at constant temperature of 450°C

Slika 7: Spremembe AES vrhov značilnih za In, Sn in O med segrevanjem oksidirane spajke InSn pri konstantni temperaturi 450°C

2 CHARACTERIZATION OF SEGREGATED Sb AND Sn UTF BY AES

2.1 Introduction

Physical properties of metals and alloys depend on the composition and on the surface and interface structure of the material. These properties are affected by segregation processes of alloying elements and impurity elements during their manufacturing and use. Some of these elements which segregates on free surfaces (surfaces, grain boundaries, interfaces) and ultra thin segregated films specifically affect adsorption, corrosion, adhesion, surface diffusion, recrystallization, catalytic activity, friction and wear[7-8].

The atomic composition of grain boundaries is also very important because it affects physical properties as well as corrosion behaviour of metals and alloys. For materials applied at high temperatures, the composition of interfaces may be drastically changed by segregation, by enrichment of dissolved surface active atoms diffusing on the surface or grain boundaries and can cause metal embrittlement.

The aim of the investigation was to examine the nature of segregation of antimony and tin and its effect on recrystallization process, grain growth and texture development of a cold rolled and annealed silicon non oriented electrical sheet to be used in generation of electrical energy.

It has been experimentally confirmed that a small addition of antimony, tin and selenium into the melt of silicon iron by microalloying affect the magnetic properties of electrical sheets by enrichment on free surfaces, i.e. surfaces and grain boundaries[9-13,15-19].

Such enrichment affects grain growth, producing an increase in the number of ferrite grains with soft magnetic lattice orientation which grow on the account of grains with other crystallographic orientations, and in

this way improves the magnetic properties. Our investigations show a strong correlation between antimony and tin surface segregation and the orientation of surface grains[17-19].

The kinetics of surface segregation is determined by bulk diffusion of the segregate to the respective interface. Surface segregation kinetics was measured on non oriented silicon steel sheet in situ by Auger Electron Spectroscopy-AES, by annealing and simultaneous analysis of the sputter cleaned sample at higher temperature in UHV.

Non oriented silicon steel is a polycrystalline multicomponent alloy of Fe, Si, Al, C, P and S. The addition of approximately 0.05 to 0.1% of single elements i.e. antimony or tin starts a competition for free surface sites[7,25].

The grain boundary segregation of Sb and Sn was studied initially on polycrystalline non oriented silicon steel. The alloys were annealed in the temperature range between 450 and 650°C to establish the equilibrium grain boundary segregation on samples quenched and mounted into UHV system, fractured in situ after cooling and analysed by AES.

The main point of the research work was the determination of the physical nature of the surface segregation and its relationship to the internal grain boundary segregation grains at the sheet surface. The investigation also included the determination and evolution of the texture of grains at the sheet surface. Emphasis was placed on the understanding how texture affects the electrical energy losses, as well as magnetic properties.

2.2 Surface segregation of antimony and tin

Most elements dissolved in iron tend to enrich at elevated temperatures at surfaces, grain boundaries and interfaces and distribution equilibrium $A_{dissolved} \leftrightarrow A_{segregated}$ are established at sufficiently high temperature[7,25,26,34].

2.2.1 Antimony

Antimony surface segregation was studied using AES method on a 2.0% Si steel, alloyed with different mass contents of Sb (0.05 and 0.1%). The dependence of surface segregation on grain orientation and on the presence of other solute atoms of S, P, C, Al and Si was investigated in situ under UHV conditions by AES in the temperature range from 450 to 900°C.

The antimony enrichment at the surface was estimated by following the peak height ratio - PHR of amplitudes between the dominant $Sb(M_5N_{4,5}N_{4,5})$ and $Fe(L M_{2,3}V)$ Auger transitions at kinetic energies of 454 and 651 eV, respectively.

The mole fraction of Sb 0.05% and 0.1% in investigated steels, is clearly in the range of solubility in α-Fe at all temperatures investigated but below the detection limit of AES method. The enrichment of Sb, caused by equilibrium segregation at the surface, can only be measured at or after annealing at elevated temperatures by AES method.

AES measurements showed a different quantity of segregated antimony on different grains (**figure 8**). All samples were metalographically polished, the orientation of single grains was determined by the etch pitting method. The temperature dependence of antimony surface segregation a) on grain with (001) and b) (111) orientation is shown on **figure 9**.

The surface of investigated steel alloyed with 0.1% Sb was clean sputtered with Ar^+ ions and in situ annealed in the analyzing chamber of the Auger spectrometer. The temperature was increased every 20 minutes for 50°C. The antimony segregation rate was perceived at temperature T > 650°C and it increased with the increasing temperature, while at T > 850°C the antimony segregation rate declined. If the influence of a possible channelling effect is neglected, it is possible to estimate the Sb surface concentration by comparison with the results on Sb surface segregation on single crystal surfaces of Fe - 4% Sb of defined orientation. For the same primary energy of exciting electrons, the saturation PHR were measured for single crystal surfaces of (100), (110) and (111) orientation. For the (100) oriented surface, the saturation coverage is half of a monolayer corresponding to LEED c(2x2) overlay pattern. For other surface orientations, no well defined ordered structure of surface coverage was observed. The PHR was of the same order; for (111) oriented grain 0.6, and for (100) oriented grain 0.4. In the investigated steels other solute elements such as C, S and P are present. Two or more elements can simultaneously segregate to the surface. In such cases a competition for the sites available occurs[24-32]. The relative amount of segregating elements on the surface depends on their free energy of segregation and their concentration in the bulk[29-32,347-37]. Also the kinetics of antimony surface segregation was measured (**figure 10**).

There are two possible explanations for this effect, simultaneous antimony and sulphur segregation and competition for sites available on the surface, and/or desorption from the segregated layer.

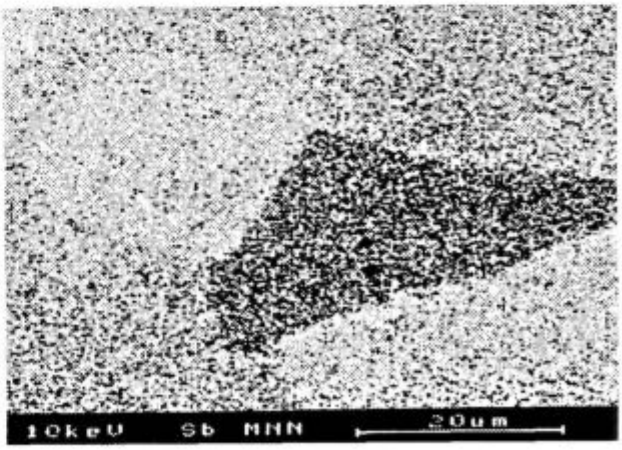

Figure 8: SAM image of the surface of steel with 0.05% Sb. A different quantity of segregated antimony was measured on grains with different orientation in the plane of the sheet

Slika 8: SAM posnetek površine jekla legiranega z 0.05%Sb. Površinska segregacija Sb je odvisna od kristalografske orientacije zrn.

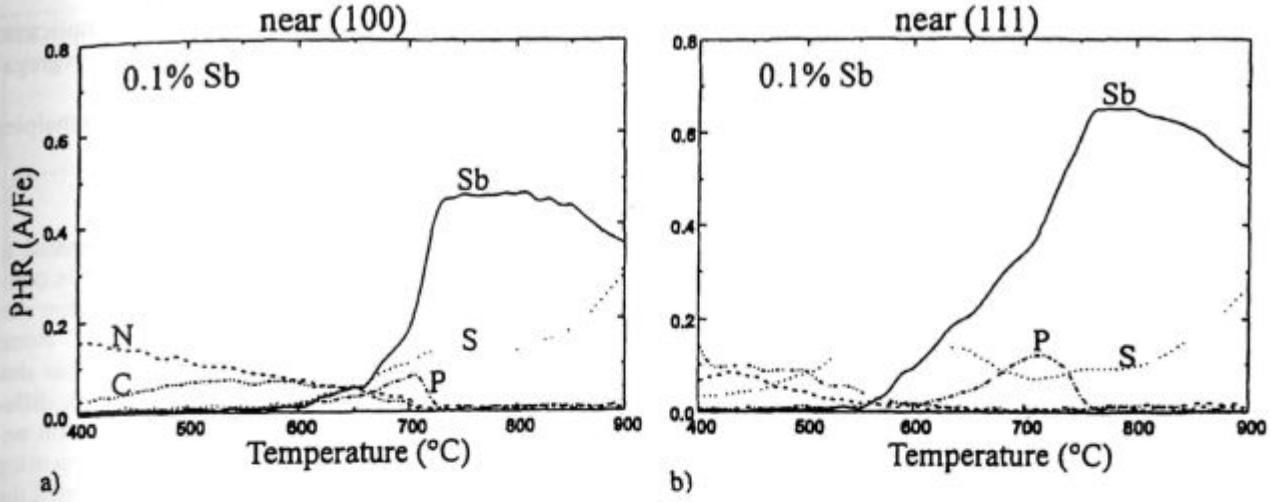

Figure 9: Temperature dependence of surface segregation on steel with 0.1% Sb on a) (100) and b) (111) oriented grain
Slika 9: Temperaturna odvisnost površinske segregacije na jeklu z 0.1%Sb a) na zrnu (100), b) na zrnu (111)

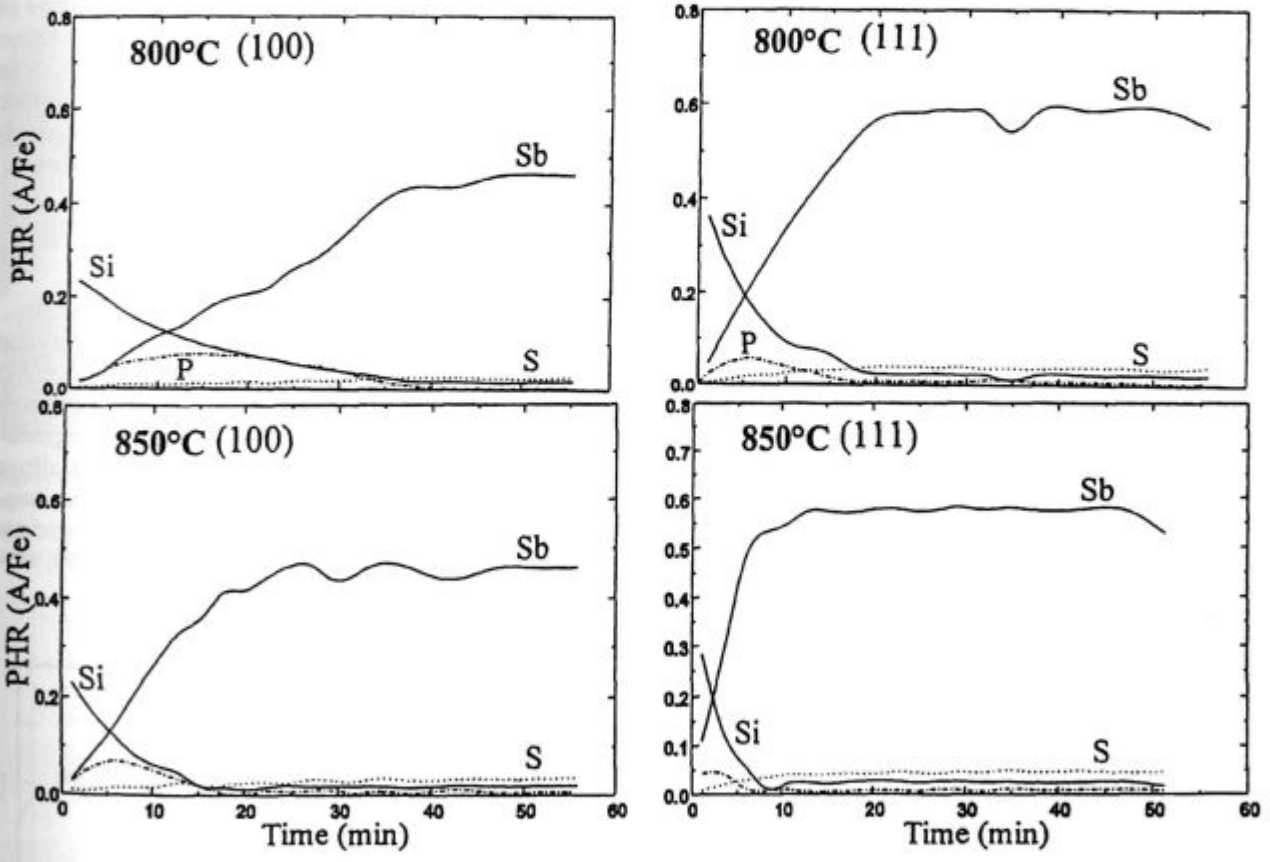

Figure 10: Sb surface segregation on steel with 0.1% Sb on a) (100) and b) (111) oriented grain at 800 and 850°C
Slika 10: Površinska segregacija Sb na jeklu z 0.1% Sb a) (100) zrno in b) (111) zrno pri 800 in 850 °C

The competitive surface segregation of antimony and sulphur is described by the following equations[25]:

$$\frac{\Theta_{Sb}}{1-\Theta_{Sb}-\Theta_S} = x_{Sb}\exp(-\Delta G_{Sb}/RT) \quad (1)$$

$$\frac{\Theta_{Sb}}{1-\Theta_S-\Theta_{Sb}} = x_{Sb}\exp(-\Delta G_S/RT) \quad (2)$$

where Θ_{Sb} and Θ_S are saturation coverage, χ_{Sb} and χ_S are mole fractions and ΔG_{Sb} and ΔG_S are free energies

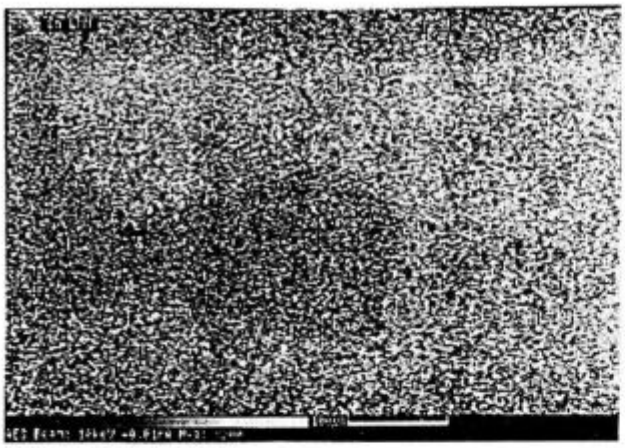

Figure 11: SAM image of the surface of steel with 0.1% Sn. A different quantity of segregated tin was measured on grains with different orientation in the sheet plane
Slika 11: SAM posnetk površine jekla z 0.1% Sn. Površinska segregacija Sn je odvisna od kristalografske orientacije zrn v ravnini pločevine.

of Sb and S surface segregation, respectively, R is the specific gas constant, and T absolute temperature.

Antimony desorption from segregated layer was established using Thermal Desorption Spectrometry -TDS at T > 750°C.

2.2.2 Tin

A scanning Auger image - SAM of non-oriented electrical steel annealed 10 minutes at 800°C was taken. The orientation of individual grains was determined by the etch pit method. **Figure 11** shows SEM and SAM images of the surface of the investigated steel. A different surface tin segregation rate on different grains was measured. Different grain orientation provided different sites for segregated tin atoms.

Figure 12 shows the temperature dependence of surface segregation of alloying and tramp elements of non-oriented electrical steel alloyed with 0.05% Sn on grain orientations (001) and (111) respectively. Electrical steel is a multicomponent system with a very complicated temperature dependence behaviour of surface segregation on binary alloys.

The relations of the surface segregation enthalpies and volume diffusivitiy are as follows:

$\Delta H^0_{Si} < \Delta H^0_C < \Delta H^0_P$ and $D^C_V >> D^{Si}_V > D^P_V$

At lower temperature, about 300°C, C segregated to the surface due to very high diffusion coefficient in comparison to Si and P, although the bulk concentration was very low, only 15 ppm. At higher temperature, C atoms were displaced by Si atoms and P while S atoms displaced silicon at higher temperatures. Their bulk diffusion coefficient is rather low, but their segregation enthalpy is very high, therefore tin started segregating significantly above 600°C. Kinetics study confirmed the orientation dependence of tin surface segregation and of the thickness of the segregated layer.

It was ascertained[17] that on grains with (100) and (111) orientation in the sheet plane, the segregation of tin was beyond one monolayer, due to the strong decrease of surface energy. On a surface with a (111) orientation FeSn intermetallic compound of one unit cell thickness was found. Our measurements showed that tin surface coverage dependence on tin bulk concentration and Θ value approached one for (100) and (111) orientations.

2.3 Grain boundary segregation

2.3.1 Antimony

Grain boundaries of FeSi steel alloyed with 0.05 and 0.1% Sb were also analyzed by AES after ageing for 200 and 500 hours at 550°C. The fracture facets were almost completely transgranular, only on some areas intergranular decohesion was noticed. In the investigated alloys there was no indication of antimony grain boundary segregation (**figure 13**). Only a negligible grain boundary segregation of other solute elements such as carbon, silicon and aluminium was established.

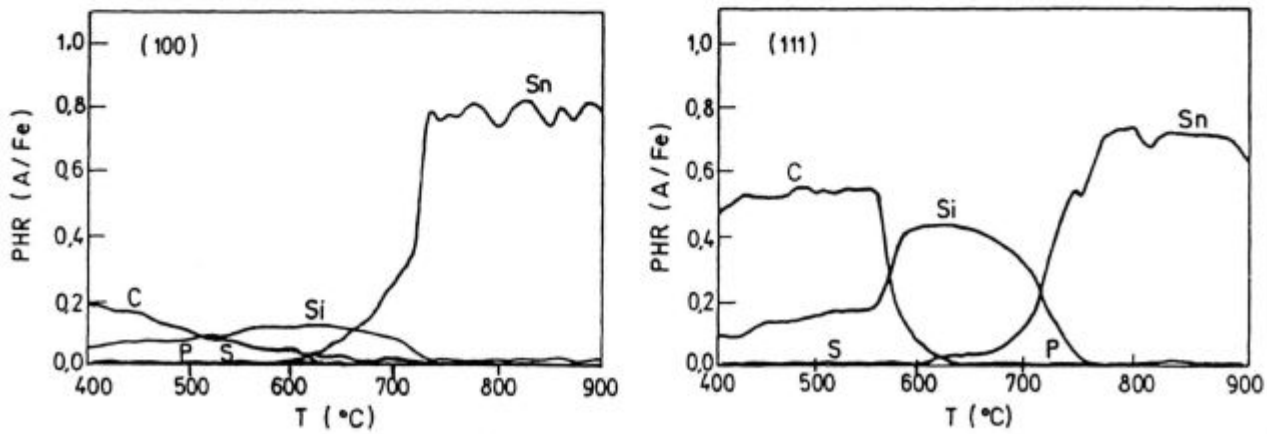

Figure 12: Temperature dependence of surface segregation on steel with 0.1% Sn on a) (100) and b) (111) oriented grains
Slika 12: Temperaturna odvisnost površinske segregacije na jeklu z 0.1%Sn a) (100) in b) (111) orientirana zrna.

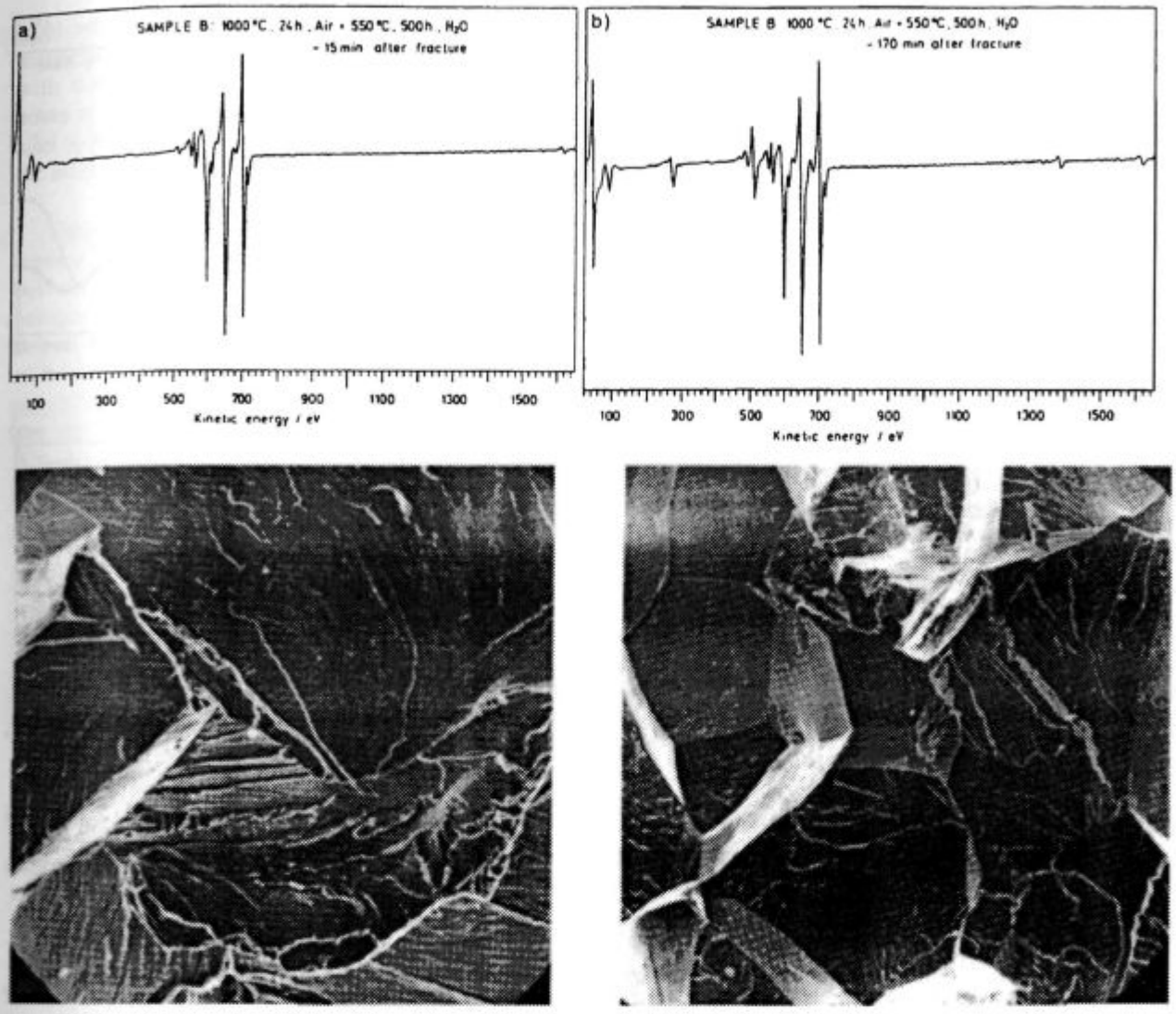

Figure 13: AES spectra taken on a) transgranular facets and SEM image of fractured sample and b) an intergranular facet of non oriented silicon steel with 0.1% Sb and SEM image of transgranular facet

Slika 13: AES spekter posnet na a) transkristalni ploskvi in SEM posnetek prelomljenega vzorca in b) interkristalni prelom silicijevega jekla za neorientirano pločevino z 0.1%Sb

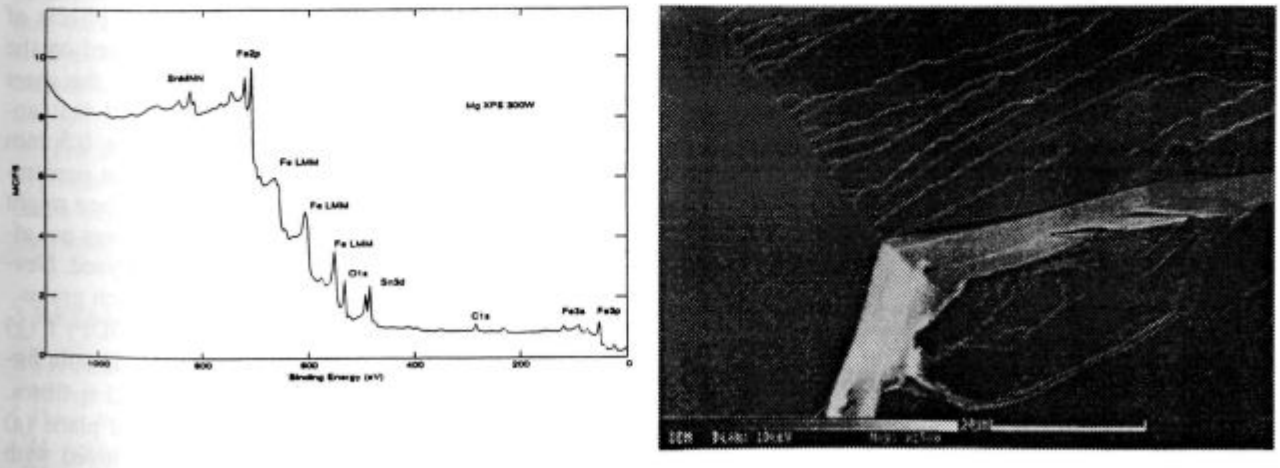

Figure 14: XPS spectra taken on intergranular facet and SEM image of fractured non oriented silicon steel with 0.1% Sn

Slika 14: XPS spekter posnet na interkristalni ploskvi in SEM posnetek prelomljenega vzorca silicijevega jekla za neorientirano elektro pločevino z 0.1%Sn

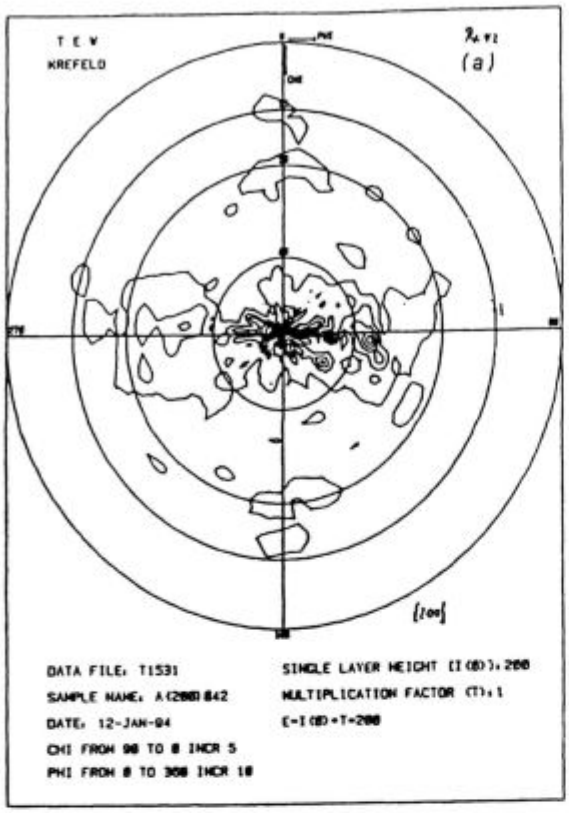

Figure 15: Pole figure of (200) grains obtained by X-ray difractometry shows the share of grains with (001)(100) texture in the steel sheet with 0.05% Sb

Slika 15: Polove figure zrn (200) narejene z rentgensko difraktometrijo prikazujejo delež zrn (001)(100) v teksturi elektro pločevine z 0.05% Sb.

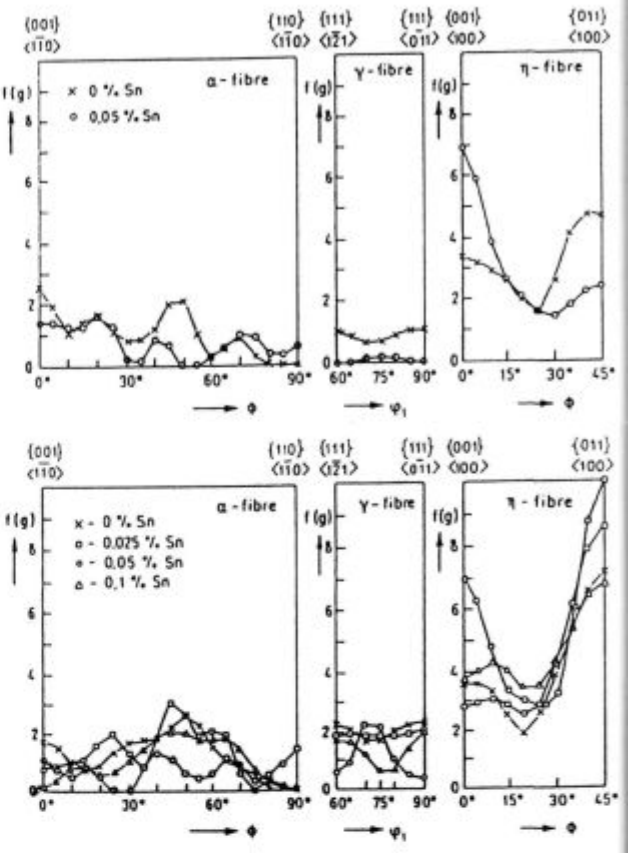

Figure 16: Texture fibres in the middle plane a) and b) on the surface of electrical steel with 0.05% Sn and without Sn

Slika 16: Tekstura vlaken v sredini vzorca a) in b) na površini elektro pločevine z 0.05% Sn in brez Sn.

2.3.2 Tin

The equilibrium segregation of tin was attained after annealing the specimen alloyed with 0.1% Sn for 200 hours at 550°C, **figure 14**.

Considering that tin is equally distributed on both fractured sides, a coverage of grain boundary surface of 0.05 ML was estimated. The scattering of results was rather large due to the strong dependence of tin segregation to grain boundary orientation. Steel alloyed with 0.05% Sn had much less intergranular facets. The evaluated equilibrium segregation was smaller than in steel alloyed with 0.1% Sn. Detailed AES analyses of free surfaces between inclusion (AlN, Al_2O_3) and matrix clearly indicated that a considerable tin segregation occurs also at their interfaces.

2.4 Texture determination

2.4.1 Antimony

The results support the hypothesis that the texture formation results from orientation dependent effects of antimony and tin on the surface energy. The texture of sheets from antimony and antimony free steels was determined by X-ray difractometry. The pole figure obtained (**figure 15**), shows that only a small share of grains with (001)(100) texture was found in the investigated 0.05% Sb steel.

2.4.2 Tin

The results support the hypothesis that the texture formation results from orientation dependent effects of tin on surface energy. The texture was measured on the surface and in internal plane after the half of the sheet thickness was removed. Taking into account that approximately six crystal grains constitute the 0.5 mm thick cross-section steel sheet and the fact that penetration depths of X-rays was less than 0.01 mm one might conclude that also some grains whose growth was not affected by the surface tin segregation were analysed. Nevertheless, there were not more than 10% of such grains.

The orientation distribution functions (ODF) f (g) were calculated from the (200), (110) and (211) pole figures. The textures were presented as α, γ and η fibres. **Figure 16** shows texture fibres in the internal plane (a) and on the surface (b) of electrical steels alloyed with and without tin. The volume fraction of grains with the (100) planes measured on the surface and in the middle plane increased by the order of two when compared the

steel without tin and the steel with 0.05% tin. Softer magnetic orientations were found on the surface. Steel with 0.05% Sn, which had previously been aged 25 hours at 550°C, showed an increase of (100) planes parallel to the rolling direction by three times, compared to the steel without tin.[36]

During annealing antimony and tin segregated at steel surface at temperatures T > 650°C. A strong correlation between the antimony or tin surface segregation and the orientation of the grains at the sheet surface was established. The maximum equilibrium Sb surface segregation of 0.6 monolayer was measured after annealing at 750°C on grains with the (111) crystallographic orientation in the sheet plane. The maximum equilibrium Sn segregation on the surface was reached also at 750°C and approached in the majority of orientations one monolayer.

Grain boundary segregation of antimony and other solute elements, such as C, S, P, Al and Si were negligible in non oriented silicon steel with 0.05 and 0.1% Sb.

Tin surface segregation was much higher than grain boundary segregation. At equilibrium grain boundary segregation only 7 and 3% of tin atoms were found on a grain boundary for steel alloyed with 0.1 and 0.05% Sn, respectively.

Antimony as well as tin surface segregation decreased the surface energy of grains with (100) surface orientation in the sheet plane, and these grains grow on account of grains with other surface crystallographic orientations, such as (110) and (111). Only a certain level of surface segregation promoted selective grain growth. By excessive surface coverage of segregated atoms, the surface energy of all orientations is not affected selectively and no preferential grain growth is obtained.

Textures represented as sections through three-dimensional orientation distribution space in fixed directions showed that the volume fraction of magnetically soft grains increased for three times in tin steel sheets when compared to steel without tin. Better textures were obtained near the surface than in the middle plane of 0.5 mm thick steel sheet. The best results were obtained for steel alloyed with 0.05% Sn. It is concluded that only a certain level of segregation promoted the desired selective grain growth.

The results of the present investigation support the hypothesis that the texture formation results from orientation dependent effects of antimony and tin on the surface energy.

3 REFERENCES

[1] I. P. Csorba, *Image Tubes*, Howard W. Sams, Indianapolis 1985

[2] M. Jenko, *Surface phenomena at Fluxless vacuum soldering* Ph.D Thesis, University of Ljubljana, Ljubljana 1988

[3] M. Jenko, B. Erjavec, B. Praček, *Vacuum*, 40 (1990) 77

[4] M. Jenko, S. Jerič, B. Praček, B. Erjavec, *Vuoto*, Vol. XX. N2 (1990) 350

[5] D. Brigs, M. P. Seah Eds, *Practical Surface Analysis, Vol. 1 Auger and X-ray Photelectron Spectroscopy* 2nd Edition, John Wiley&Sons Chichester 1994

[6] R. C. Weast, M. J. Astle, Eds, CRC Handbook of Chemistry and Physics, 76th Edition, Chemical Rubber, Palm beach 1995/96

[7] O. Kubaschewski, C. B. Alcock, P. J. Spencer, *Materials Thermochemistry*, 6th Edition, Pergamon, Oxford 1993

[8] H. J. Grabke, *Iron and Steels, ISIJ Int.*, 35 (1995) 2, 95-113

[9] G. Lyudkovski, P. K. Rastogi, *Metall. Trans. A.*, 15A (1984) 257

[10] H. Shimanaka, T. Irie, K. Matsumura and K. Nakamura, *J. Magn. Magn. Mat.*, 19 (1980) 63

[11] P. Marko, A. Šolyom, V. Frič, *J. Magn. Magn. Mat.*, 41 (1984)

[12] S. Nakashima, K. Takashima, J. Harase and K. Kuroki, *J. Japan Inst. Metals*, 55, (1991) 12, 1392-1399

[13] F. Vodopivec, F. Marinšek, D. Gnidovec, B. Praček, M. Jenko, *J. Magn. Magn. Mat.*, 97 (1991) 281

[14] F. Kovač Niznik, *Metallography 95*, Proceedings, Slovakia, April 1995, Paper 14, 84-87

[15] M. Jenko, F. Vodopivec, B. Praček, *App. Surf. Sci.*, 70/71 (1993) 118

[16] M. Jenko, F. Vodopivec, B. Praček, M. Godec and D. Steiner, *J. Mag. Mag. Mat.*, 133 (1994) 229

[17] M. Jenko, F. Vodopivec, H. J. Grabke, H. Viefhaus, B. Praček, M. Lucas, M. Godec, *Steel Research*, 65 (1994) 11, 500

[18] M. Jenko, H. Viefhaus, M. Lucas F. Vodopivec, M. Godec, D. Steiner Petrovič, M. Milun, T. Valla, *Metals, Alloys, Technologies*, 28 (1994) 4, 561-565

[19] M. Jenko, F. Vodopivec, H. Viefhaus, M. Godec, D. Steiner Petrovič, *Journal de Physique IV*, Colloque C7, 5, novembre 1995, C7-225-231

[20] R. Mast, H. J. Grabke, M. Jenko and M. Lukas, in print

[21] P. Ševc, J. Janovec, M. Lucas, H. J. Grabke, *Steel Research*, 66 (1995) 12, 537-542

[22] Rusenberg, H. Viefhaus, *Surf. Sci.*, 172 (1986) 615

[23] H. Viefhaus and M. Rüsenberg, *Surface Science*, 159 (1985) 1-23

[24] H. Viefhaus, *Analytica Chimica Acta*, 297 (1994) 43-53

[25] H. J. Grabke, *Kovine, zlitine, tehnologije*, (1993) 1-2, 9

[26] C. Lea, M. P. Seah, *Phil. Mag.*, 35 (1977) 1, 213

[27] E. D. Hondros, M. P. Seah, *Metal Trans.*, 8A (1977) 1363

[28] C. L. Briant, M. Ritter, *Acta metall.*, 32 (1984) 2031

[29] P. Gas, M. Guttman, J. Bernardini, *Acta metall.* 30 (1982) 1309

[30] K. Iwayama, K. Kuroki, Y. Yoshitomi, K. Homma and T. Wada: *J. Appl. Phys.*, 55 (1984) 2134

[31] V. Rüsenberg, H. Viefhaus, *Surf. Sci.*, 172 (1986) 615

[32] Beguinot and P. Lesbats, *Metalography*, 10 (1977) 115-119

[33] M. Godec, M. Jenko, F. Vodopivec, M. Ambrožič, Đ. Mandrino, L. Kosec, M. Lovrečič Saražin, *Kovine, zlitine, tehnologije*, 28 (1994) 1-2, 105-109

[34] W. Jager, H. J. Grabke, R. Möller, *4th International Conference*, Portorož, Jugoslavija, 1985

[35] H. De. Rugy and H. Viefhaus, *Surface Science*, 173 (1986) 418-438

[36] M. Godec, The influence of the segregated tin on the recrystalization behaviour of non oriented electrical steel sheet, PhD Thesis, University of Ljubljana, Ljubljana 1997

[37] D. Marton, J. Fine, *Optical Socoiety of America, Technical Digest*, 3 (1992) 146-148

[38] M. H. Mintz, P. Shukeer, J. Fine, *Surface Science Letters*, 238 (1990) L473-L477

Acknowledgement

The investigation was supported by the Ministry of Science and Technology of Slovenia, Contract No J2-7228-96.

I M T®
INŠTITUT ZA KOVINSKE MATERIALE IN TEHNOLOGIJE
INSTITUTE OF METALS AND TECHNOLOGY

1001 LJUBLJANA, LEPI POT 11, SLOVENIJA, POB 431
Phone.: +386 61/125 11 61, Fax: +386 61/213 780

VACUUM HEAT TREATMENT LABORATORY

Vacuum Brazing

Universally accepted as the most versatile method of joining metals. Vacuum Brazing is a precision metal joining technique suitable for many component configurations in a wide range of materials.

ADVANTAGES

- Flux free process yields clean, high integrity joints
- Reproducible quality
- Components of dissimilar geometry or material type may be joined
- Uniform heating & cooling rates minimise distortion
- Fluxless brazing alloys ensure strong defect free joints
- Bright surface that dispense with expensive post cleaning operations
- Cost effective

Over five years of Vacuum Brazing expertise at **IMT** has created an unrivalled reputation for excellence and quality.

Our experience in value engineering will often lead to the use of Vacuum Brazing as a cost effective solution to modern technical problems in joining.

INDUSTRIES

- Aerospace
- Mechanical
- Electronics
- Hydraulics
- Pneumatics
- Marine
- Nuclear
- Automotive

QUALITY ASSURANCE

Quality is fundamental to the **IMT** philosophy. The choice of process, all processing operations and process control are continuously monitored by **IMT Quality Control Department**.

The high level of quality resulting from this tightly organised activity is recognised by government authorities, industry and International companies.

ISSN 1318-0010
KZLTET 31(6)519(1997)

THE NEW RESEARCH EQUIPMENT FOR SURFACE CHARACTERIZATION OF MATERIALS AT THE INSTITUTE OF METALS AND TECHNOLOGY, LJUBLJANA

NOVA RAZISKOVALNA OPREMA ZA RAZISKAVE POVRŠIN TRDNIH SNOVI NA IMT, LJUBLJANA

MONIKA JENKO

Institute of Metals and Technology, Lepi pot 11, Ljubljana, Slovenia

At the INSTITUTE OF METALS AND TECHNOLOGY, LJUBLJANA is installed a field emission scanning Auger microprobe MICROLAB 310-F of VG Scientific from UK for research of solid surfaces, grain boundaries and phases, micro analysis of materials as well as research of physical phenomena on the free surfaces of metals and inorganic materials: adsorption, segregation of surface active elements, oxidation, corrosion, characterization of thin films, recrystallization, catalysis etc.

The new instruments allows the following methods:

- Auger Electron Spectroscopy - AES
- Scanning Auger Electron Spectroscopy - SAM
- Secondary Electron Microscopy - SEM
- Reflected Electron Energy Loss Spectroscopy - REELS
- X-Ray Photoelectron Spectroscopy - XPS

One of the most important features of Microlab 310-F is its high spatial resolution in both SEM and SAM. It has field emission electron source with very high brightness, high performance electron column, very low drift stage simultaneous peak and background acquisition when mapping and image registration software.

Microlab 310-F has a spherical sector analyser which can be operated with high energy resolution. Adding a dual anode X-ray source therefore allows the instrument to perform high quality XPS analysis. The instrument is fitted with high quality ion gun, which allows the ability to perform high quality, rapid depth profiles.

The instrument is additionally equipped with fracture stage. This device allows the fracturing of specially

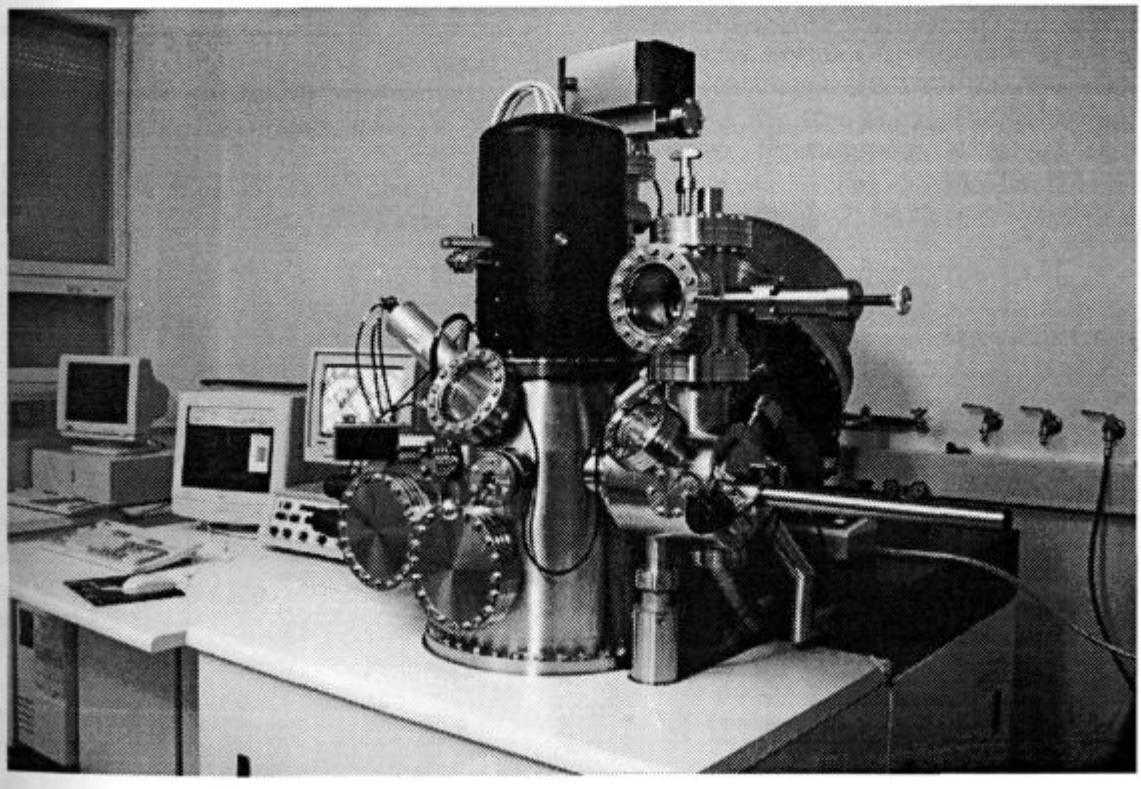

Figure 1: Microlab 310-F, AES/XPS instrument installed at the Institute of Metals and Technology Ljubljana

Figure 2: A view through the monitoring window into the UHV analysis chamber on the sample, electron gun, ion gun and X-Ray source (see cover)

shaped brittle samples in UHV; the stage allows that both halves of the fractured samples can be collected for analysis.

The purchase of instrument was financially supported by industrial partners, research institutes and university:

- Institute of Metals and Technology; Ljubljana
- Institute Jožef Stefan, Ljubljana
- National Institute of Chemistry, Ljubljana
- Concern Slovenian Steelworks, Ljubljana
- Nuclear Power Plant Krško
- Kolektor, Idrija
- Talum Kidričevo,
- Impol, Slovenska Bistrica
- Department for Materials and Metallurgy, University of Ljubljana
- Centre for Tribology and Technical Diagnostic, Faculty of Mechanical Engineering, University of Ljubljana

The purchase was subsidized by Ministry of Science and Technology of Republic Slovenia.

ISSN 1318-0010
KZLTET 31(6)521(1997)

INFLUENCE OF HEAT TRANSFER DYNAMICS ON HARDNESS DISTRIBUTION AFTER QUENCHING

VPLIV DINAMIKE PRENOSA TOPLOTE NA PORAZDELITEV TRDOTE PO KALJENJU

BOŽIDAR LIŠČIĆ

Faculty of Mechanical Engineering and Naval Architecture, Ivana Lučića 5, Zagreb, Croatia

Prejem rokopisa - received: 1997-10-01; sprejem za objavo - accepted for publication: 1997-10-21

The pattern of hardness distribution on round bars' cross-section after quenching was studied in relation to the change of heat transfer on the workpiece surface. It was found that a 'delayed quenching', producing a discontinuous change of cooling rate, may result in higher hardness in the core, than at the surface. This phenomenon called 'inverse hardening' has been theoretically explained by Shimizu and Tamura. It depends on: hardenability of the steel, cross-section size of the workpiece and on quenching condition, and is related to the incubation period consumed before the cooling rate was changed. Own experiments using cylindrical specimens of 50 mm Dia, made of AISI-4140 steel, have shown that Controllable Delayed Quenching (CDQ) technology has a great potential to increase the depth of hardening, compared to conventional quenching practice. Bending fatigue tests with inverse hardened and tempered specimens have shown a significant increase of the fatigue life compared to specimens having normal hardness distribution after quenching. CDQ-technology and 'inverse hardening' can reproducibly be realized using adequate steel hardenability and cross-section size of the workpiece, by quenching in PAG polymer-solution of high concentration, or in high pressure-circulated gases.

Key words: quenching, heat transfer

Raziskane so bile značilnosti porazdelitve trdote na preseku kaljene okrogle palice v odvisnosti od spremembe prenosa toplote na površini palice. Kaljenje z zadržanjem, ki povzroča diskontinuirno spremembo hitrosti ohlajanja, lahko ustvari večjo trdoto v jedru kot na površini. Ta pojav imenovan "inverzna utrditev" sta teoretično razložila Shimizu in Tamura. Odvisen je od kaljivosti jekla, preseka kaljenca in od pogojev kaljenja ter je povezan z inkubacijsko dobo, ki je bila porabljena pred spremembo hitrosti ohlajanja. Naši poiskusi na valjastih vzorcih ϕ 50 mm iz jekla AISI-4140 so pokazali, da ima "kontrolirano kaljenje z zadržanjem" velik potencial za povečanje globine kaljenja v primerjavi s klasičnim kaljenjem. Upogibni utrujenostni preizkusi na inverzno kaljenih in popuščenih vzorcih so pokazali pomembno povečanje življenjske dobe v primerjavi z vzorci z normalno porazdelitvijo trdote po kaljenju. CDQ - tehnologija in "kaljenje z zadržanjem" sta lahko reproduktibilna, če ima jeklo primerno kaljivost in je presek kaljenca ustrezen s kaljenjem v polimerni PAG raztopini velike koncentracije ali v visokotlačni krožeči atmosferi.

Ključne besede: kaljenje, prenos toplote

1 INTRODUCTION

The practice of quenching ferrous metals has a very long history, but development of quenching technology was first of all concentrated on choosing the proper quenchant and quenching parameters, i.e. its temperature and possibly the agitation rate. Once this was fixed for a specific case, the heat transfer from the workpiece surface was governed solely by the selected quenchant and quenching parameters. Generally the idea prevailed that, for achieving a better through-hardening, a more severe quenching intensity should be applied right at the beginning of quenching. If workpieces having bigger cross-section have to be hardened through, the heat extraction from the core is the main problem. All efforts were concentrated on shortening the quenching time i.e. cooling the core of the workpiece, if possible, below M_s temperature before (according to the hardenability of the steel used) the transformation to ferrite and pearlite begins. As a result of applying a severe quenchant, high temperature gradients developed causing high thermal stresses and distortion. Using this approach two factors on which the through hardening depends, have not been taken into consideration:

a) The cooling rate in every specific point of the cross-section from the austenitizing temperature to the transformation temperature (A_1) is not critical for the microstructure and hardness after quenching. Instead the cooling rate below A_1 to the M_s point is critical, and *different points* of the cross-section pass through this temperature range (A_1 to M_s) at *different times*.

b) When severe quenching intensity is applied right from the beginning of the quenching process, the surface temperature of the workpiece is rapidly decreased to low values while the core still retains high temperature. So, when heat has to be extracted from the core, the temperature difference between surface temperature of the workpiece (T_s) and the quenchant temperature (T_0) is low and according to the Newton's law $\dot{q} = \alpha\ (T_s - T_0)$, the heat extracted is also low. This situation can only be improved if the heat transfer (characterized by the heat transfer coefficient α (W/m^{2}K)) would be increased later during quenching, but this is not the case in normal quenching practice.

In 1977 the investigation published in USA by Loria[1] has shown that 'delayed quenching' can in some instances increase the depth of hardening, compared to conventional quenching practice. 'Delayed quenching'

means a relatively slow heat transfer from the workpiece surface at the beginning of quenching, followed by a fast cooling with high quenching intensity.

In the same time in Japan, Shimizu and Tamura[2,3] have given theoretical explanation of this phenomenon stating that it is caused by *discontinuous* change in cooling rate and the incubation period (at relevant temperature) consumed, before the cooling rate was abruptly changed. Latter, experimental investigation by Liščić and Totten[4] on one side, and numerical calculation by Chen and Zhou[5] on the other side, have shown that at 'delayed quenching' the average cooling rate may be higher below the surface of the workpiece, than at the surface itself. While in case of normal quenching (without discontinuous change of cooling rate) the cooling rates constantly decrease from the surface towards the core, in case of 'delayed quenching' the cooling rate is lower at the surface (because of mild cooling at the beginning of the quenching process), becoming greater below the surface towards the core because of the latter abrupt change of heat transfer at the workpiece surface.

Through these works it became evident that *the heat extraction dynamics* during quenching, and not the quenching time itself is responsible for the hardness distribution on the worpiece's cross-section after quenching.

Studying the pattern of hardness distribution on round bars' cross-section after quenching Shimizu and Tamura[3] have introduced the expression of 'inverse' hardening. Opposite to normal hardness distribution it shows lower hardness at the surface and higher hardness in the core.

The experiments have shown that the 'inverse' hardness distribution caused by the phenomenon of 'delayed quenching', depends on steel hardenability and on cross-section size of the workpiece. They have also shown that (in case of adequate hardenability and corresponding cross-section size) the 'delayed quenching' has a great potential to increase the depth of hardening, compared to conventional quenching practice.

Chen and Zhou[5] state also that 'delayed quenching' can reduce residual stresses and distortion. This state of the art gives, in some instances, the possibility to achieve the biggest possible depth of hardening, simultaneously with minimum residual stress and distortion, by a Controllable Delayed Quenching.

When quenching in evaporable liquid quenchants, however, the possibility to control a preprogrammed cooling cycle and cause intentionally a 'delayed quenching' is very limited, because the only parameter that can be changed *during* the quenching process is the agitation rate.

Among all liquid quenchants only the PAG polymer-solutions possess a mechanism that enables them to realize a preprogrammed Controllable Delayed Quenching by changing the polymer concentration. The advantage of PAG solution quenchants seams to be that it is possible to achieve the proper balance of the film thickness and film strength, depending of course on two other parameters, namely the bath temperature and the agitation rate. As it is well known higher polymer concentration gives thicker film on the workpiece surface, prolonging the vapor blanket stage i.e. causing a 'delayed quenching'.

Recently, Liščić, Grubišić and Totten[6] have shown that bending fatigue as well as impact strength of mechanical components can be increased by 'delayed quenching'.

2 HEAT EXTRACTION DYNAMICS

It is interesting to analyse why 20 years have passed since the phenomenon of 'delayed quenching' was first published by Loria and by Shimizu and Tamura until a Controllable Delayed Quenching of real components has been investigated more in details. The answer may be found in two following reasons:

a) There was no an adequate method to test and record the quenching intensity during quenching in real practice, that could describe the heat extraction dynamics. Neither the magnetic quenchometer method, nor the cooling curve analysis of small diameter (12.5 mm Dia x 60 mm length) inconel or silver specimens can describe the heat extraction dynamics when quenching real components.

b) Only just recent investigations[7] have revealed that polymer solutions (PAG) of higher concentration can be used as a quenchant for preprogrammed Controllable Delayed Quenching.

The newly developed Temperature Gradient Quenching Analysis System (TGQAS) using the LISCIC/NANMAC probe[8] of 50 mm Dia x 200 mm length, made of AISI-304 steel, representing a real workpiece, is capable of measuring, recording and evaluation of every quenching process in workshop practice, describing the heat extraction dynamics by corresponding thermodynamic functions. The probe itself is instrumented with three thermocouples at the mid-length cross-section, measuring the temperature at the very surface, 1.5 mm below surface and in the center.

Figure 1 shows cooling curves recorded in two quenching tests: TEST-1 mineral oil of 20°C without agitation and TEST-26 PAG polymer-solution (UCON-E) of 25% concentration, 40°C bath temperature and 0.8 m/s agitation rate. **Figure 2** shows calculated heat flux density vs. time between different thermocouple positions.

The characteristic feature in each of quenching tests with regard to heat extraction dynamics is the time period from the immersion up to the moment the maximum heat flux density occurs (t_{qmax}).

While for particular oil quenching (TEST-1) t_{qmax} is 14 seconds it is for the described polymer-solution quenching (TEST-26) 72 seconds. The latter one is obviously a 'delayed quenching'.

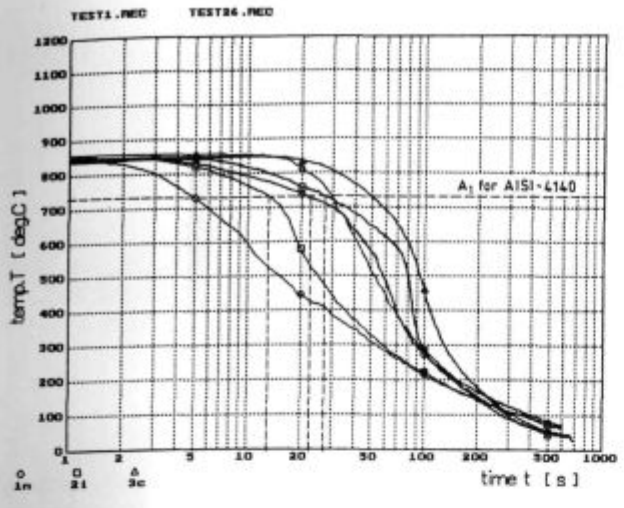

Figure 1: Two quenching tests recorded by the LISCIC/NANMAC probe (50 mm Dia x 200 mm): TEST-1 - mineral oil, 20°C, without agitation; TEST-26 - PAG polymer-solution (UCON-E), 25%, 40°C, 0.8 m/s agitation rate. Cooling curves for: surface (○), 1.5 mm below surface (□) and center (Δ)

Slika 1: Dva preizkusa kaljenja registrirana z LISCIC/NANMAC preizkušancem (ϕ 50 x 200 mm). Pr. 1 - mineralno olje, 20°C, brez mešanja: Pr. 26 - PAG raztopina (UCON-E), 25%, 40°C, hitrost mešanja 0.8 m/s. Ohlajevalne krivulje za površino (○), 1.5 mm pod površino (□) in sredino (Δ)

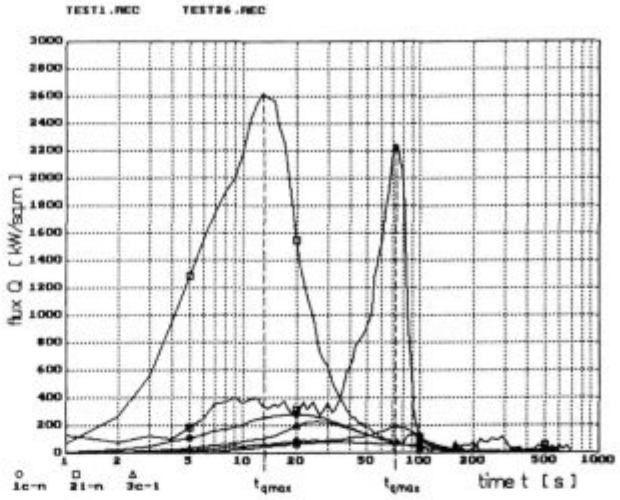

Figure 2: Heat flux densities vs. time for TEST-1 and TEST-26 calculated from recorded cooling curves. Heat flux density between 1.5 mm below surface and the surface itself (□); between center and surface (○); between center and 1.5 mm below surface (Δ)

Slika 2: Gostota toplotnega toka v odvisnosti od časa za pr. 1 in 26 izračunana iz ohlajevalnih krivulj. Gostota toplotnega toka med globino 1.5 mm in površino (□), med sredino in površino (○) ter med sredino in globino 1.5 mm (Δ)

quenching (TEST-26) 72 seconds. The latter one is obviously a 'delayed quenching'.

Because the heat flux density (W/m²) is the real physical measure of the heat extraction, it is interesting to analyse and compare the heat flux density (between 1.5 mm below surface and the surface itself) v.s. time curves for both mentioned tests, shown in **Figure 2**. For particular oil quenching (TEST-1) only 12.5 seconds, right in the beginning of the quenching process, were necessary for increasing the heat flux density from a low value of 200 kW/m² to its maximum of 2600 kW/m², and 35 seconds were necessary for the heat flux density to fall back to 200 kW/m². For particular polymer-solution quenching (TEST-26), 67 seconds or 5.4 times more were necessary for increasing the heat flux density from 200 kW/m² to its maximum of 2250 kW/m², but only 23 seconds or 1.5 times less were necessary for the heat flux density to fall back to 200 kW/m².

This analysis clearly shows a distinct difference in heat extraction dynamics between the described oil quenching characterized by a fast cooling from the beginning, and the described polymer-solution quenching characterized by a long period of relatively slow cooling followed by a sudden change in heat extraction, after burst of the polymer film, which has caused a pronounced discontinuous change in the cooling rate, having a specific influence on transformation behavior of the steel concerned.

The discontinuous change in cooling rate, when quenching in the used polymer solution (TEST-26) can be seen in **Figure 1** as a distinct change in the slope of the cooling curve for the thermocouple at 1.5 mm below surface, at 570°C.

The best way to compare the heat transfer dynamics between both described tests is to compare the amount of heat extracted at different time intervals after immersion of the probe. The curves marked with □ in **Figure 3** represent the values of the integral (∫qdt) below the heat

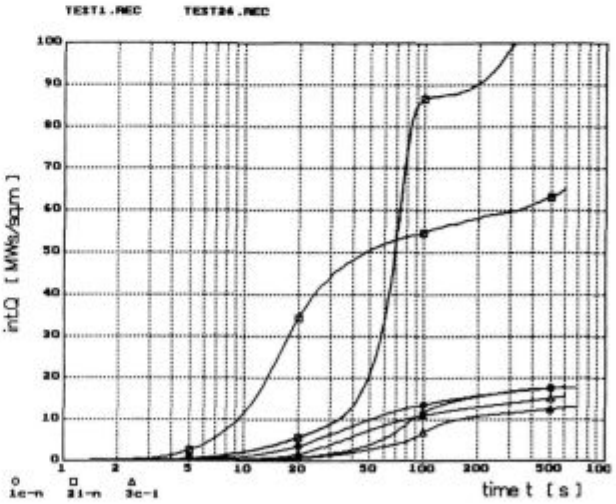

Figure 3: Integral (∫qdt) below heat flux density curves vs. time for TEST-1, and TEST-26, representing the amount of heat extracted. Heat extracted between 1.5 mm below surface and the surface itself (□); between center and surface (○); between center and 1.5 mm below surface (Δ)

Slika 3: Integral (∫qdt) toplotnega toka v odvisnosti od časa za pr. 1 in 26, ki predstavlja ekstrahirano toploto. Toplota ekstrahirana med globino 1.5 mm in površino (□), med sredino in površino (○) ter med sredino in globino 1.5 mm (Δ)

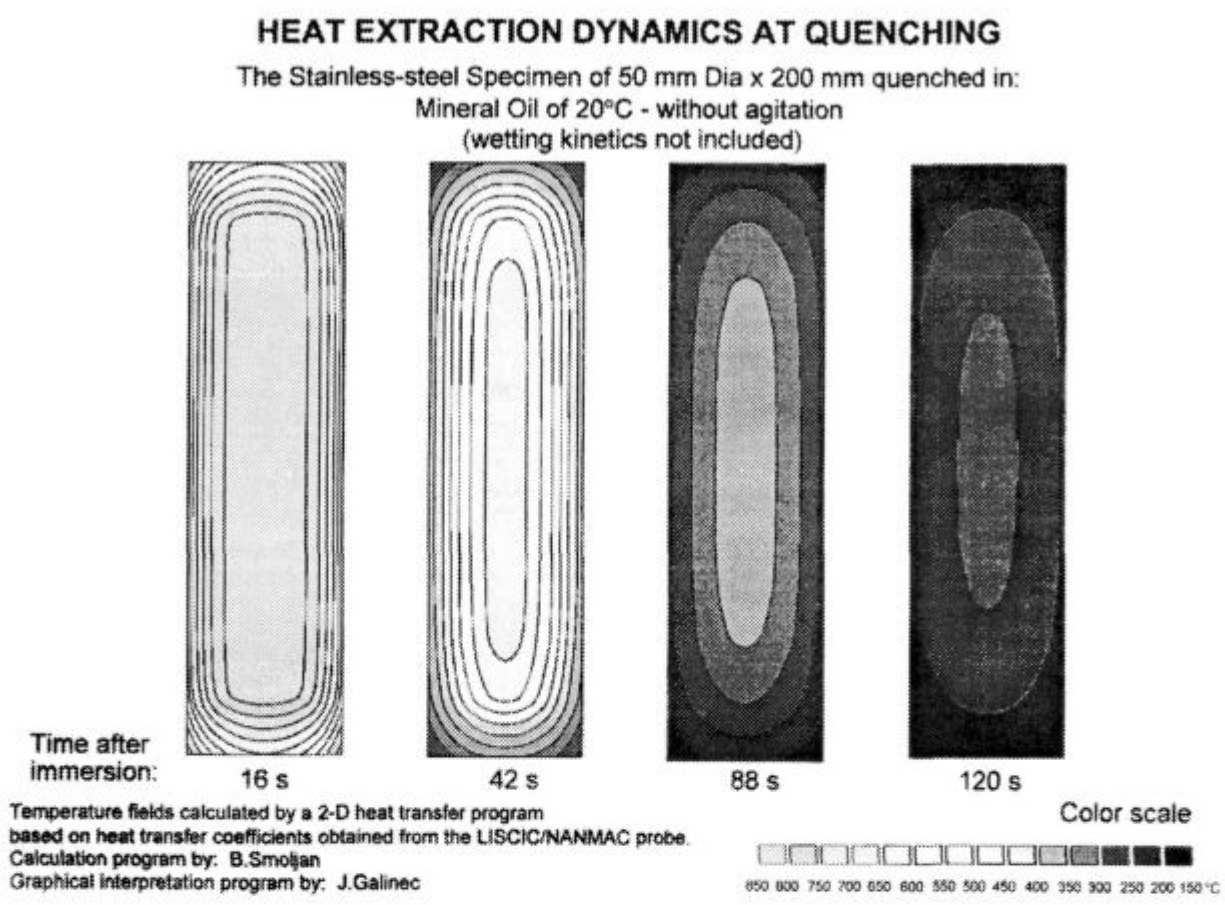

Figure 4: 2-D simulation of temperature fields when quenching the stainless steel specimen of 50 mm Dia x 200 mm in standard mineral oil of 20°C, without agitation. The calculation is based on heat transfer coefficients obtained from the LISCIC/NANMAC probe

Slika 4: 2-D simulacija temperaturnega polja med kaljenjem preizkušanca ϕ 50 x 200 mm iz nerjavnega jekla v standardnem mineralnem olju in brez mešanja. Izračunano na osnovi koeficientov prenosa toplote pridobljenih z LISCIC/NANMAC sondo

extracted (MJ/m^2), vs. time. In oil quenching (TEST-1), the amount of heat extracted starts to rise immediately in third second after immersion, reaching already after 20 seconds a value of 35 MJ/m^2. During next 80 seconds it amounted to 55 MJ/m^2. In the used polymer-solution quenching (TEST-26) only 5 MJ/m^2 was extracted until 20 seconds, but in next 80 seconds it reached 87 MJ/m^2.

Using the heat transfer coefficient vs. time values calculated from the measured temperatures at the mid-length cross-section of the LISCIC/NANMAC probe, a 2-D heat transfer programme was developed for calculating temperature fields during quenching. **Figure 4** shows a graphical presentation of the cooling a stainless steel specimen of 50 mm Dia x 200 mm length at: 16, 42, 88 and 120 seconds by quenching it in mineral oil of 20°C without agitation (TEST-1). **Figure 5** shows the same when quenching the specimen in PAG polymer-solution (UCON-E) of 25% concentration, 40°C bath temperature and 0.8 m/s agitation rate (TEST-26). Comparison of **Figure 4** and **Figure 5** clearly reveals the difference in heat extraction dynamics between those two tests.

It should be emphasized that for transformation kinetics not the cooling rates from austenitizing temperature to A_1, but the *cooling rates below* A_1, are critical. For the steel grade AISI-4140 e.g. the A_1 temperature is 730°C. Analysing the average radial temperature gradients between core and surface in half length cross-section from **Figure 4** and **Figure 5** respectively, one gets the values given in **Table I**.

Table I

Austenitizing temperature: 850°C; Radius of specimens: 25 mm					
Time after immersion (seconds)		16	42	88	120
Average temperature gradient between core and surface in half length cross-section °C/mm	TEST-1	10	12	6	4
	TEST-26	2	4	10	6

From the calculated temperature fields in **Figure 4** and **Figure 5** respectively, and the values given in **Table I** we can derive the following:

In TEST-1 (normal case of quenching with continuous cooling rates), a cooling within the critical tempera-

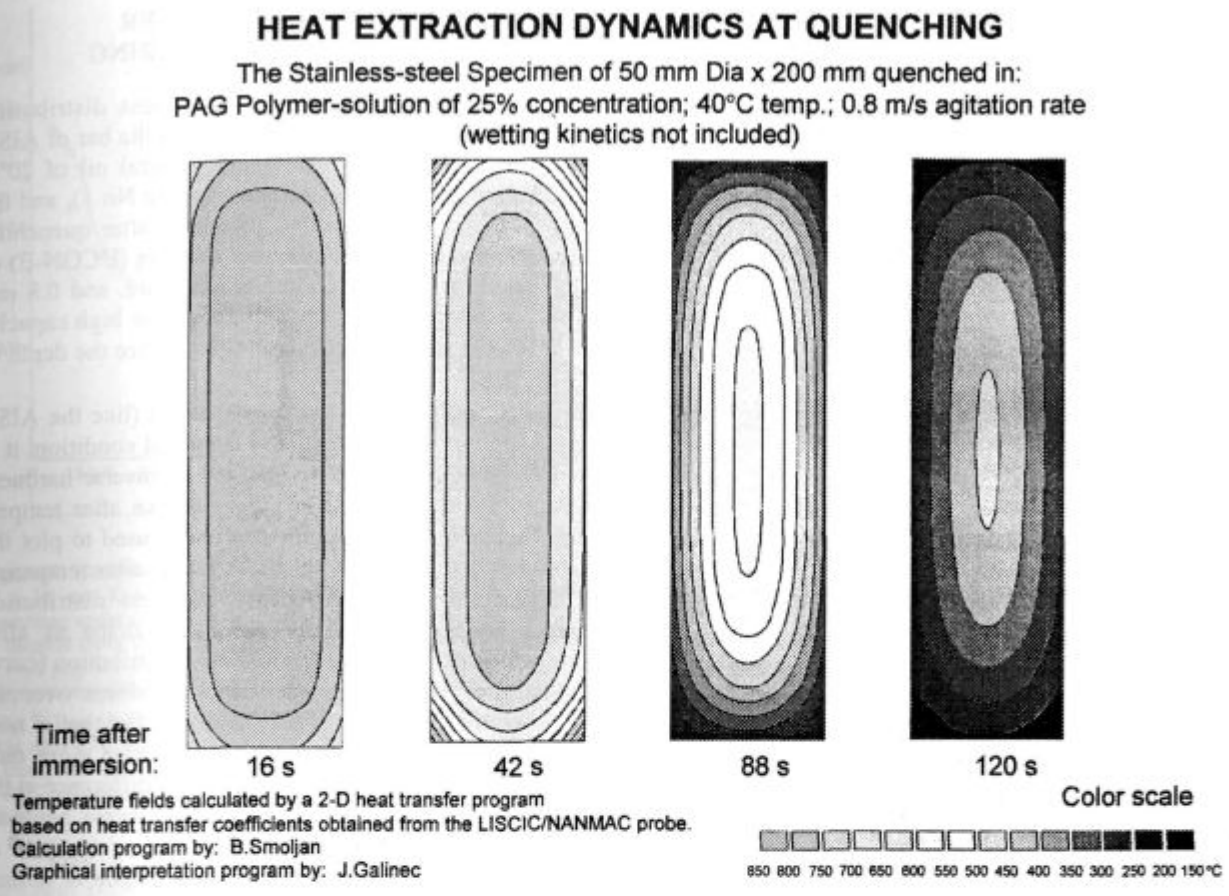

Figure 5: 2-D simulation of temperature fields by quenching the stainless steel specimen of 50 mm Dia x 200 mm in PAG polymer-solution (UCON-E) of 25% concentration; 40°C; 0.8 m/s agitation rate. The calculation is based on heat transfer coefficients obtained from the LISCIC/NANMAC probe

Slika 5: 2-D simulacija temperaturnega polja pri kaljenju preizkušanca ϕ 50 x 200 mm iz nerjavnega jekla v PAG polimerni raztopini (UCON-E) s koncentracijo 25%, 40°C in hitrostjo mešanja 0.8 m/s. Izračunano z uporabo koeficientov prenosa toplote pridobljenih z LISCIC/NANMAC sondo

ture range (700°C to 400°C) for the core, between 42 and 88 seconds is obtained with a decreasing temperature gradient, i.e. decreasing heat extraction flux from the core to the surface. Once the surface temperature has fallen to low values (about 200°C after 88 sec.), the heat transfer has decreased very much, because of the small temperature difference between the workpiece surface and the surrounding fluid. This heat extraction dynamics results in the normal hardness distribution i.e. substantially lower core than surface hardness.

In TEST-26 (a delayed quenching with discontinuous change of cooling rates), cooling of the core from 42 to 88 sec. (i.e. between 750°C and 600°C) is obtained with increasing temperature gradient, i.e. increasing the heat extraction flux from the core to the surface, resulting in increased core hardness.

3 TRANSFORMATION KINETICS WHEN DISCONTINUOUS CHANGE OF COOLING RATE OCCURS

From the moment the austenitized workpiece is immersed in the quenching fluid, two different processes start: the thermodynamic process of heat extraction and the metallurgical process of structure transformation. The latter one starts actually in *different times for different points* of the cross-section, when the temperature in each point falls to A_1. These times depend on the cross-section size and the cooling intensity of the quenching fluid. The resulting hardness in a particular point depends on constituents of the structure transformed, which depend heavily on the hardenability of the steel concerned i.e. on incubation times at every isotherm. Because incubation times are counted only at temperatures below A_1, for each particular point of the cross-section the *cooling rate in the critical temperature range A_1 to M_s is of paramount importance.*

Shimizu and Tamura[2] have found that the pearlitic transformation behavior with cooling rates discontinu-

ously changed during cooling was different from that given by an usual CCT diagram, and that this transformation is related to the incubation period consumed before changing the cooling rate. In case of delayed quenching some of the incubation period is consumed at the surface of the workpiece, while it is not at the center. The incubation period at any given isotherm is the time until the transformation starts (Z), while (X) is the incubation period consumed before the discontinuous change of the cooling rate has taken place. **Figure 6** which is a schematic illustration of delayed quenching, shows that at time t_1 and temperature T_1 (point P) a discontinuous change of cooling rate occurred. Up to this moment the surface of the workpiece has consumed a share (X) of the total incubation time (Z), but the center has not, because at the moment t_1 the center had a temperature above A_1. Further cooling below the point P has proceeded with substantially increased cooling rate, changing the transformation start curve as shown in **Figure 6**. Because for the center no incubation time has been consumed, the cooling curve for center starts from temperature A_1 at zero time! In this way the cooling curve for center, which doesn't intersect any pearlitic region, results in higher hardness than the cooling curve for the surface which has started from the point P and intersected a portion of pearlitic region. This is the theoretical explanation of 'inverse' hardness distribution.

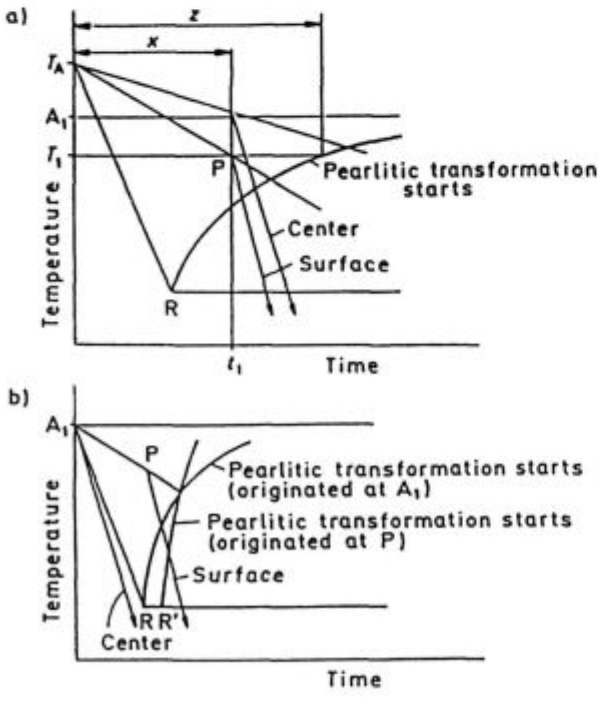

Figure 6: Schematic illustration how delayed quenching causes inverse hardening, according to[2]

Slika 6: Shematična predstavitev kako kaljenje z zadržanjem ustvari inverzno utrditev. Po viru [2]

4 HARDNESS DISTRIBUTION AFTER QUENCHING AND AFTER TEMPERING

Figure 7 shows the normal hardness distribution measured across the section of a 50 mm dia bar of AISI-4140 after quenching in ordinary mineral oil of 20°C bath temperature without agitation (curve No 1), and the inverse hardness distribution measured after quenching the same bar in the PAG polymer solution (UCON-E) of 25% concentration, 40°C bath temperature, and 0.8 m/s agitation rate (curve No 2). This shows the high capacity of delayed quenching technique to influence the depth of hardening.

Because low-alloyed structural steels (like the AISI-4140) are used in hardened and tempered condition, it is of interest to see how a normal and an inverse hardness distribution curve, respectively, look like after tempering. **Figure 8** shows this for specimens used to plot the hardness distribution curves in **Figure 7**, after tempering at 480°C for 2 hours. Normal hardness distribution (curve No 1) has retained the same shape as after quenching, while the inverse hardness distribution (curve No 2) gave a uniformly distributed hardness over the cross section. This is result of the known fact that *at tempering the higher hardness values decrease more than the lower hardness values*. The hardness difference at the center of about 6 HRC indicates that inverse hardness distribution guaranties after tempering a structure of tempered martensite in the core, while in case of normal hardness distribution, besides tempered martensite other (softer) structure constituents are present in the core. With regard to mechanical properties, as it is well known (especially for high strength levels), that tempered fine-grained martensite yields the highest toughness of all microstructures.

5 INFLUENCE OF HARDNESS DISTRIBUTION ON FATIGUE PROPERTIES

For bending fatigue tests[9] especially designed specimens of 300 mm length with the critical diameter of 50 mm were machined of the same heat of the American made steel AISI-4140. All specimens were austenitized in a protective atmosphere to 860°C for 80 minutes. The specimens having normal hardness distribution were quenched one by one, vertically, in used mineral oil of 20°C without agitation. The specimens having inverse hardness distribution were quenched in PAG polymer-solution (UCON-E) of 25% concentration, 40°C bath temperature and 0.8 m/s agitation rate. After quenching all specimens have been tempered in a vacuum furnace at 500°C for 2 hours.

Figure 9 shows the used test rig for bending fatigue tests. All tests were performed in normal environmental conditions under a specific load programme. One round of the used load programme consisted of 7,000 cycles which were subdivided into two parts:

– 5,000 load cycles with the regular load amplitude

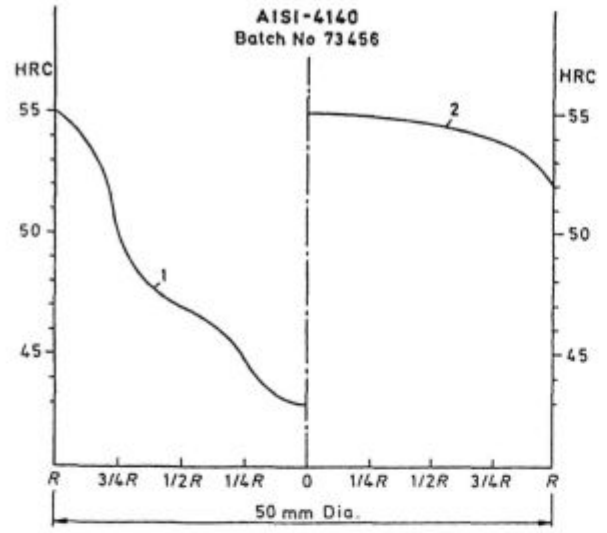

Figure 7: Hardness distribution curves measured on the cross-section of a 50 mm Dia x 200 mm cylinder made of AISI-4140, after quenching under the following conditions:
1) Mineral oil of 20°C, without agitation
2) PAG polymer-solution (UCON-E) of 25% concentration; 40°C bath temperature and 0.8 m/s agitation rate

Slika 7: Porazdelitev trdote po preseku preizkušanca ϕ 50 x 200 mm iz jekla AISI-4140 po kaljenju v naslednjih pogojih:
1) mineralno olje, 20°C, brez mešanja
2) PAG polimerna raztopina (UCON-E), 25%, 40°C in hitrost mešanja 0.8 m/s

– 2,000 load marker cycles with 25% higher than the regular load amplitude.

The 2,000 load marker cycles were used to obtain information about the crack growth rate and a possible influence of the hardness distribution on it. The information about the crack growth rate is expressed in form of share of the crack growth phase in the total test life:

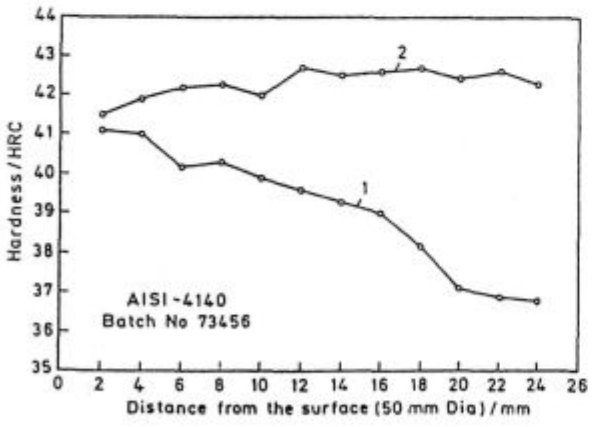

Figure 8: Hardness distribution after tempering at 480°C for 2 hours:
1) Specimen of 50 mm Dia x 200 mm, quenched in mineral oil of 20°C, without agitation
2) Specimen of 50 mm Dia x 200 mm, quenched in UCON-E; 25%; 40°C; 0.8 m/s

Slika 8: Porazdelitev trdote po popuščanju 2 uri pri 480°C:
1) Preizkušanec ϕ 50 x 200 mm kaljen v mineralnem olju pri 20°C brez mešanja
2) Preizkušanec ϕ 50 x 200 mm kaljen v UCON-E 25%, 40°C, 0.8 m/s

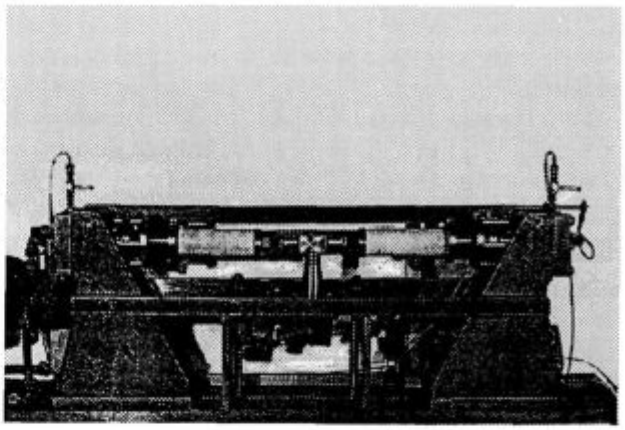

Figure 9: Test rig for bending fatigue tests
Slika 9: Priprava za preizkus upogibne utrujenosti

$$\frac{N_f - N_c}{N_f}$$

in %, where N_f is the number of cycles of the total test life and N_c is the number of cycles to the initial crack. During the tests the cylinder displacement and the load amplitude were recorded to determine N_c and N_f values. The N_c value refers to the beginning of the stiffness loss of the specimen due to initiated crack.

The fatigue tests were performed on different loading levels under pulsating sinusoidal loads with the frequency of f = 16 Hz and a stress ratio $R = F_{min}/F_{max} = 0$ which led to the nominal stress amplitudes in the critical area of the specimens. The test results represented by fatigue life to the initial crack versus the nominal stress amplitude (S - N curves) are shown in **Figure 10**.

Summarising these results it can be concluded, (although the number of tested specimens was low for a statistically confirmed data), that an increased fatigue life was achieved with specimens having inverse hardness distribution compared to specimens having normal

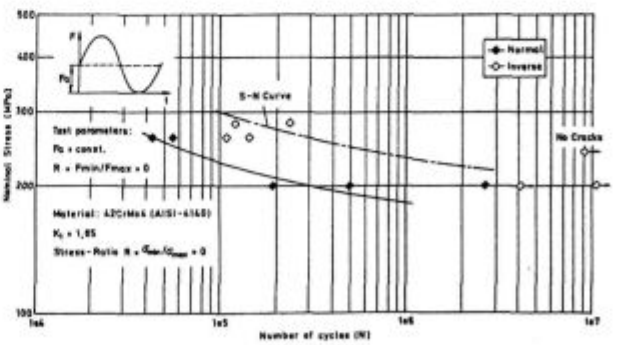

Figure 10: Bending fatigue test results of specimens with normal and with 'inverse' hardness distribution after quenching (both tempered to 500°C for 2 hours)

Slika 10: Rezultati preizkusov upogibne utrujenosti preizkušancev z normalno in z inverzno porazdelitvijo trdote po kaljenju (oba sta bila popuščena 2 uri pri 500°C)

hardness distribution. At the stress level of 270 MPa, at which most tests have been performed, this increase is expressed by a factor of about 7. The crack propagation phase, compared to the total fatigue life was more uniform for specimens with inverse hardness distribution and amounted to 13 to 20%, depending on the stress level. Additional fatigue tests are planned to increase the statistical validity of the achieved results.

6 CONCLUSION

The above described investigation shows that the hardness distribution on the cross-section of the workpiece after quenching can be influenced and greater depth of hardening and better mechanical properties can be achieved by a predetermined and controllable heat transfer dynamics. In future, therefore, the quenching technology will most probably adopt the *control of heat transfer* from the surface of the workpiece instead of letting it occur by itself (depending only on the quenchant and quenching parameters selected), as in today's practice. If so, the question will arise: By which means a controlled heat transfer at quenching is possible?

For liquid, evaporable quenchants (as the hitherto investigations show), this is possible by using polyalkylene-glicol (PAG) polymer-solutions of sufficiently high concentration of adequate temperature and agitation rate. In gas quenching applications (especially in vacuum furnaces with pressurized high velocity gases), more time is available during quenching than in case of liquid quenchants, to change the main cooling parameters i.e. the gas pressure and gas velocity.

In order to find out whether in a particular case the workpiece's cross-section size and hardenability of the steel grade in question are suitable for *quenching with controlled heat extraction dynamics* and to optimize the relevant quenching parameters the computer simulation will be necessary.

The base for such a simulation are the two following requirements:

- The CCT-diagram of the steel-grade in question, which characterizes its hardenability and allows to overlay the calculated cooling curves for different points on the cross-section, to evaluate the transformation kinetics.
- Heat transfer coefficient values $\alpha = f(t)$ (W/m^2K) between the workpiece surface and the quenching medium for the whole quenching process, characterizing the changes in quenching intensity, which allows to calculate the relevant cooling curves in every cross-section point of different bar diameters.

To get relevant heat transfer data, a workshop designed method to measure and record the quenching intensity of different quenchants, as described in[8], is required.

7 REFERENCES

[1] E. A. Loria: Transformation Behavior on Air Cooling Steel in A_3-A_1 Temperature Range, *Metals Technology*, (1977) october, 490-492

[2] N. Shimizu and I. Tamura: Effect of Discontinuous Change in Cooling Rate During Continuous Cooling on Pearlite Transformation Behavior of Steel, *Transactions ISIJ*, 17 (1977) 469-476

[3] N. Shimizu and I. Tamura: An Examination of the Relation Between Quench-hardening Behavior of Steel and Cooling Curve in Oil, *Transactions ISIJ*, 18 (1978) 445-450

[4] B. Liščić, G. E. Totten: Controllable Delayed Quenching, *Proceedings of the International Heat Treating Conference Equipment and Processes*, April 1994, Schaumburg, Illinois, USA, 253-262

[5] M. Chen and H. Zhou: Numerical Heat Transfer Analysis on the Effect of Enhancing the Thickness of the Hardened Layer by Delayed Quenching, Jinshu Rechuli Xuebao *(Transactions of Metal Heat Treatment)*, 14 (1993) 4, 1-6 (in Chinese)

[6] B. Liščić, V. Grubišić and G. E. Totten: Inverse Hardness Distribution and its Influence on Mechanical Properties, *Proceedings of the 2nd International Conference on Quenching and the Control of Distortion*, 4-7 November 1996. Cleveland, Ohio, 47-54

[7] B. Liščić: Investigation of the Correlation Between Polymer-Solution (PAG) Concentration and Inverse Hardening Distribution Curves, *Internal Report No 11/92 of Laboratory for Heat Treatment*, Faculty of Mech. Engineering and Naval Architecture, Zagreb, March 1992

[8] B. Liščić, S. Švaić and T. Filetin: Workshop Designed System for Quenching Intensity Evaluation and Calculation of Heat Transfer Data, *Proceedings of the 1st International Conference on Quenching and Control of Distortion*, 22-25 Sept. 1992, Lincolnshire, Illinois, 17-26

[9] *Test Report Nr 7710*, 24 Nov 1994 from the Fraunhofer Institut für Betriebsfestigkeit, Darmstadt, Germany

ISSN 1318-0010
KZLTET 31(6)529(1997)

METHODS FOR THE VALIDATION OF ADVANCED THIN HARD PROTECTIVE COATINGS - AN EUROPEAN PROGRAM

METODA ZA VALIDACIJO NAPREDNIH TANKIH ZAŠČITNIH PLASTI - EVROPSKI PROGRAM

PETER MAYR, H. VETTERS, A. SCHULZ

Stiftung Institut für Werkstofftechnik, Bremen, Badgasteinerstr. 3 D, 28359 Bremen

Prejem rokopisa - received: 1997-10-01; sprejem za objavo - accepted for publication: 1997-10-21

Specific surface engineering technologies are widely used to improve decisively product characteristics whereas thin hard coatings are increasingly adopted in a broad range of industries. The quality assurance infrastructure for coated products is essential to determine their functional properties. For the reliable assessment of the intrinsic properties (coating thickness, hardness, chemical compositon, adhesion) as well as the tribological performance standardised test methods are required. International groups from research institutes and industries are working on this actual topic to develop comprehensive test methodologies including instrument calibration and reference samples. These will then be proposed to committees for standardisation for adoption as European standards.

Key words: thin hard coatings, characterisation methods, properties, standards

Specifične površinske inženirske tehnologije se široko uporabljajo za povečanje karakterističnih proizvodov in tanke trde prevleke se uporabljajo v širokem spektru te industrije v naraščajočem obsegu. Zagotovitev kakovsti infrastrukture za prekrite proizvode je bistvena za določitev njihovih funkcionalnih lastnosti. Za zanesljivo opredelitev specifičnih lastnosti (debelina, trdota, kemijska sestava in adhezija prekritja) in triboloških lastnosti so zahtevane standardne testne metode. Mednarodne skupine iz raziskovalnih institutov in iz industrije delajo na tej aktualni temi s ciljem, da razvijejo razumljive metodologije za testiranje vključno s kalibracijo instrumentov in referenčnimi etaloni. Te bodo kasneje predložene komitetom za sprejem kot evropski standardi.

Ključne besede: tanke trde prevleke, metoda karakterizacije, lastnosti, standardi

1 SURFACE ENGINEERING GAINING ADVANCED THIN HARD PROTECTIVE COATINGS

Specific surface engineering technologies are widely used to improve decisively product characteristics. Thin hard coatings are increasingly adopted in a broad range of industrial sectors as a means of achieving advanced products. The mechanical properties of these advanced coatings will determine the service life because elastic and plastic behaviour control fracture and adhesion of the coating. The use of wear resistant coatings can lead the retention of better tolerances through the lifetime of tools or machine parts. In all these cases mechanical reliability requires optimum matching of the different components to be "assembled", that can only be obtained by model calculations requiring precise knowledge of the characteristics and functional properties[1]. It is established that surface coatings and treatments can lead to considerable improvements in the performance of a wide range of components. Modern PVD and CVD hard coating techniques often allow for alternative, environmentally friendly solution to wear protection[2-4].

2 QUALITY ASSURANCE - A KEY OBJECTIVE

As reported[5,6], a broad selection of materials is being offered for ceramic coatings. When selecting a coating for certain application, the substrate, the interface and possible interlayer and the environment influence strongly the on service condition of the coated part. A wide variety of coating procedures leads to a wide range in functional properties, which can be classified by methods of test[7]. In order to allow industry to take full advantage of this rapidly developing area it is essential to establish a quality assurance infrastructure for coated products by standardised test methods. In view of fostering international collaboration between research organisations, standard bodies and industry on pre-standardisation research in advanced materials the "Versailles Project on Advanced Materials and Standards" (VAMAS) is fulfilling a unique role. Within several technical working areas (TWA) formal links with international standards organisations and increasing industrial involvement have been formed. In fact one activity on developing methods of test of thin hard coatings is now established[9]. The European Committee for Standardisation (CEN) has also established a technical committee on ceramic materials with a working group "Methods of test of ceramic coatings" (CEN TC 184/WG 5).

3 CHARACTERISATION OF PROPERTIES

Many methods exist for the measurement of properties of coatings (**table 1**), but for thin hard coatings is a great paucity of standards. Improved test methods, there-

fore need to be developed or the existing procedure should be formalised and draft standards prepared. The test routine should lead to a subsequent process control during the production routine which includes preliminary quality control as well as quality control after the coating procedure. Their properties are defined as: hardness, residual strain, composition, morphology, microstructure, thickness of coating, elasticity, electrical conductivity, magnetic susceptibility, thermal conductivity, etc., and on service conditions are indicated by wear and corrosion resistance, fatigue and life time oriented behaviour, thermoshock stability, and other characteristics[8-10].

Table 1: Characterisation of reference samples

composition bulk materials	spectroscopy, wet chemical analysis
composition of coatings	X-ray fluorescence, EPMA, AES, GDOS, SIMS, SNMS
thickness of coatings	cap grinding, cross-sectioning, X-ray diffraction, step height measurement, NDT-test methods
roughness	3D profilometry
microstructure	optical microscopy, SEM, TEM, XRD phase-analysis
grain size and texture	XRD, quantitative metallography
coating internal stress	X-ray diffraction, flexural strain, Rayleigh wave analysis
density	weighting and volumina evaluation
hardness, hardness gradient	indentation method
adhesion of coatings	scratch testing, indentation method
modulus of elasticity	ultrasonics, acoustic microscopy

4 THE VALIDATION OF METHODS OF TEST

In practice, many of the qualitative tests are used and recommended, because they are suitable for several coating materials, simply to handle and commonly based on visual examination[13]. Because of limited applicability of the standard pull test a modified shear test is recommended for the test of adhesion of ceramic coatings[12]. In practice often accepted is the Rockwell indentation test[13] for the qualitative examination of thin hard coatings, where the remaining plastic deformation after indentation causes a "spalling off" of the layer, so an area of failure remains. But in spite of reference samples producing calibration data under reproducible measurement conditions this method of test is not valuable until now to be adapted as a standard.

4.1 Reference specimens for calibration

Calibration requires the production of an ensemble of well characterised specimens with hard coatings of perfectly controlled chemical composition, microstructure, and thickness uniformity, likely to become certified ultimately as reference specimens. The following methods are used to assess these properties.

4.2 Measurement of the coating thickness

For the measurement of the coating thickness the methods of stylus profilometry[14] and cap grinding[15] are employed. A further development of the cap grinding method allows the in-situ detection of the coating relief during abrasive extraction[16]. This method can also be modified for the determination of the coating resistance against abrasive wear under defined friction control.

4.3 Measurement of the chemical composition

Chemical analysis[23] was carried out from various layers of defined (N/Ti)-composition which has been realised by reactive magnetron sputtering with nitrogen where the N-concentration has been varied by trimming the gas flow[18]. The spectrochemical analysis of the layer led to a constancy of the composition of ±1% atomic%, which has been certified by reference labs[18].

4.4 Measurement of the coating hardness

It was found by round robin comparison that existing standards methods of hardness tests on hard coatings are rarely valuable for certification. Hardness measurement by load-indentation[18,19] on TiN coated test plates of tool steel showed under certain conditions, regarding the surface quality, chemical homogeneity, smooth interface morphology, hard substrate material, reproducible hardness values of 20 GPa by means of a test force between 250 mN (HU 0.25) and 1 N (HU 1) within an error width of less than ±2,5% of the value as determined above. These platelets, described in[18], could act as calibration samples for hardness measurement.

The surface morphology, respectively the surface roughness, plays an important role on accuracy and reproducibility. Doubtless, the calibration of the instruments, their stability and constancy during the test periods give a guarantee for exact results. Several procedures, especially for the nanohardness scale, have been developed and controlled through various round robin tests[19].

4.5 Adhesion of the coating

In the same way the influences on scratch test sensitivity and reproducibility of results are carried out. Obeying the whole system, stylus geometry and adhesive debris, surface quality, the existence of lubricants, humidity and temperature the function of influencing parameters is studied[22]. Then, using various coating/substrate composites of defined combination, scratch test failure modes are analyzed and various features catalogued. Improving the NDT techniques for in-situ control during process routines, ultrasonic test procedures are validated[20]. For thin hard films it will be realised by surface acoustic measurement techniques. The input of one specified research work is to enhance and calibrate the surface acoustic wave velocity measurement technique vis a vis reference coated substrate standards with

the aim of developing a comprehensive test methodology for coating thickness. This measurement methodology will then be proposed to CEN for adoption as an European standard.

5 ASSESSMENT OF TRIBOLOGICAL PERFORMANCE

Engineering components often suffer from wear and friction resulting at best in energy inefficiencies and losses in performance, and in the worst cases catastrophic failure. There has been considerable recent interest in improving the tribological performance of components by the application of wear resistant coatings to the surface of the components[22].

For reliable assessment of the tribological performance of potential coating systems, robust and effective testing procedures are required. Testing of the cavitation erosion by ultrasonic affects in water can be estimated as a valuable method for standardisation[18].

Current friction and wear testing procedures are not sufficiently well defined to allow data comparisons, and evaluation of the significance of reported data is difficult. The work to be carried out in one prenormative research[22] involves the development of improved procedures for uniaxial sliding wear testing; reciprocating sliding wear testing and abrasive testing.

6 ASSESSMENT OF LIFE TIME OF COATED PARTS

Whatever the main technological function may be, in practice mechanical properties of the coating substrate compound will determine the life time with on service conditions because the interactive elastic and plastic behaviour of coating and substrate controls the fatigue endurance, fracturing conditions and the adhesion of the coating. At first, the aims of the research work conducted in one current program[22] are to develop and validate the methods of test to determine the elastic properties of the surface layer. In comparison to the tribological test procedures quantitative assessments based on scientific investigations due to structure and composition of reference samples are provided. These items will involve the development of reference materials and the conduction of round-robin intercomparisons.

7 REFERENCES

[1] D. S. Rickerby & A. Matthews: Advanced surface coatings, A handbook for surface engineering, Blackie, London, 1991

[2] S. Bull & D. S. Rickerby: Compositional, microstructure and morphological effects on the mechanical and tribological properties of chromium nitrogen films, Surface and Coatings Technology, 43/44 (1990) 732 -744

[3] E. Lugscheider, P. Jokiel: Particle reinforced coatings - processing and mechanical properties, Surface Engineering (ed. P. Mayr, Proc. Of the International Conf. On Surf. Eng. 1993, Bremen, FRG, DGM Informations GmbH Frankfurt/Oberursel ISBN 3-88355-189-9, 1993, 159-164

[4] K. Keller: Economical and ecological aspects as design criteria for coating processing, Surface Engineering (ed. P. Mayr, Proc. Of the International Conf. On Surface Engineering 1993, Bremen, FRG, DGM Informations GmbH Frankfurt/Oberursel ISBN 3-88355-189-9, 1993, 3-12

[5] D. S Rickerby et al.: The development of advanced erosion resistant coatings for gas turbine compressor applications, BRITE-EURAM Rep. BE-3339 Rep. (Brussels, 1994)

[6] H. Holleck: Binäre und Ternäre Carbid- und Nitridsysteme der Übergangsmetalle, Materialkundl, Techn. Reihe 6, Verl. Gebr. Borntraeger, Berlin, Stuttgart, 1984

[7] W. Gissler, H. Jehn: Advanced Techniques for Surface Engineering, Dordrecht, 1992

[8] S. Ronkainen et al.: Mechanics of Coatings (Ed. D. Dawson, C. M. Taylor, M. Godet) Elsevier Sci. Publ., 1990, 453-462

[9] S. R. J. Saunders: VAMAS (Versailles Project on Advanced Materials and Standards), Technical Working Area Project Initiation Form: Property Measurement of Thin Films and Coatings, Tokyo, Dec. 1992

[10] J. P. Celis et al: Corrosion of Electrodeposited, PVD and CVD Coated Metallic Materials, Surface Engineering (ed. P. Mayr, Proc. Of the International Conf. On Surface Engineering 1993, Bremen, FRG, DGM Informations GmbH Frankfurt/Oberursel ISBN 3-88355-189-9, 1993, 43-53

[11] European Envisaged Standard ENV 1071-5, Methods of Test of Ceramic Coatings: Determination of the Porosity, 1995

[12] ISO standard 2819, Metallic Coatings on Metallic Substrates - Electrodeposited and Chemically Deposited Coatings - Review of Methods for Testing Adhesion

[13] H. Jehn, G. Reiners: Charakterisierung dünner Schichten, DIN Fachbericht 39, Beuth Verlag GmbH., Berlin, Wien, Zürich, 1993, ISSN 0179-275X

[14] European Envisaged Standard CEN ENV 1071-1, Determination of the Coating Thickness; Step height measurement by means of a contact profilometer, 1992

[15] European Envisaged Standard CEN ENV 1071-2, Determination of the Coating Thickness; Cap grinding method, 1992

[16] H. Klümper-Westkamp: Prakt. Metallographie (German DGM, Spec. Vol. 26, 1994), Mikrotribometer zur Qualitätssicherung von Randschichten (Pat. DE-P 4434661.1) 433-442

[17] European Envisaged Standard CEN ENV 1071- 3: Characterization of adhesion: Scratch adhesion test, 1992

[18] A. Schulz, H.-R. Stock, H. Vetters and P. Mayr: Qualifizierung von Prüfverfahren und Standards für die Dünnschichttechnologie, Final Report Programme OSTEC 13N6242, (German Fed. Ministry of Education and Research BMBF, Feb. 1996)

[19] S. R. J. Saunders et al.: Hardness (Mechanical Property) Testing of Surfaces, NPL Report DMA (D) 198, BCR MAT CT 92 - 0027, 1996

[20] BRITE EURAM BE 4398: Non Contacting Surface Characterization of Ceramics and Coatings with Micro Acoustic Waves (C-MAW), Final Report R/CJG/1093/95, 1996

[21] K. Holmberg: Friction and Wear Mechanisms of Thin Surface Coatings on Metal Substrates, Surface Engineering (ed. P. Mayr, Proc. Of the International Conf. On Surf. Eng. 1993, Bremen, FRG, DGM Informations GmbH Frankfurt/Oberursel ISBN 3-88355-189-9, 1993, 13-22

[22] Development and Validation of Test Methods for Thin Hard Coatings (FASTE) EU- MS&T MAT1-CT 940045, Workprogramme, 1994 - 1997

[23] European Envisaged Standard CEN ENV 1071-4; Determination of the chemical composition, 1995

slovenske železarne

ŽELEZARNA JESENICE

ACRONI

IZDELUJE:

- nerjavna jekla
- jeklo za elektro pločevino
- nelegirana in legirana jekla
  - za poboljšanje
  - za cementacijo
- nelegirana, mikro in malolegirana konstrukcijska jekla

- toplo valjane pločevine, trakove in lamele
- hladno valjane pločevine, široke in vzdolžno razrezane trakove
- hladno oblikovane profile
- kovinske podboje za vrata
- izsekance
- varnostne ograje

ELEKTRO PLOČEVINE IN TRAKOVI

NERJAVNA JEKLA

MIKROLEGIRANA JEKLA

VISOKO OGLJIČNA JEKLA za poboljšanje

NUDIMO TUDI STORITVE:

- prevaljanje
- izsekovanje (štancanje)
- krojenje
- ravnanje
- toplotne obdelave pločevin

SŽ ŽJ ACRONI d.o.o. Cesta železarjev 8, 4270 Jesenice, tel. centrala: +386 64 861-441,
tel. direktor: 861-443, tel. komerciala: 861-474, fax: 861-379, telex: 37219 ZELJSN SI

Slovenija

ISSN 1318-0010
KZLTET 31(6)533(1997)

AS-ROLLED MULTI-PHASE MICROALLOYED STEEL BARS WITH IMPROVED PROPERTIES

VALJANE VEČFAZNE MIKROLEGIRANE JEKLENE PALICE Z IZBOLJŠANIMI LASTNOSTMI

DJORDJE DROBNJAK[1], A. KOPRIVICA[2]

[1]Faculty of Tech & Met University of Belgrade, Belgrade, Yugoslavia
[2]Institute for Ferrous Metallurgy, Niksic Yugoslavia

Prejem rokopisa - received: 1997-10-01; sprejem za objavo - accepted for publication: 1997-10-21

A series of experimental steels, based on a 0.3 C, 1.5 Mn, 0.1 V composition, with and without 0.01% Ti addition, was made by laboratory and full-scale casting, and fabricated into 22 mm dia bars by full-scale hot-rolling. Multi-phase Polygonal Ferrite-Pearlite-Non Polygonal Ferrite (PF-P-NPF) structures, with varying amount of NPF, are obtained in as-rolled bars. Acicular Ferrite (AF) and classical Bainite Sheaves (BS) are found to be dominant NPF morphologies in steels with a low (<30%) and a high (>40%) fraction of NPF, respectively. In Ti-bearing PF-P-AF steels, the PF-grain and P-colony size control, obtained through fine TiN particles, which also provide preferential sites for intragranular nucleation of AF, a tensile strength of 800/850 MPa and 900/950 MPa in 0.2 and 0.3 C steels was obtained, while maintaining the room temperature CVN impact energy at a level of 65/75 J and 40/50 J, respectively. A high fraction of grain boundary nucleated BS is promoted by increasing the content of Cr, Mo or Mn above the base level. The main effect of introducing BS into structure is a drop in impact toughness. Even so, in some BS dominated steels (notably Cr treated) an impact energy of 30/35 J is maintained at a tensile strength level of 1050/1100 MPa. These results have provided a bases for the development of as-rolled medium carbon microalloyed engineering bars, that achieve satisfactory properties in the as-rolled conditions without the need for subsequent heat treatment.

Key words: microalloying, bar-rolling, polygonal ferrite, pearlite, non-polygonal ferrite, bainite, acicular ferrite, strength, toughness

Vrsta eksperimentalnih jekel z osnovno sestavo 0.3 C, 1.5 Mn in 0.1 V z ali brez dodatka 0.01% Ti je bila izdelana z laboratorijskim in z industrijskim vlivanjem ter industrijsko izvaljana v 22 mm palice. Dosežene so več fazne poligonalni ferit-perlitne - poligonalni ferit (PF-P-NPF) mikrostrukture z različnim deležem NPF. Acikularni ferit (AF) in klasični bajnitni snopi (BS) so prevladujoče NPF morfologije v jeklih z majhnim (<30%) in velikim (>40%) deležem NPF. V PF-P-AF jeklih z dodatkom Ti, kjer je dosežena kontrola velikosti zrn PF in P kolonij z izločki TiN, ki so tudi prednostna mesta za intragranularno nukleacijo AF, je bila dosežena pri 0.2 in 0.3 C jeklih natezna trdnost 800/850 in 900/950 MPa. Pri tem je ostala CVN udarna energija pri temperaturi ambienta 65/75 oz. 40/50 J. Velik delež BS z nukleacijo na kristalnih mejah se doseže z dodatkom Cr, Mo ali Mn nad osnovno vsebnostjo. Glavna posledica prisotnosti BS v mikrostrukturi je zmanjšanje udarne žilavosti. Vendar je bila tudi v nekaterih jeklih s prevladujočo BS (predvsem z dodatkom Cr) ohranjena udarna energija 30/35 J pri trdnosti 1050/1100 MPa. Ti rezultati so bili osnova za razvoj srednje ogljičnih konstrukcijskih jekel, ki imajo v valjanem stanju dobre lastnosti brez dodatne toplotne obdelave.

Ključne besede: mikrolegiranje, valjane palice, poligonalni ferit, perlit, ne poligonalni ferit, bainit, acikularni ferit, trdnost, žilavost

1 INTRODUCTION

Medium-carbon microalloyed (MA) forging steels have been extensively studied over the past decade, and the results are reported at several international conferences (e.g.[1-3]). There are many examples to show that MA steels can replace Q&T steels in as-forged and air-cooled conditions, without subsequent heat treatment. However, in the ferrite-pearlite (FP) version, these steels suffer from inferiors notch toughness. In the last few years, bainite (B) and martensite (M) type grades, have received considerable attention as viable candidates to replace FP steels. Compared to M type (e.g.[4,5]) the air-hardened B-type grades need not quench, but the improvement in toughness is not as-spectacular[4,6-13], and in some instances a deterioration in toughness is claimed[14-16]. This as well as other disadvantage of B-grades, such as a low yield ratio[13,17] and poor machinability[7], may be among the reason why they are scarcely used[17].

The strength and toughness of as-hot rolled bars have been less extensively studied in comparison to forgings. However, while considerable work has been done to improve the toughness of conventionally or controlled rolled bars in FP version (e.g.[13,18,19]), little effort has been made to improve the toughness of bars by introducing B into structure. Improvements achieved in this work are mostly based on recent results which show[20,21] that, while some B-morphologies are beneficial, the other are detrimental to toughness.

2 EXPERIMENTAL DETAILS

2.1 Material

A series of experimental heats, based on 0.3% C, 1.5% Mn, 0.1% V composition (small variations among different heats are included in **Table 1**) with and without 0.01% Ti addition, is used in this work. A number of heats were modified by either reducing the content of some additions (e.g.: C to 0.2%; N to 15-60 PPM; V, Ni and Cu to traces) or increasing the content of other additions above the base level (e.g.: Mn to 1.55/1.65 or

1.72/1.78%; Cr to 0.37/0.38 or 0.57%; Mo to 0.21%; V to 0.16/19%; N to 160/240 ppm; S to 150/250 ppm).

Table 1: Steel compositions (in wt.%)
Tabela 1: Sestava jekel (v ut.%)

C	Si	Mn	P	S	Cr	Mo	Ni	Al	Cu	N	V
0.27	0.29	1.47	0.006	0.006	0.21	0.03	0.15	0.02	0.18	0.010	0.10
0.32	0.39	1.57	0.010	0.010	0.30	0.06	0.19	0.03	0.31	0.012	0.13

2.2 Casting and hot working of steels

Either laboratory vacuum or full-scale casting was used to produce 60 kg and 2630 kg ingots, labeled L and I-ingots, respectively. L-casting practice proved[20] to be effective in producing the fine TiN particles in Ti-bearing steel, capable of imposing a pinning effect on austenite grain boundaries during subsequent reheating and rolling. The ingots were fabricated into 22 mm dia bars on production facilities. They were first fabricated into 120 mm (I-ingots) and 80 mm squares (L-ingots) by hot-rolling on a bloom mill or by press-forging, respectively. Then, the squares were hot-rolled to 22 mm bars, on either a continuous (120 mm squares) or a cross-country (80 mm squares) bar mill, using the conventional rolling practice, which involved soaking at 1150°C and finish-rolling above 950°C.

2.3 Testing

Room temperature properties are evaluated from round tensile (l_0 = 40 mm; d_0 = 8 mm) and standard Charpy V-notch (CVN) longitudinal specimens, which were taken mid-radius from the as-rolled bars. A few impact tests were run at -50°C. Conventional metallographic techniques were used for revealing the microstructure.

3 RESULTS

3.1 Structure

A multi-phase Polygonal Ferrite-Pearlite-Non Polygonal Ferrite (PF-P-NPF) structure, with varying amount of NPF, is developed in the as-hot rolled bars. Acicular Ferrite (AF) and classical Bainite Sheaves (BS) are found to be dominant NPF morphology in steels with a low (<30%) and a high (>40%) fraction of NPF (to be referred to as PF-P-AF and PF-P-BS steels), respectively.

Intragranularly nucleated, mostly needlelike plates, which radiate in many directions, referred to as AF, are shown in **Figure 1a**, and as a part of PF-P-AF structure, in **Figure 1b**. The former austenite grain boundaries are decorated by Grain Boundary Idiomorphs (GBI) in **Figure 1a**, but Grain Boundary Alotriomorphs (GBA) or Widmanstatten Sideplates (WSP) are also frequently observed[20]. Grain boundary nucleated parallel ferrite plates, referred to as BS, are shown in **Figure 2a**, and as a part of a PF-P-BS structure, in **Figure 2b**.

AF is dominant NPF morphology in steels with composition within the limits given in **Table 1**, while a high fraction of BS is promoted by increasing Mn, Cr and Mo content above the base level. The two morphologies (including some transient variants) generally coexist in various proportions. In PF-P-AF steels, the addition of Ti increases the AF/BS ratio (Ti addition also refines the PF-grain and P-colony size). In PF-P-BS steels the BS/AF ratio depends upon the alloying addition. Thus, in 0.57% Cr and 0.21% Mo steels, BS coexist with a detectable fraction of AF (**Figure 3a**), while in 1.72/1.77% Mn steels BS are the only morphology present (**Figure 3b**). All three steels are L-cast and Ti-treated, but the two latter are virtually free of PF and P.

3.2 Structure-Property Relationship

Strength and Impact Properties (YS = Yield Strength; TS = Tensile Strength; CVN_{20} = Charpy V-Notch impact energy at 20°C) are, in terms of NPF fraction, shown in **Figures 4a and 4b**, respectively. Each data point represents an average of two (strength) and three to five tests (toughness). The TS remains virtually unchanged with increasing fraction of NPF up to about 70% and then

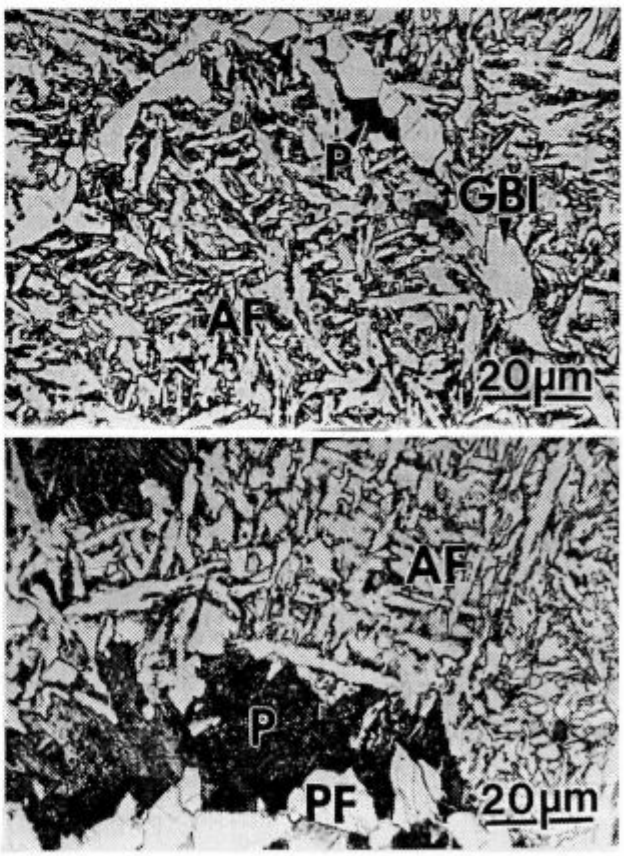

Figure 1: (a) Acicular Ferrite (AF), Grain Boundary Idiomorphs (GBI) and Pearlite(P); (b) Polygonal Ferrite-Pearlite-Acicular Ferrite (PF-P-AF)
Slika 1: (a) Acikularni ferit (AF), idiomorfi (GBI) in perlit (P) po kristalnih mejah; (b) poligonalni ferit perlit - acikularni ferit (PF-A-AF)

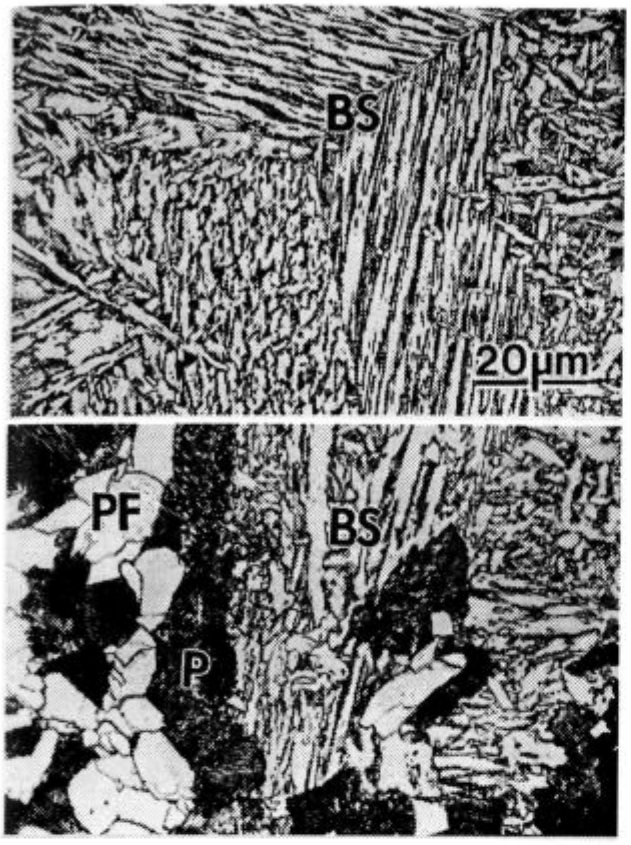

Figure 2: (a) Bainite Sheaves (BS); (b) Polygonal Ferrite-Pearlite-Bainite Sheaves (PF-P-BS)
Slika 2: (a) Bainitni snopi (BS); (b) poligonalni ferit perlit - bainitni snopi (PF-B-BS)

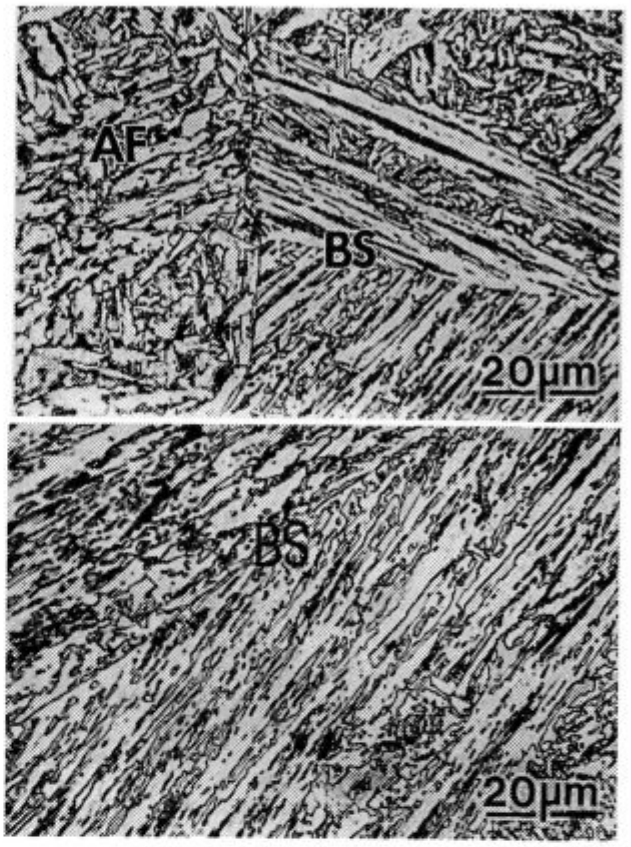

Figure 3: (a) Bainite Sheaves (BS) and Acicular Ferrite (AF); (b) Bainite Sheaves (BS)
Slika 3: (a) Bainitni snopi (B) in acikularni ferit (AF); (b) bainitni snopi (BS)

slightly increases, while the YS first decreases and than, at 30-40% of NPF, attain a constant level. These changes are neither consistent with variations in fraction nor in morphology of NPF (AF = open symbols; BS = closed symbols, in **Figure 4**). A relatively broad scatter band in **Figure 4a** is presumably a reflection of small variations in composition. For instance, decreasing C from 0.3% to 0.2% produces a drop in YS and TS from 600/650 to 550/600 and from 900/950 to 800/850 MPa, respectively. Moreover Ti, Cr and Mn produce an effect which can be discriminated within the scatter-band itself. Thus, Ti-free PF-P-AF steels (**Region 1a**) exhibit a higher strength level then Ti-bearing steels (**Region 1b**), while 0.57% Cr PF-P-BS and 1.72/1.77% Mn B-steels (**Region 2a**) exhibit a higher TS level (1050/1100 and 1150/1200 MPa, respectively) than the other PF-P-BS grades (**Region 2b**).

Data of **Figure 4b** show that an increase in impact energy with increasing fraction of NPF is interrupted by a pronounced drop on passing from AF dominated - **Region 1** to BS dominated - **Region 2**. Within the PF-P-AF **Region 1c**, the energy attains a level of 65/75 J at 20°C (33 J at -50°C), corresponding to YS = 550/600 MPa and TS = 800/850 MPa; and within the **Region 1b**, a level of 40/50 J at 20°C (32 J at -50°C), corresponding to YS = 600/650 MPa and TS = 900/950 MPa, in 0.2% C/10% AF and 0.3% C/30% AF steels, respectively. Both steels are L-cast and Ti-treated. In general, the L-cast/Ti-treated steels exhibit a higher impact energy level (+Ti band in **Figure 4b**) than the Ti-free steels (-Ti band). The I-cast/ Ti-treated steels take an intermediate position (open squares). Within the PF-P-BS **Region 2**, the energy attains a level of 30/35 J at 20°C (25/30 J at -20°C), corresponding to YS = 600 MPa and TS = 1050/1100 MPa; and within the **Region 2c**, a level of 15/25 J at 20°C, corresponding to YS = 550/600 MPa and TS = 1150/1200 MPa, in 0.57% Cr/70% BS and 1.75% Mn/98% BS steels, respectively. In 0.57% Cr steel, in addition to BS, the NPF morphology comprises a detectable fraction of AF (**Figure 3a**), while in 1.75% Mn steels, BS is the only NPF morphology present (**Figure 3b**).

4 DISCUSSION

4.1 Structure

A slight difference in composition of the steels studied in this work seems to be decisive in controlling not

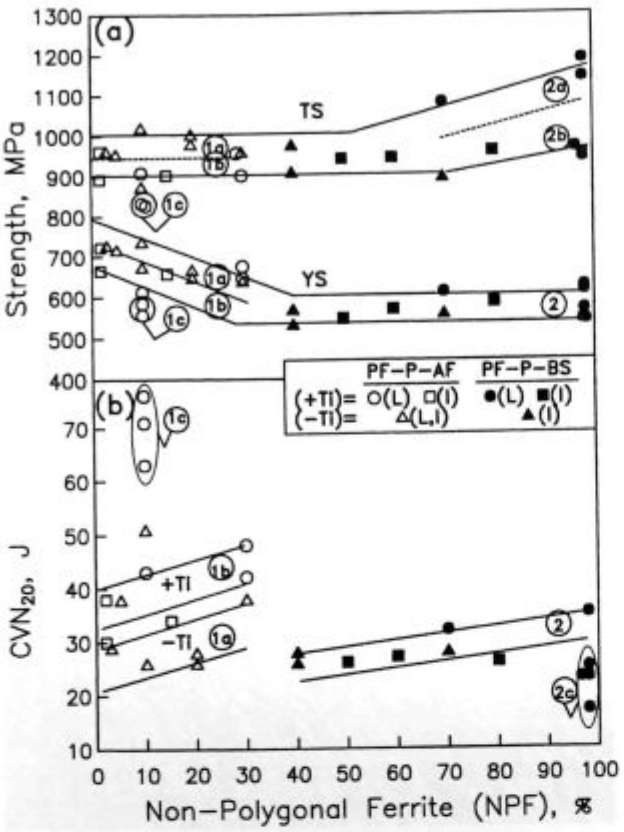

Figure 4: (a) Yield Strength (YS) and Tensile Strength (TS) as a Function of Non-Polygonal Ferrite (NPF) Fraction; (b) Charpy V-Notch Impact Energy at 20 (CVN_{20}) as a Function of NPF Fraction (PF = Polygonal Ferrite; P = Pearlite; AF = Acicular Ferrite; BS = Bainite Sheaves; L = L-Cast Ingots; I = I Cast-Ingots; +Ti = Ti-Bearing Steels; -Ti = Ti-Free Steels)

Slika 4: (a) Meja plastičnosti (YS) in natezna trdnost (TS) v odvisnosti od deleža ne poligonalnega ferita (NPF); (b) Charpy V udarna energija pri 20°C (CVN_{20}) v odvisnosti od deleža NPF (PF - poligonalni ferit, P - perlit, AF - acikularni ferit, BS - bainitni snopi, L-L - liti ingoti, I-I - liti ingoti, +Ti - jekla s Ti, -Ti - jekla brez Ti)

only the fraction of NPF but, together with inclusions, its morphology also.

Thus, the AF, which is assumed to be either intragranulary nucleated bainite[22] or Widmanstatten ferrite[23], together with various proportions of PF (e.g. Grain Boundary Idiomorphs, GBI) and pearlite, P (**Figure 1**), is produced in PF-P-AF grades, with a relatively low hardenability (<30% NPF). The Grain Boundary Ferrite (GBF) is assumed[24] to render austenite grain boundaries inactive in respect to intergranular nucleation of BS, what in turn promotes the intragranular nucleation of AF on TiN or MnS inclusions[20]. The nucleation potential of inclusions varies with composition, crystal structure and dispersion, i.e. with their number, size and spacing[22,25-29]. For example, a low degree of misfit between the ferrite matrix and the substrate crystal lattice is assumed[25-31] to increase the nucleation potential of inclusions. Therefore, TiN with a misfit ratio of 3.8[27] should be much more effective than MnS with misfit ratio of 8.8[25]. This could account for a higher fraction of AF observed in Ti-bearing (fine and coarse particles, which are presumably developed in L and I-cast ingots respectively, seems to be equally potent nucleation sites) than in Ti-free (high S) steels. However, in steels with high V and N, VN particles can be precipitated on MnS, before austenite is transformed to ferrite[30,31]. Since the misfit ratio of VN, estimated at 1.3 for (001) plane[27], is lower than that of TiN, the former particles, i.e. MnS coated by VN, should be more potent nucleation sites for AF. While the effect is not quite apparent in the present steel, the fact remains that the fraction of AF is higher in high-S than in low-S/Ti-free steels.

The BS are produced in PF-P-BS grades with relatively high hardenability (>40% NPF). The nucleation of GBF is considerably suppressed, and an abrupt transition from AF dominated to BS dominated NPF morphology occurs not only in Ti-free but also in Ti-bearing steels. This supports the assumption that removal of GBF frees the boundaries to nucleate BS concurrently with intragranular AF.

4.2 Properties

Yield and Tensile Strength (YS, TS). It is well known (e.g.[6-8]) that the YS of Polygonal Ferrite-Pearlite (PF-P) steels increases with increasing fraction of P. Additional strengthening is obtained by precipitation of V (C,N) particles in ferrite. Precipitation strengthening effect decreases with decreasing N-content. In Ti-bearing PF-P-AF steels tested in this work, Ti forms nitride particles which reduce the N available for VN precipitation and hence, reduce (from **Region 1a** to **1b** in **Figure 4a**) the strengthening associated with this precipitation. Gradual replacement of PF-P structure with NPF structure reduces the YS, as shown in **Figure 4a**, due to suppression of precipitation within the NPF phase (e.g.[8,11]). However, the TS is maintained at the same level (**Region 1**), and even increases (**Region 2a**) in some steels. This latter observation can be associated with a high strain-hardening rate imposed by bainite[32].

CVN_{20} Impact Toughness (CVN_{20}). The present results, together with data presented in previous papers[20,21], indicate that AF and BS are beneficial and detrimental to toughness, respectively. The brittle fracture of low-C bainites can be related to the cleavage facet size[33], which in the present steels can be related to either AF-plate or BS-packet size. AF-plates give rise to a finer facet size, and thus to a higher toughness, while BS, in addition to being coarser itself (individual laths within a sheaf have little effect, since the cleavage crack is deflected at the sheaf and not at the lath boundary[33]), contain coarse interlath carbides (a feature characteristic of upper bainite), which are detrimental to toughness[33].

The Ti-bearing PF-P-AF steels (**Region 1b** in **Figure 4b**) exhibit a considerably higher toughness in comparison to Ti-free steels (**Region 1a**). This is because the PF-grain and P-colony size is finer and the AF fraction is presumably higher in Ti-bearing steels which contain

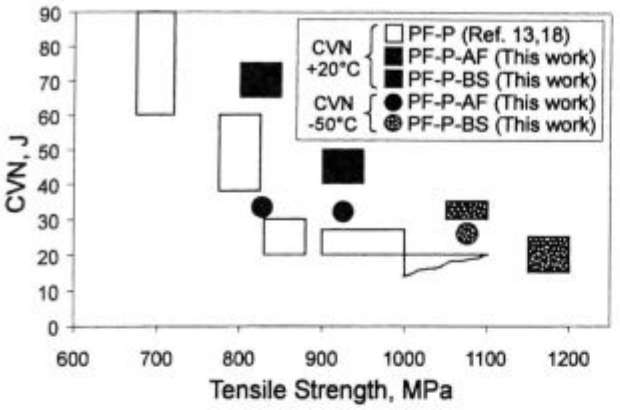

Figure 5: Tensile Strength (TS) vs. Charpy V-Notch Impact Energy (CVN_{20} = 20°C; CVN_{-50} = -50°C) of Conventionally Hot Rolled 0.2-0.5% C Polygonal Ferrite-Pearlite (PF-P), and 0.2-0.3% C Polygonal Ferrite-Pearlite-Acicular Ferrite (PF-P-AF) and Polygonal Ferrite- Pearlite- Bainite Sheaves (PF-P-BS) Bar Steels

Slika 5: Natezna trdnost (TS) v odvisnosti od Charpy V udarne energije (CVN_{20} = 20°C CVN_{50} = 50°C) pri konvencionalno vroče valjanih 0.2 - 0.5% C poligonalni ferit perlit (PF-P) in 0.2 - 0.3% C poligonalni ferit perlit - acikularni ferit (PF-P-AF) in poligonalni ferit perlit - bainitni snopi (PF-P-BS) jeklenih palicah

fine TiN particles. The role of particles is twofold, first they inhibit the austenite grain growth, and second, they provide the nucleation sites for intragranular nucleation of AF. However, Ti-bearing/I-cast steels exhibit a lower toughness than Ti-bearing/L-cast steels, in spite of AF is a dominant NPF morphology in both. Coarser TiN particles in I-cast steels are not as effective in pinning austenite grain boundaries as fine particles in L-cast steels and lead to a coarser austenite grain, and consequently coarser PF-grain and P-colony size.

5 CONCLUDING REMARKS

The conventionally hot-rolled and air-cooled multiphase Polygonal Ferrite-Pearlite-Non Polygonal Ferrite (PF-P-NPF) microalloyed Ti-bearing steels, tested in this work (closed and shaded symbols in **Figure 5**), exhibit improved impact properties in comparison to conventionally hot rolled Polygonal Ferrite-Pearlite (PF-P) steels (open symbols), tested previously (e.g.[18,19]).

The 0.2% C/10% AF and 0.3% C/30% AF PF-P-AF steels, based on a 1.5% Mn - 0.1% V - 0.01% Ti composition, with an impact energy level of 65/75 J and 40/50 J at 20°C (33 and 32 J at -50°C), and tensile strength level of 800/850 MPa and 900/950 MPa respectively, can replace Q&T steels which currently achieve these property levels.

The use of a higher Cr or Mn contents give rise to PF-P-BS structure with 70-98% BS and increased tensile strength level up to 1050/1200 MPa at the expense of reduced toughness.

Acknowledgment

This work was supported by Steel Mill, Niksic, Yugoslavia and permission to publish this paper is acknowledged.

6 REFERENCES

[1] Fundamentals of Microalloying Forging Steels, eds. G. Krauss and S. K. Banerji, The Metallurgical Society, Warrendale, PA 1987
[2] Microalloyed Bar and Forging Steels, ed. M. Finn, The Canadian Institute of Mining and Metallurgy, Montreal, QU 1990
[3] Fundamentals and Applications of Microalloying Forging Steels, eds. C. J. Van Tyne, G. Krauss and D. K. Matlock, The Minerals, Metals and Materials Society, Warrendale, PA 1996
[4] W. A. Szilva et al., As Ref. 2, p. 227
[5] M. Katsumata et al., Phys. Metall. of Direct-Quenched Steels, eds. R. A. Taylor et al., The Metallurgical Society, Warrendale, PA 1993, p. 247
[6] H. Hara and M. Kobayashi, Hot Forged Microalloyed Steels in Automobile Components, Vanadium Award, The Institute of Metals, 1987
[7] Vanadium As Forged Steels for Automobile Components, Vanitec Monograph No3, 1987
[8] W. E. Heitmann and P. B. Babu, As Ref. 1, p. 55
[9] G. Tither, T. B. Cameron and D. E. Diesburg, As Ref. 1, p. 269
[10] P. H. Wright et al., As Ref. 1, p. 541
[11] P. A. Khalid and D. V. Edmonds, As Ref. 2, p. 1
[12] Y. Koyasu et al., As Ref. 2, p. 202
[13] M. Cristinacce and P. F. Reynolds, As Ref. 3, p. 29
[14] J. F. Held, *Metal Progress*, 128 (1985) 12, 17
[15] V. Ollilainen, H. Hurmola and H. Pantinen, *Journal of Materials Energy Systems*, 5 (1984) 221
[16] B. Garbarz and R. Kuziak, Microalloying '95, The Iron and Steel Society, Warrendale, PA 1995, p. 409
[17] H. Tokada and Y. Koyasu, As Ref.3, p. 143
[18] P. E. Reynolds and J. H. Reynolds, As Ref. 3, p. 79
[19] D. Tostenson, R. Bertolo and B. Glasgal, As Ref. 3, p. 327
[20] Dj. Drobnjak and A. Koprivica, As Ref. 3, p. 93
[21] Dj. Drobnjak and A. Koprivica, Metal 97, Ostrava, Czech Republic 1997, p. 162
[22] H. K. D. H. Bhadeshia, Bainite in Steels, The Institute of Materials, London, 1992, p. 245
[23] R. A. Ricks, P. R. Howell and G. S. Barritte, *Journal of Materials Science*, 17 (1982) 732
[24] S. S. Babu and H. K. D. H. Bhadeshia, *Materials Science and Technology*, 6 (1990) 1005
[25] A. R. Mills, G. Thewlis and J. A. Whiteman, *Ibid.*, 3 (1987) 12, 1051
[26] G. Thewlis, *Ibid.*, 10 (1994) 2, 110
[27] Y. Tomita et al., *ISIJ International*, 34 (1994) 10, 829
[28] J. L. Lee, *Acta Metallurgica and Materialia*, 42 (1994) 10, 3291
[29] J. L. Lee and Y. T. Pan, *ISIJ International*, 35 (1995) 8, 1027
[30] F. Ishikawa and T. Takahashi, *Ibid.*, 35 (1995) 9, 1128
[31] F. Ishikawa, T. Takahashi and T. Ochi, *Metallurgical and Materials Transactions A*, 25A (1994) 5, 929
[32] K. Irvine and F. B. Pickering, *ISI Spec. Rep. 93*, London, 1965, 110
[33] D. V. Edmonds and R. C. Cohrane, *Metallurgical Transaction*, 21A (1990) 6, 1527

ISSN 1318-0010
KZLTET 31(6)539(1997)

TWO-WAY SHAPE MEMORY EFFECT AND ITS DEGRADATION DURING THERMAL CYCLES IN Ni-Ti ALLOYS

DVOSMERNI SPOMINSKI EFEKT V Ni-Ti ZLITINAH IN NJEGOVA DEGRADACIJA MED TOPLOTNIMI CIKLI

HEINRICH SCHERNGELL, A. C. KNEISSL

Institute of Physical Metallurgy and Materials Testing, University of Leoben, A-8700 Leoben, Austria

Prejem rokopisa - received: 1997-10-01; sprejem za objavo - accepted for publication: 1997-10-21

This work presents a study of the degradation of the Two-Way Shape Memory Effect (TWSME) due to working cycles. An intrinsic TWSME was induced in wire specimens of a near equiatomic Ni-Ti alloy by thermomechanical training. The development of the two-way strain was analysed and discussed with respect to the different training parameters and the preliminary heat treatment of the samples. Subsequent to the training, the stability of the obtained TWSME was examined by thermal cycling under stress-free conditions. Possible reasons and mechanisms for the degradation of the effect during thermal cycling are discussed.

Key words: shape memory, two-way-effect, Ni-Ti alloy, stability, martensitic transformation, fatigue

V delu se predstavlja raziskava degradacije dvosmernega spominskega efekta (TWSME) zaradi delovnih ciklov. Intrinsičen TWSME je bil induciran v žice iz equiatomske Ni-Ti zlitine s termomehanično obdelavo. Razvoj dvosmerne deformacije je bil raziskan in ocenjen glede na obremenilne in predhodno toplotno obdelavo vzorcev. Po obremenitvah je bila stabilnost dosežene TWSME preiskana s toplotnim cikliranjem brez napetosti. Razpravlja se o možnih vzrokih in mehanizmih degradacije efekta med termičnim cikliranjem.

Ključne besede: oblikovni spomin, dvosmerni efekt, zlitina Ni-Ti, stabilnost, martenzitna premena, utrujenost

1 INTRODUCTION

The term Shape Memory refers to the ability of certain alloys, to recover large strains perfectly either right after unloading (pseudoelasticity) or after heating (pseudoplasticity). Several alloys can show this phenomenon as a consequence of martensitic transformation[1]. In the case of the intermetallic phase Ni-Ti, such a transformation occurs between the high temperature modification (austenite) with a CsCl-type B2 superlattice and the low temperature phase (martensite) with a monoclinic B19' structure[2]. Furthermore, a TWSME may be obtained in these alloys after a suitable thermomechanical treatment, which is often termed training. This special behaviour refers to the ability to produce spontaneous shape changes on heating as well as on cooling, both without the application of external forces. Consequently, trained elements can directly be used as temperature-sensitive actuators. The actuators are usually electrically actuated and cooled by natural convection. One important criterion for the actual use of Shape Memory components in such multiple cycle applications is the stability of the functional parameters throughout application. A reliable component should exhibit constant transformation-temperatures and a two-way strain independent of number of cycles. In this work, the stability of an intrinsic TWSME during repeated thermal cycling has been investigated.

2 EXPERIMENTAL

The investigations have been carried out on a binary Ni-Ti alloy with a nominal composition of Ni-50,3 at% Ti. The material was melted from pure metals in an arc-furnace, hot extruded and cold-drawn with intermediate annealings. The as-received wire material was cold worked by 13,5% with a diameter of 3 mm. Wire specimens of 20 cm in length were prepared and some of them annealed at 550°C / 20 min. The transformation temperatures were deduced from resistivity measurements and are listed in **Table 1**. All transformation temperatures are above room temperature, with M_s, M_f indicating the start and finish temperature for the forward transformation, and A_s, A_f describing the reverse transformation. The mechanical properties of the alloy were investigated by tensile tests carried out at room temperature. The obtained stress-strain-curves of the martensitic phase are illustrated in **Figure 1**. The training procedure was simulated on a tensile testing machine. The specimens were fixed at room temperature, loaded with the constant training stress σ_{train} and repeatedly thermally cycled between M_f and a temperature above the highest temperature, at which martensite can be stress-induced (M_d). Heating was done by Joules-Effect, cooling by natural convection in air. According to the applied training stress σ_{train} and number of training cycles N_{train}, different magnitudes of the TWSME were obtained. Some of the values are given in **Table 2**. Subsequently to the training, the magnitude of the TWSME was measured

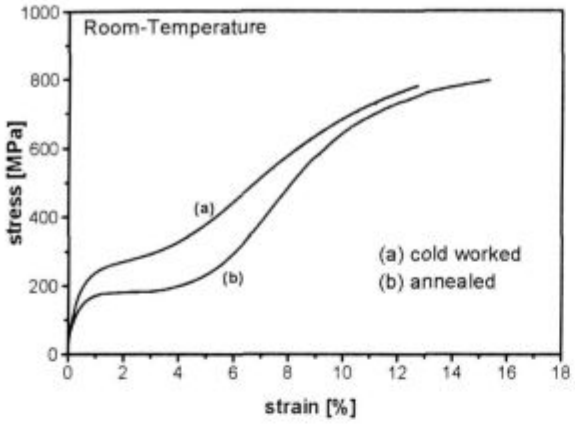

Figure 1: Stress strain curves of the martensitic modification

and its degradation during repeated stress-free thermal cycling studied.

Table 1: Transformation temperatures obtained by resistivity measurements

HT	M_s(°C)	M_f(°C)	A_s(°C)	A_f(°C)
none	52	38	82	141
550°C	55	42	84	127

Table 2: TWSME achieved with different numbers of training cycles and heat treatments

HT	σ_{train}	(MPa) N_{train}	ε_{2w} (%)
550°C	50	20	1,65
none	100	20	1,18
550°C	100	20	1,80
550°C	100	10	2,15

3 RESULTS AND DISCUSSION

It is very useful to study the strain temperature relationship in order to understand the shape memory behaviour. **Figure 2** illustrates the strain-temperature-curves as they have been recorded by microstrain measurement during the training cycles. On cooling the loaded wire specimen from a temperature above M_d, martensite is stress induced on reaching the M_s-temperature. Normally, the Ni-Ti martensite consists of 24 variants, that are crystallographically equivalent[3]. But the applied stress causes a preferred nucleation and growth of those variants, that have the highest compatibility with the strain-field. This orientation of the martensite results in a macroscopic strain in direction of the applied stress, as can be observed in **Figure 2**. On heating, the alloy transforms back to the B2 structure of the austenitic modification, forced to restore the associated original shape. A careful look on **Figure 2** shows, that the restoration does not succeed completely, but there is a small amount of irreversible strain. This irreversible strain consists as well of locally stabilised martensite as of true plastic strain[4]. During the growth of the martensite plates, stress concentrations may arise on the B2/B19' interfaces, locally exceeding the true plastic yield strength. Actually, this generation of dislocations during the thermomechanical training procedure is a precondition for the development of the two-way effect. The generated dislocation pattern is a characteristic feature of the deformed low-temperature shape, which is repeatedly formed during training. On subsequent stress-free thermal cycling, these dislocations are effective in guiding the martensite formation, causing the martensite to form at least partly oriented. The resulting two-way strain ε_{2w} has the same direction as the reversible strain during the training, but it is smaller in magnitude, as the efficiency of dislocations in the formation of a preferential martensite morphology is weaker compared to the stress field caused by an external force.

Furthermore, it can be observed in **Figure 2** that the temperature interval (A_f - M_f) increases throughout training. This is thought to be likewise due to the increase of the dislocation density. The increase of the internal stress that is connected with it reduces the mobility of the B2/B19' interfaces. As the martensitic transformation in near equiatomic NiTi occurs by the way that the martensite plates grow continuously on cooling and shrink on heating, the rise of frictional stress leads to an increase of A_f and a decrease of M_f.

The development of the TWSME can be observed best by studying the course of the different strains during training. **Figure 3** shows the labelling of the different strains describing a training cycle. If one follows the course of these strains throughout training, it becomes evident, that a high temperature and a low temperature shape is being established. The pseudoplastic strain ε_{pp} increases very fast during the first few cycles as a consequence of the stress-biased martensite formation. A certain σ_{train} is able to orient a certain amount of martensite variants. Consequently, ε_{pp} saturates after having reached a certain magnitude. To increase σ_{train} beyond a certain limit has no sense in the case of a thermomechanical training procedure as one obtains excessive irreversible strain, leading to a deterioration of the high temperature

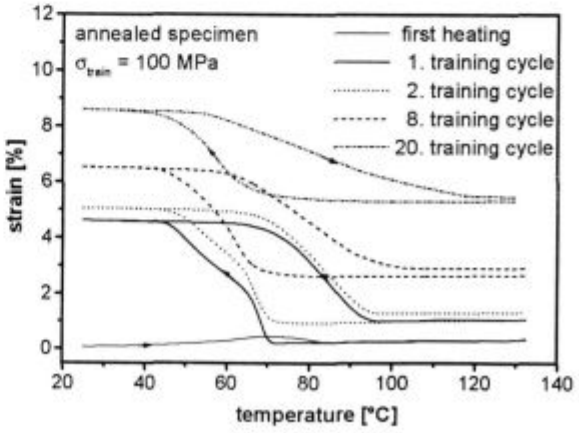

Figure 2: Illustration of some training cycles

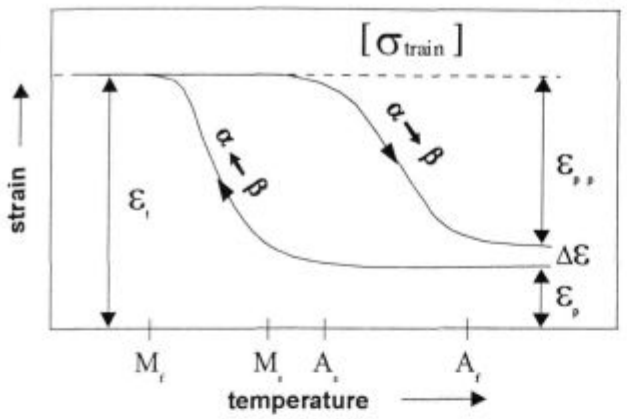

Figure 3: Schematic illustration of a training cycle indicating the labelling of the different strains: ε_t: total strain, ε_{pp}: pseudoplastic strain, ε_p: irreversible strain

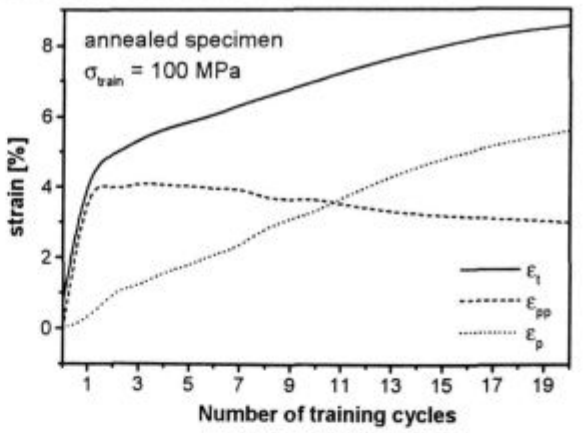

Figure 5: Development of the different strains during training, annealed specimen, 100 MPa

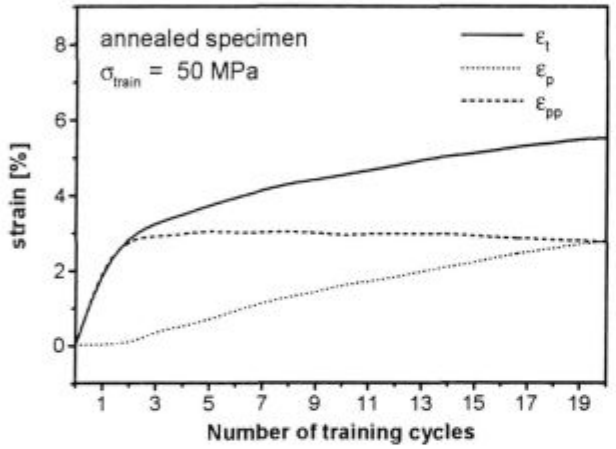

Figure 4: Development of the different strains during training, annealed specimen, 50 MPa

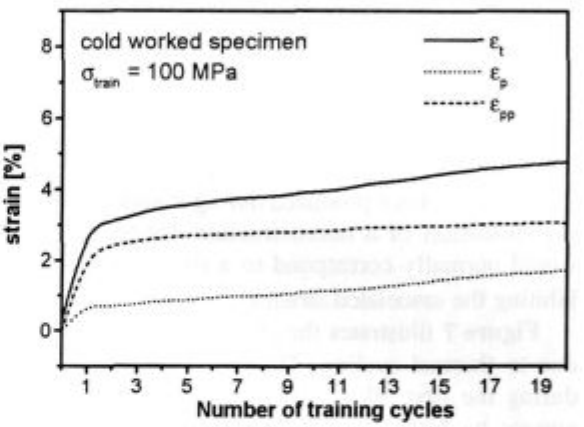

Figure 6: Development of the different strains during training, cold worked specimen, 100 MPa

shape. It has been shown by other authors that generally those training parameters (combination of training stress and number of training cycles) give the highest two-way memory, which result in the least permanent strain, while producing a full one-way strain[5]. The maximum transformation strain for a certain heat-treatment condition may be estimated from the extension of the martensite plateau in the stress-strain curve in **Figure 1**. As can be observed from **Figure 4**, 50 MPa is not enough to take advantage of the whole orientation capacity. The ε_{pp} in this plot is considerable smaller than the extension of the martensite plateau in **Figure 1**, which reaches about 4%. It is evident from **Figure 5** that an increase of σ_{train} to 100 MPa leads to a ε_{pp} of the aimed magnitude. It is interesting to note in this plot that the pseudoplastic strain decreases after having passed a maximum value after about 4 training cycles. Apparently, the irreversible strain rises too fast in the case of 100 MPa. This is quite important as it has been concluded elsewhere[5], that there exists a near proportionality between the pseudoplastic strain and the obtained two-way strain. This suggests that in order to maximise ε_{2w}, fewer than 20 training cycles should be applied. This is confirmed by the values listed in **Table 2**. In the case of σ_{train} = 100 MPa, the two-way strain obtained after 10 training cycles is larger than after 20 cycles. **Figure 6** shows the course of the strains for the work hardened specimen. Due to the high internal stresses, the σ_{train} is not as efficient in biasing the martensite formation as in the annealed specimens. A pseudoplastic strain of only 2,5% is reached and it has neither saturated nor passed a maximum after 20 training cycles. It may therefore be concluded that ε_{pp} would increase further, if training was continued.

In order to repeatedly achieve the same low temperature shape during stress-free thermal cycling it is essential, that the transformation follows the same transformation paths over and over again. The thermoelastic martensitic transformation occurs sequentially. Those martensite variants that have formed first, are the last to revert. A thermodynamic balance exists at all times on the B2/B19' interfaces between chemical and not chemical energy terms. The latter one is essentially the elastic

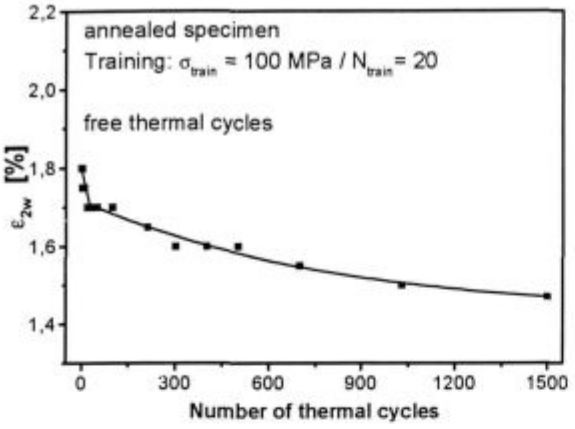

Figure 7: Degradation of the TWSME during thermal cycling, annealed specimen

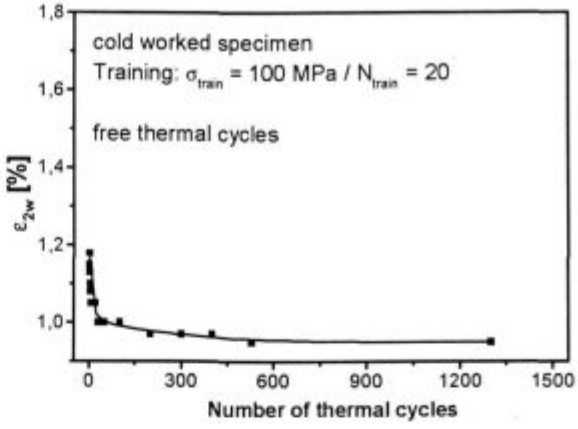

Figure 8: Degradation of the TWSME during thermal cycling, cold worked specimen

strain energy developed as the microstructural units of new phase nucleate and grow in the original phase[6]. By this energy term, the substructure can exercise some influence on the selection of variants, that are assisted in their nucleation and growth. In an asymmetric substructure, as it has been produced during training, this leads to the formation of a microstructure during cooling, that would normally correspond to a strained condition, exhibiting the associated strain ε_{2w}.

Figure 7 illustrates the change of the two-way strain due to thermal cycling. There is a rather strong decay during the first 50 to 100 cycles, which gradually decreases by further cycling. After about 500 cycles, the degradation rate becomes fairly small. Considering the importance of the asymmetric microstructure for the appearance of the TWSME, it appears very likely, that the decrease of ε_{2w} is the consequence of changes in the substructure. Investigations by Miyazaki et al.[7] showed, that thermal cycling causes a rearrangement and annihilation of existing dislocations as well as the introduction of additional ones. Both processes change considerably the dislocation pattern that has been created during the training cycles and will therefore lead to an increasing amount of unfavourably oriented martensite. Some hints about the actually controlling mechanism may be obtained by comparing the degradation of the annealed specimen in **Figure 7** to a cold worked one in **Figure 8**. While the initial decay cannot be avoided, the decrease in the latter stage shows a sensitivity from the initial dislocation density. In the annealed specimen, the two-way strain keeps degrading throughout the investigated range of 1500 thermal cycles whereas in the cold worked sample it stays almost stable. It may be suggested from this observation, that the degradation in this stage is primarily due to the introduction of dislocations. In the cold worked sample it is more difficult to generate additional dislocations as the dislocation density is already very high. This results in a more stable TWSME in the latter stage.

On the other hand, the sharp decay at the beginning of thermal cycling appears to be not affected by a higher dislocation density. Moreover, it seems to be a transient phenomenon which is limited to the first 50 to 100 cycles, reaching a saturation at the end of the initial period. It appears very likely that the decrease in this range corresponds to a continual change in the dislocation substructure - by rearrangement and annihilation - until a stable configuration, representative of the saturated state, is reached.

It should be further noted, that even on variation of the training parameters, the characteristic features of the degradation curve remain more or less the same. It becomes evident, that for the applied training procedure, the initial microstructure of the alloy influences the stability of the intrinsic TWSME far more than the training parameters.

4 CONCLUSIONS

With the chosen training procedure, a maximum two-way strain of 2,1% could be achieved. The induced intrinsic TWSME shows a sharp decay in the early stage of cyclic application. This is ascribed to the rearrangement and annihilation of dislocations during the first few thermal cycles until a new saturated state is reached. In the latter stage, the degradation rate is smaller and it shows a dependence from the preliminary heat-treatment. It is suggested that the controlling mechanism in this stage is the introduction of additional dislocations. For the practical point of view it may be concluded from this work, that trained shape memory elements should be cycled several times before application until the mechanism, responsible for the sharp decay in the initial stage, has been exhausted. The stability in the latter stage, especially in cold worked specimens, should be suitable for technical applications. The preliminary heat-treatment appears to be the crucial parameter to optimise the TWSME regarding magnitude and stability.

ACKNOWLEDGEMENT

The authors gratefully acknowledge financial support of this work by the "Jubiläumsfond der Österreichischen Nationalbank".

5 REFERENCES

[1] E. Hornbogen, *Pract. Met.*, 26 (1989) 279
[2] J. Perkins, *Metall. Trans.*, 4 (1973) 2709
[3] S. Miyazaki, K. Otsuka, *ISIJ Int.*, 29 (1989) 353
[4] R. Stalmans, J. van Humbeeck, L. Delaey, *Acta metall. mater.*, 40 (1992) 501
[5] Y. Liu, P. G. McCormick, *Acta metall. mater.*, 38 (1990) 1321
[6] J. Perkins, *Mat. Sci. Eng.*, 51 (1981) 181
[7] S. Miyazaki, Y. Igo, K. Otsuka, *Acta metall.*, 34 (1986) 2045

ISSN 1318-0010
KZLTET 31(6)545(1997)

INTRODUCTION OF UNSHAPED REFRACTORIES IN THE WEAR LINING OF STEEL LADLES

UPORABA NEOBLIKOVANEGA OGNJESTALNEGA MATERIALA ZA OBRABNO OBSTOJNO OBZIDAVO JEKLARSKIH PONOVC

F. ETIENNE[1], E. ZIAROVSKI[2]

[1]Lafarge Monolithics (LRM)
[2]Lafarge Feuerfest GmbH, Kaltenbornweg 6, 50679 Köln

Prejem rokopisa - received: 1996-10-04; sprejem za objavo - accepted for publication: 1997-10-21

Steel ladles are essential tools in steelmaking. In the past, research was almost entirely centred on converters but nowadays attention has focused on ladles. The determining factor for the choice of a lining is the cost per tonne of steel as well as reliability, security, availability and metal purity. The cost per tonne of steel has now reached a constant level with shaped products and can hardly be improved. The introduction of new technology and radical changes are the only possible means to make improvements in the economic situation. The application of unshaped products to the ladle may provide a solution. Experience in Japan has shown that improvements are possible when techniques utilising monolithics in ladles are adapted. Here we intend to describe the trials carried out by Lafarge Réfractaires Monolithiques and the first significant industrial results with the use of monolithic ladles in European conditions.

Key words: steel ladles, wear lining, monolithic lining, industrial experience

Jeklarske ponovce so bistveno orodje za izdelavo jekla. V preteklosti je bila pozornost usmerjena predvsem v konvertorje, sedaj pa se pozornost usmerja v ponovce. Odločujoči dejavnik pri izbiri obzidave so strošek na tono jekla ter zanesljivost, varnost, razpoložljivost in čistost kovine. Strošek na tono jekla je pri oblikovanih proizvodih sedaj dosegel konstantni nivo in ga bo težko izboljšati. Razvoj nove tehnologije in radikalne spremembe so edina možnost za izboljšanje gospodarskega položaja. Uporaba neoblikovanih proizvodov za ponovce bi lahko bila rešitev. Izkušnje iz Japonske so pokazale, da je mogoč napredek z uporabo monolitov v ponovcah. Tu želimo opisati preizkuse, ki so bili izvršeni pri Lafarge Réfractaires Monolithiques in prve pomembne industrijske rezultate pri uporabi monolitskih ponovc v evropskih pogojih.

Ključne besede: jeklarske ponovce, obrabno obstojna obzidava, monolitska obzidava, industrijske izkušnje

1 EUROPEAN CONDITIONS AND THE LAFARGE CONCEPT

a) LININGS IN EUROPE

In the steelmaking and secondary steelmaking process, the lining is submitted to different thermomechanical stresses. If the evolution of refractories in Europe is taken into account, it is not surprising that a wide range of ladle linings is found on the market.

- Brick linings
  - Basic linings: The slag line is often magnesia-carbon bricks, the other areas are magnesia or dolomite. The basicity of the lining may be considered a favourable factor for secondary steelmaking.
  - Aluminosilicate linings: only the sidewalls and the bottoms are in such bricks, generally bauxite. Alumina-spinel is rarely used.
- Raw materials

Let us compare the relative costs of the raw materials for the above compositions:

Spinel	100
Tabular alumina	75
Bauxite	15 - 40
Magnesia	15 - 40
Dolomite	5 - 10

Ladle linings have previously been made from less expensive raw materials (bauxite, magnesia, dolomite). In Japan, this was not the case and mostly more expensive materials were used. Therefore, from an economic point of view, the starting point for monolithic design differs in Japan and Europe.

- Metal quality

The steel ladle has become a metallurgical reactor where many operations of secondary steelmaking are carried out. Ladle refractories in contact with steel may influence the steel quality, either directly or through secondary effects. For example, refractories may cause alterations in slag composition, or indirectly affect steel quality as a result of the performance of the refractory involved in the stirring operation.

Consequently refractories play an important role in metal quality. Basic linings, in particular dolomite, have been developed for metallurgical reasons and in addition also offered to European steelmakers a cheap solution. In the past steelmakers where also concerned by the presence of alumina in ladle linings.

b) THE CONCEPT

For technical reasons, basic slag line products will not be considered in this paper. Basic castables with properties competing with basic bricks in this area have

not yet been developed to a commercial level. Therefore to date our solutions exclude the slag line and our experiences are concentrated on the monolithic sidewall, prefabicated and the casting of the in-situ bottom. Our designs are based on the following five principles:

1 The various zones of the lining

Alumina-spinel products are not considered necessary for the whole ladle, since the raw material is relatively expensive in Europe. Examples are found where this design proved to be wrong from the economic point of view. It is necessary to have different properties for the different conditions encountered in the ladle, i.e. the best quality/price ratio in each zone of the lining.

2 Deskulling and repairs

The cost of high technology alumina castables is greater than those of alumina or basic brick. However the repair/veneering of the initial lining after cleaning, not only allows the ladle availability to improve, but also reduces the refractory cost of the ladle.

For subsequent repairs/veneers we propose a self flowing castable (MONROX RANGE) which are specifically designed for this type of repair. Their special characteristics give a free flowing product which readily fills the lining profile between the former and residual lining, and has an excellent adhesion to the residual materials.

3 The development of silica-free products

With the exception of the slag line which must remain basic, the sidewall and the bottom of the ladle are lined with alumina materials. Bearing in mind the metal quality, LRM developed silica-free products for monolithic ladles.

4 Appropriate placing

Mixing, vibrating and drying together account for 50% of the achievement of the maximum campaign life. These features are specific to unshaped materials.

5 User and supplier as partners

The key to progress for the user and the supplier is co-operation. Monolithic ladles are a good replacement for shaped linings, but full co-operation is required to optimise the economic factors, a difficult but not impossible task. The following solutions may be proposed.

2 DEVELOPMENT OF SILICA-FREE PRODUCTS

Monolithic materials have vastly improved over the last few years. Highly compact products and increased refractoriness have been obtained through the technology of ultrafine particles and defloculation.

Corrosion resistance can be improved by the addition of fine particles to protect the matrix taking care to avoid possible reactions between the lining and the liquid steel, which may lead to contamination. These fine particles additions can be classified as:

- *Anti-wetting-agents*

These agents impair the penetration of the refractory matrix by oxide slags and therefore limit the corrosion to surface phenomena. They are non-oxide compositions which can only be employed in products working in reducing or moderately oxidizing atmospheres. Their use is made possible by the reduction of the oxidation rate because of the great compactness of these castables.

The most effective are also those which oxidise the most readily such as: pitch, resin, and carbon black used alone or in combination.

- *Agents wich reinforce the dissolution resistance*

These agents work by increasing the viscosity of the diffusion layer and are generally oxydes, such as Cr_2O_3, ZrO_2, MgO and MgO Al_2O_3.

The use of ultra-low cement castables allows us to obtain a matrix with the characteristics close to those of the aggregate materials. Therefore, means limiting the penetration of the corrosive elements using the two methods indicated and employing alumina ultra-fines (no silica) were developed.

Anti-wetting castables

In castables with alumina matrix moderate sintering leaves a very fine capillary structure which is easily and deeply penetrated by the slag.

With the addition of silicon carbide (**table 1- castable A**), test shows a slight improvement of corrosion resistance while the slag still penetrates deeply. This behaviour is verified by the analysis of a panel used in a ladle wall: after 50 heats, by the total residual thickness 185 mm, the thickness of the impregnated layer is 60 mm.

The transformed area no longer contains silicon carbide as this has been completely oxidised with reaction with the slag, mullite and anorthite have been formed.

Carbon is the key element to avoid penetration (**table 1 - castables B, C, D**). However, carbon addition weakens mechanical strength since it diminishes the sintering of the alumina matrix. A compromise, as in castable D, through the choice of the carbon type and the content of carbon and silicon carbide is required depending on the anticipated degree of oxidation and silicon carbide content and according to the risk of oxidation.

The principle has been applied to both corundum and bauxite castables.

Alumina-spinel castables

In several Japanese papers the use of spinel as addition to tabular alumina castables to reduce impregnation is described. The mechanism may be explained as follows:

- Spinel magnesia fixes in solid solution iron oxide from slag;
- Slag lime reacts with the alumina of the matrix to form refractory CA6

Table 1: Castables with antiwetting agents

	A	B	C	D
Al_2O_3	72	67	67	73
SiC	10	10	5	5
C	0,9	0,9	0,9	0,6
Water	4	4,2	4,8	4
Density after 1550°C/5 h*	3,30	3,13	2,98	3,18
Compression Mpa 110°C	60	30	30	30
1200°C/5 h*	65	40	25	30
1600°C/5 h*	160	120	50	100
PLC 1500°C	-0,1	+0,1	+0,2	-0,1
Corrosion 1600°C-80 mn Steel XC 38-Synthetic slag	(C/S=2,4) (Fe_3O_4=20) (CaF_2=5)			
Wear (mm)	8,6	8	6,5	7,5
Impregnation (mm)	7	0	0	0

* reducing atmosphere

Table 2: Alumina-spinel castables

	E	F	G
Alumina	82	59	62
Electro-fused spinel	-	20	-
Sintered spinel	-	-	20
Magnesia	-	3	1,4
Lime	1,4	1,4	1,4
Mixing water	4,3	4,4	4,9
Apparent density	3,07	2,92	2,93
Compression Mpa			
100°C	85	55	50
1200°C/5 hr*	90	90	80
1500°C/ hr*	140	100	90
PLC 1600°C/5 hr	+0,3	+0,9	+0,7
Corrosion 1600°C-30mn Steel XC 38-Synthetic slag	(C/S=2,4) (Fe_2O_3=20) (CaF_2=5)		
Wear(mm)	not detectable completely	8	9
Impregnation		12	12

* reducing atmosphere

- Silica concentration in slag increases and consequently its viscosity increases also
- Reaction with alumina induces precipitation of C_2AS (gehlenit)

These results have been verified in a tabular alumina castable with alumina bond. Addition of 10 to 20% of spinel strongly reduces slag penetration. The introduction of silica in the system promotes the dissolution and in this case undesirable monticellite is formed.

In **table 2** the evolution of tabular alumina-spinel products is presented. Recent developments have been made considering the following parameters:

The nature of the spinel: Laboratory corrosion tests had originally shown a deeper penetration at the slag-metal interface in over-stoichiometric than in stoichiometric spinel similar crystal size.

Facility of installation: Due to their alumina bond, the castables may need care during placement.

Improvements are being made in workability and rheology to achieve a high degree of mobility. This is essential for the future.

3 INDUSTRIAL RESULTS

Many trials have been undertaken and are either still in progress in laboratory and industrial stage. Today we have a good background of industrial experiences throughout Europe, each site presenting a different scenario:

- Integrated and electric steel plants manufacturing flat products, IFS, long products, steel for roll bearings or stainless steel;
- Ladle capacities from 50 to 310 tonnes,
- Equipement for secondary steel making including RH, DH degassers, desulphurisation lances, ladle furnaces, CAS-OB...
- And the different work cultures within the European community.

Precast wear linings for Ladle Bottoms

The development of high performance castables allows competitive solutions to be put forward in order to obtain a balanced ladle life. This is currently been demonstrated by the use of pre-cast blocks in steel ladle bottoms.

The pre-cast wear lining of ladle bottom is a solution which offers a competitive and simple alternative with many advantages, including:

- quick and easy installation,
- controlled off site casting,
- pre-drying, under controlled conditions,
- design flexibility, and
- enhanced performance.

The concept uses different castables for various pieces and joints, depending on the characteristics and constraints encountered (impact area, porous plug as well as tap-hole number and position).

a- SITE 1 - Steel Teeming Ladle-Precast bottom blocks

This site is an intregrated steel plant operation with 3 No. BOF's producing approximatively 2,3 Mt/year of strip product and supplying high quality low and ultra low carbon steel to the motor industry. Ladle availability is fundamental to this plant and improved ladle bottom performances were required. The standard brick lining gave a typical campaign of 30 heats with failure occurring in the impact pad. Our objectives were to achieve 60 heats and provide a ladle with an uniform sidewalls and bottom life. The proposals for a complete precast bottom were based on:

- improvement of the impact area with introduction of a precast pad in alumina-spinel quality;
- providing an economicaly viable balanced bottom lining exhibiting an even wear. This was achieved by introducing bauxite based products in the none impact area of the bottom;
- an intregral joint in a self flowing version of our alumina-spinel castables, which are designed for this type of installation. Their special characteristics give a free flowing product which readily fills the lining profile between the precast blocks and has an excellent user friendly nature;
- elimination of additional drying time usually associated with the use of monolithics. The drying schedule is the same as that used for the bricks.

All the objectives were achieved in performance. A typical campaign of 60 heats has been attained with a stop at mid campaign to change the wellblock. In **table 3** some technical and economic benefits acquired are listed.

Table 3: Economical and technical benefits on site 1

	Actual situation	Solution: prefabicated bottom
Material cost	100	105
Manpower cost	100	28
Client profit directs costs		-6,5% on the cost ratio
Maintenance standstill	42h	26h
Duration of a ladle campaign including installation maintenance and production duration	15 days	15 days
Client profit		-38% on the maintenance time
Indirect costs		+4,5% on ladle availability

Currentely trials are ongoing to extend the wellblock life and eliminate the stop at mid campaign and further improve ladle availability. In late 1995, this site decided to convert all their teeming ladle fleet to precast bottoms.

b- SITE 2 - Steel Teeming Ladle-Cast in-situ bottom

This 2 x 300t BOF plant is similar to other large integrated plants in that there is a desire to diminish the refractory costs in ladles. The general feeling is that the cost per tonne of steel has now reached a constant level using bricks. However, the introduction of monolithic technology was felt to be a solution that could offer significant improvements. In **table 4** the clients final gains after adoption of the monolithic concept are listed.

Our alumina-spinel products were used, the cast vibration version for the initial installation, and repairs with self-flow product. The performance of these products allowed the customer's objectives to be achieved. The fleet of ladles on this site is sufficient to allow planned campaigns when the monolothic concept is adopted the clients final gain is:

Table 4: gains on site 2

	Actual situation	Solution:cast in-situ bottom
The campaign	90 heats life with one stop to repair the impact area	360 heats with 3 small repairs of the impact area
Material cost	100	92
Manpower cost	100	29
Client profit:direct cost		-14% on the ratio
Maintenance stand-still/length	336 h(4 campaigns)	208 h(4 notations)
Duration of a ladle campaign	15 days	15 days
Client profit		-38% on maintenance time
Indirect cost		+3,5% on ladle availability

The next step at this plant is to improve the ladle sidewall.

c- Monolithic sidewall and bottom lining: our references

Monolithic products either as precast shapes or in-situ casting increase the ladle life. The campaign length is the main parameter which allows the decrease of costs per tonne. Numerous trials carried out since 1989 show a favourable evolution in maintenance costs. Some benefits are in **table 5**.

Table 5: Benefits obtained at different sites

	SITE A	SITE B	SITE C	SITE D
Process	2x310t BOF Cas-OB/CC Slag	1x70t BOF DH/LF/Lances Bloom/ Billet	1x80t EAF RH/LF/CCR Bloom/Billet	1x85t EAF LF/CCR Tube/Pipe
Initial lining	80% Al_2O_3 bricks	Dolomite bricks	MgO-C bricks	Dolomite bricks
Initial life	80 heats	60 heats	50 heats	70 heats
Monolithic concept	Al_2O_3 spinel product	Al_2O_3 spinel and bauxite product	Al_2O_3 spinel products for metal quality	Al_2O_3 spinel products for metal quality
Life	400 heats with 1 relining at 240 heats	300 heats with 4 relinings every 60 heats	120 heats with one relining	420 heats with 3 relinings
Achiefed production costs	10% material and manpower	20% material and availability	10% material and manpower	10% material and manpower

4 CONCLUSION

The trend towards the use of monolithic refractories in ladle applications has been initiated by changes in steelmaking technology and associated product technology.

However, products development has to continue to further reduce wear of the steel ladle refractories and to decrease refractory costs.

Lafarge Réfractaires Monolithiques have considered the metal quality in the development of new products for secondary steelmaking. The new silica-free bond products behave very satisfactorily in industrial service and confirm the results predicted on the base of laboratory corrosion tests. The improvement of the installation techniques will have a significant effect on the use of monolithic refractories since such techniques lend themselves to automation. When the suitability of the product has been established, the required investment in installation equipment will bring increased benefits. Recent innovations have shown that there is a place within the ladle environment for monolithic refractories and that they can meet the most competitive challenges.

5 REFERENCES

M. M. Bourdet-Jeanne, F. Etienne, P. Lafargue, Evolution des Refractaires des Poches Acier D'Unimetal Normandie: Vers la Poche Monolithique; ATS Paris, décembre 1993

F. Etienne, La Rentabilite des Poches Acier Monolithiques; Commission ATS, juin 1994

P. Atkinson, F. Etienne, Development of Monolithic Refractories in Steel Ladles; Sheffield Congress, september 1994

F. Etienne, M. Jacquemier, P. Meunier, B. Clavaud, Introduction of Unshaped Products without Silica in Secondary Metallurgy for Metal Cleanliness; Unitecr Kyoto, November 1995

Gruppenbild *ohne Dame*

Reichl & Partner Werbung

sitbergbau Veitsch/Austria 1910

Männer, deren Pioniergeist unser Weltbild in vieler Hinsicht verändert hat.
Wir von Veitsch-Radex haben größte Hochachtung vor jenen, die der Welt neue Impulse verleihen.

Es ist jener Pioniergeist, der uns zum Weltmarktführer bei Feuerfestlösungen gemacht hat. Zu einer Position, die durch die Treue unserer Kunden Tag für Tag bestätigt wird. In über 150 Ländern werden Qualität und Verläßlichkeit unserer Produkte und Dienstleistungen geschätzt. Unsere höchsten Qualitätsmaßstäbe werden durch die Zertifizierung nach ISO 9001 unterstrichen.

Starke Ideen,
starke Produkte,
starke Partner.

Veitsch-Radex Aktiengesellschaft
für feuerfeste Erzeugnisse
Wien 4., Mommsengasse 35, A-1011 Wien, Postfach 143,
Tel.: ++43/1/502 13-0, Fax: ++43/1/50213-213
Telex: 111 766 Vrag

Veitsch-Radex

ISSN 1318-0010
KZLTET 31(6)551(1997)

PULSE PLASMA NITROCARBURISING OF GAS SHOCK ABSORBER TUBES FROM STEEL W.No. 1.0116

NITROKARBURIRANJE CEVI PLINSKEGA BLAŽILCA IZ JEKLA W.No. 1.0116, V PULZIRAJOČI PLAZMI

VOJTEH LESKOVŠEK[1], M. DOBERŠEK, A. RODIČ

Vacuum Heat Treatment and Surface Engineering Centre, Institute of Metals and Technology, Lepi pot 11, 1000 Ljubljana, Slovenia

Prejem rokopisa - received: 1997-10-01; sprejem za objavo - accepted for publication: 1997-10-21

Gas shock absorber tubes from steel W.No. 1.0116 were pulse plasma nitrocarburised at 560 and 580°C in atmosphere containing carbon dioxide additions. Variations in compound layer structure, thickness, porosity, hardness-depth profiles and stability of the process were investigated. It was found that the formation of predominantly ε phase compound layer structure is promoted by high nitrogen atmosphere. The compound layer thickness was found to increase with increasing nitrogen content, temperature, and pulse as well as decreasing carbon dioxide content. The experiments showed that by use of high nitrogen atmosphere no pores appear in compound layers on steel W.No. 1.0116. Proper process control and the addition of carbon dioxide to the atmosphere with high content of nitrogen result in a reasonably thick compound layer from predominantly ε phase.

Key words: pulse plasma nitrocarburising, compound layer, structure, porosity, hardness-depth profile, thickness, stability of the process

Nitrokarburiranje cevi plinskega blažilca iz jekla W.No. 1.0116 v pulzirajoči plazmi je bilo izvršeno pri temperaturi 560°C in 580°C v atmosferi z dodatkom ogljikovega dioksida. Raziskali smo mikrostrukturo spojinske plasti, debelino, poroznost ter profil trdote nitrokarburirane plasti in stabilnost procesa. Ugotovili smo, da se lahko z uporabo atmosfere, ki vsebuje visok odstotek N_2, poveča tvorbo spojinske plasti, ki je pretežno sestavljena iz ε faze. Ugotovili smo, da debelina spojinske plasti raste z vsebnostjo N_2, temperaturo in frekvenco pulziranja ter z zniževanjem vsebnosti ogljikovega dioksida v atmosferi. Eksperiment je pokazal, da visoka vsebnost N_2 ne vpliva na nastajanje por v spojinski plasti, ki se tvori na jeklu W.No. 1.0116. Pravilno vodenje procesa ter dodatek ogljikovega dioksida v atmosfero z visoko vsebnostjo N_2 omogoča doseganje sprejemljive debeline spojinske plasti, ki je sestavljena pretežno iz ε faze.

Ključne besede: nitrokarburiranje v pulzirajoči plazmi, spojinska plast, struktura, debelina, poroznost, profil trdote, ponovljivost procesa

1 INTRODUCTION

Pulse plasma nitrocarburising has grown to a thermochemical heat treating process of particular technological and economic importance for improving the surface characteristics of components for mechanical engineering. The most important advantages are greatly improved wear, fatigue, and corrosion resistance. As a low temperature process it minimises distortion and volume change of parts treated. Pulse plasma nitrocarburising produces at the surface compound layer of a few micrometers in thickness consisting mostly of ε phase, and a significantly thicker diffusion zone. As opposed to conventional salt bath and gas processes, nitrocarburising in glow discharge pulse plasma affets several advantages. In addition to its increasingly important environmental acceptability, plasma nitrocarburising because of the possibility of freely selection at a wide variety of process parameters also makes it possible to match the properties of the layers to the specific load profile of the application.

In the present paper a short survey of theoretical aspects of pulse plasma nitrocarburising is given and its significance as industrial process is assessed. The experiments were carried out on two charges of gas shock absorber tubes with different load configurations and process parameters to produce at the surface an up to 10 μm thick compound layer consisting predominantly of ε phase.

2 SOME THEORETICAL ASPECTS OF PULSE PLASMA NITROCARBURISING

The pulse plasma nitrocarburising process is characterised by a glow discharge surrounding the workpieces surface, which appears at low pressures when a voltage is applied between the workpieces and the furnace wall. The workpieces are held at a negative potential (cathode) while the furnace bell is positive (anode). The furnace must initially be pumped down to a low pressure and subsequently refilled with a suitable gas mixture to a pressure of ~1-10 hPa. A voltage of 200-1000 V is then applied, whereupon the gas species in the reaction vessel becomes ionised. By controlling the power input the workpieces can be heated to the nitrocarburising temperature, but better control of the magnitude and uniformity of the temperature is obtained with auxiliary convection heating. Another way to control the heat input to a greater precision is to apply a pulsating voltage and supply the furnace with heating elements. In this manner the workload temperature can be controlled with the retention of a high degree of glow discharge control. The problems with arc formation, local overheating, and

the hollow cathode effect can thus be minimised. The pulse frequency that could be used ranges between DC and 33 kHz. To obtain uniform nitriding depths and uniform compound layer thickness it is important to emphasise that process parameters - applied voltage, pulsing frequency, load configuration, etc.- must be selected empirically. Load configuration is very important. If components are placed too close together the hollow cathode effect can cause severe problems.

The compound layer structure and the depth of the diffusion zone can be controlled by varying the gas mixture, pulsing frequency and temperature. Normally the compound layer contains only the γ phase. To achieve a compound layer consisting of ε phase on steels a gas mixture of nitrogen, hydrogen and carbon dioxide is used.

The base for understanding the events during the formation of the compound layer and the diffusion zone is provided by the ternary Fe-N-C phase diagram. The two significant binary systems making up the sides of the ternary system, Fe-C and Fe-N[1], are well known. However, many observations are in disagreement with this diagrams. These deviations are often explained in terms of kinetics or orientational relations between the lattices of the various phases prevailing over the pure thermodynamic equilibrium in the formation of these phases. For these reasons a new ternary phase diagram has been proposed by J. Slycke et al.[2]. This diagram eliminates all ambiguity regarding the interpretation of how structures have evolved, since all observations can be explained by the local equilibrium approach. The major difference between the new diagram and that published by Naumann et al.[1] is that it allows the frequently observed direct contact between ferrite (α) and ε phase. The new Fe-N-C phase diagram shown in **Figure 1** is characterised by two

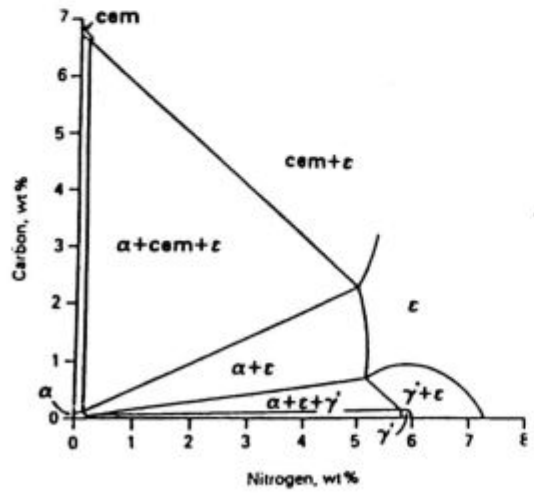

Figure 1: Schematic ternary Fe-N-C phase diagram at ~580°C suggested by J. Slycke et al.[2]

Slika 1: Shematski ternerni Fe-N-C fazni diagram pri ~580°C po J. Slycke et al.[2]

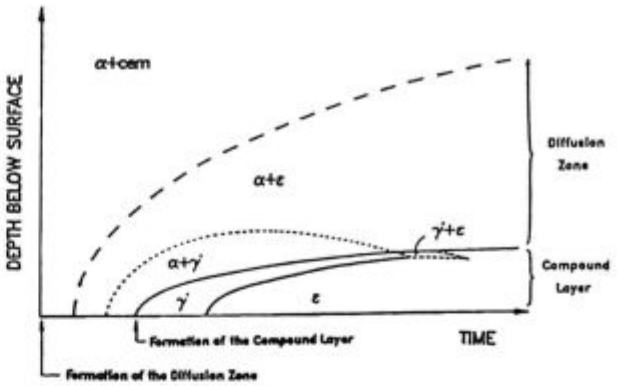

Figure 2: Schematic illustration of the evolution of the diffusion zone and compound layer during nitrocarburisig of carbon steels[3]

Slika 2: Shematska ponazoritev razvoja difuzijske in spojinske plasti pri nitrikarburiranju ogljikovih jekel[3]

three phase equilibrium (α + ε + γ and α + Fe_3C + ε) and one ternary two phase field (α + ε).

The ε phase field extends towards lower nitrogen contents with increasing carbon content as consequence of the stabilising effect of carbon on the ε phase, which can exist at a lower nitrogen content (~5% N) than the γ phase (5.9% N).

The different sequences during the nitrocarburising process of low carbon steels[3] are shown schematically in **Figure 2**. During this process ε phase and γ' phase are formed within the evolving diffusion zone, followed by the formation of γ and ε phases in the fully developed and growing compound layer.

3 EXPERIMENTAL PROCEDURE

3.1 Material and process of pulse plasma nitrocarburising

The gas shock absorber tubes ϕ 28 x 175 mm used in the present work are from steel W.No. 1.0116 with the chemical composition given in **Table 1**.

Table 1: Chemical composition of steel W.No. 1.0116, (in wt-%)
Tabela 1: Kemijska sestava jekla W.No. 1.0116 (v ut.%)

	C	Si	Mn	P	S	Cr	Mo	Ni	Al	Cu
WNr 1.0116	0,15	0,013	0,53	0,011	0,008	0,023	0,006	0,019	0,049	0,031

The pulse plasma furnace used was a GP 1000/80 M nitriding unit manufactured by Metaplas-Ionon GmbH, **Figure 3**. The furnace is equipped with a convection heating system and with an internal gas/water heat-exchanger for quick cooling.

The gas shock absorber tubes in load configuration as shown in **Figure 4** were pulse plasma nitrocarburised at 560 and 580°C at 5,2 hPa and 2,8 hPa pressure, using a total gas flowrate of 100 and 67 l h^{-1}. The gas shock ab-

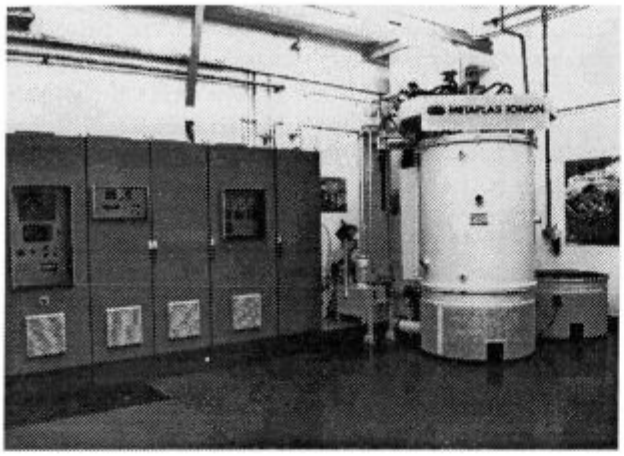

Figure 3: Pulse plasma nitriding furnace GP 1000/80 M
Slika 3: Peč za nitriranje v pulzirajoči plazmi GP 1000/80 M

sorber tube's temperature was measured with two chromel-Alumel termocouples embedded in a tubes on two different levels (top and bottom) in the first and the third circuit.

Gas atmospheres with nitrogen contents 70,5 and 87%, carbon dioxide contents 2,5 and 2% and hydrogen contents 27 and 11% respectively, were employed. The pulse frequency used was 2 and 2,5 kHz, respectively. Convection and plasma heating to process temperature took appr. 4h and the isothermal treatment lentghs were 10 and 4 hr respectively, followed by forced cooling in a flow of nitrogen.

4 RESULTS AND DISCUSSION

4.1 Compound layer structures

In pulse plasma nitrocarburising, the large number of freely definable treatment parameters make it possible to control precisely the structure, composition, and growth characteristics of the compound layer without impairing the formation of the diffusion layer.

The tubes nitricarburised for 10 and 4 hr in the pulsed plasma mode, considering the 0,480 ms glow-on time, 0,020 ms glow-of time, the 0,200 ms glow-on time, and 0,200 ms glow-of time, respectively were transversally sectioned at the middle, metallographically prepared, and etched with 3% nital for the determination of the thickness of the compound layer on an optical microscope. The thickness of the compound layer was taken by averaging five measurements for each tube.

Figure 5 shows the microstructure of the nitrocarburised layer on the outer surface of the 5 tubes taken from the third circuit from 5 different levels of the charge no.1 (560°C). The charge no.1 contain 685 tubes in 5 circuits with 20 mm intercircuit distance, processed for 10 hr in pulsed plasma mode, considering the 0,480 ms glow-on time and 0,020 ms glow-of time. The compound layers thickness appears to be 5 to 8 µm and the growth rate 0,5 to 0,8 µm/hr. Metallographical analysis (**Figure 5**) indicates that the compound layer on tubes on the top and bottom (sample 1 and 5) obtained by the above pulse plasma nitrocarburising parameters mainly consisted of γ' phase - $Fe_4(N,C)_{1-x}$. While the compound layers of the tubes between two (samples 2 - 4) consisted beside of γ' phase also of ε phase- $Fe_{2-3}(N,C)_{1-x}$ and carbide particles. In the compound layers grain boundaries are parallel to the diffusion direction and thus perpendicular to the surface. Under compound layers of these same tubes (samples 2 - 4) a 15 to 25 µm thick fringe of pearlite is found, while this fringe is not found under the compound layer on top and bottom tubes (samples 1 and 5).

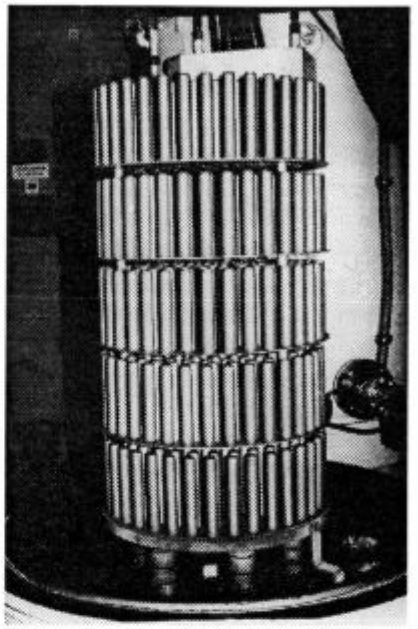

Figure 4: Gas shock absorber tubes in load configuration
Slika 4: Razporeditev cevi plinskega blažilca v sarži

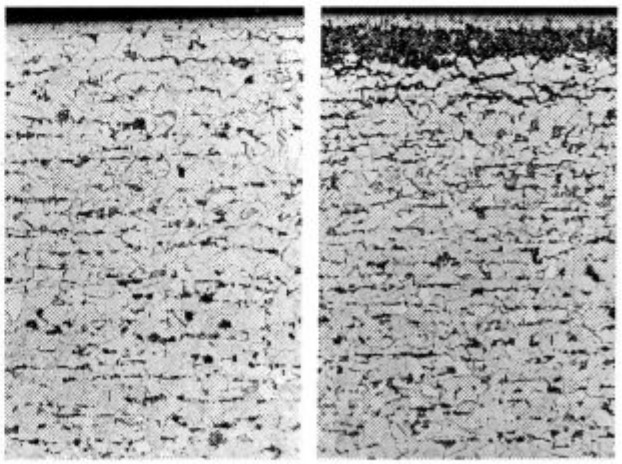

Figure 5: Microstructure of the nitrocarburised layer at the outer surface of tubes (200x)
Slika 5: Mikrostruktura nitrokarburirane plasti ob zunanji površini cevi (200x)

From the obtained microstructures it is possible to conclude that the temperature within the charge was not equalised or the distribution of gas mixture because of charge configuration was not fulfilled. The analysis of the process parameters actually shows that in spite of the relative high pressure (5,2 hPa) the temperature difference between the two thermocouples was too large (~25°C), because of the hollow cathode effect caused local overheating. This effect called the hollow cathode can occur when the cathode drops to a dimension equal to the distance between tubes.

Nitrocarburising depth on 5 tubes from top to bottom is shown in **Table 2.**

Table 2: Metallographically determined nitrocarburising depth on tubes from charge no.1

Tabela 2: Metalografsko določene globine nitrokarburirane plasti na ceveh iz sarže 1

No. of tube	Nitrocarburising depth in mm
1	0,43
2	0,48
3	0,46
4	0,43
5	0,47

Microhardness profiles HV0,3 of the nitrocarburised layers for the same 5 tubes (top and middle of the tube) are shown in **Figure 6.**

From the **figures 5 and 6**, it can be seen that the microstructure and hardness of diffusion layer on tubes from different levels are affected by the hollow cathode efffect, which causes also the irregular thickness and the type of compound layer which is also too thin.

As mentioned above the goal of the present work was to obtain at the surface of the gas shock absorber tubes a compound layer consisting predominantly of ε phase with a thickness of ≥ 10 µm. In the case of the gas shock absorber tubes the thickness of diffusion zone is not so very important. Such compound layer produced by pulse plasma nitrocarburisig process improves corrosion and wear resistance and after fine polishing one can obtain also satisfactory level of decorativeness. In order to avoid the hollow cathode effect causing local overheating of tubes it was necessary to rearrange the load configuration in such a way that the distance between tubes and each next circuit is appr. 1,3 time the distance between tubes. With new load configuration charge no. 2 processed at 580°C contains 552 tubes in 6 levels.

The thickness of the compound layer produced at 580°C with a 4 h treatment depends not only on the nitrogen and carbon dioxide levels in the treatment atmosphere, but also on the pulse frequency used. The results indicate that increasing the pulse frequency and the nitrogen level in the atmosphere an increased compound layer thickness ≥ 10 and a surface hardness in excess of 320 HV1 are obtained. The growth rate becomes greater than 2,5 µm/hr. This tendency is mostly due to the increased nitrogen "activity" in the plasma.

Figure 7 shows the typical microstructure of the nitrocarburised layer on the outer surface of the shock absorber tubes which consists predominantly of ε phase - $Fe_{2-3}(N,C)_{1-x}$. The compound layer at the surface consists of 2 µm thick monophase range of ε - $Fe_{2-3}(N,C)_{1-x}$, and it is followed by a two-phase field (ε + γ') up to 6 µm thick. In the compound layer grain boundaries are parallel with the diffusion direction and thus perpendicular to the surface. The diffusion zone below the compound layer consisted of the eutectoid constituent braunit (α + γ') from the binary Fe-N[1] system and some islands of pearlite and needles of γ'. The present experiments have confirmed that the use of high nitrogen atmospheres produces no pores in the compound layers developed on steel W.No. 1.0116.

4.2 Reliability survey

The reproducibility of the process is shown in **figure 8**, which presents the results of the processing of 23

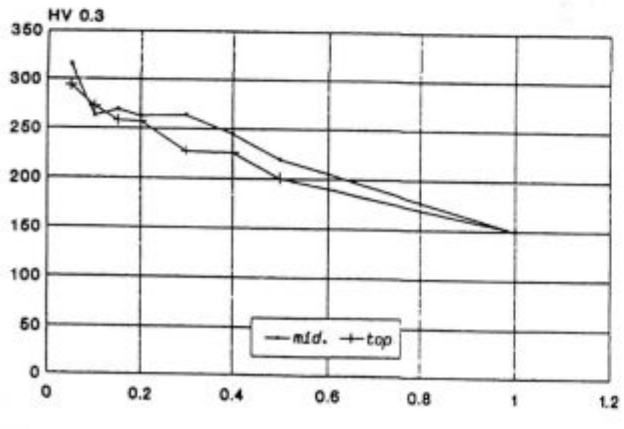

Figure 6: Microhardness profiles HV0,3 of the nitrocarburised layers
Slika 6: Profil mikrotrdote HV0,3 nitrokaburirane plasti

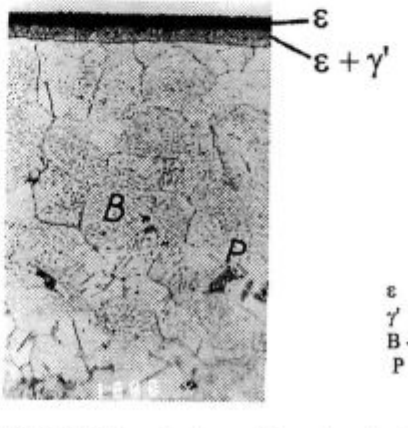

Figure 7: Microstructure of the nitrocarburised layer on the outer surface of the shock absorber tubes
Slika 7: Mikrostruktura nitrokarburirane plasti na zunanji površini cevi plinskega blažilca

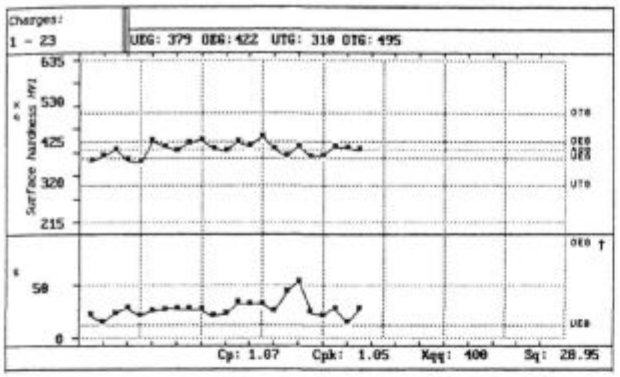

Figure 8: Reproducibility of the pulse plasma nitrocarburising process on 23 charges
Slika 8: Ponovljivost procesa nitrokarburiranja v pulzirajoči plazmi pri 23 saržah

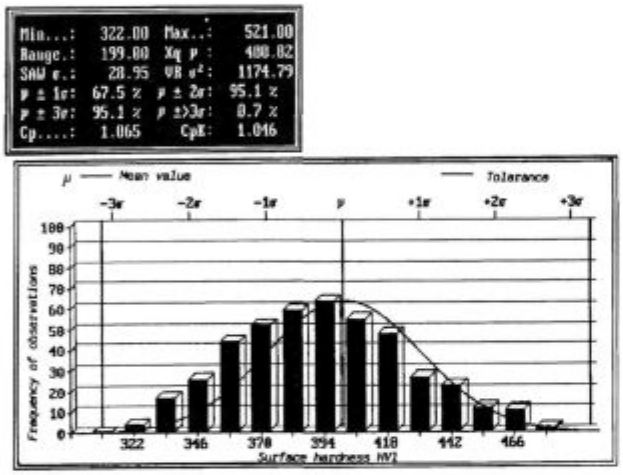

Figure 9: Statistical consideration of surface hardness HV1 data on 23 charges
Slika 9: Statistična obdelava podatkov površinske trdote HV1 pri 23 saržah

charges. A typical charge may contain up to 552 tubes with a net weight of around 94 kg.

Statistically confirmed quality control data for surface hardness HV1 are shown in **figure 9**.

These distributions satisfy customer's ± 3σ (standard deviation) quality requirements, that mean 95% of all pulse plasma nitrocarburised tubes have to meet this specification. However, it should be pointed out that fluctuations in the hardness of the core materials, i.e. 150-230 HV1 and used UIC (Ultrasonic Contact Impedance) hardness testing method[4] can affected the nitrocarburising results and are not taken into account in the statistical control. Clearly, improved control over the variations experienced in core hardness would be expected to reduce the amount of scatter observed in the nitriding results. Fortunately, the quality requirements are already satisfied to such an extent that these effects may be disregarded.

5 CONCLUSIONS

On the basis of the present experiments, it is confirmed that the atmosphere consisting of 87% N_2 + 2% CO_2 + 11% H_2 and increased pulse frequency are required in the glow discharge to produce a compound layer thickness ≥ 10 μm without pores and with a predominantly ε phase structure.

From the results is evident that higher nitrogen content in atmosphere, higher temperature and increased pulse frequency strongly influenced the compound layer growth rate which is by the second charge nearly three times higher than in by the charge no. 1 processed in a less suited atmosphere. With a new load configuration charge no. 2 and increased pulse frequency the phenomenon called the hollow cathode effect, which causes local overheating among the tubes, was also avoided.

Beside this, it is very important that pulse plasma nitrocarburisig quickly overcomes its sometimes still unfavourable image and that this modern and progressive technology is recognised as a reliable case hardening process. What good are all the remarkable technical, economical and environmentally clean properties of the process if it cannot be justified in practical use under industrial conditions? The results presented in this work prove that such a demand can be fulfilled.

6 REFERENCES

[1] F. K. Naumann and G. Langenscheid: *Arch. Eisenhüttenwes.*, 36 (1965) 677-682
[2] J. Slycke, L. Sproge, and J. Agren: *Scand. J. Metall.*, 17 (1988) 122-126
[3] J. Slycke and L. Sproge: *Surface Engineering*, 5 (1989) 2, 125-140
[4] Krautkrämer: Technical Reference and Operating Manual, 1992, Ident. No. 28894

EUROMAT '98

CONFERENCE ON

MATERIALS IN OCEANIC ENVIRONMENT

22-24 JULY

LISBON, PORTUGAL

1998

SCOPE

»Materials in Oceanic Environment« is one of the conferences in the EUROMAT series which is devoted to one main topic.

The Conference will be held in Lisbon, from 22 to 24 July 1998, and its scope is related to the behaviour of systems, structures and materials in oceanic environment. Therefore this EUROMAT '98 will be an important event and its scope is closely related to the »International Year of Oceans«, both taking place in 1998.

The place chosen – Lisbon – has a very special meaning. An exhibition at this same city will be open to the public at this occasion – EXPO '98 – which theme is »The Oceans, a Heritage for the Future«. In the XV century the Portuguese ships – the caravells – left from Lisbon to open to the World the maritime roads to the other Continents and Seas.

Understanding and prediction of the behaviour and performance of materials used in systems under marine environment are essential. The Conference will mainly discuss development related to all aspects of safety and risk, reliability and lifetime of equipments, pollution reduction and the sea as a source of resources.

EUROMAT '98 MAIN THEME:

Materials in Oceanic Environment

Specific topics:

I) Behaviour of systems and their structures.
- ships
- platforms offshore
- pipelines
- harbour systems and installations
- airplanes
- bridges and civil engineering structures

II) Behaviour of materials and protection mechanisms:
- corrosion
- biodegradation
- fatigue, fracture, stress-corrosion
- low temperatures

III) Materials characterization, testing and selection
- metals (ferrous, non-ferrous)
- concrete, reinforced concrete
- wood, plywood
- polymers, composites
- rubber
- ceramics and glass
- adhesives
- coatings, paints

IV) Influence of manufacturing processes on materials behaviour:
- metallurgical processes
- powder technology
- welding, brasing
- forming, machining
- heat treatment
- surface treatment
- gluing

V) The oceans as a source of material

VI) Recycling and disposal of waste materials

VII) Case studies

ISSN 1318-0010
KZLTET 31(6)557(1997)

POSSIBILITIES AND PERSPECTIVES FOR DEVELOPMENT OF METALLURGY IN THE REPUBLIC OF MACEDONIA

MOŽNOSTI IN PERSPEKTIVE ZA RAZVOJ METALURGIJE V REPUBLIKI MAKEDONIJI

JOVAN K. MICKOVSKI[1], N. NACEVSKI[1], B. NIKOV[2], S. MILOSEVSKI[3]

[1]Faculty of Technology and Metallurgy, University 'St. Cyril and Metodius', R. Bošković b.b., 91000 Skopje, Macedonia
[2]Department of Science 'Zletovo' - Metallurgical and Chemical Company, Veles
[3]Administration for International Scientific and Technical Cooperation, Ministry of Science

Prejem rokopisa - received: 1997-10-01; sprejem za objavo - accepted for publication: 1997-10-21

Installed metallurgical capacities in the Republic of Macedonia exceed the local market and a significant share of products is exported. These exports represent a very significant share of foreign currency inflow. The production of steel is based on scrop import. Ferroalloys industry shows improving performances because of transformation of ownership and restructuring. The increasing of production capacities is expected and especially it is planned to build facilities for exploitation of all lead in zinc concentrates produced in Macedonia.

Key words: Macedonia, metallurgical industry, production of steel, ferroalloys, lead, zinc, cadmium, silver

Instalirane metalurške kapacitete v Republiki Makedoniji presegajo absorbcijo domačega trga in precejšnja količina proizvodov se izvaža. Ta izvoz predstavlja pomemben deleže dotoka deviz. Proizvodnja jekla bazira na uvozu starega železa. Proizvodnja ferolegur kaže naraščujoče dosežke zaradi olastninjenja in restrukturiranja. Pričakuje se povečanje kapacitet, predvsem pa se načrtuje povečanje exploatacije koncentratov svinca in cinka.

Ključne besede: Makedonija, metalurška industrija, proizvodnja jekla, ferozlitine, svinec, cinka, kadmij, srebro

1 INTRODUCTION

The capacities of ferrous and non ferrous metallurgy are overextended considering the market requirements in the Republic of Macedonia. In accordance with the fifty years period of development of the Republic of Macedonia, within the former Yugoslav Federation, and the natural resources, the strategic development of ferrous metallurgy of the Republic of Macedonia was projected in accordance with the capacities in Slovenia and the previously started construction of the Steel Complex in Zenica, Bosnia and Herzegovina (BH). The strategy of the Yugoslav industrial development was strongly oriented towards the West European market and the regions more closer to Europe were developed as final exporters for western markets. Other regions should have supported the technological and the industrial development of northern regions through raw materials, and have provided food and other less finalized products for local markets.

The production of steel in Macedonia, the primary processing of steel sheets and the production of ferrochrome and ferrosilicon, combined with Slovenian production should have supplied the Yugoslav market with beaded profiles. Profiled steel should have been provided by the Republic of BH while the production of tubes was given to the Steel Complex in Sisak, Republic of Croatia.

In the former SFRY, the planed roles did not change, not even after the year 1970 and in Macedonia, two large extractive metallurgical capacities, one for ferroalloys (FeNi) and the second for lead and zinc, have been built. Processing plants for these raw materials have not been foreseen in Macedonia.

Considering the industrial structure in Macedonia with the processing of steel and other metals was far below the installed capacities for steel constructions and seam tubes, as well as the disproportion between extractive and processing units in steel industry, the Macedonian ferrous industry was forced towards foreign markets. The foreseen supply with semi finished products for the Steel Complex Skopje from the Steel Complex in Smederevo has never been accomplished since, and beside the blast furnaces and the steel plant, rolling mills for profiles almost identical to the assortment of the Steel Complex in Skopje were built in Serbia. The steel processing capacities in Macedonia, were left without raw materials, and faced with the local market competition. The solution was found in the import of semi-finished products, mainly from the former USSR and other foreign markets.

2 FERROUS METALLURGY

At present, in the Republic of Macedonia, the following metallurgic capacities for production and processing of steel and ferroalloys are in operation:

- Electric Steel Processing Plant and Rolling Mill in Skopje "Rudnici i Zelezarnica Skopje"

- Chemical Electric-Metallurgical Complex "Jugohrom", in Jegunovce (in the vicinity of Tetovo)
- Company with mixed ownership for production of ferronickel "Fenimak" in Kavadarci
- Factory for welded tubes "11 Oktomvri" in Kumanovo

2.1 Steel complex 'Skopje'

The Steel Complex in Skopje was built in accordance to the silicate ores reserves on the territory of Macedonia. Due to the lack of cocking coal, and considering the large reserves of lignite in Serbia, electrometallurgy procedure with low combustion electro reduction furnaces and prereduction in rotation furnaces with lignite, was selected. For the beneficiation of the charge up to 42% Fe, a peletisation unit for the magnetic iron ore from the Damjan Mine, in the vicinity of Radovis, was built with magnetic separation, and use of imported ferrous concentrates. The 5 electroreduction low combustion furnaces with the installed power of 195 MW and five 90 m long rotation furnaces, were projected to produce about 600.000 t/years of pig iron. However, due to unsolved technological problems, the production of pig was obtained mainly by reduction of the cold charge in the electric furnaces, which, besides the unfavorable chemical content - high concentration of silicium without manganese - significantly increased the price of pig iron. Within a period of 25 years of production, the projected capacity was not achieved because of back of reducing agents and of electric power. Because of these limiting factors and technological problems in the pre-reduction process, for which numerous pilot and semi-industrial researches have been carried out, the maximum production ever reached was 280.000 t/year[1].

The processing of pig iron with high content of silicon was achieved in two LDAC converters, 130 t each. Because of the small individual capacity of the electric furnaces for homogenization of the chemical content and maintenance of temperature two reservoirs for liquid iron were provided. Pig iron from the electric furnaces with more than 2% Si, was processed in the unit for desiliconition in pig iron ladle. The steel obtained from the converters was cast in slab ingots up to 1981, later a continuous caster for slabs was built.

In order to provide the own steel required by the rolling mill capacity, an electric arc furnace of 100 t was build and additional 200.000 t of pig steel provided. In 1988, the capacity of the electric arc furnace was increased to 350.000 t/year, while in the second phase, by melting of scrap iron steel production was planned to reach 500.000 t/year. However, due to technological problems in the computerized electric arc furnace and difficulties in the supply of appropriate and sorted scrap iron, the new furnace did reach only a yearly production of 250.000 t/year steel.

The basic product are low carbon and carbon manganese structural as well as ship plates and boiler plates. Later also the production of microalloyed steels with niobium, vanadium, titan and zirconium was developed. The converters were also suitable for the production of deep drawing steels.

The Steel Complex 'Skopje' includes the following three rolling mills:

- Hot rolling mill for 3.000 mm heavy plates with the capacity of 500.000 t/year, on a reversible four-high rolling stand, with a vertical duo-stand on line
- Hot rolling mill for 1.600 mm rolled strips with the capacity of 850.000 t/year, with a four-high rolling pre-stand and a final six stands train with four-high rolling stands; and
- Rolling mill for cold rolled strips with two lines: (a) a five stands train with the capacity of 500.000 t/year and (b) a four-high reversible stand of 300.000 t/year.

The cold rolling mill includes also a department zinc coating with the capacity of 100.000 t/year as well as a line for plastification of plates with the capacity of 25.000 t/year.

The rolling mill capacities were built for about 2.000.000 t/year of final products, while the maximal production obtained by the Steel Complex 'Skopje' was 1.250.000 t/year because of the lack of steel of own production. Considering the discrepancies in the primary metallurgical and processing production the Steel Complex was forced to import semi products or to undertake loan arrangements.

The Macedonian market could absorb maximally 100.000 t/year cold roll and plates, while the possibilities for absorption of hot mill strips are greater since the Factory for welded tubes with the capacity of about 600.000 t/year is located at a distance of about 35 km from the Steel Complex. The Steel Complex disposed of the majority of production on the markets of the former Yugoslav republics and to export markets.

After 1991 a significant decrease in production occurred due to the economic and political crisis in the former USSR, the main foreign partner and in the former SFRY. Consequently, in the following 4 years the production of the Steel Complex was significantly decreased and than even discontinued.

The cost of production of pig iron in electroreduction low combustion furnaces and steel in converters was too high and in 1988 it was stopped.

Also the costs analyses of steel production from local ores led to its stopping. Lately two electric reduction furnaces were restructured and the production of ferromanganese and siliconmanganese was started on the base on imported raw materials. The actual production amounts to 36.000 t/year of ferromanganese and 44.000 t/year siliconmanganese. Other units were preserved and the converter unit was dismantled.

2.2 Production of 'Jugohrom' Jegunovce

The enterprise 'Jugohrom' is the producer of mass ferroalloys as FeSi, FeCr, silicon metal and silicon-chrome primarily for the requirements of the ferrous metallurgy and casting industry of the former SFRY. The products are lately totally exported.

The capacity of 'Jugohrom' was rebuilt for a modern production of ferroalloys, with melting aggregates with medium and large installed power; permanently modernized in terms of technique and technology, providing:

- Increased production compared to the originally projected;
- Alternative production and quick adjustment to the market conditions, necessary for a competitive market oriented production;
- Improvement of operating conditions;
- Environment protection etc.

The production of ferroalloys in 'Jugohrom' in accordance with its assortment can be performed in nine electric furnaces with the total installed capacity of 140.2 MVA, in accordance with the schedule presented in **Table 1**.

The intensive development of processes of ladle processing for acquiring ferroalloys with improved physical-mechanical properties, as well as technological and exploitation characteristics required the application of a broad scale of complex alloys - modifficators for cast iron. Based on these trends of development in metallurgy, in the current phase of modernization, 'Jugohrom' has developed the technology for production of complex alloys-modificators based on ferrosilicon used as inoculant and nodulators.

The production of these alloys is based on FeSi, with addition of Mn, Ba, Ca, Al, Mg, Ce, MM, and C. By applying the direct procedure, a further alloy-up of melted FeSi or its alloys into a melting pot with spilling, sinking and mixing homogenous complex alloys - modificators of a broad assortment like FeSi, FeSiAl, FeSiMn, FeSiBa, FeSiBaMn, FeSiMgCeMM and composite mixtures FeSiC and FeSiBaC are obtained.

The production capacity and assortment depend of the demand on local as well as on export markets.

The metallurgical production in 'Jugohrom' was conditioned by the development of new technologies of steel production and casting of gray and nodular iron, primarily by the ladle processing by modification, alloying and microalloying, providing a high yield of metal and ferro alloys. From this point of view, the long-standing experience of 'Jugohrom' will be directed in future towards:

- quality improvement of the present assortment of ferroalloys and modificators;
- production of special, fine ferroalloys, especially of fine FeSi, by application of new technologies;
- extension of the production of complex alloys - modificators with new more efficient types and assortment of inoculators and nodulators;
- introduction of quality FeSi with low content of Si: FeSi 15 (14-16 Si) for production of resolvable anodes for cathodic protection, FeSi 15 powder for separation of ore minerals in heavy liquids;
- development of auxiliary devices for casting industry and metallurgy;

Development of dust collecting and utilization of waste gases heat and its conversion into electric power, all contributing to the environment protection and improvement of the overall operation of the enterprise.

2.3 Production of ferronickel

The Ferronickel producer 'Feninmak' in Kavadarci is organized as a share holding company and exploits local raw materials of laterite type.

The technological process includes are beneficiation and preparation for metallurgical processing based on differences in density and magnetic properties of minerals in the ore and the distribution of the nickel. The process is performed in the plant for ore pulverizing, pneumatic, dry and wet magnetic separation, as well as for

Table 1: Characteristics of the melting units in 'Jugohrom'

Furnace	Type of the furnace	Install. capacity MVA	Type of electrodes	Production of ferroalloys		
				Basic		Alternative
				Type	Production technical capacities t/year	
I	Electric-arc reduction	6.5	A	Si-metal	3.400	FeSi45/75/90
II	"	10.0	A	"	4.000	"
III	"	6.5	A	"	3.00	FeSi45/75/90 SiCr
IV	"	16.0	A	"	5.200	FeSi45/75/90 Cr
V	Electric-arc rafin.	3.5	G	LC FeCr	4.500	"
VI	Electric-arc slake	4.4	Sö	FeSi 75	13.300	FeSi 45/CaC2
VII	Electric-arc reduction	21.3	Sö	FeSi 75	13.300	FeSi 45/CaC2
VIII	"	48.0	Sö	"	34.000	FeSi 45
IX	"	24.0	Sö	"	14.000	FeSi 45HCFeCr
Total	9	140.2			77.300	

Abbrev.: A-amorphi, G-graphite, Sö-Söderberg

pelletisation of nickel concentrate. It has been foreseen that the magnetic fraction in the ore should be about 30%, representing the ferrous concentrate, with a lower content of nickel and the difference with higher nickel content.

Besides preparation and pelletisation, the technological process includes roasting of the pellets, their pre-reduction in rotation furnaces by addition of lignite and melting of the pre-reduced material into 16% FeNi, which is further refined up to 45% FeNi into oxidind converters. Two pyrometallurgical lines with separate rotating and rectangular electric furnaces with six Söderberg electrodes set in line are in operation. The projected total capacity of the plant was 21.000 t/year nickel in FeNi by average ore content of 1.03% Ni. So far only one technological line was used[2].

Changes in mining technology and unprecise previous geological investigations lead to a very small magnetic fraction with higher percentage of nickel during exploitation and affected the production costs. Consequently, magnetic concentration is being avoided and the overall ore supply is ground and pelletized.

Nickel is a stock exchange product which price in the last 10 years changed significantly. In 1984 and 1985 it was very low and the production of FeNi was interrupted only one and a half year following the start of production. As a result of changes in nickel prices on world market and after investments of several companies the production of one technological line re-started at the end of 1991. During recent years the production increased permanently, however the projected values, will not be obtained due to the decrease average content of nickel in the ore. **Table 2** indicates the trend of production in the restart period.

Table 2: Production of Ni as FeNi in 'Fenimak'

Year	1992	1993	1994	1995
Produced in t	4.220	4.493	3.981	4.960

Due to the second decrease of the nickel price in the period of 1993 to 1995, the society in the period of 1993/94 operated with loss and profit was obtained later because of the light increase of nickel price.

If the present trend of increase of nickel price will continue, the production could increase to 5.500 t/year with only one technological line and be profitable. Following the re-start, rigorous economic measures have been undertaken related with the restructuring of the production, to the decrease of the number of employees, to the improvement of the technology within given conditions related to the supply of raw materials and direct marketing. 'Fenimak' is forced to import lignite from SR Yugoslavia. The enterprise undertakes serious and detailed investigations of the mineralogy of the mine deposit, as well as for possible alternatives for economic beneficiation of the nickel ore. The production could increase only if the nickel content in the charge of furnaces is increased. This can be obtained through the supply of rich raw materials and requires additional working capital. Domestic investments are almost impossible because of the present economic situation, since Macedonia is exhausted by the political and economic changes imposed by the disintegration process and the war on the territory of the former SFRY as well as the economic and transport blockades of some neighbours of the Republic of Macedonia. New investments in the present production of 'Fenimak' and its increase with the re-start of the second technological line will be welcome and of benefit for the investors since the enterprise employs qualified managerial staff and disposes of modern technological devices with capacity non exploited.

Ferro-nickel is sold on foreign markets and only a very small quantity was sold on the local market, because of the crisis in steel metallurgy during the last years.

3 CAPACITIES OF NONFERROUS METALLURGY IN MACEDONIA

Moderate quantities of nonferrous metals are produced in the MHK 'Zletovo'. Smelter 'Zletovo' is using Imperial smelting process for exstraction of zinc, lead, cadmium and silver.

3.1 Lead and zinc

Lead and zinc ores have been exploited for centuries in the Kratovo-Zletovo ore deposit. Traces such as tools, slag, pots etc. indicate that lead has been smelted in the region during the Roman period.

'Zletovo' Metallurgical and Chemical Company in Titov Veles is the only producer of lead and zinc in the Republic of Macedonia. It is based mainly on the ore deposits and capacities of the three surrounding lead and zinc mines: Zletovo, Sasa and Toranica.

The Imperial Smelting process route was the most convenient for treating lead and zinc concentrates simultaneously. Moreover, it offered an opportunity to produce bulk concentrates, thus increasing the overall metal recovery. Therefore, an agreement was signed, the site preparation began, and the first quantities of slab zinc and lead bullion were produced in November 1972.

'Zletovo' Smelter was designed for a maximum production of 65,000 tpa of slab zinc and 35,000 tpa of lead bullion. **Figure 1** shows the annual production rates in the period from 1973 to 1995. Numerous prerequisites are required to reach the designed capacity of the ISF.

The break of the continuous growth of metal production from 1986 to 1991 was due to series of problems arising from the disintegration of former Yugoslavia, international sanctions against the Federal Republic of Yugoslavia, and Greek embargo against the Republic of Macedonia. These events created enormous difficulties in transporting both raw materials and products and led to higher production costs.

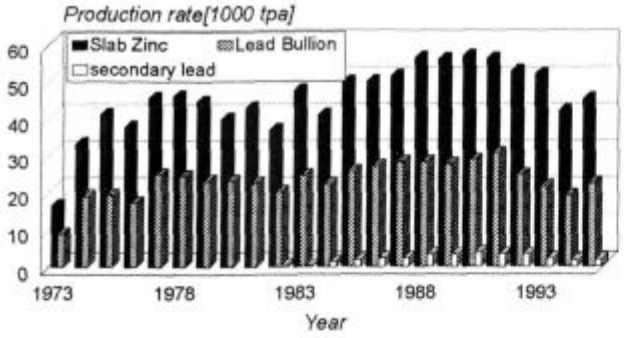

Figure 1: Annual production of slab zinc, lead bullion and secondary lead from plant start-up to 1995
Slika 1: Letna proizvodnja slabov cinka, primarnega in sekundarnega cinka od zagona podjetja do 1995.

Most of the refined lead produced at 'Zletovo' smelter is consumed within the country, mainly in the lead batteries plant having a capacity of 24000 tpa. However, due to the same reasons as above, especially the disintegration of SFR Yugoslavia, the market the battery plant was designed for, the production rate has been reduced down to 30%.

Lead and zinc production rates are increased since the Dayton and New York agreements were signed last year, but a period of several years is necessary for a full recovery.

3.2 Cadmium

Most of the cadmium fed onto the sinter machine is eliminated during the sintering process. The degree of elimination depends mainly on sulfur and cadmium contents of the raw mix, but the usual level is as high as 65 to 80%. With the construction of the cadmium plant based on the Ion Exchange Process the recovery of cadmium is accomplished with high efficiency (over 92% as shown in **figure 2**).

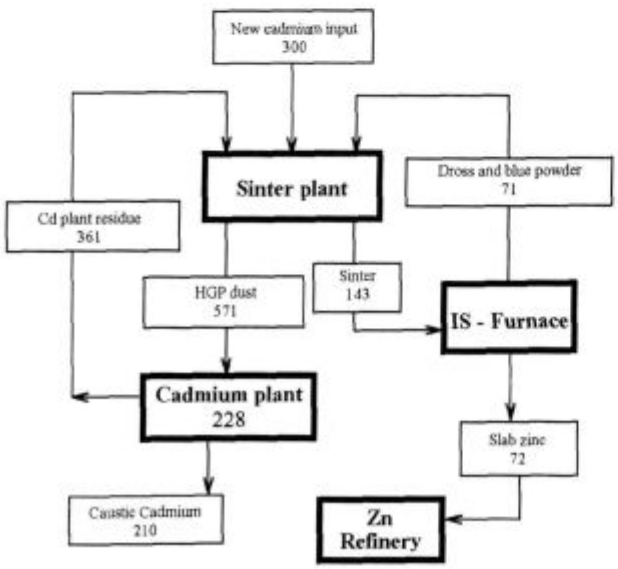

Figure 2: Overall cadmium balance
Slika 2: Celovita bilanca kadmija.

Cadmium is leached from the hot gas dust precipitator by means of weak sulfuric acid. Depending on the chemical compounds in which cadmium is present in the dust, leaching efficiencies from 30 to 60% are obtained. The resulting leach liquor is countercurrently washed in a system of three decanters, filtered through a pair of sand filters and subjected to ion exchange on IR 120 cation exchange resin. Stripping is performed by means of 10% brine solution. Cadmium sponge produced by cementation on zinc rods in suitable trammel tanks is melted in a caustic furnace and combined with the zinc refinery to a cadmium alloy for further refining.

Despite the high stage efficiencies, the magnitude of losses is high and disturbing. As shown in **figure 2**, cadmium recirculating load is very high relative to the new input and this feature must contribute considerably to the losses.

Cadmium production rate in a zinc and lead smelter depends primarily on the quantities of new cadmium fed with the raw materials. Since significant quantities of zinc concentrates have been purchased from various producers around the world, it is obvious that the Zn/Cd ratio is rather a varying parameter. However, there are two objectives that a zinc smelter must achieve:

- High cadmium elimination to provide good zinc quality
- High cadmium recovery to avoid environmental problems

The annual production of cadmium from the 'Zletovo' Smelter from its start up to 1994 is shown in **figure 3**.

3.3 Silver

Unlike cadmium, most of the silver fed with concentrates reports in the lead bullion. Desilvering of the later is performed by adding metallic zinc and removing the resulting solid intermetallic compounds (mainly Ag_2Zn_5) together with a substantial amount of mechanically entrained lead as a silver crust. Further treatment of the crust includes evaporating of zinc, oxidizing of lead and electrolytic refining of silver.

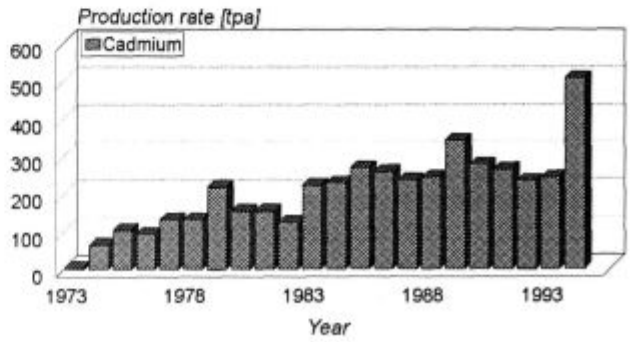

Figure 3: Annual cadmium production from plant start-up to 1995
Slika 3: Letna proizvodnja kadmijev od zagona podjetja do leta 1995.

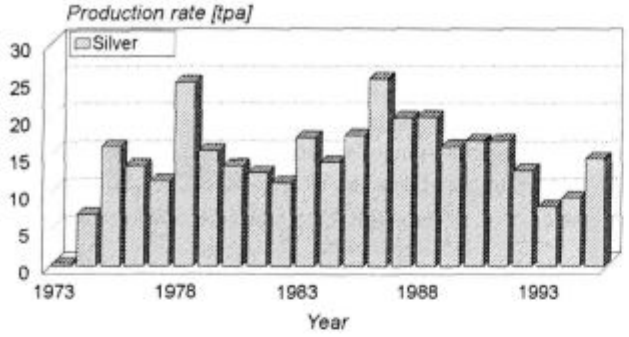

Figure 4: Annual silver production from plant start-up to 1995
Slika 4: Letna proizvodnja srebra od zagona podjetja do 1995.

The electrolytic silver refinery was introduced in 1982. Its total capacity amounts 30 tpa electrolytic silver, but the highest production achieved so far was 24.35 t in 1986.

4 CONCLUSIONS

- The installed metallurgical capacities of iron, its alloys and nonferrous metals in the Republic of Macedonia encompasses the requirements of the local market and is directed towards the foreign market;
- The participation of steel, ferro alloys and nonferrous metals alloys in the national foreign currency inflow is very significant;
- due to the discrepancies between the primary steel production and the installed melting capacities, as well as the limited possibilities for supply of raw materials, the metallurgy in Macedonia is forced to import steel in a slabs and scrap;
- considering the 30 years of experience in the steel industry and in the production of ferro alloys, following the carried out transformation of ownership and completion of the restructuring processes, more profitable operating and its further development may be expected;
- increasing the production capacities regarding various metals could also be expected, but it is intended to provide facilities for treating all the lead and zinc concentrates produced in the Republic of Macedonia. With respect to this, installing a new lead smelter plant has been considered.

5 REFERENCES

[1] Program of the restructuring for Iron and steel work 'Skopje' during the period 1991-1995, with vision to 2000, Iron and steel work 'Skopje', Department for development, Skopje, 1990

[2] Analysis of production posibilities, markets condition and financial effects of project FENI- Kavadarci, RTB Bor, Institut za bakar, Bor, 1983

ISSN 1318-0010
KZLTET 31(6)563(1997)

INVESTIGATION OF KINETICS LEACHING AND EXTRACTION OF VANADIUMPENTOXYDE AS A FUNCTION OF TEMPERATURE

RAZISKAVE KINETIKE LUŽENJA IN EKSTRAKCIJE VANADIJEVEGA PENTOKSIDA V ODVISNOSTI OD TEMPERATURE

NIKOLA NACEVSKI[1], B. NIKOV[2]

[1]Faculty of Technology and metallurgy, Skopje, Macedonia
[2]Smelter Zletovo, Veles, Macedonia

Prejem rokopisa - received: 1997-10-01; sprejem za objavo - accepted for publication: 1997-10-21

In several thermal power plants in operation in the Republic of Macedonia a substantial quantity of ash is produced by oil burning. Ashes are considered as highly hazardous for the environment due to their fine particle size. On the other hand, analyses carried out so far, indicate appreciable contents of vanadium, gallium, beryllium etc. in the ashes.

Key words: oil ashes, V_2O_5, leaching, effect of temperature and solution composition, activation energy of leaching

V Makedoniji obratuje več termoelektrarn, kjer pri zgorevanju olj nastaja pepel, ki je nevaren za okolje zaradi drobnozrnatosti. Po drugi strani pepel vsebuje pomembne količine vanadija, galija, berilija itd.

Ključne besede: oljni pepel, V_2O_5, luženje, vpliv temperature in sestave raztopin, aktivacijska energija luženja

1 INTRODUCTION

Investigations presented in this paper are aimed to examine the possibility of hydrometallurgical treatment of ashes, produced with burning of fuel in power and metallurgical plants. The topics of the present investigations are the recovery of vanadiumpentoxyde as value component and the utilization of dust which is an ecological problem. The investigations of the hydrometallurgical treatment of ashes were aimed to determine the working conditions and process laws of leaching of vanadiumpentoxyde in solution. The purification of V_2O_5 solution and its concentration of V_2O_5 is obtained with liquid-liquid extraction with D2EHPA (DI - 2 etil heksil phosphoric acid).

The effects of temperature (298 - 373 K), phase ratio (S/L : 1/50 - 1/5), concentration of H_2SO_4 in solution (0,5 ; 1 ; 1,5) mol/dm^3, were investigated by constant particle size (-0,074 mm 100 %), velocity of mixing 8000 rev./min and leaching time 3 hours.

Experimental results showing the influence of temperature, concentration of H_2SO_4 and phase ratio on V_2O_5 leaching are showed on **figures 2, 3, 4**.

2 RESULTS AND DISCUSSION

The kinetics shows that by the maximal investigated temperature of T = 373 K and the following conditions S/L 1/50, H_2SO_4 1 mol/dm^3 in the first 30 min of leaching 67,4% V_2O_5 is dissolved. Prolonging the leaching time is without significant influence on volume of V_2O_5 in solution. Changes of concentration of H_2SO_4 (0,5 - 1,5 mol/dm^3), of phase ratio (1/50 - 1/5) affect by constant temperature (343 K) also in the first period the V_2O_5 leaching efficiency.

A leaching activation energy E_a = 24,8 kJ/mole was determined through Arhenius analysis of the kinetics curves in **figure 2**.

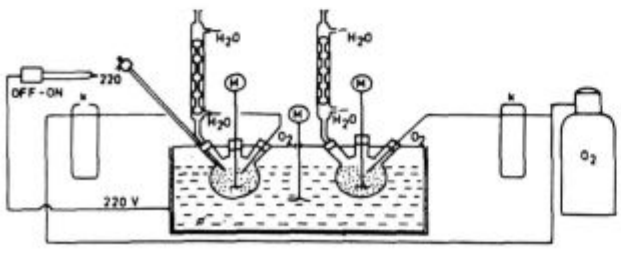

Figure 1: Apparatus for leaching
Slika 1: Naprava za izluževanje

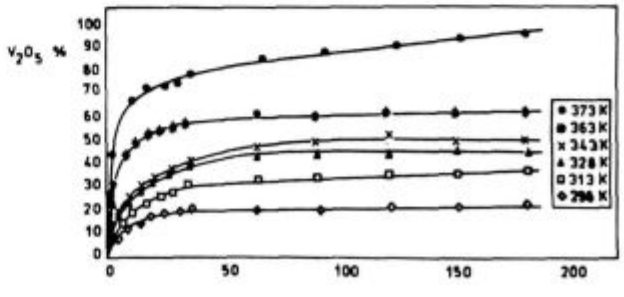

Figure 2: Kinetics of V_2O_5 leaching for different temperatures
Slika 2: Kinetika izluževanja V_2O_5 za različne temperature

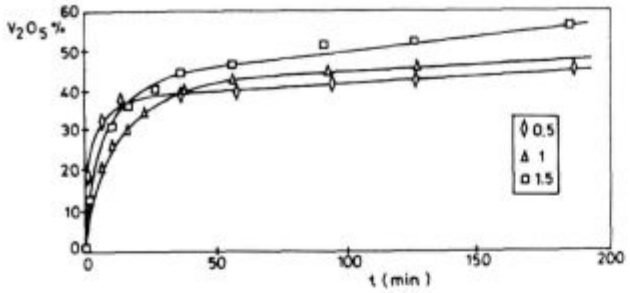

Figure 3: Kinetics of V_2O_5 leaching for different concentrations of H_2SO_4
Slika 3: Kinetika izluževanja V_2O_5 za različne koncentracije H_2SO_4

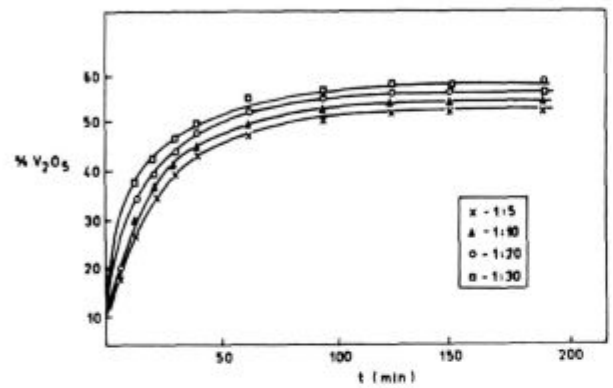

Figure 4: Kinetics of V_2O_5 leaching for different phase ratios
Slika 4: Kinetika izluževanja V_2O_5 za različna razmerja faz

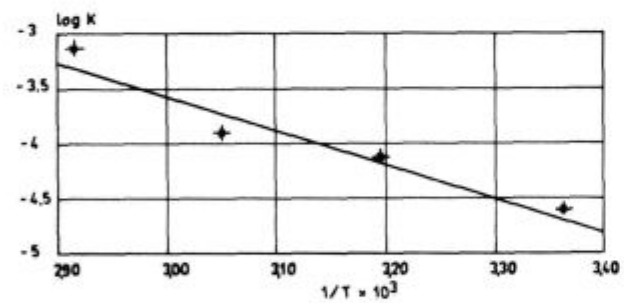

Figure 5: Graph of variables in Arhenius presentation
Slika 5: Odvisnosti v Arhenius predstavitvi

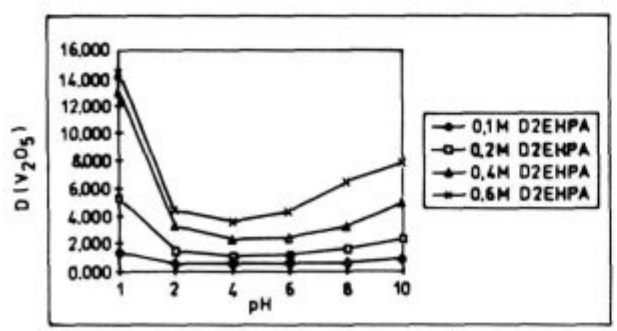

Figure 6: Effect of concentration D2EHPA on coefficient of distribution $D(V_2O_5)$ ($C_{initial}$ = 0,2 mol/dm^3)
Slika 6: Vpliv koncentracije D2EHPA na razdelitveni koeficient $D(V_2O_5)$ ($C_{začetna}$ = 0.2 mol/dm^3)

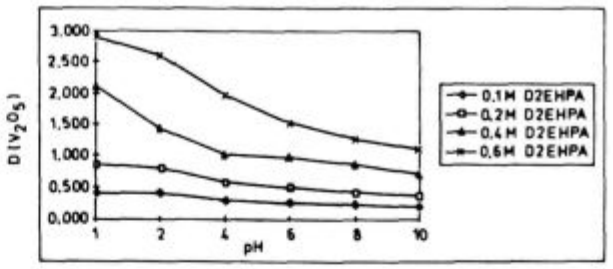

Figure 7: Effect of concentration D2EHPA on coefficient of distribution $D(V_2O_5)$ ($C_{initial}$ = 0,4 mol/dm^3)
Slika 7: Vpliv koncentracije D2EHPA na razdelitveni koeficient $D(V_2O_5)$ ($C_{začetna}$ = 0.4 mol/dm^3)

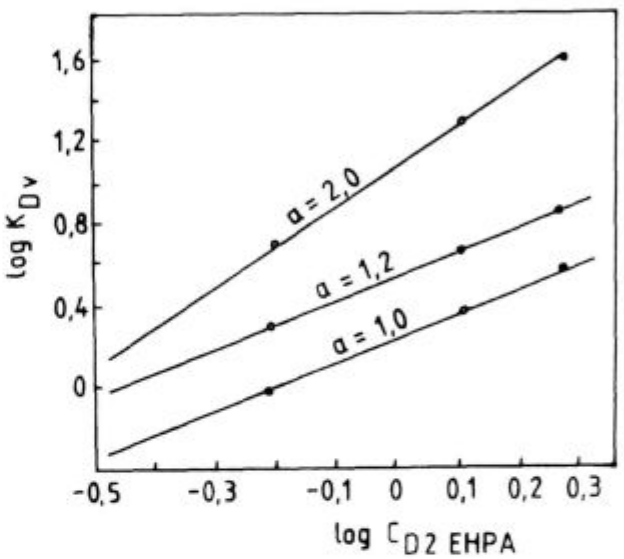

Figure 8: Log-log dependence of $D(V_2O_5)$ and (D2EHPA) for different concentrations of HCl ($C_{initial}$ = 0,2 mol/dm^3)
Slika 8: Log-log odvisnost med $D(V_2O_5)$ and (D2EHPA) za različne koncentracije HCl ($C_{začetna}$ = 0.2 mol/dm^3)

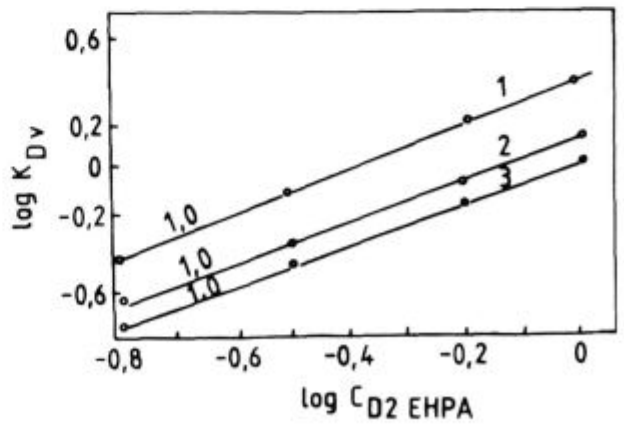

Figure 9: Log-log dependence of $D(V_2O_5)$ and (D2EHPA) for different concentrations of HCl ($C_{initial}$ = 0,4 mol/dm^3)
Slika 9: Log-log odvisnost med $D(V_2O_5)$ in (D2EHPA) za različne koncentracije HCl ($C_{začetna}$ = 0,4 mol/dm^3)

The experimental investigation of liquid-liquid extraction using D2EHPA was carried out with initial concentrations of V_2O_5 of 0,2 mol/dm^3 and of 0,4 mol/dm^3. In the tests sulfate solutions were used and the liquid-liquid extraction investigated as function of the following parameters:

a) pH of solution: 1 ; 2 ; 4 ; 6 ; 8 ; 10 mol/dm^3
b) Concentration of D2EHPA: 0,1 ; 0,2 ; 0,4 ; 0,6 mol/dm^3

3 RESULTS AND DISCUSSION

The experimental results showing the coefficient of distribution $D(V_2O_5)$ and the level of extraction $E(V_2O_5)$ as a function of parameters a) and b) are given in **table 1** and **2** and **figure 6** and **7**.

The analyses of the experimental data show by determined changes of the coefficient of distribution and level of extraction V_2O_5 as a function of pH an intial period of decreasing grade of extraction while by increasing of pH, the extraction efficiency of V_2O_5 is increased.

In logarithmic presentation the functions are straight lines which slopes represent the solvent coefficients. In **figure 8 and figure 9** the line slope have a tangents value of 2. It is concluded that vanadium will be recovered with a phase ratio $C_{D2EHPA}/L_{phase} = 2$. With increasing the pH solutions until 10 mol HCl the slope is tangent decreased to 1, 2 and in this case extraction will be realized with a ratio phase $D2EHPA/L_{phase} = 1 : 1$.

4 REFERENCES

[1] A. N. Zelikman, T. M. Voldman, A. B. Beloevsija: Teorija gidrometalurgicheskih procesov Moskva, Metalurgija, 1983

[2] Processing of petroleum coke for recovery vanadium, Hazen Research Inc. 4601 Indiana str. Golden C.O. 80403, USA, 1986

[3] O. B. Michesen: Recovery of vanadium from dust in the aluminum industry, Institute for energy technology P.O. 40 Norway, 1987

[4] N. Nacevski, F. Popovska, B. Nikov: Extraction of indium from sulphate solutions with D2EHPA solutions; *Journal de Physique III*, 5, (1995) nov.

ISSN 1318-0010
KZLTET 31(6)567(1997)

THE DIFFERENCE BETWEEN THE MAGNETO-CRYSTALLINE ANISOTROPY OF THE INTERMETALLIC ALLOY $Pr_2(Co_{0.5}Fe_{0.5})_{17}$ AND INTERSTITIALLY MODIFIED $Pr_2(Co_{0.5}Fe_{0.5})_{17}N_{3-\delta}$

RAZLIKA MED MAGNETNO KRISTALNO ANIZOTROPIJO $Pr_2(Co_{0.5}Fe_{0.5})_{17}$ IN $Pr_2(Co_{0.5}Fe_{0.5})_{17}N_{3-\delta}$

MATEJ KOMELJ, S. KOBE

Institut Jožef Stefan Jamova 39, 1000 Ljubljana, Slovenija

Prejem rokopisa - received: 1997-10-01; sprejem za objavo - accepted for publication: 1997-10-21

The alloy with the composition $Pr_2(Co_{0.5}Fe_{0.5})_{17}$ has an easy-axis magneto-crystalline anisotropy. The anisotropy is changed to the easy-plane by introducing nitrogen on interstitial sites. We proved the difference between the anisotropy of the basic alloy and the nitrided composition directly by the magnetic measurements and by observing the domain structure by means of optical and magnetic force microscopy. The transition from one to another type of anisotropy can be explained by a simple model based on crystal structure and shape of the electronic cloud of the Pr ion.

Key words: permanent magnet materials, magneto crstalline anisotropy, nitriding

Intermetalna zlitina $Pr_2(Co_{0.5}Fe_{0.5})_{17}$ ima osno magneto-kristalno anizotropijo. Z uvajanjem dušika na intersticijska mesta anizotropija preide v ravninsko. Razliko med tipoma anizotropij med obema spojinama dokažemo neposredno z magnetnimi meritvami in opazovanjem domenske strukture z mikroskopom na magnetno silo (MFM). Prehod iz ene anizotropije v drugo kot posledico spremenjene sestave lahko razložimo s preprostim modelom, ki temelji na kristalni strukturi in obliki elektronskega oblaka iona Pr.

Ključne besede: trajno-magnetni materiali, magneto-kristalna anizotropija, nitriranje

1 INTRODUCTION

It is well known that R_2T_{17}, where R stands for a rare earth and T for a transition metal, intermetallics exhibit interesting magnetic properties and represent important permanent magnet material[1]. To obtain high coercivity of the magnet it is necessary that the material has an easy-axis magneto-crystalline anisotropy and that the value of the coefficient K_1, which is a measure for the energy of the magneto-crystalline anisotropy, is as high as possible[2]. The magneto-crystalline anisotropy of the basic compound can be influenced by introducing nitrogen on interstitial sites in the crystal lattice[3]. The $Pr_2(Co_{0.5}Fe_{0.5})_{17}$ compound crystallizes in the rhombohedral Th_2Zn_{17} type structure and it has easy-axis magneto-crystalline anisotropy[4,5]. But the anisotropy is too weak and the magnet based on this material does not exhibit desired properties. In our work we studied the influence of nitrogen in the $Pr_2(Co_{0.5}Fe_{0.5})_{17}$ alloy. In Sm_2Fe_{17} intermetallic alloy the magnetic properties were successfully improved by introducing nitrogen to the interstitial sites of the crystal lattice[6].

2 EXPERIMENTAL

The samples were prepared from 99.9% pure elements by arc melting. Excess of Pr was added to a nominal composition to offset Pr evaporation losses during melting. After the fourth melting the samples were wrapped in a Ta foil and encapsulated after evacuation in quartz tubes and then annealed at 1000°C for 24 hours. Before and after the heat treatment their phase purity was determined by JEOL JXA 840 SEM/EPMA electron probe microanalysis. Nitriding, as a gas-solid reaction, was performed at 450°C for 10 hours in a high purity N_2 1 bar gas atmosphere. The nitriding temperature was previously determined by using DTA/TGA facilities (Netzch). The parent alloy and the nitrided powder were characterized by XRD. The magnetization measurements on the powdered and aligned samples were provided by the magnetometer-susceptometer (Manics) based on the Faraday principle. Magnetic domains were examined by magnetic force microscopy (MFM) using a Dimension 3000 scanning probe microscope (Digital Instruments, Inc.), which allows separate atomic force and magnetic force images to be collected in the course of one scan. Surface topography was obtained using Tapping Mode[7] AFM. High resolution MFM image was obtained by using Lift Mode software[7] and the ultra-soft Fe-SiO_2 tip. Images of the domain patterns were previously taken by Kerr microscopy using a Nikkon Optiphot XP-2 polarizing light microscope with a 150W Xe lamp.

3 RESULTS OF THE MEASUREMENTS

The magnetization versus applied field curves of the $Pr_2(Co_{0.5}Fe_{0.5})_{17}$ bonded powder measured parallel and perpendicular to the direction of the alignment are shown

in **Figure 1**. From these curves it is evident that the anisotropy field is greater then 30 kA/cm which implies the existence of weak easy-axis magneto-crystalline anisotropy. The domain pattern of this alloy, observed by optical microscope in a polarized light using the magneto-optic Kerr effect is shown in **Figure 2**. A star shaped or "labyrinth" pattern in the grains cut perpendicular to the c-axis and a banded or "strip" structure within the grains cut parallel to the c-axis are present. Such domain structure applies for materials with easy-axis type of magneto-crystalline anisotropy where the crystallographic c-axis defines the easy direction[8]. **Figure 3** shows the same area observed by the magnetic force microscope (MFM) which appears to be in a good agreement with Kerr microscopy. Both magnetization curves of the nitrided powder, measured parallel and perpendicular to the direction of the alignment are essentially the same (**Figure 4**) that means that the nitrided material does not have an easy-axis magneto-crystalline anisotropy. This fact was confirmed also by observation of the domain structure. **Figure 5** shows the Kerr image of a large (~100 μm) particle. Because of the slow nitrogen bulk diffusion[9] just a layer of width ~5 μm was nitrogenated. The core area represents the basic $Pr_2(Co_{0.5}Fe_{0.5})_{17}$ material. The shell resolution is low, and no magnetic structure was observed in the nitrided layer. Only strip domains were found in the core region. On **Figure 6** is shown a MFM detail image of the core-shell border area of the same particle with a sharp demarcation between the strip domain pattern in the core area and the labyrinth domain structure in the nitrided shell with the star domain width of ~1-1.2 μm which is significant for easy-plane magneto-crystalline anisotropy[10].

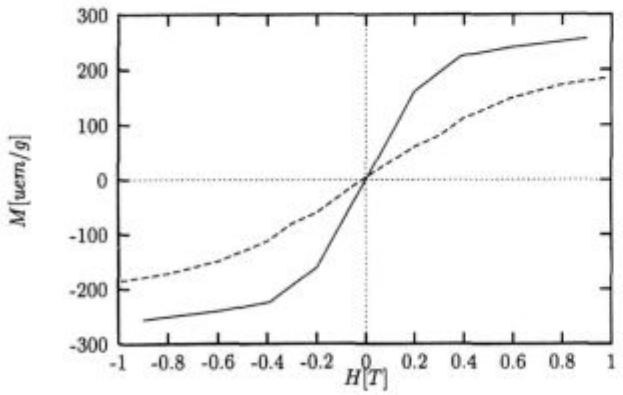

Figure 1: Magnetization versus applied field of the $Pr_2(Co_{0.5}Fe_{0.5})_{17}$ bonded powder measured parallel (upper curve) and perpendicular (lower curve) to the direction of the aligment. The anisotropy field is greater then 30 kA/cm

Slika 1: Magnetizacija prašnega vzorca $Pr_2(Co_{0.5}Fe_{0.5})_{17}$ v odvisnosti od zunanjega magnetnega polja merjena vzporedno (zgornja krivulja), in pravokotno (spodnja krivulja), glede na smer predhodne namagnetenosti prahu

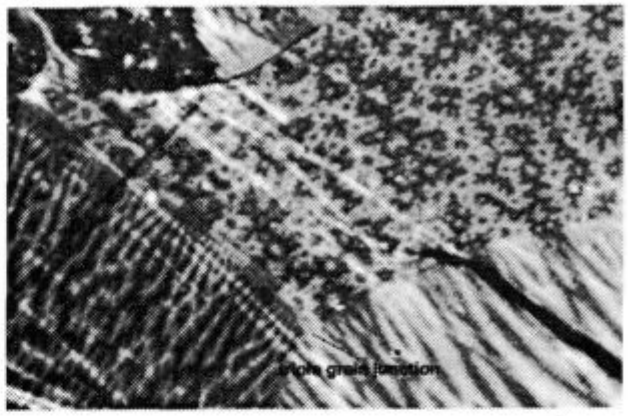

Figure 2: The domain pattern of the alloy $Pr_2(Co_{0.5}Fe_{0.5})_{17}$ observed by optical microscope in a polarized light using magneto-optic Kerr effect. Star shaped or "labyrinth" pattern in grains cut perpendicular to the c-axis and a banded or "strip" structure within grains cut parallel to the c-axis are present

Slika 2: Domenska struktura zlitine $Pr_2(Co_{0.5}Fe_{0.5})_{17}$, opazovana z optičnim mikroskopom v polarizirani svetlobi s pomočjo Kerrovega efekta. V zrnih, odrezanih pravokotno glede na os c, vidimo labirintno strukturo domen zvezdaste oblike. V zrnih, ki so odrezana vzporedno z osjo c pa so črtaste domene v obliki pasov

4 THEORETICAL

Undesired transition from the easy-axis to the plane magneto-crystalline anisotropy due to the introduced nitrogen in the case of $Pr_2(Co_{0.5}Fe_{0.5})_{17}$ contrary to the case of Sm_2Fe_{17} [6] can be explained in the frame of the simplified crystal field theory[11]. We assume that the energy of the magneto-crystalline anisotropy is given by the electrostatic interaction between the 4f charge distribution of the rare earth atom and the non-4f charges present in the

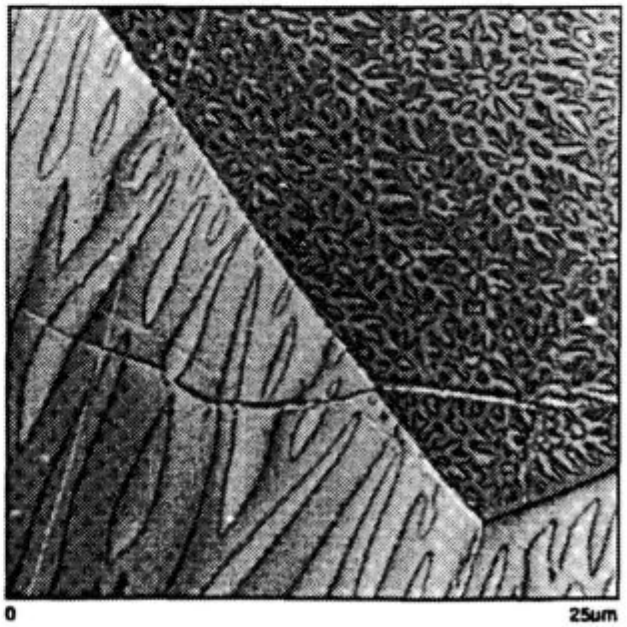

Figure 3: MFM image of the same area as in **Figure 2**

Slika 3: MFM posnetek istega območja kot na **sliki 2**

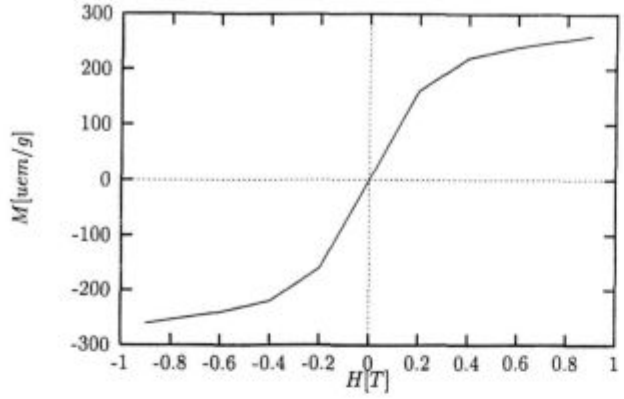

Figure 4: Magnetization curves of nitrided powder measured parallel, and perpendicular, to the direction of the alignment are the same
Slika 4: Krivulja magnetizacije nitriranega prahu, merjena pravokotno in vzporedno glede na smer predhodne namagnetenosti prahu

lattice. The change of the coefficient K_1 upon the interstitial modification in the first approximation depends:

- on the angle θ between the directions of the nitrogen atom and the magnetization relative to the position of the rare earth atom: **Figure 7**
- and to the quadrapole contribution n_2 to the 4f charge density.

One can schematically conclude that rare earth atoms with $n_2<0$ (Pr, Nd, Dy etc.) have the oblate shape of the 4f electron cloud while in the case of Sm with $n_2>0$ it can be described as a prolate. To estimate whether the K_1 is increased or decreased after the nitriding there is a simple rule[11]:

$$\mathrm{sgn}(\Delta K_1) = \mathrm{sgn}(n_2)\ \mathrm{sgn}(\theta)$$

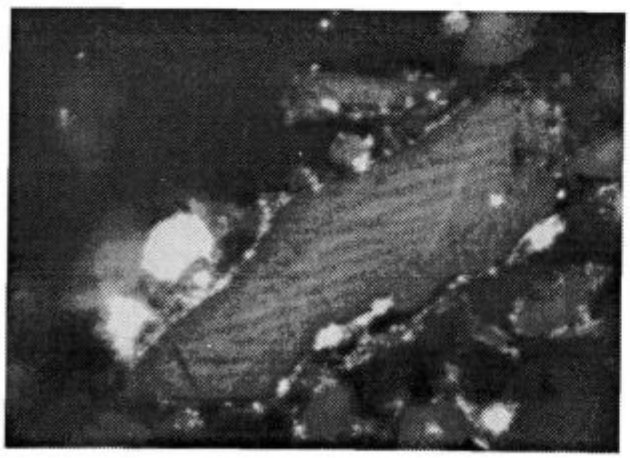

Figure 5: Kerr image of a large (~100 μm) particle. Just a layer of width ~5 μm was nitrogenated. The core area represents the basic $Pr_2(Co_{0.5}Fe_{0.5})_{17}$ alloy
Slika 5: Posnetek velikega (~100 μm) delca s pomočjo Kerrovega efekta. Nitrirana je samo zunanja plast debeline ~5 μm. Jedro predstavlja osnovna zlitina $Pr_2(Co_{0.5}Fe_{0.5})_{17}$

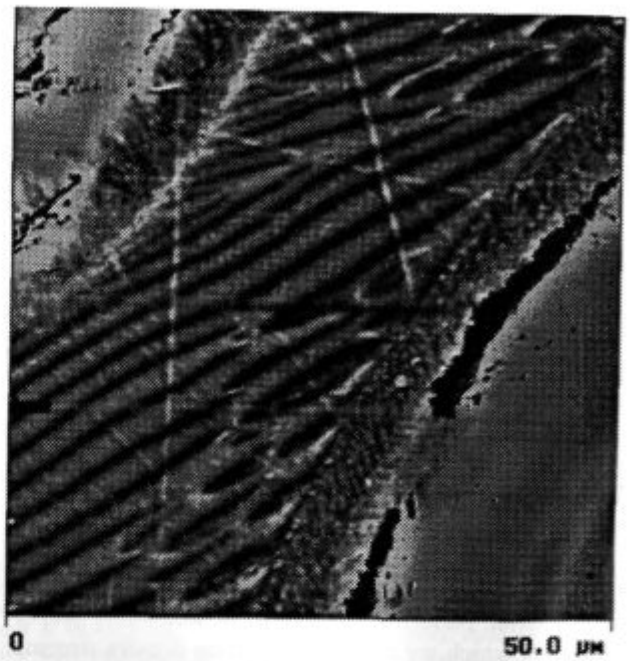

Figure 6: MFM detail image of the core-shell border of the same particle as in **Figure 5**. A sharp demarcation between the strip domain pattern in the corearea and the labyrinth domain structure in the nitrided shell is shown
Slika 6: MFM detajlni posnetek meje med nitriranim in nenitriranim območjem delca iz **slike 5**. Ostro se vidi razlika med črtastimi domenami v nenitriranem območju ter zvezdastimi domenami iz nitrirane plasti

where $\mathrm{sgn}(\theta = 0°) = -1$ and $\mathrm{sgn}(\theta = 90°) = 1$. It implies that in the case of Pr ($n_2<0$) we have to look for interstitial sites with the axial coordination ($\theta = 0°$) which is not the case for the site 9e in Th_2Zn_{17} type of crystal structure. It has in-plane interstitial coordination ($\theta = 90°$) which is favorable for the Sm ($n_2>0$) based materials.

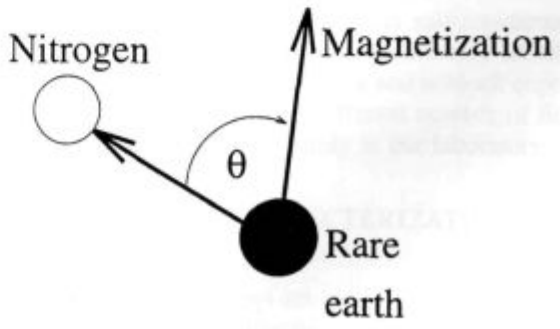

Figure 7: Angle θ between the directions of the nitrogen atom and the magnetization relative to the position of rare earth atom
Slika 7: Kot θ med zveznico atoma dušika ter atoma redke zemlje in smerjo magnetizacije

5 CONCLUSION

It was shown that besides the magneto-optic Kerr effect MFM can be used as an important technique for rapid and simple characterization of the magnetic structure of new magnetic materials. When the magnetic structure is too fine for optical microscopy, MFM can serve as a very convenient method in observing and characterizing the magnetic structure of different and unknown magnetic materials. After the successful interstitial modification of the Sm_2Fe_{17} [3,6] and some other intermetallics[3] it was hoped that the same procedure could be applied also to the $Pr_2(Co_{0.5}Fe_{0.5})_{17}$ alloy. Instead of the increasing of magneto-crystalline anisotropy even a transition from the easy-axis to the undesired easy-plane type was observed. Therefore the nitrided alloy $Pr_2(Co_{0.5}Fe_{0.5})_{17}$ can not be used as a permanent magnet material. Nevertheless it has very interesting properties from which we can learn much on domain structure and the effects of nitriding. Finally the experimental results obtained on the investigated alloy agree with the predictions of a model based on a crystal field theory[11].

6 REFERENCES

[1] K. H. J. Buschow: *Ferromagnetic Materials*, Vol. 2, ed. E. P. Wohlfarth (North-Holland Publishing Co., Amsterdam, 1980) p. 297

[2] A. H. Morrish: *The Physical Principles of Magnetism*, (John Wiley & Sons, Inc., New York, 1965)

[3] K. H. J. Buschow, G. J. Long and F. Grandjean: Interstital Intermetallic Alloys (Kluwer Academic Publishers, Dordrecht, 1995)

[4] M. Jurczyk, *Phys. Stat. Sol.*, (a) 80 (1989) 657-662

[5] H. Y. Chen, B. M. Ma, S. G. Sankar and W. E. Wallace, *Journal de Physique*, Colloque C8, Suppl. no 12, 49 (1988) C8, 507-508

[6] B. Saje, B. Reinsch, S. Kobe, D. Kolar, I. R. Harris: Nitrogenation of Ta Modified Sm_2Fe_{17} Alloy, *Metals, Alloys, Technologies*, 30 (1966) 307-309

[7] Trademark of Digital Instruments, Santa Barbara, CA

[8] U. Schafer, G. Schneider, G. Petzow, *Pract. Met.*, 26 (1989) 59-67

[9] T. Mukai, T. Fujimoto, *JMMM*, 103 (1992) 165-173

[10] B. Grieb, H. H. Stadelmaier and E.-Th. Henig, *Materials Letters*, 8 (1989) 396-399

[11] R. V. Skomski, Interstitial Nitrogen, Carbon and Hydrogen: Modification of Magnetic Properties, Interstitial Intermetallic Alloys, Kluwer Academic Publishers, Dordrecht, 1995

ISSN 1318-0010
KZLTET 31(6)571(1997)

MODEL POLYMERS WITH DIMETHYLAMINE AND SULFOZWITTERIONIC END-GROUPS. SYNTHESIS AND SELF ASSEMBLY IN SOLUTION AND IN BULK

MODELNI POLIMERI Z DIMETILAMINSKIMI IN SULFOZWITTERIONSKIMI KONČNIMI SKUPINAMI

NIKOS HADJICHRISTIDIS, S. PISPAS, M. PITSIKALIS

University of Athens, Department of Chemistry, Panepistimiopolis Zografou, 15771 Athens, Greece

Prejem rokopisa - received: 1997-10-01; sprejem za objavo - accepted for publication: 1997-10-21

The dilute solution and bulk properties of a variety of well-defined polymers of different architectures (linear homopolymers, diblock and triblock copolymers and star homopolymers) having dimethylamine and sulfobetaine end groups mainly synthesized in our laboratory are reviewed. The end functionalized polymers were synthesized by means of anionic polymerization high vacuum techniques, using 3-dimethylaminopropyl-lithium as initiator for the introduction of the dimethylamine group at the chain end. This group was converted to sulfozwitterionic by reaction with cyclopropanesultone. Extensive molecular characterization proved the high homogeneity of these model materials. Their aggregation properties in dilute solutions, of solvents of different polarity and selectivity towards different parts of the molecules, were studied by viscometry, static and dynamic light scattering. The ω-functionalized polystyrenes and the block copolymers of styrene have a much lower degree of association, than the homopolydienes, probably due to the polarizability of the phenyl group. The bulk properties of end-functionalized homopolymers and diblocks were studied by SAXS, reology and dielectric spectroscopy revealing new features of self organization at this low ionic content and extraodinary phase behavior at high temperatures. The adsorption behavior of stars with different number of functionalized arms in dilute solutions was also investigated by ellipsometry showing different behavior compared to linear polymers.

Key words: end-functionalized polymers, anionic polymerization, macromolecular architecture, association, phase separation, adsorption

V delu je podan pregled lastnosti vrste dobro definiranih polimerov z različnimi arhitekturami (linearni homopolimeri, diblok in triblok kopolimeri, zvezdasti homopolimeri) z dimetilaminskimi in sulfobetainskimi končnimi skupinami, v razredčenih raztopinah in v masi. Polimere s funkcionalnimi končnimi skupinami smo sintetizirali z anionsko polimerizacijo z visoko-vakuumsko tehniko. Z iniciatorjem 3-dimetilaminopropilitijem smo na konec verige uvedli dimetilaminsko skupino, ki smo jo z reakcijo s ciklopropansultonom prevedli v sulfozwitterionsko. Temeljita molekularna karakterizacija je potrdila, da so sintetizirani modelni materiali zelo homogeni. Z viskozimetrijo ter statičnim in dinamičnim sipanjem svetlobe smo raziskali njihove agregacijske lastnosti v razredčenih raztopinah, v topilih različne polarnosti in selektivnosti do določenih delov molekul. ω-funkcionalizirani polistireni in blok kopolimeri stirena imajo, verjetno zaradi polarizabilnosti fenilne skupine, mnogo nižjo stopnjo asociacije kot homopolidieni. S SAXS reologijo in z dielektrično spektroskopijo smo študirali lastnosti ω-funkcionaliziranih homopolimerov in diblokov v masi ter ugotovili nove oblike samoorganiziranosti pri tej nizki koncentraciji ionov ter nenavadno obnašanje faz pri visoki temperaturi. Z elipsometrijo smo raziskali tudi adsorpcijske lastnosti zvezdastih polimerov z različnim številom funkcionaliziranih vej v razredčenih raztopinah in ugotovili, da se razlikujejo od lastnosti linearnih polimerov.

Ključne besede: polimeri s funkcionalnimi končnimi skupinami (ω-funkcionalizirani polimeri), anionska polimerizacija, makromolekularna arhitektura, asociacija, fazna separacija, adsorpcija

1 INTRODUCTION

The presence of even a few highly polar groups distributed along or fixed at the ends of nonpolar chains changes dramatically the properties of polymers[1-7]. These changes are caused by association of polar groups in the nonpolar environment of the hydrocarbon chains in the bulk or of the aliphatic solvents in solution.

The least complicated examples of polymeric associating species are chains with one polar group[8-9]. These simple materials offer an essential starting point for testing theories and establishing the basic structure-properties relationships, which will help to design associating polymers for practical applications.

Although many routes exist for the synthesis of end functionalized polymers[10-12], living anionic polymerization has been proven to be the most efficient method for synthesizing well defined macromolecules[13,14], since it gives the possibility to control many structural variables including placement of the ionic groups.

This review will be focused on the dilute solution and bulk properties of dimethylamine and sulfozwitterionic end-functionalized polymers having different architectures (linear homopolymers, diblock and triblock copolymers and star polymers with a different number of functional groups), synthesized mainly in our laboratory.

2 SYNTHESIS AND CHARACTERIZATION

Homopolymers

3-Dimethylaminopropyl-lithium (DMAPLi) was used as initiator for the introduction of the dimethylamine group at the end of the polymer chain in all cases. DMAPLi was prepared by reaction of the corresponding chloride (DMAPCl) and Li dispersion according to Stewart et al.[15]. Styrene (St), Isoprene (Is) and butadiene

(Bd) were polymerized with DMAPLi. The molecular weight distributions are low in the case of polydienes. Stoichiometric molecular weights are in very good agreement with the number average molecular weights, measured by osmometry. These results indicate that DMAPLi is an efficient initiator for the polymerization of isoprene and butadiene.

The microstructure of the polydienes was investigated using ^{1}H-NMR spectroscopy. The results clearly show an increase of the vinyl content with decreasing chain length, due to the presence of the polar dimethylamine group in the initiator.

The slow initiation rate was readily observed during the polymerization of St by the gradual appearance of the orange color[16], which is characteristic of the living polystylyllithium chains. This fact in combination with the very fast propagation rate for the polymerization of St resulted in very broad molecular weight distributions (I=1.23-1.27). In addition, the M_n(SEC) of samples with stoichiometric molecular weights M_s<9300 were much higher than the stoichiometric ones, with the difference being higher by decreasing M_s. This behaviour can be explained by partial consumption of the initiator. This was verified by the subsequent addition of Is, which produced polymers having bimodal distribution (**figure 1**). The lower molecular weight peak, not seen by the UV detector, corresponds to NPI homopolymer, produced by the DMAPLi, which remained unreacted during the polymerization of St. The higher molecular weight peak is attributed to the NPSt-b-PI block copolymer with the amine group at the PSt chain end, produced by the crossover reaction of NPStLi with Is. Addition of THF to the mixture of St and DMAPLi ([THF]/[Li] > 3) gave polymers with close agreement between M_s and M_n and lower polydispersities.

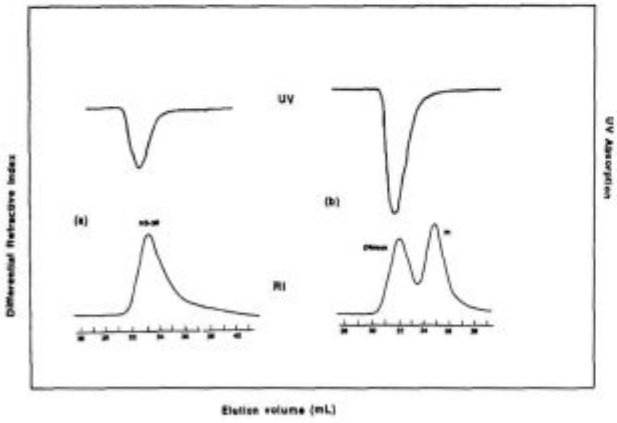

Figure 1: SEC chromatograms of (a) NS-3B (purified DMAPLi; polymerization in pure benzene) and (b) NS-3B after the addition of isoprene (first peak, diblock formed; second peak, homopolyisoprene formed by reaction of isoprene with unreacted DMAPLi). The UV detector sees only the PS part

Slika 1: SEC kromatogrami (a) NS-3B (očiščen DMAPLi; polimerizacija v čistem benzenu) in (b) NS-3B po dodatku izoprena (prvi vrh ustreza diblok kopolimeru; drugi vrh ustreza homopoliizoprenu, ki nastane v reakciji med izoprenom in nezreagiranim DMAPLi). UV detektor zazna samo polistirenski del blok kopolimera

3 DIBLOCK AND TRIBLOCK COPOLYMERS

Block copolymers of styrene and isoprene having dimethylamine end-groups at the one or the other chain end were prepared using DMAPLi and sequential addition of monomers[17]. When Is is polymerized first, a small amount of THF is added after the polymerization of the diene is completed to accelerate the crossover reaction with St. The reaction scheme is the following:

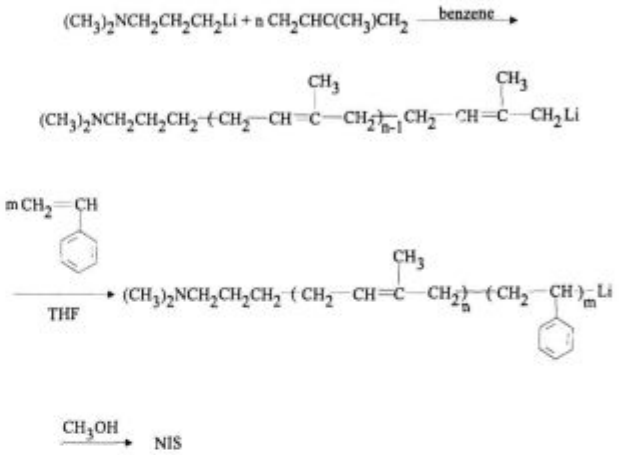

Triblock copolymers, having dimethylamine groups at both chain ends were prepared by coupling diblock chains with dimethyldichlorosilane, $(CH_3)_2SiCl_2$. The products are characterized by compositional and chemical homogeneity and low molecular weight distributions. The samples are designated with the letter N corresponding to the end-amine group, followed by the sequence of blocks starting with the block at which the functional group is attached.

4 ω-FUNCTIONALIZED STAR POLYISOPRENES AND Mono-, Di- AND Tri-ω-FUNCTIONALIZED THREE ARM STAR POLYBUTADIENES

Three and twelve arm PI stars[18] and three arm star PBd with all ends functionalized with dimethylamine groups[19] were synthesized by the reaction of end-functionalized living polymers with suitable chlorosilanes. As an example the 3-arm polybutadienes have been prepared according to the following scheme:

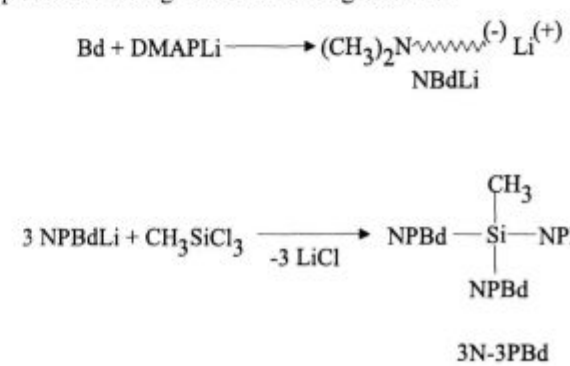

Three arm stars PBd with one or two end-amine groups were prepared using controlled chlorosilane chemistry[19]. The presence of one or two functional groups is denoted by the symbols 1N- and 2N- respectively, whereas the symbol 3PBd denotes a three arm star PBd. So 1N-3PBd is a three arm star PBd with one end-amine group. The following numbers differentiate samples of the same series. A schematic representation of the reaction sequence used for the synthesis of samples 1N-3PBd is shown below:

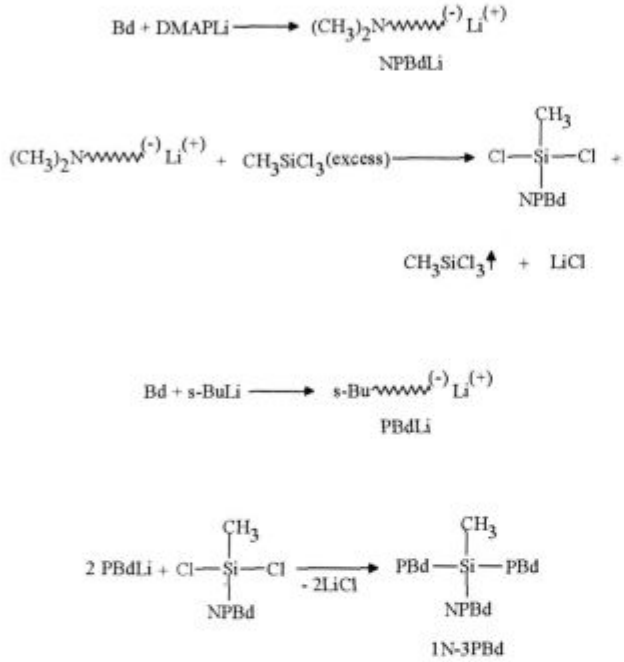

A living end-functionalized PBd chain was prepared in benzene using DMAPLi as initiator. The living polymer solution was added to a large excess of methyltrichlorosilane (Si-Cl/C-Li ≈100/1) in order to prepare the methyldichlorosilane-capped PBd. The excess of linking agent was removed under vacuum line conditions. The polymer was repeatedly redissolved and pumped to extract traces of silane from the bulk polymer. Finally benzene was distilled into the reactor to dissolve the ω-methyldichlorosilane PBd arm.

The next step involved the synthesis of the unfunctionalized arm, using s-BuLi as initiator. A small excess of this living polymer was coupled with the macromolecular linking agent to produce the final product. Termination of the residual active anions with degassed MeOH and subsequent fractionation to remove the excess PBd arm gave the pure 1N-3PBd star polymer.

A similar procedure is followed for the synthesis of 2N-3PBd stars, starting from the reaction of the living unfunctionalized arm with excess methyltrichlorosilane followed, after the removal of the excess linking agent, by the coupling reaction of the dichlorosilane-capped arm with a small excess of the amine-functionalized living arm. All these procedures were monitored by SEC.

In the case of samples with low arm molecular weight ($M_n<10^4$) and in order to prevent the formation of the diadduct the steric hindrance of the living arm PB$^-$ was increased by reaction with diphenylethylene (DPE). A few drops of THF were added to accelerate the cross-over reaction. The coupling reaction was minimized using this procedure giving less than 3% of the byproduct.

The molecular characteristics of representative samples synthesized as described above are given in **Table I**.

Table I: Molecular characteristics of diblock, triblock and three-arm PBd stars with one, two, or three dimethylamino end groups
Tabela I: Molekularne lastnosti zvezdastih PBd polimerov z dvema blokoma, s tremi bloki in tremi vejami, z eno, dvema ali tremi dimetilaminskimi končnimi skupinami

Sample	$M_w x10^{-4}$	$M_n x10^{-4}$	$I=M_w/M_n$ (SEC)	%wt PS
NPI	4.56	4.53	1.04	
3NPI	7.2	6.6	1.05	
NIS-3	2.44	2.25	1.06	28
NSI-1	6.96	6.12	1.06	30
NSISN-1	7.63	7.02	1.05	36
NISIN-1	6.98	6.27	1.05	27
1N-3PBd30	11.1	10.4	1.06	
2N-3PBd30	62.4	61.8	1.06	
3N-3PBd40	93.1	91.4	1.06	

5 POST-POLYMERIZATION REACTION OF THE AMINE-FUNCTIONALIZED POLYMERS

The amine end groups can be easily transformed to ionic dipoles by reaction with 1,3 cyclopropane sultone[20,21], illustrated in the following scheme:

The reaction takes place in dilute THF solutions (2-3 w/v%) at 70°C for several days using an excess of the sultone over the amine groups (sultone/amine = 10/1). For the PBd samples inert atmosphere was used. Under these conditions this post-polymerization reaction is free of side reactions (crosslinking, degradation etc.) as was verified by SEC. Similar peaks with the corresponding amine-capped polymers were observed in $CHCl_3$ in all cases.

It is difficult to determine the extent of the conversion of the t-amine groups to sulfobetaines due to the low concentration of these groups in the polymer chains. However, qualitative results by ^{1}H-NMR show that the reaction yield is very high[17,22]. In **figure 2** the ^{1}H-NMR spectra of linear block copolymer NIS-5 and the corresponding zwitterion sample are given. The peak at 2.2 ppm is assigned to the methyl protons of the carbons attached to the nitrogen atom. This peak has completely disappeared after the reaction with 1,3 cyclopropane sul-

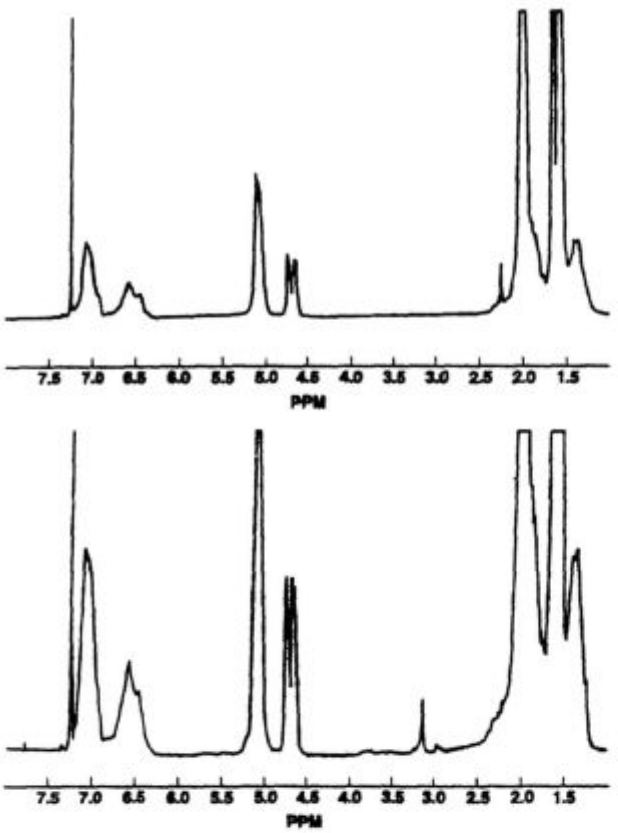

Figure 2: ^{1}H-NMR spectra of samples NIS-5 (top) and ZwIS-5 (bottom) in $CDCl_3$

Slika 2: ^{1}H NMR spektri vzorcev NIS-5 (zgornji) in ZwIS-5 (spodnji spekter) v $CDCl_3$

tone and two new peaks at 3.15 and 2.95 ppm have emerged. These peaks are assigned to the methyl protons attached to the positively charged nitrogen atom of the zwitterionic group and to the methylene protons of the carbon attached to the sulfur atom respectively[21,23].

6 DILUTE SOLUTION AND BULK PROPERTIES

Homopolymers

The dilute solution properties of ω-functionalized linear homopolymers were studied by membrane osmometry (MO), low angle laser light scattering (LALLS) viscometry, and dynamic light scattering (DLS) in various non-polar solvents[18,24,25]. The conclusions obtained from this study are the following:

a) The dimethylamine-cappped samples present no evidence of association in non-polar solvents (cyclohexane, CCl_4, toluene)
b) The zwitterion-capped samples form large aggregates in these solvents with aggregation numbers increasing with decreasing molecular weight of the parent material. However, aggregation numbers for PS homopolymers are lower than those obtained for polydiene homopolymers probably because of the solvating effect of phenyl rings on the dipolar groups
c) The aggregates are polydisperse as concluded by LALLS, MO and DLS measurements
d) The associates behave hydrodynamically as star polymers as evidenced by the increasing k_H values with increasing degree of association and by the good agreement between experimental aggregation numbers and those calculated assuming the star model
e) The linear head packing model describes fairly well the structures of the associates.

Detailed studies by small angle x-ray scattering (SAXS) were performed on low molecular weight zwitterion-capped polyisoprenes[26]. For samples having $14000 < M_w < 28000$ the scattering profiles show that the aggregates form a body-centered cubic lattice.

Figure 3 shows the corresponding scattering profiles for the lower molecular weight samples ($2200 < M_w < 4650$). The peaks can be indexed on a two dimensional hexagonal lattice of tubes. In other words the aggregates have a tubular structure with the tubes closed packed on a two dimensional hexagonal lattice with crystalline order. The core is formed by dipoles which are arranged in an antiparallel configuration as shown in **figure 4**.

It is characteristic that a very small weight fraction of ionic species (3.5-7.5%) is able to promote a hexagonal cylinder morphology with long range order in contrast to usual block copolymers.

The viscoelastic behavior in the melt state of end-functionalized polyisoprenes was also investigated[27]. The amine-capped samples behave more or less as conventional polyisoprenes indicating that only weak associa-

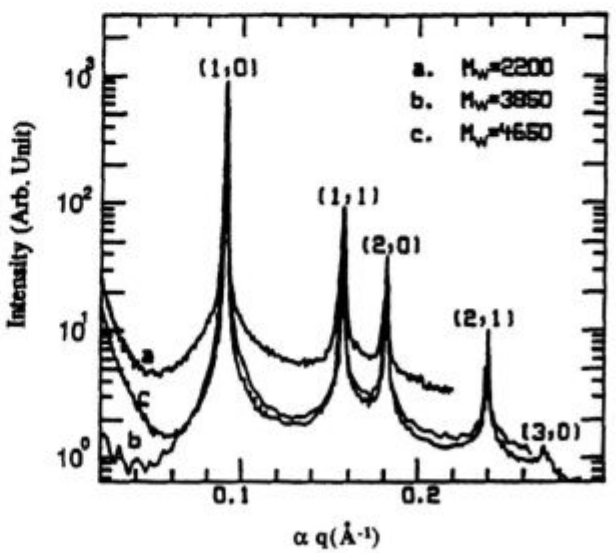

Figure 3: X-ray scattering profiles of zwitterion-capped polyisoprene samples with molecular weights of 4650, 3850, and 2200. The profiles of the last two samples were shifted by a factor (α) to make the first peak positions overlap

Slika 3: Krivulje sipanja rentgenskih žarkov vzorcev poliizoprena s končnimi zwitterionskimi skupinami z molskimi masami 4650 (c), 3850 (b) in 2200 g/mol (a). Zaradi lažje primerjave krivulj sta krivulji zadnjih dveh vzorcev premaknjeni za faktor (α)

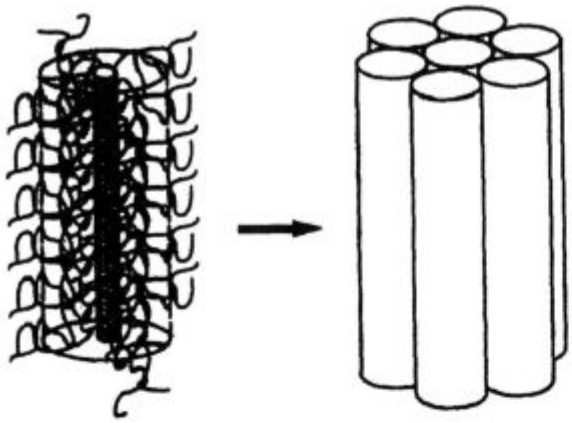

Figure 4: A schematic representation of the formation of two-dimensional lattices of close-packed tubular aggregates
Slika 4: Shematska predstavitev nastanka dvodimenzionalnih mrež tesno zloženih cevastih agregatov

tion may exist in the melt state. The situation is very different for the zwitterion-cappped polymers with the dynamic moduli broadened and shifted to much lower frequencies. For samples with high base molecular weights the viscoelastic behaviour more closely resembles the behaviour of conventional star polymers.

Samples with intermediate and lower molecular weights show a second relaxation regime at very low frequencies. A characteristic example is given in **figure 5**. It is observed that some resemblance exist between the zwitterion and star polymer only at intermediate and high frequencies.

The viscosities of the zwitterion polymers, especially of low and intermediate molecular weights are much larger than those predicted assuming the star model. Consequently, it is reasonable to consider that aggregates have extended morphologies (lamellae, strings etc.). Only in the case of low aggregation numbers, observed for samples of high base molecular weight, the behavior is similar to those of star polymers because the core size is rather small and can be considered as the star's center. The extended structures are delicate in a mechanical sense making it possible to explain the remarkable strain sensitivity observed at low frequencies. It is noted that there is close aggrement with the results obtained by melt rheology and SAXS.

7 ω-FUNCTIONALIZED BLOCK COPOLYMERES OF STYRENE AND ISOPRENE

The association behavior of end-functionalized diblock and triblock copolymers of isoprene and styrene was studied in CCl_4, which is a nonpolar and good solvent for both blocks[17,28]. The aggregation numbers, N_w are almost the same whether the zwitterion group is linked at the PI or the PS chain end. Their value depends strongly on the M_w of the base polymer. N_w decreases with increasing molecular weight of the precursor polymer, M_0. The variation of N_w with M_0 for the case of ZwPI in cyclohexane[18] and CCl_4[17], PS in CCl_4[27] di- and triblock copolymers in CCl_4[17] is given in **figure 6**. The aggregation numbers for ZwPI are lower in CCl_4 than in cyclohexane due to the higher polarizability of the former solvent. Another point to be noticed is that the degrees of association of copolymers are closer to those determined for the ZwPS samples than to those of ZwPI samples in CCl_4. The aromatic rings, due to their high polarizability cause some kind of solvation, and lead to reduced N_w values. The aggregation numbers are almost the same for the monofunctional and difunctional samples. This is rather surprising, since the difunctional polymers form gels at concentrations lower than c_{gel}

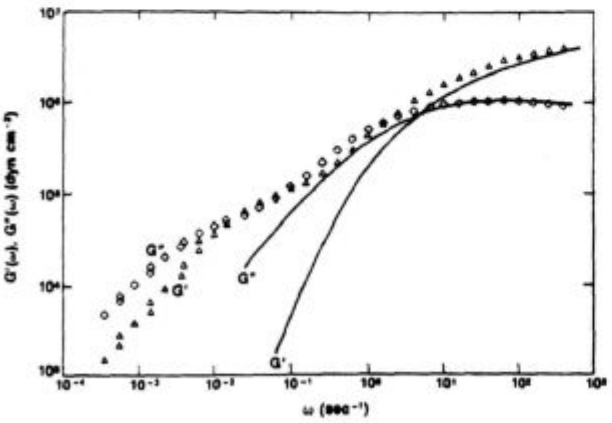

Figure 5: Comparison of dynamic moduli for a four-arm polyisoprene star and a monofunctional zwitterion polyisoprene in the melt state at 25°C. Data for the star (M_a=4.4 x 10^4) are shown by the solid lines; the points are data for a sample with M_0=4.61 x 10^4
Slika 5: Primerjava dinamičnih modulov zvezdastega poliizoprena s štirimi vejami in monofunkcionalnega zwitterionskega poliizoprena v talini pri 25°C. Neprekinjena črta - zvezdasti poliizopren (M_a=4,4 x 10^4), točke - vzorec z M_0=4,61 x 10^4

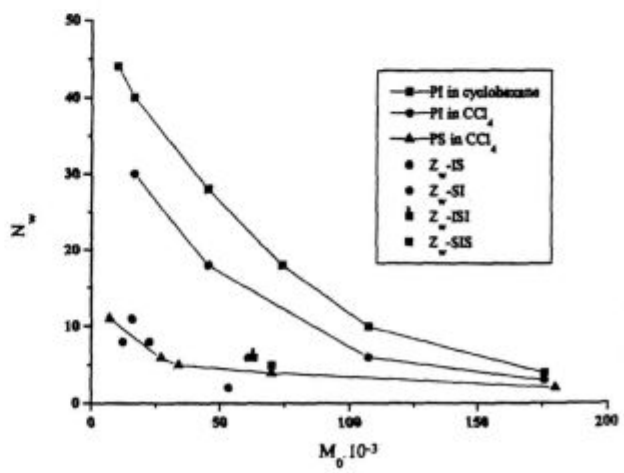

Figure 6: Dependence of the weight average aggregation number, N_w from the base molecular weight, M_0 for various polymer series
Slika 6: Odvisnost utežnega povprečja števila agregacije N_w od molekulske mase M_0 za različne serije polimerov

(c_{gel}=0.5 c^*) and can be seen as evidence of intramolecular association in very dilute solutions.

DLS was used to study the hydrodynamic properties of the end-functionalized copolymers. The zwitterionic polymers have a substantially different behaviour than their precursors, due to the formation of aggregates in CCl_4. The values of diffusion coefficient at infinite dilution, D_0 are lower, the R_H values higher, and the aggregates are polydisperse. The k_D values are negative in most cases, due to the aggregation process and are consistent with the low A_2 values obtained by LALLS.

Viscosity measurements were also performed to complement the DLS data. The [η] values for the zwitterionic samples are considerably higher than those for the amine-capped samples and the reduced viscosity vs concentration plots are not always linear. The Huggins plots are concave upwards in some cases and especially for the difunctional samples.

The nonlinear dependence of the reduced viscosity on concentration is an indication that the association number changes by increasing concentration, something which is expected to be more pronounced in the case of the difunctional triblocks.

The stability of aggregates was tested by adding small amounts of an alcohol, namely 2-methylcyclohexanol (at 1% and 5% content). The association is reduced in the presence of the alcohol, but even by 5% alcohol samples remained aggregated. With increasing alcohol content the aggregation numbers decreased, the A_2 values increased and the k_H values are decreased also.

SAXS, rheology, and dielectric spectroscopy were used to study the statics and dynamics of the end-functionalized block copolymer[29,30]. SAXS profiles from amine and the corresponding zwitterion-capped samples confirm the existence of ionic aggregation. A characteristic example is given in **figure 7**. The following features were observed:

a) a background originating from density and concentration fluctuations
b) an excess intensity at low Q related to heterogeneities with long correlation lengths in the case of ionomers[31]
c) the microdomain peak[32] characteristic of the microphase separation process between PI and PS phases and
d) the peak related to the polar groups, which emerged in the case of the zwitterionic sample.

The last three characteristics are temperature dependent with the aggregate peak intensity being much less sensitive to changes of temperature for the specific experiment temperature range. The microdomain peak intensity has a similar temperature dependence for both the amine and the zwitterion-capped copolymers.

A completely different behavior is observed when the functional group is attached to the PS chain-end, as shown in **figure 8**. The microdomain peak dominates the scattering pattern in this case. The peak increases in intensity, sharpens, and moves to slightly higher Q values with increasing temperature. The absence of any dissolution process clearly indicates that the microdomain structure is stabilized by the ionic aggregates. In the case of ZwSI samples the ionic groups are trapped within the PS phase without being able to aggregate. The increase of temperature increases the mobility of the polar groups leading to the formation of aggregates within the "hard" phase. This is schematically shown in **figure 9** for both systems, ZwIS and ZwSI. As a consequence the incompatibility of PI and PS is enhanced and a completely different phase behavior is observed. So only by changing the position of the polar group, from the PI to the PS chain-end it is possible to change the phase diagram.

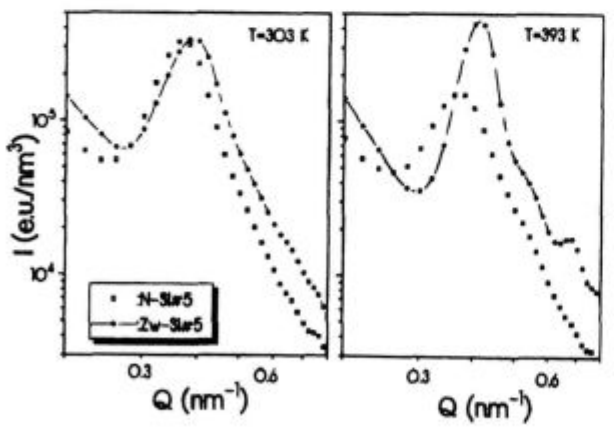

Figure 7: SAXS profiles for two ω-functionalized IS diblock copolymers at T=303 K. Data were corrected for density fluctuations and the intensities are given in absolute units

Slika 7: SAXS krivulje dveh ω-funkcionaliziranih izopren-stirenskih (IS) diblok kopolimerov pri T=303 K. Pri podatkih so upoštevane fluktuacije gostote, intenzitete so podane v absolutnih enotah

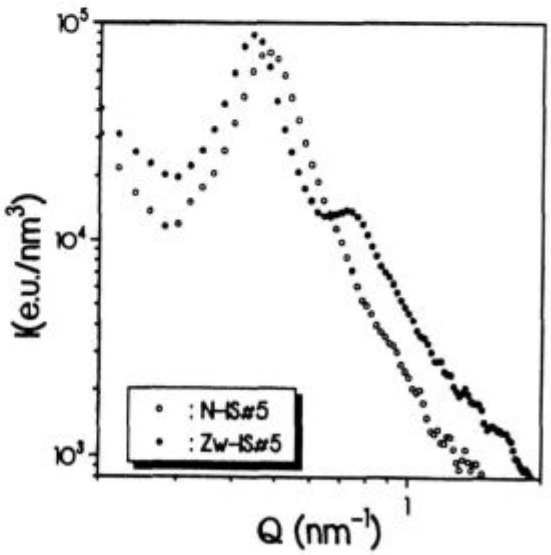

Figure 8: Comparison of the SAXS profiles for the dimethylamino- and zwitterion-substituted ω-functionalized copolymers at two temperatures

Slika 8: Primerjava SAXS krivulj dimetilamino- in zwitterionsko substituiranih ω-funkcionaliziranih kopolimerov pri dveh temperaturah

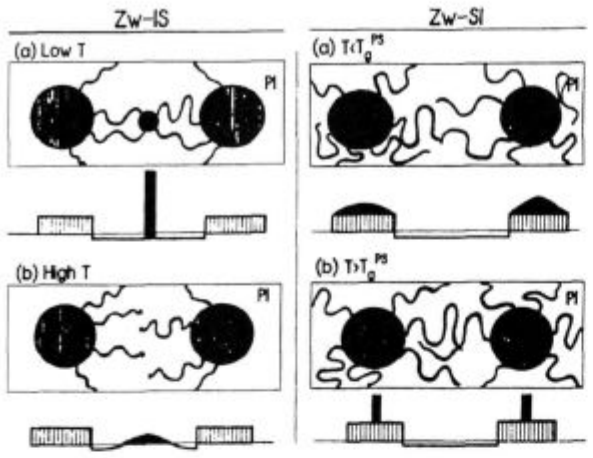

Figure 9: Schematic illustration of the microstructures in ω-functionalized SI block copolymers, showing the Zw-IS (left) and Zw-SI (right) cases at low (upper) and high (lower) temperatures. The corresponding electron density distributions are also shown

Slika 9: Shematska predstavitev mikrostrukture ω-funkcionaliziranih SI blokkopolimerov pri nižji (zgoraj) in višji temperaturi (spodaj) za Zw-IS (levo) in Zw-SI (desno). Prikazana je tudi ustrezna porazdelitev elektronske gostote

The conclusions derived by SAXS studies were confirmed by rheology. In the case of the zwitterionic copolymers an extension of the rubbery plateau is observed. This behaviour is explained considering that the aggregates act as physical crosslinks within the PI phase. Furthermore, within the temperature range investigated no sign of an order-disorder transition was observed in agreement with SAXS results, meaning that the cubic microdomain structure is stable up to high temperatures.

Dielectric spectroscopy also offers the means to verify the conclusions drawn so far through the selective probing of the PI chains. In the case of ZwIS copolymers in addition to the fast segmental and the slow normal mode an intermediate process, with activation parameters which are reminiscent of the segmental process, is observed. This intermediate process arises from regions of the reduced mobility created around the aggregates impending the motion of the PI chains in their immediate environment. However differential scanning calorimetry, DSC is not so sensitive and the size of these regions very small in order to detect an intermediate Tg value, although an increase on the Tg of the polyisoprene block has been observed at low molecular weights[33].

The combination of the association process caused by the presence of polar groups in a nonpolar solvent with the micellization procedure, promoted in selective solvents leads to interesting solution behavior. The dilute solution properties of ω-functionalized diblock copolymers having dimethylamine or zwitterion groups at the PS chain-end were studied in n-decane a nonpolar selective solvent for the PI blocks[34].

The presence of the polar groups introduces another factor capable to enhance the aggregation numbers for the zwitterionic samples in n-decane. Much lower N_w

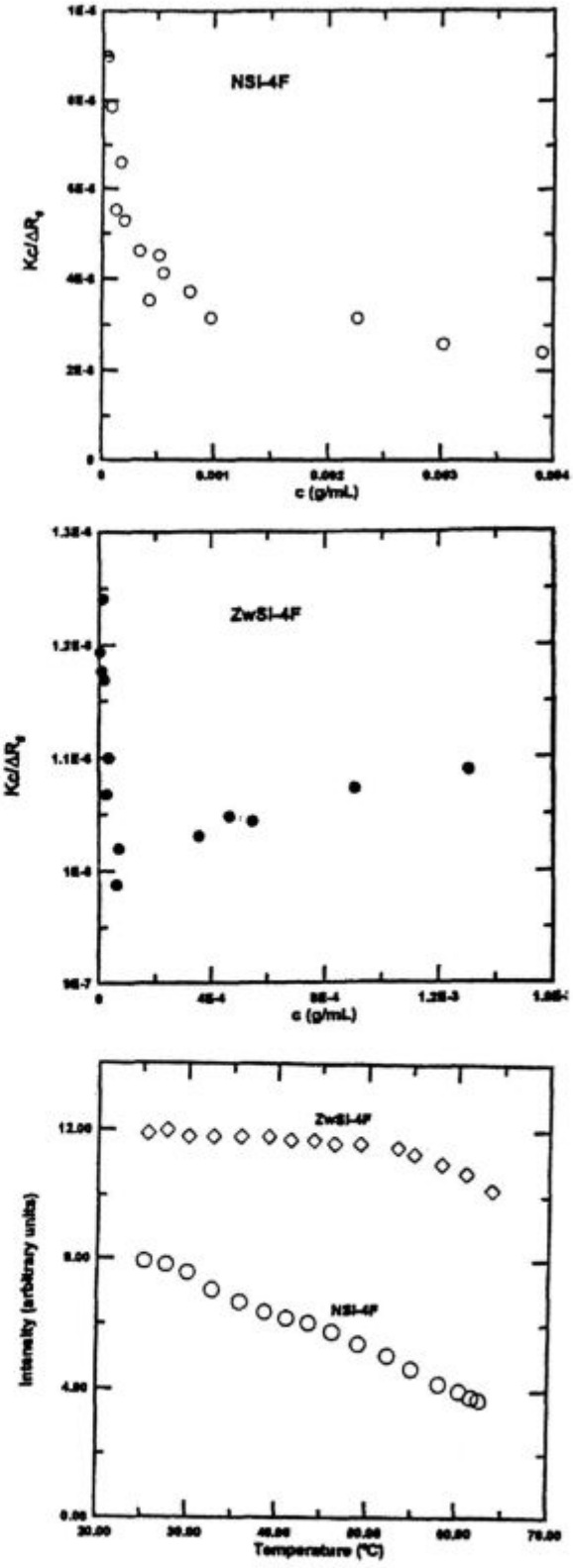

Figure 10: $Kc/\Delta R_\Theta$ vs concentration plots given for (a) sample NSI-4F and (b) sample ZwSI-4F in n-decane at 25°C. (c) Intensity vs temperature plot for the same samples at c=2.800 x 10^{-3} g/mL for NSI-4F and c=1.629 x 10^{-3} g/mL for ZwSI-4F

Slika 10: $Kc/\Delta R_\Theta$ v odvisnosti od koncentracije za vzorca (a) NSI-4F in (b) ZwSI-4F v n-dekanu pri 25°C; (c) odvisnost intenzitete od temperature za NSI-4F pri c=2,8 x 10^{-3} g/mL in za ZwSI-4F pri c=1,629 x 10^{-3} g/mL

values were observed for the amine-capped copolymers, meaning that the amine groups are not polar enough to enhance the association process. Typical LALLS plots are given in **figure 10**.

From DLS measurements negative k_D values were obtained for the amine-capped polymers as expected having in mind the negative A_2 values. For the zwitterionic samples the k_D values were positive meaning that the equilibrium is shifted in favor of the micelles.

Viscometry measurements were also performed. The Huggins coefficients increase with increasing molecular weight for the amine-capped polymers. This behavior is consistent with a star-like structure. For the zwitterionic samples constant k_H values, around 1.1 were obtained, meaning that rather compact structures exist in solution.

The R_v and R_H values are identical within experimental error for the amine polymers but for the zwitterionic polymers R_H is much higher than R_v. The former result is consistent with star-like structures, whereas the latter can be explained considering the high sensitivity of DLS to large structures and/or to the development of shear forces in the capillary tube able to disrupt the larger aggregates. The fact that the polar core probably has an elongated structure with antiparallel placement of the zwitterionic groups is able to support the above assumption, since a break of the association at one point can cause a large reduction of the micelle's size.

Intensity vs temperature measurements at concentrations where micelles are the dominant species revealed that the micelles formed by the zwitterionic copolymers are stable at much higher temperatures than the ones made of amine-capped precursors. It seems that in the former case the high temperature resistive ionic cores stabilise the micelles (**figure 10(c)**).

8 STAR SHAPED POLYBUTADIENES WITH END-FUNCTIONAL GROUPS

The amine-capped star polymers provide no evidence of association in cyclohexane, whereas strong association is observed in the case of zwitterionic samples. It is evident that (a) among the different series of polymers the aggregation number decreases with increasing number of functional groups and (b) among the samples with the same number of polar groups the degree of association decreases with increasing molecular weight of the precursor polymer, due to excluded volume repulsions. These results are given schematically in **figure 11**.

Multifunctional samples, especially the trifunctional stars form gels even at low concentrations. This result connected with the low aggregation numbers for these samples leads to the conclusion that in very dilute solution intramolecular association dominates and by increasing concentration there is a rather sharp transition from intramolecular to intermolecular association able to produce stable gels.

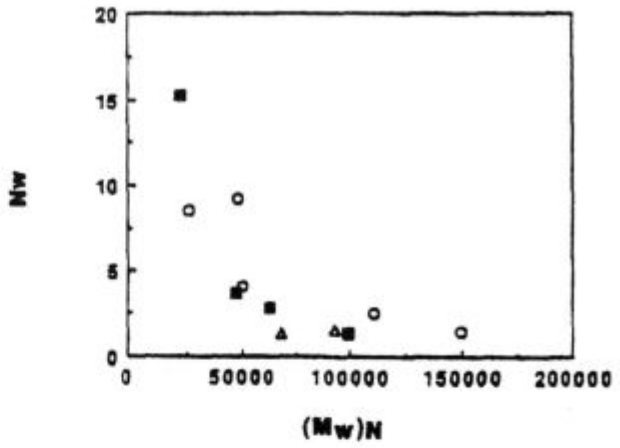

Figure 11: Weight-average aggregation number, N_w vs base molecular weight $(M_w)N$ of the star polymers: Zw-1N-3PBd (o), Zw-2N-3PBd (■), and Zw-3N-3PBd (Δ)

Slika 11: Utežno povprečje števila agregacije N_w v odvisnosti od molske mase $(M_w)N$ zvezdastih polimerov: Zw-1N-3PBd (o), Zw-2N-3PBd (■) in Zw-3N-3PBd (Δ)

The degrees of association of monofunctional stars are lower than those measured for the linear ω-functionalized PBd, meaning that the star structure prevents the association due to the steric hindrance caused by the unfunctionalized arms.

The hydrodynamic behavior of the functionalized stars was studied by DLS and viscometry[35]. The increased values of μ_2/Γ^2 (>0.2) indicate that the aggregates produced by the zwitterionic samples are polydisperse in agreement with the MO and LALLS results. Low k_D values were observed in most cases as a concequence of the decreased second virial coefficients.

The strongly negative k_D values for the trifunctional stars indicate the existence of strong hydrodynamic interactions between macromolecular chains eventhough these samples have low aggregation numbers and show only small increases in R_H compared to their precursors. This behavior can be seen as evidence of intramolecular association in very dilute solutions. For the case of difunctional stars the above analysis is not straightforward. It is clear that intermolecular association cannot be ruled out.

For monofunctional samples there is no possibility of intramolecular association. The star model can be used for these samples considering that the aggregates correspond to star polymers and their precursors to the arms of these stars. Consequently, it is possible to calculate the aggregation numbers from DLS measurements, N_{DLS}. The results show that the aggregates formed from the monofunctional samples behave hydrodynamically as star polymers with functionality equal to $2N_w$. It seems that the two unfunctionalized arms anchored at the periphery of the aggregates are responsible for the overall size of micelles.

The conclusions drawn by DLS are verified by viscometry for the amine-capped polymers. Zwitterionic trifunctional samples have lower intrinsic viscosities than their precursors but the k_H values are extremely high, indicating the presence of strong hydrodynamic interactions. This behavior implies that in very dilute solutions compact structures are formed through intramolecular association. This result is in agreement with LALLS and DLS data.

Comparative examination of R_v and R_H values shows that $R_v<R_H$ for the zwitterionic polymers, meaning that the aggregates dissociate to some extent in the capillary tube, due to the shear forces applied therein. It seems that the increased steric repulsions introduced by the unfunctionalized arms lead to the formation of not so strong associates as in the case of linear polymers.

The adsorption behavior of functionalized linear and three arm star PBd was studied by ellipsometry at 20°C in a mixed solvent of cyclohexane and toluene (50% by volume)[36]. A mixture of cyclohexane and toluene was used. In this mixture association is not detected up to the concentration of 2.0 mg/ml from DLS measurements and the dn/dc values (0.050 ml/g at 589.4 nm at 20.0°C) provide enough contrast for accurate measurements.

Various parameters of the adsorption behavior of samples are reported in **Table II**. The adsorbed amount A is increased with decreasing molecular weight for the linear samples. The longer the PBd chains adsorbed the bigger space they occupy and the stronger the repulsion between them. The ratio $\delta=D_{inter}/D_{over}$ of the interchain distance (D_{int}) over the space needed to accomodate a swollen polymer coil in a good solvent in it's unperturbed state on the surface (D_{over}) is much lower than unity. This indicates that the adsorbed chains are stretched adopting a brush-like conformation.

In the case of the zwitterionic stars the adsorbed amount increases with increasing number of functionalized arms. The grafting density, defined as $\sigma=AN_A/M_w$, where A is the adsorbed amount, N_A the Avogadro number and M_w the weight average molecular weight of the star seems to present stronger dependence on the molecular weight than the functionality of the stars. The σ values of the samples Zw-2N-3PBd30 and Zw-3N-3PBd25 are very close indicating that despite the fact that the adsorption energy is high the entropic loss involved in the attachment of the third arm when two arms are already attached may be very high.

The adsorption kinetics, studied by time-ressolved ellipsometry shows two processes. In the initial stages the adsorption is diffusion controled. By longer times the polymers must penetrate the barrier formed by the initially adsorbed chains. It was found that the star polymers penetrate this barrier faster than the linear chains, due to the different conformations adopted by the stars.

Table II: Various adsorption parameters of ω-functionalized linear (L) and mono-(1N)-, Di-(2N)-, and tri-(3N)-ω-functionalized polybutadienes

Tabela II: Adsorpcijski parametri ω-funkcionaliziranega linearnega (L) in mono- (1N)-, di- (2N)- in tri- ω-funkcionaliziranih polibutadienov

Sample	$A_{plateau}$ (mg/m^2)	σ (chains/ nm^2)	D_{inter} (nm)	D_{over} (nm)	$\delta=D_{inter}/D_{over}$
Zw-L-PBd12	2.47+0.01	0.125	2.8	10.5	0.27
Zw-L-PBd20	2.410+.25	0.07	3.8	14.5	0.26
Zw-L-PBd80	1.69+0.18	0.012	9.1	33.3	0.27
Zw-1N-3PBd30	1.77+0.17	0.0096	10.2	25.2	0.4
Zw-2N-3PBd30	1.86+0.06	0.0179	7.5	19.1	0.39
Zw-2N-3PBd40	1.90+0.12	0.0128	8.8	25.2	0.35
Zw-3N-3PBd25	2.14+0.18	0.0191	7.2	19.7	0.37
Zw-3N-3PBd40	2.3+0.2	0.0148	8.2	24.3	0.34

9 REFERENCES

[1] R. D. Lundberg and R. R. Phillips, *J. Polym. Sci. Polym. Phys. Ed.*, 20 (1982) 1143

[2] R. D. Hegedus and R. W. Lenz, *J. Polym. Sci.*, Part A: Polym. Chem., 26 (1988) 367

[3] M. Hara and J. Wu, Multiphase Polymers: Blends and Ionomers, Utracki L. A., Weiss R. A Eds., ACS Symposium Series 395, American Chemical Society: Washington, DC, 1988, Chapter 19

[4] N. Nagata, T. Kobatake, H. Watanabe, A. Veda and A. Yoshioka, *Rubber Chem. Technol.*, 60 (1987) 837

[5] Z. Zhou, B. Chu, G. Wu and D. G. Peiffer, *Macromolecules*, 26 (1993) 2968

[6] J. J. Fitzgerald and R. A. Weiss, *J. Macromol. Sci.*, Rev. Macromol. Chem. Phys., C28 (1988) 1

[7] K. A. Mauritz, *J. Macromol. Sci.*, Rev. Macromol. Chem. Phys., C28 (1988) 65

[8] G. Broze, R. Jerome and P. Teyssie, *Macromolecules*, 14 (1981) 224

[9] G. Broze, R. Jerome and P. Teyssie, *Macromolecules*, 15 (1982) 1300

[10] R. W. Lenz, Organic Chemistry of Synthetic High Polymers, Interscience, New York 1967

[11] J. P. Kennedy, *Rubber Chem. Technol. Reviews*, 56 (1983) 639

[12] D. Y. Sogah and O. N. Webster, *J. Polym. Sci. Polym. Lett. Ed.*, 21 (1983) 927

[13] R. N. Young, R. P. Quirk and L. J. Fetters, *Adv. Polym. Sci.*, 56 (1984) 1

[14] S. Bywater, Anionic Polymerization in Encyclopedia of Polymer Science and Engineering Vol. 2

[15] M. J. Stewart, N. Shepherd and D. M. Service, *Br. Polym. J.*, 22 (1990) 319

[16] S. Pispas, M. Pitsikalis, N. Hadjichristidis, P. Dardani and F. Morandi, *Polymer*, 36 (1995) 3005

[17] S. Pispas and N. Hadjichristidis, *Macromolecules*, 27 (1994) 1891

[18] N. S. Davidson, L. J. Fetters, W. G. Funk, W. W. Graessley and N. Hadjichristidis, *Macromolecules*, 21 (1988) 112

[19] M. Pitsikalis and N. Hadjichristidis, *Macromolecules*, 28 (1995) 3904

[20] U. Bahr, H. Weiden, H.-A. Rinkler and G. Nische, *Makromol. Chem.*, 161 (1972) 1

[21] V. M. Monroy Soto and J. C. Galin, *Polymer*, 25 (1984) 121

[22] M. Pitsikalis, Ph. D. Thesis, University of Athens, 1994

[23] D. N. Schulz, D. G. Peiffer, P. K. Agarwal, J. Larabee, J. J. Kaladas, L. Soni, B. Handwerker and R. T. Garner, *Polymer*, 27 (1986) 1734

[24] A. Borlenghi, M. Pitsikalis, S. Pispas, N. Hadjichristidis, *Macromol. Chem. Phys.*, 196 (1995) 4025

[25] M. Pitsikalis, E. Siakali-Kioulafa and N. Hadjichristidis, *J. Polym. Sci.*, Part B: Polym. Phys. Ed., 34 (1996) 249

[26] Y. Shen, C. R. Safinya, L. J. Fetters, M. Adam, T. Witten and N. Hadjichristidis, *Phys. Rev.*, 43 (1991) 1886

[27] L. J. Fetters, W. W. Graessley, N. Hadjichristidis, A. D. Kiss, D. S. Pearson and L. B. Younghouse, *Macromolecules*, 21 (1988) 1644

[28] S. Pispas, N. Hadjichristidis N. and J. W. Mays, *Macromolecules*, 27 (1994) 6307

[29] G. Floudas, G. Fytas, S. Pispas, N. Hadjichristidis, T. Pakula, A. R. Khokhlov, *Macromolecules*, 28 (1995) 5109

[30] G. Floudas, G. Fytas, S. Pispas, N. Hadjichristidis, T. Pakula, A. R. Khokhlov, *Macromol. Symp.*, 106 (1996) 137

[31] B. Chu, J. Wang, Y. Li and D. Peiffer, *Macromolecules*, 25 (1992) 4229

[32] P.-G. de Gennes, Scaling Concepts of Polymer Physics, Cornell University Press, Ithaca, New York 1979

[33] S. Pispas, N. Hadjichristidis and J. W. Mays, *Polymer Comm.*, 37 (1996) 17, 3989

[34] S. Pispas, S. Allorio, N. Hadjichristidis and J. W. Mays, *Macromolecules*, 29 (1996) 2903

[35] M. Pitsikalis, N. Hadjichristidis and J. W. Mays, *Macromolecules*, 29 (1996) 179

[36] D. F. Siqueira, M. Pitsikalis, N. Hadjichristidis and M. Stamm, *Langmuir*, 12 (1996) 1631

ISSN 1318-0010
KZLTET 31(6)581(1997)

RECENT ADVANCES IN SYNTHESIS OF MONOSUBSTITUTED ACETYLENE POLYMERS

RAZVOJ NA PODROČJU SINTEZE MONOSUBSTITUIRANIH ACETILENSKIH POLIMEROV

JIŘÍ VOHLÍDAL[1], J. SEDLÁČEK[1], M. ŽIGON[2]

[1]Department of Physical and Macromolecular Chemistry Faculty of Science, Charles University Albertov 2030, CZ-128 40 Prague 2 Czech Republic
[2]National Institute of Chemistry, Hajdrihova 19, 1000 Ljubljana, Slovenia

Prejem rokopisa - received: 1997-10-01; sprejem za objavo - accepted for publication: 1997-10-21

During the last three years, a considerable progress has been achieved in development of catalyst systems for living polymerization of various substituted acetylenes. Nowadays, there are available single-component catalysts of this type based on stable carbene complexes and multicomponent catalysts based on $MoOCl_4$ and $WOCl_4$, both operating in metathesis mode, as well as Rh(diene) complexes operating in the ZN mode. Within that time period, similar progress has been attained in polymerization of novel substituted acetylene monomers, including those bearing functional groups like $-NO_2$, $-NR_2$, $-C{\equiv}N$, etc. and those bearing ionic or zwitterionic pendant groups. These advancements provide an improved basis for more systematic study of functional properties of these electrically and fotonically active polymers and a better comprehension of relations between the covalent structure and functional properties of this class of polymers.

Key words: substituted acetylene polymers, living polymerization, functional polymers

V obdobju zadnjih treh let je bil dosežen znaten napredek pri razvoju katalizatorskih sistemov za živo polimerizacijo različnih substituiranih acetilenov. Danes so tako na razpolago enokomponentni katalizatorji te vrste na osnovi stabilnih karbenskih kompleksov in večkomponentni katalizatorji na osnovi $MoOCl_4$ in $WOCl_4$, ki delujejo po metateznem načinu, ter Rh(dienski) kompleksi, ki delujejo po načinu Ziegler-Natta (ZN). Za isto obdobje je značilen tudi napredek na področju polimerizacije novih substituiranih acetilenskih monomerov, vključno z monomeri s funkcionalnimi skupinami, kot so npr. $-NO_2$, $-NR_2$ ali $-C{\equiv}N$, in z ionskimi ali zwitterionskimi stranskimi skupinami. Razvoj na tem področju zagotavlja boljšo osnovo za sistematičen študij funkcionalnih lastnosti teh električno in fotonsko aktivnih polimerov ter za boljše razumevanje povezav med kovalentno strukturo in funcionalnimi lastnostmi te skupine polimerov.

Ključne besede: substituirani acetilenski polimeri, živa polimerizacija, funkcionalni polimeri

1 INTRODUCTION

For at least two decades, conjugated polymers attract significant interest of both academics and industry due to their potential applicability as functional materials for future electronic devices[1-8]. One class of these materials are substituted acetylene polymers, SAP, that are insulators in native state and do not show metallic conductivity neither after doping. However, they exhibit other useful functional properties like photoconductivity, electroluminescence, nonlinear optical properties, etc. originating from their ability to capture, transport and mediate mutual conversions of charge and energy and from their increased higher-order optical susceptibility. Besides, they are candidates for molecular wires transporting the charge and/or energy (signals) through membranes of supramolecular systems, see, e.g. ref.[9]. Actually, carotenoid pigments like carotenes and zeaxanthines, serving as molecular wires in living systems, are oligomers of the SAP type. It can be thus said that the research on synthesis and properties of substituted acetylene polymers really meets material demands of future electronics based on the molecular and supramolecular devices.

There are a few published reviews and book chapters summarizing the state of art in the field of synthesis of substituted acetylene polymers until 1995[2,3,5,8]. In this paper a brief survey of recent developments in the field of living polymerization systems and synthesis of novel substituted acetylene polymers is presented.

2 LIVING POLYMERIZATION OF SUBSTITUTED ACETYLENES

Living polymerization systems provide: (i) the most efficient control of the polymer molecular weight, and (ii) possibility to synthesize block copolymers of substituted acetylenes that can show some new interesting properties originated from their domain interfaces.

First living metathesis polymerizations of substituted acetylenes have been reported in 1987 for o-Me_3Si-phenylacetylene[5,10,11] and tert-butylacetylene[12]. Most effort has been paid to systems with phenylacetylenes bearing bulky ortho substituents and $MoOCl_4/Bu_4Sn$/EtOH catalyst that give polymers with polydispersity I_n<1.10. Analogous systems without ethanol or bulky substituents do not show living polymerization. Monomers with medium-size substituents yield only living-like systems providing I_n values about 1.2 to 1.3 and m- and p-substituted phenylacetylenes provide systems in which a termination takes place[5,13,14]. An exception is 1-chloro-1-octyne that also provides living polymerization system[15].

In 1994, Schrock et al.[16] reported of the living metathesis polymerization of o-trimethylsilyl phenylacetylene induced by (1-adamantyl-N=)[$OCH(CF_3)_2$]$_2$(2,4-lutidine)-Mo=CH-CMe_2Ph carbene complex (I_n = 1.05). They found that other carbene initiators with bulkier ligands do not provide living polymerization systems. Buchmeiser and Schrock have reported of the living stereoregular polymerization of three organometallic acetylenes, ethynylferrocene and ethynylruthenocene[17] and 4-(ferrocenylethynyl)-4'-ethynyltolan (tolan is a trivial name for diphenylacetylene)[18] induced by another Mo-carbene complex: (2,6-Me_2-C_6H_3-N=)[$OCH(CF_3)_2$]$_2$Mo=CH-CMe_2Ph in THF and toluene.

Recently, Masuda et al. reported living polymerization of o-CF_3-phenyl-acetylene in anisole induced by $WOCl_4$/Bu_4Sn/t-BuOH catalyst (I_n<1.1)[19]. Again, alcohol was found to be essential for the living polymerization to be achieved. Similar behaviour has been observed for the systems $MoOCl_4$/Et_3Al/EtOH (1:1:4), $MoOCl_4$/Et_2Zn/EtOH (1:1:4) and $MoOCl_4$/BuLi (without alcohol) for which polymer polydispersities about I_n=1.02 to 1.03 are reported[19].

Rh^I(diene) complexes represent another class of living polymerization initiators because, unlike the previous, they operate in the Ziegler-Natta mode and induce living polymerization of sterically uncrowded acetylenes including unsubstituted phenylacetylene, PA. Kishimoto, Nyori et al. reported[20] of the living polymerization of PA induced by [Rh(nbd)(PPh_3)$_2$(-C≡CPh)] and the synthesis of block copolymers of PA with p-methoxy-PA. Living system is only obtained if a strong base like 4-(dimethylamino)pyridine, DMAP, is added into polymerization mixture. Later on, the same authors reported of the living polymerization of PA and p-($OCH_2CH_2CH_2O$-Ph-Ph-OCH_3)-PA by bridged binuclear Rh^I complex [Rh(nbd)(OCH_3)]$_2$ in a presence of DMAP[21]. In all cases, stereoregular head-to-tail cis-transoid structure is reported for polymers prepared on catalysts derived from Rh(diene) complexes.

In summary, it can be said that a development of living polymerization systems has achieved considerable advances in recent years and further progress in this field seems quite promising. Besides, the catalysts forming living polymerization systems often give stereoregular polymers which is promising for a progress in analysis of microstructure of substituted acetylene polymers.

3 NEW SUBSTITUTED ACETYLENE POLYMERS

Functional properties of SAPs depend on their structure that, in the first place, is predetermined by pendant groups attached to their main chains. Great attention is, therefore, paid to design and synthesis of new polymers with more sophisticated structure that are expected to possess better functional properties. In addition, the investigation of these new polymers brings up new knowledge improving our general understanding of the relations between the polymer structure and functional properties that is rather poor till now. Some interesting, recently prepared substituted acetylene polymers are presented in the next survey.

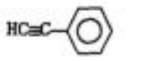

1

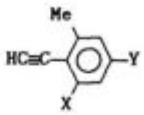

X = Y = H 2

X = Y = Me 3

X = Me Y = tBu 4

Demonstration of positive effect of bulky ortho substituents on the molecular weight, thermal stability, UV/vis absorption and other properties of PPA[22]. Rate of polymerization decreases from **1** to **4**. Tert-butyl group improves polymer solubility: poly(**3**) is insoluble whereas poly(**4**) is soluble and provides free standing films. Copolymers of **4** with **1** and **2** were prepared. Gas permeability and dark conductivity measurements are reported.

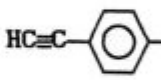

5

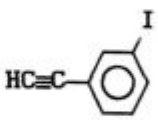

6

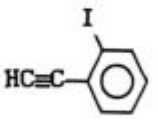

7

First polymerization of iodophenylacetylenes by various Mo, W and Rh based catalysts. Poly(**5**)s formed on $MoCl_5$ based catalysts are insoluble, on Rh catalyst partly soluble, and on $WOCl_4$ based catalyst soluble. Dioxane cosolvent increases MW of polymers prepared on $WOCl_4$ based catalyst. Unusual, negative effects of common cocatalysts like Ph_4Sn and Bu_4Sn have been observed. Content of cis-units decreases in the following order: Rh>Mo>W/dioxane>W/benzene. Poly(**7**) is stable in solutions exposed to air whereas poly(**5**) and poly(**6**) are not. Photoconductivity of soluble polymers prepared by $WOCl_4$ based catalyst is reported[23-25].

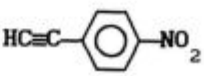

8

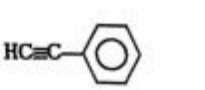

1

First polymerization of **8** and its copolymerization with PA by $WOCl_4/Me_4Sn$ in dioxane/benzene and [Rh(nbd)(PPh_3)$_2$(-C≡CPh)]. $WOCl_4$ by itself does not transform **8** to any oligomer or polymer. Homopolymers of **8** are insoluble. Photoconductivity measurements on the copolymer of **8** with PA are reported. Nitro group was found to act as a trap for photogenerated charge carriers[25,26].

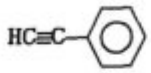

1

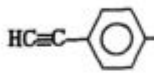

9

Polymerizations in water, THF, Et_3N and toluene induced by various Rh^I(nbd) and Rh^I(cod) complexes: other ligands: tosyl, H_2O, Cl, piperidine, o-phenylenediamine, N-methylimidazole, bis(4-tBu)-2-pyridylmethanethiolate, $tBuNH_2$, NH_3. [Rh(cod)(tosyl)(H_2O)] complex yields all-cis polymers. Acetylenes of aliphatic type (1-octyne, 1-butyne-4-ol, 5-hexyne carboxylic acid and 2-butyne dicarboxylic acid) do not polymerize on this Rh catalyst[27].

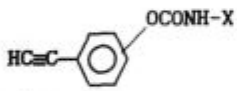

where X = :

(R)-CH(CH_3)-Ph	*m*-	**10**
	p-	**11**
(R)-CH(CH_3)-α-naphtyl	*p*-	**12**
-O-$SiMe_2$-*t*Bu	*m*-	**13**
	p-	**14**
-O-$SiPh_2$-*t*Bu	*p*-	**15**

PA	**1**
4-ethynylbiphenyl	**16**
a-ethynylnaphtalene	**17**

Homopolymerization of phenylacetylenes with bulky, optically active groups linked to phenyl ring and their copolymerization with non-chiral monomers. [Rh(nbd)Cl]$_2$ in THF solvent was found to be efficient initiator yielding high cis-transoidal polymers whereas WCl_6/Ph_4Sn and $MoCl_5/Ph_4Sn$ systems have provided oligomers and/or low-MW polymers only. Upfield shifts of olefinic protons' NMR signal up to 0.25 ppm are correlated to increasing co-monomer bulkiness resulting in twisting up of the main chain. Polymers of **10**, **11** and **12** as well as their copolymers with achiral acetylenes **1** and **13** to **17** show circular dichroism, CD, in 300 to 500 nm range. Stereoregularity of main chains was found to be essential for CD activity (non stereoregular polymers of chiral monomers do not show significant CD bands). Computational study of the polymers' helical structure is presented[28].

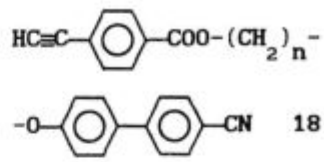

18

n = 6, 12

Successful transformation of both monomers **18** into cis-transoid stereoregular PPAs with pendant polar mesogenic groups by using [Rh(nbd)Cl]$_2$ catalyst. WCl_6/Ph_4Sn yields either cyclotrimers (in THF) or their mixture with low MW polymer (in toluene). $MoCl_5/Ph_4Sn$ catalyst has not shown activity in any solvent. DSC records as well as slow polymer dissolving prove to a formation of mesogenic structures[29].

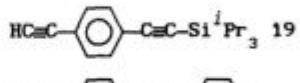

19

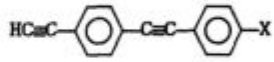

where X = C≡C-Si ^{i}Pr$_3$ **20**

Selective polymerization of **19** and **20** by Mo, W and Rh based initiators taking place on terminal ethynyl group is reported. Polymer formed by $WOCl_4Ph_4Sn$ catalyst in benzene involves a small amount of soluble high-MW fraction. Dioxane cosolvent suppresses this fraction formation and increases content of cis units in poly(**19**) and poly(**20**). Content of cis units increases in order: W/benzene<W/dioxane<Mo<Rh and it is well correlated even with UV spectra of polymers. Introduction of ethynylenephenylene spacer increases photoconductivity and fluorescence activity of the polymer. Autoxidation kinetics of polymers is reported[30,31].

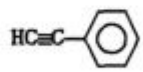

1

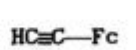

21

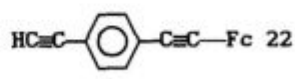

22

(Fc is ferrocenyl). $TaCl_5$ quantitatively cyclotrimerizes **21** to 1,2,4- and 1,3,5-triferrocenylbenzenes (mole ratio 3:2). Solid state structure of 1,3,5-isomer was established: up-up-down arrangement of Fc groups. **21** was copolymerized with **1** to a soluble statistical copolymer. **22** was selectively polymerized on terminal ethynyl group by using W and Rh based catalysts to partly soluble polymers[32,33].

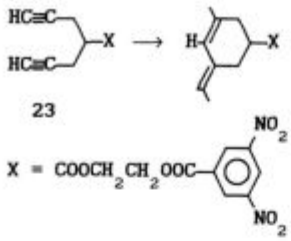

23

X = $COOCH_2CH_2OOC$–(2,4-$(NO_2)_2$-phenyl)

The first reported polymerization of acetylene bearing nitro group. Cyclopolymerization of dipropargylic monomer induced by $MoCl_5/Ph_4Sn$ and $PdCl_2$ catalysts. The former yields only partly soluble (solubility depends on the solvent used in polymerization), whereas the latter completely soluble poly(**23**). W-based catalysts were found as inactive. Polymer shows UV/vis absorption up to ca 650 nm[34].

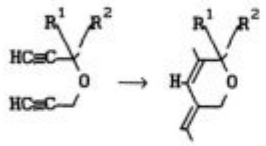

$R^1 = R^2 = H$ **24**

$R^1 = H$ $R^2 = Me$ **25**

$R^1 = H$ $R^2 = pentyl$ **26**

$R^1 = Me$ $R^2 = Ph$ **27**

$R^1 = R^2 =$ cyclohexyl **28**

Cyclopolymerization of series of dipropargyl ethers. $MoCl_5$ based catalysts ($EtAlCl_2$ and Bu_4Sn cocatalysts) were found to be most active providing high yields of medium-MW polymers. WCl_6 based catalysts are almost inefficient and $PdCl_2$ gives only 25% yield of poly(**27**). Poly(**24**) is insoluble. Solubility of poly(**25**) and poly(**26**) depends on the monomer concentration in polymerization mixture (above [M] = 0.5 mol/L, the formed polymers are insoluble). On the contrary, poly(**27**) and poly(**28**) are well soluble. Bulky α-substituents are suggested to support intramolecular cyclization and suppress intermolecular crosslinking, thus ensuring good polymer solubility. UV/vis absorption up to 600 nm and dark conductivity in both native and iodine doped state are reported[35].

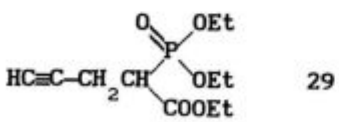

29

By itself $MoCl_5$ and WCl_6 do not induce polymerization of **29** but together with $EtAlCl_2$ or Ph_4Sn cocatalysts provide good yields of low-to-medium-MW yellow polymers (<M>$_w$ below 10000). $PdCl_2$ gives only lower yield of brown poly(**29**). UV/vis absorption up to 500 nm is reported[36].

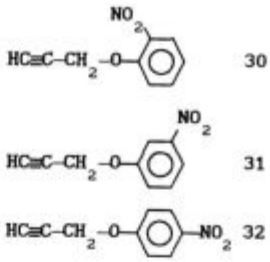

30

31

32

$MoOCl_4/Me_4Sn$ and $MoCl_5/EtAlCl_2$ polymerize **30** to insoluble polymer, **31** to insoluble polymer and methanol-soluble fraction, and **32** to soluble, high-MW polymer (<M>$_w$ value up to 480 000) and methanol soluble fraction. Methanol soluble fractions formed on $MoOCl_4$ consist of oligomers only (MW below 1000), whereas in those formed on $MoCl_5$ involve polymers of <M>$_w$ value up to 35000. The former catalyst is more active than the latter one. $WOCl_4/Me_4Sn$ system in dioxane/benzene (highly active in polymerization of nitroPA, **8**) shows low activity at room temperature (only methanol soluble polymer is reported) but no activity at 60°C [37].

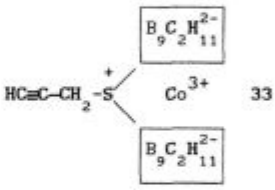

33

First preparation of polyacetylene with deltahedral sandwich carborane pendant groups is reported. $WOCl_4/Ph_4Sn$ catalyst induces polymerization of **33** to a polymer partly soluble in DMSO. Strong intermolecular interactions of zwitterionic carborane groups (dipole moment 17.7×10^{-30} Cm) are perhaps responsible for low solubility. The same catalyst copolymerizes **33** with **1** to a soluble statistical copolymer[38].

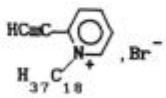

34

Quaternization of 2-vinylpyridine with 1-bromooctadecane is accompanied by a spontaneous polymerization of formed **34**. Poly(**34**) was also prepared by quaternization of thermally prepared poly(2-vinylpyridine). Multilayers thin films of poly(**34**) were prepared by LB technique and their properties were investigated. Electrical conductivity of native and iodine doped polymer and oxygen and nitrogen permeation of membranes deposited on Nafion as substrate are reported. The multilayer membranes have shown excellent long term stability[39,40].

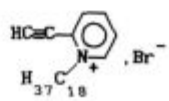

34

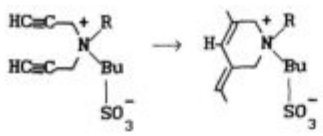

R = Et	35
R = Bu	36
R = hexyl	37
R = octyl	38

Synthesis of amorphous, conjugated polybetaines by cyclopolymerization of **35** to **38** induced by $MoCl_5$, WCl_6 and $PdCl_2$ catalysts. Negative effect of cocatalysts ($EtAlCl_2$ and Bu_4Sn) has been observed for the first two catalysts (viz. also polymerization of iodophenylacetylene **5**). Solubility of polymers in various solvents, UV/vis absorption up to 600 nm, dark conductivity in native and iodine doped state are reported[41].

ACKNOWLEDGEMENT

Financial supports from Grant Agency of Charles University (contract No. 189/97/B-CH) and EU Commission (PECO, supplementary contract ERBCIPDCT 940617) are greatly acknowledged.

4 REFERENCES

[1] J. C. W. Chien, *Polyacetylene - Chemistry, Physics and Material Science*. Academic Press, New York, 1984

[2] T. Masuda, T. Higashimura, *Adv. Polym. Sci.*, 81 (1987) 121

[3] J. L. Brédas, R. Silbey (Eds), *Conjugated Polymers*. Kluwer Academic Publishers, Dordrecht, 1991

[4] G. H. Kiess (Ed.), *Conjugated Conducting Polymers*. Springer Verlag, Berlin, 1992

[5] H. Shirakawa, T. Masuda, K. Takeda, in: *The Chemistry of Triple-Bonded Functional Groups, Supplement C2* (Patai S. Ed.), Wiley, New York, 1994, p. 945

[6] S. Nešpůrek, V. Cimrová, J. Pfleger, I. Kmínek, *Polym. Adv. Technol.*, 7 (1996) 459

[7] R. Giesa, *J. Macromol. Sci. Macromol. Chem. Phys.*, C36 (1996) 4, 631

[8] K. J. Ivin, J. C. Mol, *Olefin Metathesis and Metathesis Polymerization*, Academic Press, London, 1997

[9] A. C. Benniston, V. C. Goule, A. Harriman, J.-M. Lehn, B. Marczinke, *J. Chem. Phys.*, 98 (1994) 7798

[10] T. Masuda, T. Yoshimura, J. Fujimori, T. Higashimura, *J. Chem. Soc. Chem. Commun.*, (1987) 1805

[11] T. Yoshimura, T. Masuda, T. Higashimura, *Macromolecules*, 21 (1988) 1899

[12] J. Kunzler, V. Percec, *Polym. Bull.*, 18 (1987) 303 and ibid. 29 (1992) 335

[13] T. Mizumoto, T. Masuda, T. Higashimura, *Macromol. Chem. Phys.*, 196 (1995) 1769

[14] H. Seki, T. Masuda, T. Higashimura, *J. Polym. Sci. Polym. Chem. Ed.*, 33 (1995) 117

[15] K. Akiyoshi, T. Masuda, T. Higashimura, *Makromol. Chem.*, 193 (1992) 755

[16] H. H. Fox, M. O. Wolf, R. O'Dell, B. L. Lin, R. R. Schrock, M. S. Wrighton, *J. Am. Chem. Soc.*, 116 (1994) 2827

[17] M. Buchmeiser, R. R. Schrock, *Macromolecules*, 28 (1995) 6642

[18] M. Buchmeiser, R. R. Schrock, *Macromolecules*, 30 (1997) 2274

[19] T. Masuda, *Proceedings of ISOM 12 Symposium on Metathesis and Related Chemistry*, Flagler College, St. Augustine, Florida, July 13-18, 1997, p. 25, papers in preparation

[20] Y. Kishimoto, P. Eckerle, T. Miyatake, T. Ikariya, R. Noyori, *J. Am. Chem. Soc.*, 116 (1994) 12131

[21] Y. Kishimoto, T. Miyatake, T. Ikariya, R. Noyori, *Macromolecules*, 29 (1996) 5054

[22] T. Yoshida, Y. Abe, T. Masuda, T. Higashimura, *J. Polym. Sci. Polym. Chem.*, 34 (1996) 2229

[23] J. Vohlídal, J. Sedláček, M. Pacovská, O. Lavastre, P. H. Dixneuf, H. Balcar, J. Pfleger: *Polymer*, 38 (1997) 3359

[24] J. Pfleger, S. Nešpůrek, J. Vohlídal, *Adv. Mat. Opt. Electronics*, 6 (1996) 325

[25] J. Vohlídal, J. Sedláček, M. Pacovská, N. Patev, H. Balcar, S. Cabioch, O. Lavastre, P. H. Dixneuf: *Proceedings of ISOM 12 Symposium on Metathesis and Related Chemistry*, Flagler College, St. Augustine, Florida, July 13-18, 1997, p. 97; papers in preparation

[26] J. Sedláček, J. Vohlídal, S. Cabioch, O. Lavastre, P. H. Dixneuf, H. Balcar, M. Štícha, J. Pfleger, V. Blechta: *Macromol. Chem. Phys.* 199 (1998) 155

[27] B. Z. Tang, W. H. Poon, S. M. Leung, W. H. Leung, H. Peng, *Macromolecules*, 30 (1997) 2209

[28] E. Yashima, S. Huang, T. Mitsushima, Y. Okamoto, *Macromolecules*, 28 (1995) 4184

[29] B. Z. Tang, X. Kong, X. Wan, X.-D. Feng, *Macromolecules*, 30 (1997) 5620

[30] J. Vohlídal, J. Sedláček, N. Patev, M. Pacovská, S. Cabioch, O. Lavastre, P. H. Dixneuf, H. Balcar, J. Pfleger, V. Blechta, P. Matějka, *Macromolecules* (submitted)

[31] J. Sedláček, M. Pacovská, T. Etrych, M. Dlouhý, N. Patev, S. Cabioch, O. Lavastre, H. Balcar, M. Žigon, J. Vohlídal, *Polym. Mate. Sci. Eng.*, 77 (1997) 52

[32] P. Štěpnička, I. Císařová, J. Sedláček, J. Vohlídal, M. Polášek, *Collect. Czech. Chem. Commun.*, 62 (1997) 1577

[33] J. Sedláček, J. Vohlídal, N. Patev, M. Pacovská, S. Cabioch, O. Lavastre, H. Balcar, P. Matějka, V. Blechta, *Macromol. Chem. Phys.*, (submitted)

[34] J.-H. Lee, J.-W. Park, J.-M. Oh, S.-K. Choi, *Macromolecules*, 28 (1995) 377

[35] H.-J. Lee, Y.-S. Gal, W.-C. Lee, J.-M. Oh, S.-H. Jin, S.-K. Choi, *Macromolecules*, 28 (1995) 1208

[36] Y.-S. Gal, B. Jung, W.-C. Lee, H.-J. Lee, S.-K. Choi, *Macromolecules* 28 (1995) 2086

[37] H. Balcar, T. Kalisz, J. Sedláček, V. Blechta, P. Matijka, *Polymer*, in print

[38] J. Vohlídal, J. Plešek, J. Sedláček, I. Císařová, P. Matějka, S. Heřmánek, *Collect. Czech. Chem. Commun.*, 61 (1996) 877

[39] P. Zhou, A. Blumstein, *Polymer*, 37 (1996) 1477

[40] P. Zhou, L. Samuelson, K. S. Alva, C.-C. Chen, R. B. Blumstein, A. Blumstein, *Macromolecules*, 30 (1997) 1577

[41] D.-C. Choi, S.-H. Kim, J.-H. Lee, H.-N. Cho, S.-K. Choi, *Macromolecules*, 30 (1997) 176

ISSN 1318-0010
KZLTET 31(6)???(1997)

INTERFACIAL PHENOMENA IN THIN POLYMER FILMS STUDIED BY DIRECT PROFILING TECHNIQUES

ŠTUDIJ POJAVOV NA MEJNIH PLOSKVAH TANKIH POLIMERNIH PLASTI Z DIREKTNIMI TEHNIKAMI PROFILIRANJA

ANDRZEJ BUDKOWSKI

Institute of Physics Jagellonian University Reymonta 4, 30-059 Krakow, Poland

Prejem rokopisa - received: 1997-10-01; sprejem za objavo - accepted for publication: 1997-12-11

Various interfacial phenomena, such as: phase coexistence, surface segregation and wetting, as well as surface directed phase separation, determine many properties of polymer mixtures. These phenomena are studied in blends confined in a thin film geometry. Direct composition vs. depth profiling techniques are used, which have been developed in the last decade. Present paper describes briefly direct profiling methods and interfacial phenomena observed with their help. Discussion is illustrated by experimental results obtained for homopolymer mixtures with nuclear reaction analysis and secondary ion mass spectroscopy.

Key words: polymer blends, liquid thin films, ion beam analysis, composition vs. depth profiling techniques, miscibility conditions, surface segregation, wetting, phase separation

Razni pojavi na mejnih ploskvah kot so npr. soobstoj faz, površinska segregacija in omakanje na površini pa tudi s površino usmerjena ločitev faz, določajo mnoge lastnosti polimernih mešanic. Te pojave smo študirali na polimernih mešanicah (blendih) z geometrijo tankih plasti. Uporabljene so bile direktne tehnike profiliranja koncentracije z globino plasti, ki so bile razvite v zadnjem desetletju. Članek na kratko opisuje direktne metode profiliranja in pojave na mejnih ploskvah, ki smo jih opazovali s pomočjo omenjenih metod. V diskusiji so predstavljeni eksperimentalni rezultati homopolimernih mešanic z jedrsko reakcijsko analizo in sekundarno ionsko masno spektroskopijo.

Ključne besede: polimerne mešanice, tekoče tanke plasti, analiza z ionskimi snopi, tehnike profiliranja koncentracije z globino, pogoji mešljivosti, površinska segregacija, omakanje, ločitev faz

1 INTRODUCTION

Alloying polymers provides an inexpensive method to produce new materials with desired properties, often superior to either blend component alone[1]. The spatial blend structure is rarely homogeneous. Compositional inhomogeneities are related with *internal* interfaces, separating coexisting phases inside the blend, and *external* interfaces exposed by the blend (**Figure 1**). The most complex situation occurs in blends confined in a thin film geometry.

Various phase domain morphologies are encountered in thin films, and exemplified in **Figure 1**. Their characterization precedes an enforcement of the proper performance of many low- and high- tech applications. The local concentration of the surface *segregation* 'cuticle' of one- phase layer (**Figure 1a**) is different from the composition in the bulk, modifying e.g. the surface wettability by paints. Complex 3- dimensional two- phase structure (**Figure 1b**), expected for the *separation* of polystyrene (PS)/ polybutadiene blends, results in very tough 'high impact PS'. The separation process can be directed by external surfaces leading to self- stratified films (**Figure 1c**), where individual domains have often different properties (e.g. gas permeation and mechanical characteristics in gas separation membranes).

Apart from these technology oriented aspects[2,3], the interfacial phenomena pose a fundamental scientific challenge to soft matter physics[4]. They can be categorized according to complexity. The *internal* interface specifies miscibility conditions (Section 3a). These conditions, augmented by the knowledge of the specific segment interactions at given *external* interface, explain *surface segregation* (Section 3b). Finally, when all interfaces are treated explicit, the self- stratified films, created in the due course of *surface directed phase separation* (Section 3c), can be described.

Nowadays the spatial structure of blend films (phase morphology and local composition) can be determined with a nanometer precision, comparable with the polymer chain dimensions. Even the 3-dimensional complex morphology of two- phase systems can be resolved, e.g. with transmission electron microtomography[5]. The concentration vs. depth profiles $\phi(z)$ are examined by modern techniques[6] yielding the volume fraction ϕ of the blend component(s) as the function of depth z within the thin film (**Figure 1**). Indirect profiling techniques, such as X-ray and neutron reflectivity, yield model dependent profiles $\phi(z)$ (although with excellent resolution $\delta \approx 1$ nm). To contrary, the straightforward profiles $\phi(z)$ are obtained with the commonly used *direct methods*[6].

2 DIRECT PROFILING TECHNIQUES

The direct methods analyze the film composition with ion beams of medium (3-7 keV in dynamic Secondary Ion Mass Spectroscopy (SIMS)) or higher (0.7 - 7

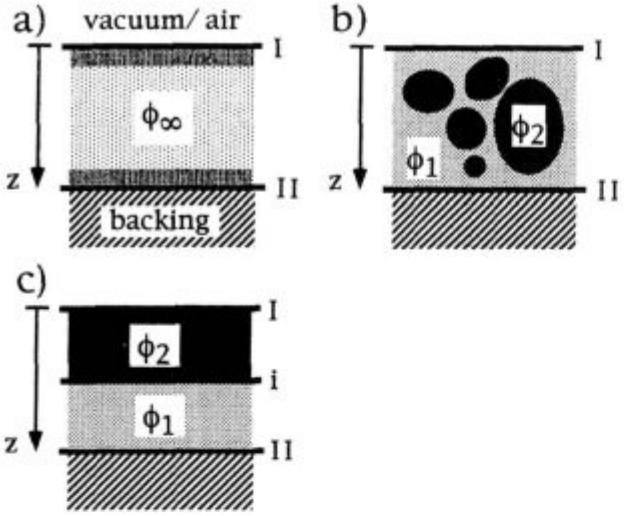

Figure 1: Thin polymer films composed of one phase ϕ (a), or two coexisting phases ϕ_1 and ϕ_2 (b, c) are not homogeneous. External interfaces **I** and **II** cause segregation (a), internal interface **i** separates coexisting phases (b and c)

Slika 1: Tanke polimerne plasti, sestavljene iz ene faze ϕ (a) ali iz dveh soobstoječih faz ϕ_1 in ϕ_2 (b, c), niso homogene. Zunanji mejni plasti **I** in **II** povzročita segregacijo (a), notranja mejna plast **i** ločuje soobstoječi fazi (b, c)

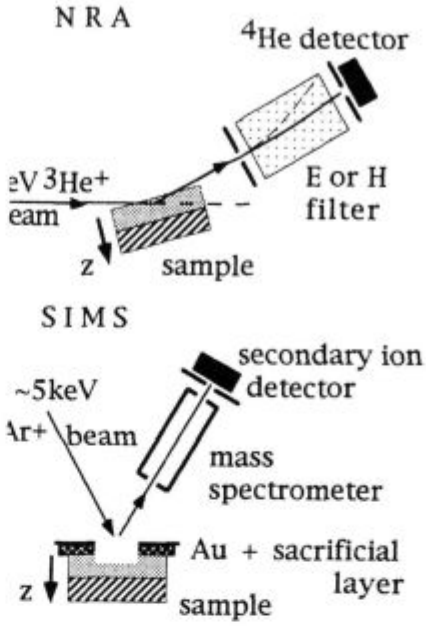

Figure 2: Schematic illustration of setups used to yield the composition ϕ vs. depth z profiles $\phi(z)$ in thin film samples with nuclear reaction analysis (NRA) (a) and dynamic secondary ion mass spectroscopy (SIMS) (b)

Slika 2: Shematska predstavitev priprav za merjenje koncentracije ϕ z globino z profila $\phi(z)$ v vzorcih tankih plasti z jedrsko reakcijsko analizo (NRA) (a) in dinamično sekundarno ionsko masno spektroskopijo (SIMS) (b)

MeV) energy (Rutherford Back Scattering (RBS), Forward Recoil Spectrometry (FRES), Nuclear Reaction Analysis (NRA)).

Bulk of polymers are made up of elements which rarely provide an effective contrast for high energy techniques. RBS can in principle yield composition profiles of heavy elements present in polymers, but it is exceptionally used to trace polymers themselves[6]. This is because the labeling a polymer with a heavy element severely alters the extent of its mixing with other polymers. Therefore a deuterium labeling is commonly used instead, which allows for the profiling of 'stained' polymers in such methods as FRES and NRA. The deuterium 'staining' of one of the chemically distinct blend components introduces much smaller thermodynamic perturbation, visible only for longer chains, and easily evaluated[7].

Non-resonant NRA[8] is the high energy method of choice providing profiling deuterium in polymer films with the highest range (even of few microns) and best resolution (δ ′ 7 nm at the free surface deteriorating to δ ′ 30 nm at depth z = 600 nm). As a standard procedure thin polymer films are mounted on Si wafers (spin cast from solution either directly on Si, or cast on mica, floated on water, and picked up by Si backing bearing a precast film to form a multilayer if necessary), annealed at temperatures above polymer glass transition, and measured at room (or lower) temperature. The monoenergetic ^{3}He$^+$ beam (with mm diameter) impinges on and penetrates into the thin film sample, as illustrated in **Figure 2a**. At different depths z the reaction: ^{3}He + ^{2}H ⊗ ^{4}He + ^{1}H + 18.4 MeV takes place and the magnetic or electric filter allows only ^{4}He$^+$ particles to reach the detector. The measured ^{4}He energy is related with the depth z, which can be calculated based on reaction kinematics and known energy losses of ^{3}He and ^{4}He in the sample. Finally, the correction of ^{4}He count rate with respect to the reaction cross section provides a relative profile $\phi(z)$ of the polymer 'stained' by deuterium. The absolute values of the volume fractions $\phi(z)$ are determined from the known (from preparation) overall amount of the deuterated material in the sample[9], or by profiling the studied sample covered with an additional reference layer built of pure deuterated material[10]. Typical NRA profiles are shown in **Figures 3a and 4a**.

An alternative profiling method of dynamic SIMS[11,12] is accomplished by monitoring individual atomic and molecular secondary ions emitted when the polymer sample is exposed to the primary ion (Ar$^+$ or another) beam with a medium energy (**Figure 2b**). The primary beam is scanned over an area of mm diameter, thereby eroding the sample and forming a flat crater with a growing depth. The secondary ions ejected from the central region of the crater are analyzed with mass spectrometer (with respect to their mass- to- charge ratio) and monitored as a function of the sputtering time. Prior to SIMS measurements, the polymer samples are covered by a polymer sacrificial layer and evaporated with Au. This is

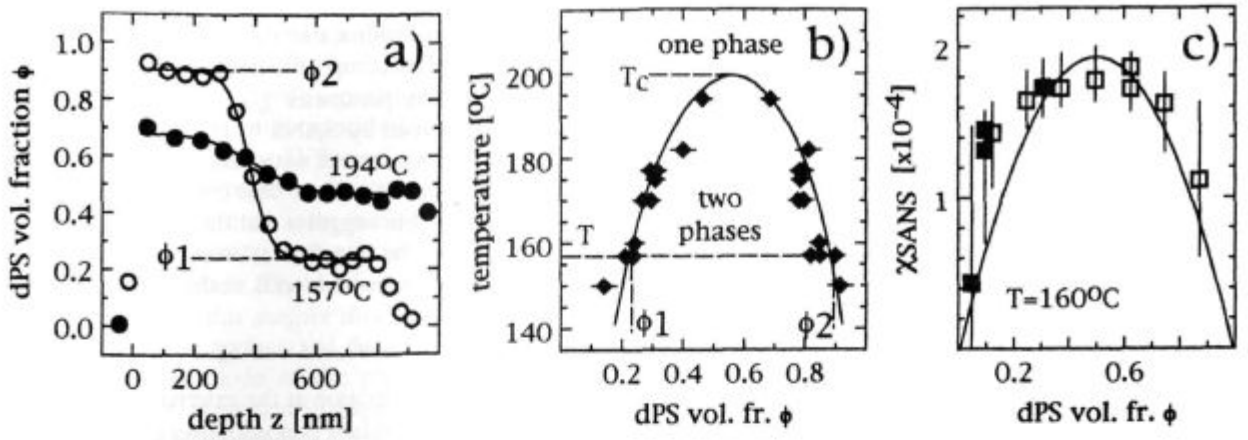

Figure 3: Relaxation of an initially sharp interface between pure polystyrene (PS) (N = 27.8 k) and pure deuterated polystyrene (dPS) (N = 9.2 k) leads (here after a month long annealing at varied T) to coexisting profiles $\phi(z)$ (a). NRA profiles, tracing local dPS concentration, determine coexisting compositions, ϕ_1 and ϕ_2, used to plot experimental phase diagram (b). This is well fitted by theory (see solid line in b) to yield the specific form of segmental parameter $\chi_{SANS}(\phi)$ presented (for T=160°C) in (c) as a solid line. The $\chi_{SANS}(\phi)$ values measured by SANS for bulk blends of PS (N = 15.4 k)/dPS (N = 11.5 k) and PS (N = 8.7 k)/dPS (N = 11.5 k) are marked in (c) as open and solid symbols, respectively

Slika 3: Relaksacija na začetku ostre mejne površine med čistim polistirenom (PS) (N = 27,8 k) in čistim devteriranim polistirenom (dPS) (N = 9,2 k) vodi (tu po enomesečnem kondicioniranju pri različnih T) do soobstoječih profilov $\phi(z)$ (a). NRA profili, ki spremljajo lokalno dPS koncentracijo, določajo soobstoječe sestave, ϕ_1 in ϕ_2, so bili uporabljeni za eksperimentalni fazni diagram (b). Ta se dobro ujema s teorijo (neprekinjena črta v b), tako da dobimo specifično obliko segmentnega parametra $\chi_{SANS}(\phi)$, ki je prikazan (pri T = 160°C) v (c) kot neprekinjena črta. Vrednosti $\chi_{SANS}(\phi)$, izmerjene s SANS za polimerne mešanice v masi, so pri (c) označene z odprtimi simboli za PS (N = 15,4 k)/dPS (N = 11,5 k) in s polnimi simboli za PS (N = 8,7 k)/dPS (N = 11,5 k)

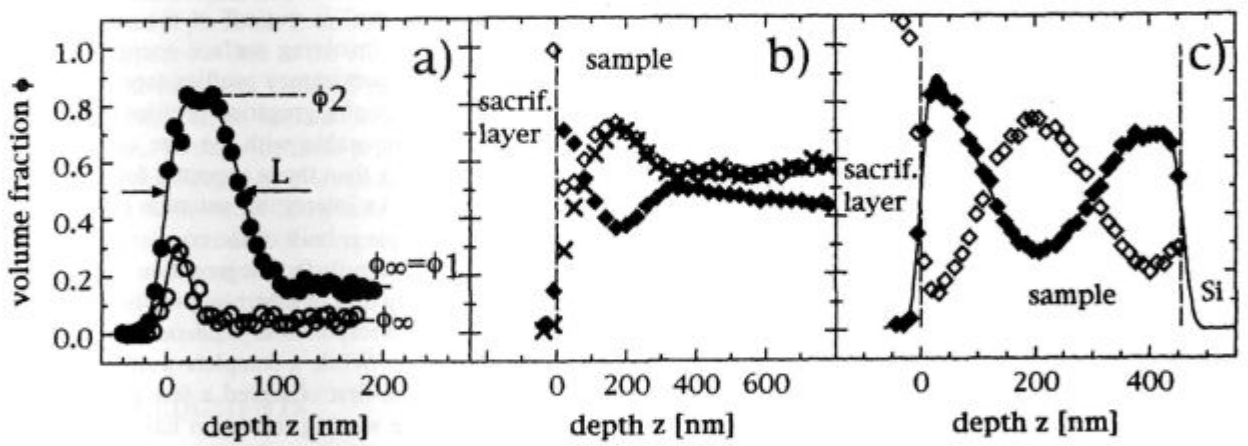

Figure 4: (a) NRA profiles $\phi(z)$ of the surface exposed by the mixture of random olefinic copolymers $[(C_4H_8)_{1-x}(C_2H_3(C_2H_5))_x]_N$: a hydrogenous h52 (x=52%, N=1510) and a partly deuterated d66 (x=66%, N=2030), after a few hours of annealing at T= 99°C. The open and solid symbols correspond to the surface enriched in d66 and completely wetted by the d66- rich phase ϕ_2, respectively. (b and c) SIMS profiles $\phi(z)$ illustrating surface directed phase separation. Its initial stages were recorded (see b) for the blend of dPS (N= 6.4k)/ brominated polystyrene PBr_xS (N=1.7k, x=0.08) annealed for 1 day at T=180°C. Its late stages (see c) were observed in the blend of dPS (N=17.4k) / PS (N=27.8k) annealed for 20 days at T=190°C. (Br^-, $^1HC^-/C^-$ and $^2HC^-/C^-$ profiles are marked by crosses, open and solid symbols, respectively)

Slika 4: (a) NRA profili $\phi(z)$ za površine, ki so bile izpostavljene zmesi naključnih olefinskih kopolimerov $[(C_4H_8)_{1-x}(C_2H_3(C_2H_5))_x]_N$: vodikov h52 (x=52%, N=1510) in delno devterirani d66 (x=66%, N=2030) po nekaj urah kondicioniranja pri T=99°C. Odprti simboli ustrezajo površini, ki je obogatena z d66 in polni simboki površini, ki je popolnoma omočena z d66 - bogato fazo ϕ_2. (b in c) SIMS profili $\phi(z)$ predstavljajo s površino usmerjeno ločitev faz. Začetne stopnje so posnete (glej b) za polimerno mešanico dPS (N=6,4 k) / bromirani polistiren PBr_xS (N=1,7 k, x=0,08), ki je bila kondicionirana en dan pri T=180°C. Kasnejše stopnje (glej c) so prikazane za polimerno mešanico dPS (N=17,4 k) / PS (N=27,8 k), ki je bila kondicionirana 20 dni pri T=190°C. (Br^- je označen s križci, $^1HC^-/C^-$ z odprtimi simboli in $^2HC^-/C^-$ s polnimi simboli)

to obtain a steady sputtering state before the real sample is reached by primary ions, and to avoid charging effects, respectively. Sputtering rates are determined by NRA (FRES or ellipsometric) measurements of selected control samples. This allows us to evaluate the absolute depth scale for each sample. The very good depth resolution of $\delta \approx 5$ nm, which deteriorates only slightly with depth z, is the one of two main SIMS advantages. The simultaneous profiling of various species such as ^1H, ^2H, C, O, Br, Si, N, etc., labeling polymers or present in the sample, is the second virtue. Most of these species are detected however only in semi- quantitative fashion. It

has been concluded that the absolute local concentrations $\phi(z)$ can be determined for polymers 'stained' with deuterium (based on the $^2H^-$ [11] or relative $^2HC^-/C^-$ [12] signals). The concentration calibration seems to hold also for hydrogenous (traced by $^1HC^-/C^-$) and for brominated (monitored by Br^-) polymers[12] (see **Figure 4b**). Typical SIMS profiles are shown in **Figures 4b and c**.

3 INTERFACIAL PHENOMENA IN THIN FILMS

3.a Phase coexistence

Two different polymer chains composed of N ($\approx 10^3$) segments would mix, when a gain in the entropy of mixing outweighs unfavorable interaction χ between unlike polymer segments[1]. Entropy of mixing scales as 1/N, and therefore the critical interaction χ_c necessary to cause the phase separation is 1/N times smaller as compared to simple liquid (N=1) alloys. In most cases χ, related with different cohesive energy of blend components, reduces with temperature as $1/T$[7]. Therefore homogeneous one-phase mixture is expected (**see Figure 3b**) at higher temperatures ($T>T_c$), while two adjacent macroscopic phases (ϕ_1 and ϕ_2) are expected to coexist in thermodynamic equilibrium at temperatures below critical point ($T<T_c$). The balance of three factors, related with the entropy of mixing, the segment-segment interaction and the configurational entropy of polymer coils, determines the composition profile $\phi(z)$ across the internal interface[4]. As the temperature is elevated the interfacial width increases and diverges to infinity for a miscible blend at $T>T_c$.

Until recently the phase coexistence of high polymer mixtures have been evaluated with a dynamic method determining cloud-point loci or with Small Angle Neutron Scattering (SANS). While the first technique is problematic due to extremely low molecular mobility, the second one measures the segmental interaction χ_{SANS} away from coexistence curve. A new direct approach has been developed[13,14] in which the profiles $\phi(z)$ are measured (for different T) across the internal interface between two coexisting phases forming a bilayer morphology as in **Figure 1c**. Such samples are obtained from bilayers composed of pure blend components as a result of an annealing process, involving the relaxation of the initial sharp internal interface and a material transport across the interface.

Figure 3a presents the exemplary coexistence profiles obtained with this novel method for the isotopic PS blend[14]. The corresponding coexistence curve presented in **Figure 3b** shows $T_c = 197°C$, which is much elevated as compared to $T_c \approx 0.9°K$ characterizing the isotopic mixture of simple liquids ^3He and ^4He. While unfavorable segment-segment interaction is comparable in both cases, the mixing entropy is reduced only for the isotopic PS blend. The question of accordance between the coexistence conditions determined by the novel approach[13,14] involving thin submicron films, and evaluated by SANS for bulk samples (with a size of c.a. 1 mm) is addressed by **Figure 3c**. The composition dependence of the segmental interaction parameter χ_{SANS} for the isotopic PS mixtures determined by SANS[15] (and marked by points) is in very good agreement with that (denoted by a solid line) based on the thin films data corresponding to **Figures 3a and b**. This suggests that the coexistence conditions yielded by the interface relaxation method should be valid also for polymer blends in the bulk.

3.b Surface segregation and wetting

The local concentration at the external surface differs usually from the constant concentration ϕ_∞ of one-phase in the bulk of the sample[16]. This is demonstrated in **Figure 4a** for the free surface of an olefinic blend[17]. The reason for this *surface segregation* (or *enrichment*) is the specific surface interaction of polymer segments, lowered when the surface blend concentration is changed. The amount of the segregation is a result of a trade-off between this specific surface energy f_s and the bulk term, expressing the free energy of mixing (three factors mentioned in Section 3a) and opposing the segregation. For known bulk concentration ϕ_∞ the segregation profile $\phi(z)$ is generated by the bulk energy term, specified by coexistence conditions. $\phi(z)$ is cut off at the surface by a boundary condition involving surface energy f_s[4]. Similarly to the case of coexistence profiles (**see Figure 3a**) also the spatial scales of segregation profiles (**see Figure 4a**) are at least comparable with the size of a polymer coil, and much larger than those expected for simple liquid (metal) alloys. An interesting situation occurs when the bulk of the sample is built of the coexisting phase ϕ_1. The thickness L of the surface segregation layer can be then microscopically thin or macroscopically thick (**as in Figure 4a**). This corresponds to a *partial* and *complete wetting*, respectively. While a complete wetting for polymer blends has been first observed a few years ago[18], a partial- to complete wetting transition has just been reported[19].

According to a conventional view point the surface of the polymer mixture is enriched in the component with lower cohesive energy, regardless of the value of the composition ϕ_∞ in the bulk of the sample. This is not necessary true. First, entropy- related forces driving the segregation have been concluded[20] besides those related to cohesive energy difference. Second, an *enrichment-depletion duality* has been advocated by theory[21] and computer simulations[22], and just observed in real polymer blends[23]. The surface is *enriched* in one blend component when the bulk composition is below a certain value $\phi_\infty < Q$, and it is *depleted* in this component for larger bulk concentration $\phi_\infty > Q$.

3.c Surface directed phase separation

A binary mixture is thermodynamically unstable when its average composition corresponds to the two-

phase region bounded by a spinodal curve. In such conditions spontaneous bulk- and surface- driven phase separations occur. The bulk separation, driven by thermal fluctuations, results in composition waves with random directions and phases. Different scenario is expected when a surface segregation is observed. Then a concentration gradient, created at the surface, induces composition waves propagating with a fixed phase in a direction normal to the surface. The concentration oscillation $\phi(z)$, characteristic for this *surface directed phase separation*, extends from the surface and decays inside the sample, where the bulk mode of the phase separation dominates[24]. This is presented in **Figure 4b** for the mixture composed of deuterated and brominated PS[12]. Finally, at the late stages of this process, a stratified plate morphology can be obtained[25] as presented in **Figure 4c** for the isotopic PS mixture. This layered structure can be controlled in a tunable fashion by a surface active copolymer admixed to the polymer blend[25].

4 CONCLUSIONS

Binary polymer blends are usually incompatible or only partly compatible. Already very weak interactions between unlike segments, as in isotopic mixtures, would lead to phase separation. Even miscible polymer 'alloys' are inhomogeneous due to the effects related with an external blend interface. Ordered segregation and separation processes can be initiated at the external interfaces of thin films. To describe them properly coexistence conditions needed first to be evaluated. Nowadays thin films are studied with direct composition vs. depth profiling techniques, which are best represented by SIMS and NRA. The advent of real 3- dimensional profiling is expected, which would enable to study directly complex two- phase morphologies.

ACKNOWLEDGMENTS

The author thanks Dr. A. Bernasik and J. Rysz for their help in performing SIMS experiments.

5 REFERENCES

[1] F. S. Bates, *Science*, 251 (1991) 898
[2] a special issue of *Physics World*, March (1995)
[3] a special issue of *MRS Bulletin*, January (1996)
[4] K. Binder, *Acta Polymer.*, 46 (1995) 204
[5] J. H. Lauer, J. C. Fung, F. S. Bates, et al., *Langumir*, 13 (1997) 2177
[6] E. J. Kramer, *Physica B*, 174 (1991) 189; MRS Bulletin, January (1996) 37
[7] A. Budkowski, J. Klein, U. Steiner, et al., *Macromolecules*, 26 (1993) 3858
[8] U. K. Chaturvedi, U. Steiner, J. Klein, et al., *Appl. Phys. Lett.*, 56 (1989) 1228
[9] A. Budkowski, J. Klein, U. Steiner, et al., *Macromolecules*, 26 (1993) 2470
[10] A. Budkowski, U. Steiner, J. Klein, *J. Chem. Phys.*, 97 (1992) 5229
[11] S. A. Schwarz, M. H. Rafailovich, et al., *Molecular Phys.*, 76 (1992) 937
[12] A. Bernasik, J. Rysz, A. Budkowski, K. Kowalski, J. Camra, J. Jedlinski, ECASIA 97, ed. by I. Olefjord, L. Nyborg and D. Briggs (J. Wiley & Sons, Chichester 1997) pp. 775-778
[13] F. Bruder, R. Brenn, *Macromolecules*, 24 (1991) 5552
[14] A. Budkowski, U. Steiner, J. Klein, G. Schatz, *Europhys. Lett.*, 18 (1992) 705
[15] J. D. Londono, F. S. Bates, et al., *Macromolecules*, 27 (1994) 2864
[16] Q. S. Bhatia, D. H. Pan and J. T. Koberstein, *Macromolecules*, 21 (1988) 2166
[17] A. Budkowski, F. Scheffold, J. Klein, et al., *J. Chem. Phys.*, 106 (1997) 719
[18] U. Steiner, J. Klein, E. Eiser, A. Budkowski, et al., *Science*, 258 (1992) 1126
[19] J. Genzer, E. J. Kramer, *Phys. Rev. Lett.*, 78 (1997) 4946, in press
[20] M. Sikka, A. Karim, F. S. Bates, et al., *Phys. Rev. Lett.*, 70 (1993) 307
[21] R. A. Jerry and A. Dutta, *J. Colloid Int. Sci.*, 167 (1994) 287
[22] S. K. Kumar, H. Tang and I. Szleifer, *Molecular Physics*, 81 (1994) 867
[23] A. Budkowski, J. Rysz, F. Scheffold, J. Klein, L. J. Fetters, *17th Disc. Conf.* 'Surface and Int. Phenomena in Macromol. Systems', Inst. Macromol. Chem. Ac. Sci. Czech Rep., Vol. K67, 1997
[24] R. A. L. Jones, L. J. Norton, et al., *Phys. Rev. Lett.*, 66 (1991) 1326
[25] J. Rysz, A. Bernasik, H. Ermer, A. Budkowski, R. Brenn, T. Hashimoto, J. Jedlinski, Europhys. Lett. 40 (1997) 503

ISSN 1318-0010
KZLTET 31(6)593(1997)

MECHANICAL AND MICROSTRUCTURAL PROPERTIES OF DUPLEX STEEL

MIKROSTRUKTURA IN MEHANSKE LASTNOSTI DUPLEKS JEKEL

MIRKO GOJIĆ[1], L. KOSEC[2], L. VEHOVAR[3]

[1]Željezara Sisak, Sektor za razvoj, B. Adžije 2, 44000 Sisak, Croatia
[2]OMM, Naravoslovnotehniška fakulteta, Ljubljana
[3]Inštitut za kovinske materiale in tehnologijo, Ljubljana

Prejem rokopisa - received: 1997-05-26; sprejem za objavo - accepted for publication: 1997-10-21

In this work mechanical properties and microstructure of duplex steel after heat treatment are shown. Heat treatment of the steel consisted of water quenching from 1050°C. A ferrite-austenite microstructure was obtained and the brittle σ-phase was avoided. The results show that the impact energy depends on the direction of rolling. In rolling direction the share of ferrite and austenite was approximately equal.

Key words: duplex steel, mechanical properties, ferrite-austenite microstructure, impact energy

V članku so opisani rezultati raziskav mikrostrukture in mehanskih lastnosti dupleks jekel po gašenju v vodi s 1050°C. Na ta način je jeklo dobilo mikrostrukturo iz ferita in austenita in brez krhke σ-faze. Rezultati kažejo, da je udarna energija odvisna od smeri valjanja. Na vzdolžnem prerezu cevi sta deleža ferita in austenita približno enaka.

Ključne besede: dupleks jeklo, mehanske lastnosti, feritno-austenitna mikrostruktura, udarna energija

1 INTRODUCTION

Because of excellent strength and toughness as well as high resistance to corrosion the high alloy stainless steels are used in car, electronic and petrochemical industries. Investigations of the development of high alloy steels which have simultaneously a high strength and other physical-chemical characteristics are important[1]. Depending on chemical composition, especially the content of chromium, nickel, and carbon as well as heat treatment high alloy steels can have a ferrite, austenite, martensite or duplex microstructure. Between the high alloy steels duplex stainless steel (DSS) with austenite-ferrite microstructure has an important role[2-6]. It is a relatively new class of engineering material for different applications because of the excellent combination of mechanical and corrosion characteristics. DSS offer benefits over austenite stainless steels and carbon steels because of their higher strength, good toughness and ductility in combination with equivalent resistance to general corrosion, as well as better resistance to localized corrosion and stress corrosion cracking. Today DSS have low carbon content (<0.002 wt.%) and contain optimal contents of chromium, nickel, molibdenum, copper and nitrogen for obtaining the required properties.

In process industries materials with a favorable microstructure are used because it determines their mechanical and corrosion behavior. DSS with a austenite-ferrite microstructure are desirable, if free of brittle σ-phase[7]. In the present work the investigation of mechanical and microstructural properties of DSS after heat treatment are presented with the accent on impact energy and the share of phases.

2 EXPERIMENTAL

2.1 Material

A section of commercially produced duplex stainless tubing was used for this investigation. The thermal treatment consisted of solution annealing at 1050°C and water quenching. The chemical composition the steel is given in **Table 1**.

Table 1: Chemical composition of duplex stainless steel, wt. %

C	Si	Mn	P	S	Cr	Mo	Al	Ni	N
0.02	0.45	0.88	0.024	0.018	24.97	3.19	0.04	8.20	0.12

2.2 Mechanical and microstructural testing

The mechanical properties were assessed on an Instron 1196 tensile testing machine in accordance with standard ASTM procedures[8]. The average hardness was determined by the Brinell method (HB), while the microhardness of austenite and ferrite grains was determined using the indentor on a Leitz-Wetzlar optical microscope 8196. Impact testing was performed at room temperature in both directions of rolling.

Microstructural tests were carried out with optical microscopy (OM), scanning electron microscopy (SEM), transmission electron microscopy (TEM), image analysis system and X-rays diffraction (XRD). Specimens for metallographic analysis were mechanically polished and

Table 2: Results of mechanical properties of duplex steel

R_g MPa	R_m MPa	A %	Z %	Hardness HB	Microhardness $HV_{0.10}$	Impact energy J
645	774	33	53	225	α = 140 γ= 292	dir.of rolling: 41 transverse to dir. of rolling: 33

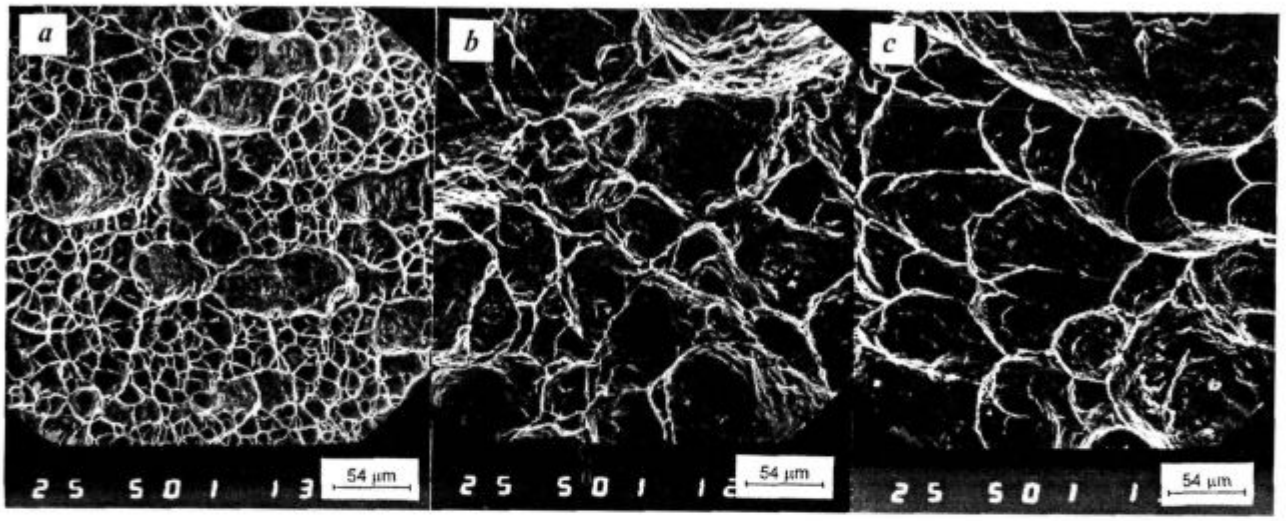

Figure 1: Microfractography of fracture surface of duplex steel after tensile testing (a) and impact testing in longitudinal (b) and transverse direction (c)
Slika 1: Mikrofraktografije prelomnih površin dupleks jekla po raztržnem preiskusu (a) in preiskusu udarne žilavosti v vzdolžni (b) in v prečni smeri valjanja (c)

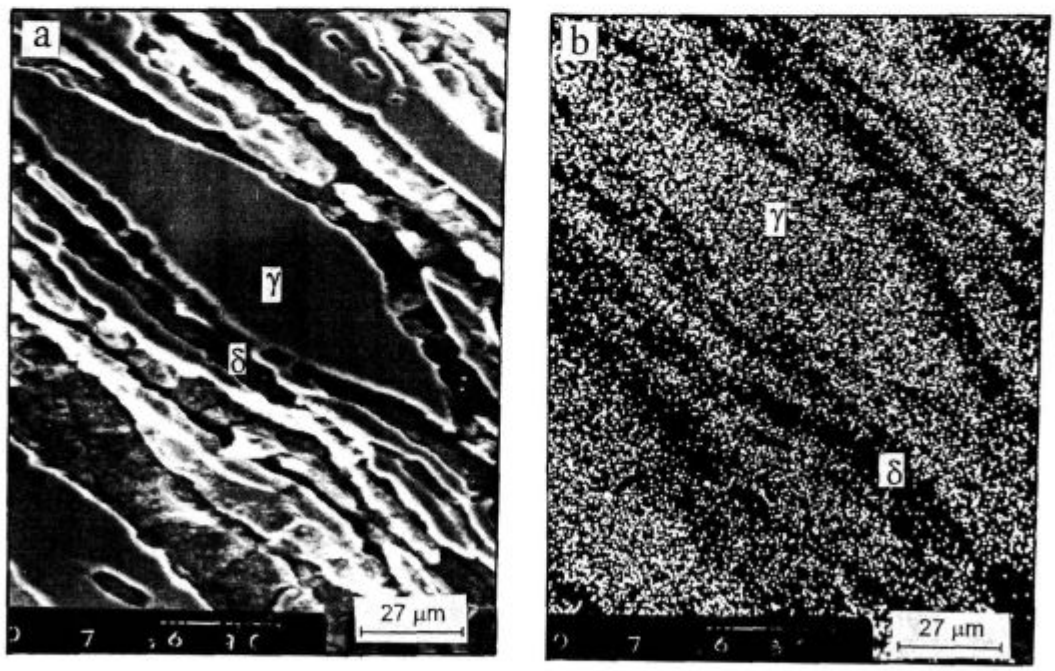

Figure 2: Scanning electron microscopy image of duplex steel in longitudinal direction (a) and the scanning picture for nickel (b)
Slika 2: Raster elektronski posnetek dupleks jekla v vzdolžni smeri valjanja (a) in x slika niklja (b)

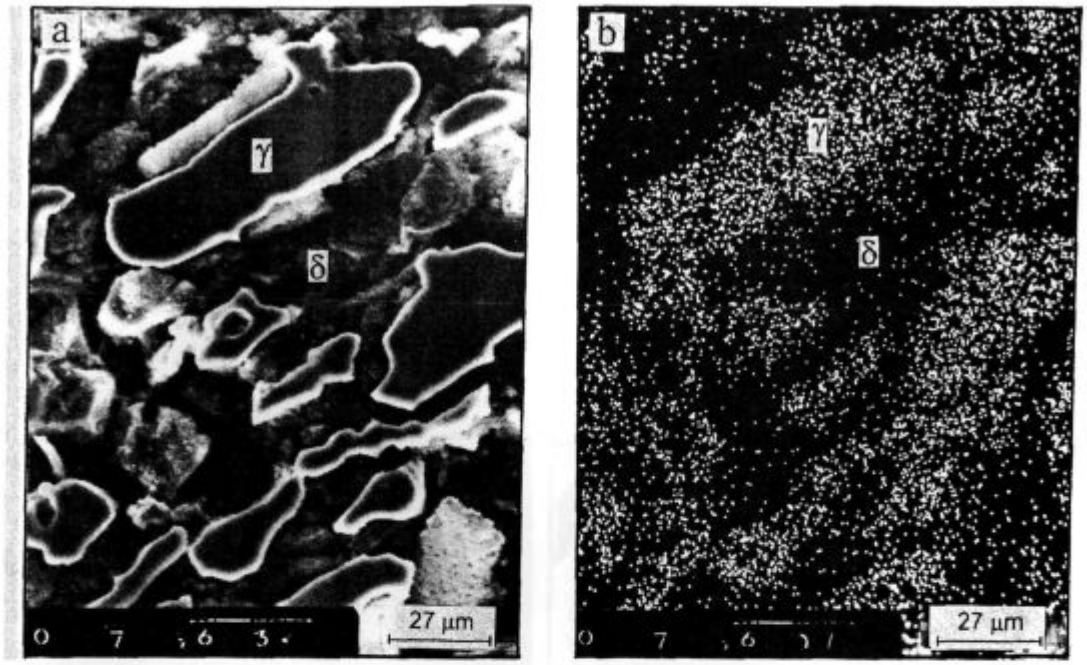

Figure 3: Scanning electron microscopy image of duplex steel in transverse direction (a) and the scanning picture for nickel (b)
Slika 3: Raster elektronski posnetek dupleks jekla prečno na smer valjanja (a) in x slika niklja (b)

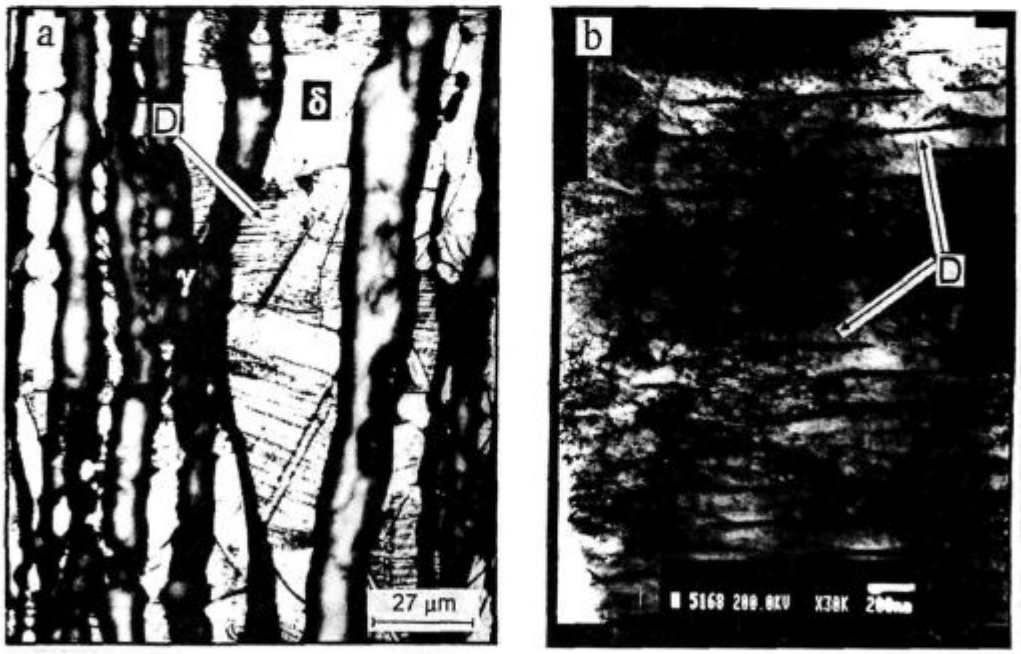

Figure 4: Optical (a) and transmission electron bright-field micrographs (b) of duplex steel. D - twins
Slika 4: Optični (a) in transmisijski elektronski posnetek (b) dupleks jekla. D - dvojčki

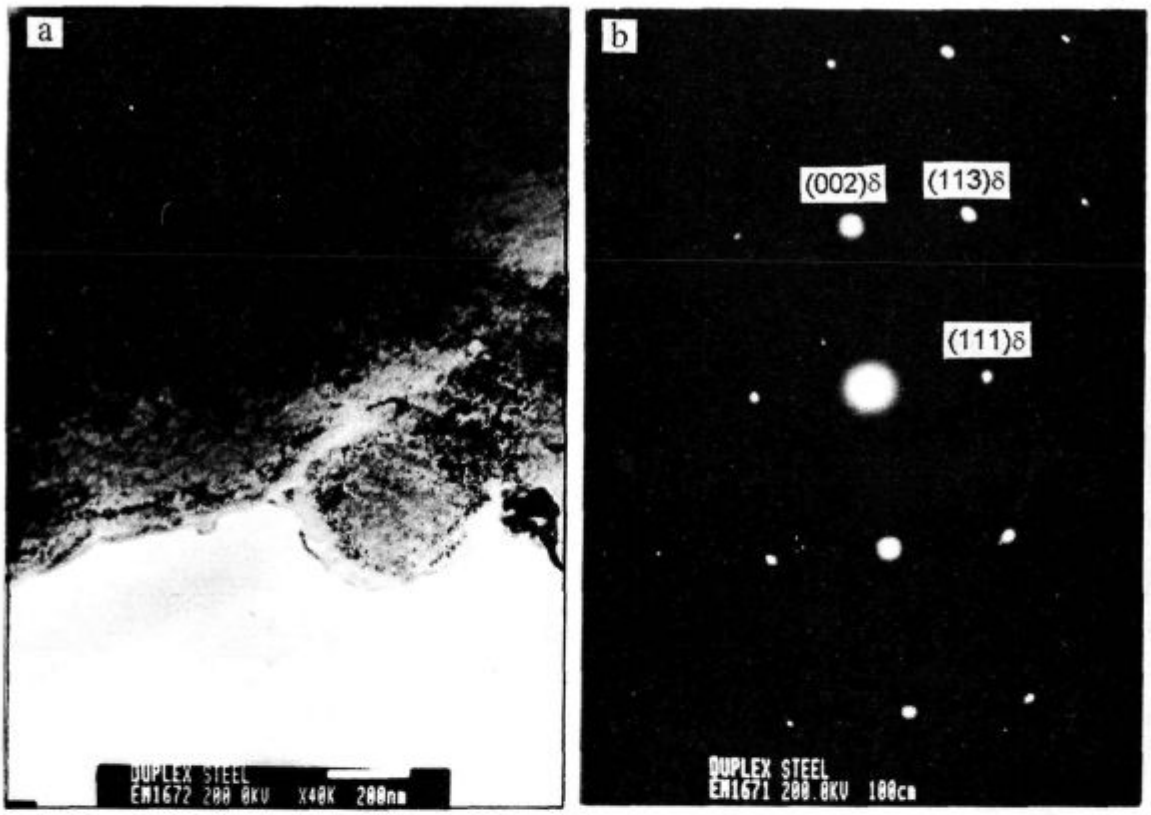

Figure 5: Transmission electron microscopy bright-field micrograph of ferrite phase (a) with indexed area diffraction pattern (b)
Slika 5: Transmisijski elektronski posnetek feritne faze (a) z indeksirano difrakcijo za ferit (b)

etched in the Kallings reagent, an acid chloride solution (1.5 g of $CuCl_2$, 33 ml of HCl, 33 ml alcohol and 33 ml of distilled water)[9]. The microstructure was examined in optical and SE microscopes, which was equipped for wave dispersive X-ray (WDX) analysis. The quantitative shares of ferrite and austenite were determined using an image analysis system. Thin foil samples for transmission electron microscope were prepared electrochemically and examined TEM operated at 200 kV and equipped for diffraction analysis. The phase identification was obtained by X-rays diffraction using CuKα radiation.

3 RESULTS

Mechanical properties (R_e -yield strength, R_m - tensile strength, A - elongation and Z - reduction of area), impact energy, hardness and microhardness of DSS were measured at room temperature on three specimens. The average values of the properties are given in **Table 2**. When compared to usual stainless steels DSS have a significantly higher yield strength (twice that of austenite steels) and a good impact energy. However, the steel showed also a significant anisotropy in impact energy. The fracture process and valuable evidence concerning the cause of failure can be obtained through microfrac-

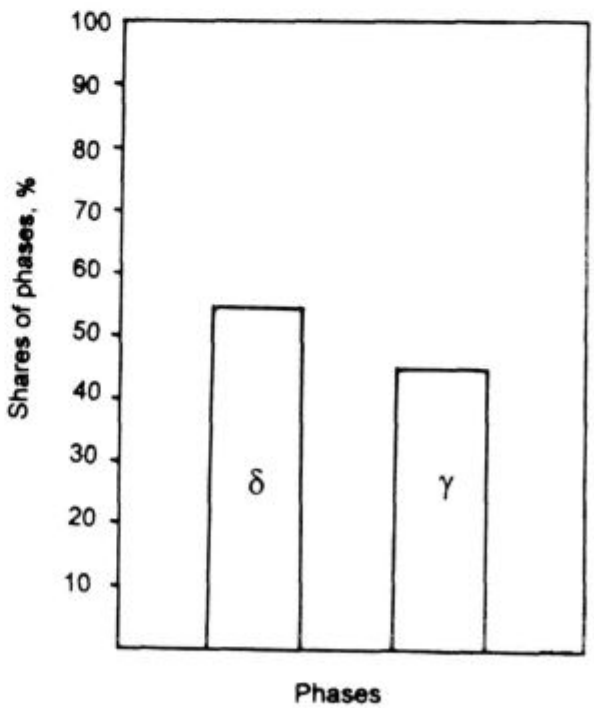

Figure 6: Quantitative shares of the ferrite-austenite microstructure in rolling direction
Slika 6: Kvantitativni delež ferita in austenita v mikrostrukturi v vzdolžni smeri valjanja

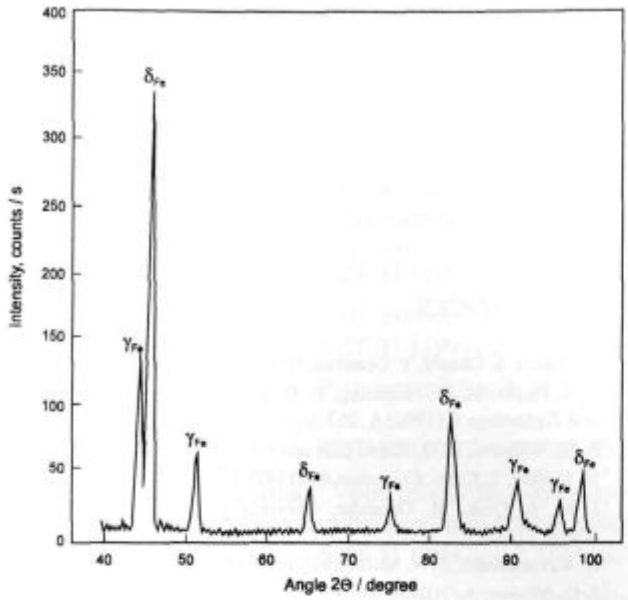

Figure 7: X-ray diffraction spectrum of duplex stainless steel
Slika 7: X-ray difrakcijski spekter dupleks jekel

tography[10]. **Figure 1** shows the fracture surfaces of DSS after tensile and impact testing. The difference in fracture surfaces is only in size of dimples. At tensile testing DSS fracture in the ductile mode by microvoid coalescence mechanism (**Figure 1a**). The fracture surfaces after impact testing are also ductile but with elongated dimples (**Figures 1b and 1c**).

Figures 2 and **3** show the microstructure of DSS in both rolling directions. In both directions the microstructure is similar and consists of austenite grains embeded in ferrite. In rolling direction austenite grains are more elongated. Austenite grains contain more and ferrite grains less nickel (**Figures 2b and 3b**). No σ-phase was found also by TEM observation, while frequent twins were observed in ferrite grains (arrow D, **Figure 4a**), which was identified by selected area diffraction (SAD) pattern (**Figure 5**). **Figure 6** shows the results of the quantitative phase analysis in rolling direction. An average of the ten continuous fields was used for estimation of the phase share. In the longitudinal direction the shares of ferrite and austenite were approximately equal. **Figure 7** shows the X-ray spectrum the steel. The phases were identified using of JCPDS data[11]. Only the presence of ferrite and austenite was confirmed by X rays diffractometry.

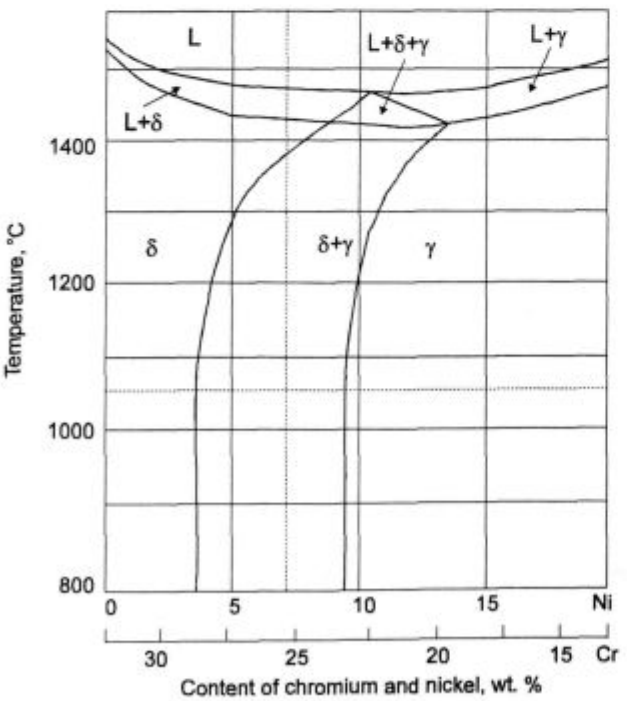

Figure 8: Quasi binary diagram of FeCrNi alloy with located duplex steel
Slika 8: Kvazi binarni diagram Fe-Cr-Ni zlitin z lokacijo dupleks jekel

4 DISCUSSION

The microstructure and the depending mechanical and corrosion properties are explained the best through the solidification process according to the quasi binary FeCrNi phase diagram, which is shown shematically in **Figure 8**[12] with dashed lines locating the DSS. By equilibrium solidification, δ-ferrite is the primary solidification phase. δ-ferrite then undergoes solid-state transformation in a two-phase region consisting of austenite (γ) and ferrite (δ) as the temperature is lowered. The nucleation of austenite occurs at grain boundaries enriched in carbon and nitrogen because of their limited solubility in ferrite. Given sufficient time, soluble carbon and nitrogen in solid solution diffuse uniformly throughout the austenite phase. It is known that a slow cooling under 815°C or aging at about 850°C can result in the formation of σ-phase[13], which is prevented by a final solution annealing at 1050°C and water quenching, as shown already. In this case a microstructure consisting of approximately equal shares of austenite and ferrite in the rolling direction is obtained. Taking into account the chromium and nickel equivalents[14] the properties of both phases (δ and γ) and their respective compositions can be approximately calculated for a given alloy and annealing temperature. The DSS tested here was represented in **Figure 8** by the dashed lines. It can be seen that at 1050°C for the composition given in **Table 1**, the steel is located in the two phases δ+γ region having an approximate δ/γ fraction of 55:45 in accordance to the share of phases shown in **Figure 6** for the rolling direction.

The high tensile strength (**Table 2**) is the result of several simultaneous mechanisms[15]: interstitial solid solution hardening (carbon and nitrogen); substitutional solid solution hardening (chromium, molibdenum and nickel) and strengthening by grain refinement (the presence of two phases prevents their mutual growth during heat treatment). The values of impact energy are higher in the longitudinal than in the transverse direction of rolling. Thus, the properties of DSS depend on the shape and arrangement of both phases as well as on the direc-

tion of rolling. The difference in micromorphology fracture is explained through the fracture stresses and shape of both phases. The effect of deformation mode is usually explained in terms of localized shear deformation[16]. Probably, also the interface between the austenite and ferrite in DSS plays a considerable role in the fracture process. Crack propagation may take place through austenite and ferrite grains. The propagation is associated with the interface it depends greatly on the orientation of ferrite and austenite stringers[17]. There is a tendency of the propagation cracks to deflect along the interface to produce delamination when stringers lie parallel to the applied stress.

Taking into consideration the microstructural texture **(Figure 2a)**, as well as their microhardness lower impact energy in transverse to the direction was expected. A higher ductility of DSS in the longitudinal direction of rolling could indicate to the crack propagation along the δ/γ boundaries because of axial stress, in contrast to the transverse direction of rolling where the fracture is produced by orthogonal stresses. This is in agreement with the results by Odelstam[18] showing that elongation is by DSS lower in the transverse than in longitudinal direction.

5 CONCLUSION

In this work the results of investigation of mechanical and microstructural properties of the duplex stainless steel (DSS) are shown the heat treating consisted of annealing at 1050°C and water quenching, which produced a ferrite-austenite microstructure free of brittle σ-phase. Compared with usual stainless steels the DSS has a significantly higher mechanical strength (twice higher yield strength than that of austenite steels) with a good impact energy. It was found that the impact energy depends on the direction of rolling. In the longitudinal direction of rolling the fractions of the ferrite and austenite were approximately equal. A higher ductility of steel in rolling direction could indicate to the crack propagation along the boundaries because of axial stress, in contrast to the transverse direction of rolling where the fracture produced by orthogonal stress.

6 REFERENCES

[1] Y. Murata, S. Ohashi, Y. Uematsu, *ISIJ International* 33 (1993) 7, 711

[2] F. H. Hayes, M. G. Hathering, R. D. Longbotton, *Materials Science and Technology* 6 (1990) 6, 263

[3] S. M. Wilhelm, R. D. Kane, *Corrosion* 40 (1984) 8, 431

[4] N. Sridhar, J. Kolts, *Corrosion* 43 (1987) 11, 646

[5] J. M. A. Quik, M. Geudeke, *Chemical Engineering Progress* 11 (1994) 11, 49

[6] K. Ravindranath, S. N. Malhotra, *Corrosion Science* 37 (1995) 2, 121

[7] J. O. Nilsson, A. Wilson, *Materials Science and Technology* 9 (1993) 7, 545

[8] ASTM standard E 370

[9] *Metals Handbook* vol.8, Metals Park, OH: ASM, 1973, p. 99

[10] Y. Tomita, *Materials Science and Technology* 11 (1995) 7, 508

[11] Search Manual for Selected Powder Diffraction Data for Metals and Alloys, JCPDS International Centre for Diffraction Data (eds. S. Weissmann), Pennsylvania, Swarthmore, 1978

[12] C. J. Long and W. T. Delong, *Welding Journal* 62 (1983) 4, 281

[13] Y. Maehara and Y. Ohmory, *The Sumitomo Search* 31 (1985) 11, 147

[14] L. Pryce and K. W. Andrews, *Journal Iron Steel Institute* 196 (1969) 6, 415

[15] J. Charles, M. Verneau and B. Bonnefois, *Preceedings 12th International Corrosion Congress*, Houston, Vol. 4, 1993, p. 2926

[16] A. ul-Haq, H. Weiland and H. J. Bunge, *Materials Science and Technology* 10 (1994) 4, 289

[17] T. P. Perng and C. J. Altstetter, *Metallurgical Transactions* 18A (1987) 2, 123

[18] T. Odelstam, *Proc. Conf. Pulp and Paper Industry Corrosion*, Stockholm Vol. 4, 1983, p. 140

LETNO KAZALO - INDEX
KOVINE ZLITINE TEHNOLOGIJE, 31, 1997, 1-6

Kronološko kazalo

Avtorsko kazalo

Stvarno kazalo - Subject Index

Poslovno tehnični del - Managing Technical Part

Kovine - Metals

Polimeri - Polymers

Vakuumska tehnika - Vacuum Technique

Wirtz BUEHLER

Buehler Ltd.

Leader in the field of automatic materials preparation.

For over a half century Buehler has been the leading manufacturer of scientific instruments and supplies for cross sectional analysis. Buehler products are used throughout the world by metallurgical laboratories, quality control departments, and failure analysis facilities for the analysis of all types of materials including ceramics, composites, semiconductors, metals, rocks and plastics.

Corporate headquarters of Buehler Ltd., Lake Bluff, Illinois

AUTOMATION, A BUEHLER FOCUS

The all new VANGUARD™ System brings affordability to the area of fully automatic sample preparation systems. For under $35,000, laboratories can completely automate their preparation process. Productivity increases as well, because laboratory personnel are freed to perform more critical duties, like sample analysis.

The VANGUARD is a fully automatic system that will grind, polish, clean and dry samples without any operator intervention. This PC based system allows the user to select from an array of stored polishing routines that can be tailored to the material being prepared. Single sample pressure allows 1 to 6 samples to be prepared simultaneously.

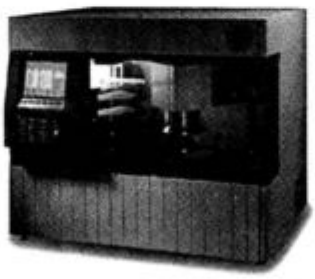

THE PHOENIX 4000, A NEW STANDARD FOR SEMIAUTOMATIC POLISHING

The PHOENIX 4000 offers an extremely vibration resistant, stable, and corrosion proof platform for semiautomatic grinding and polishing. This system offers single sample pressure, which will allow the operator to inspect individual samples at any time during the preparation process. Available in single or dual wheel models, with 10″ or 12″ diameter wheels, the PHOENIX 4000 sets the industry standard for semiautomatic preparation.

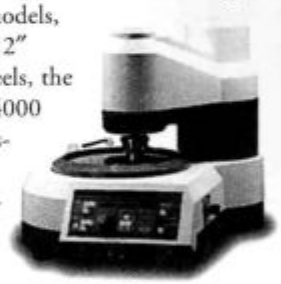

AUTOMATE YOUR MATERIAL ANALYSIS

The Buehler OMNIMET® Image Analysis systems provide the speed and productivity your lab personnel demand in today's competitive environment. These Windows based systems represent the culmination of Buehler's long commitment to automating the analysis process. No other product can provide the speed, accuracy and quality of analysis found in the OMNIMET family of systems.

CODA TRADE

REPRESENTATIONS
IMPORT - EXPORT

CODA TRADE Ltd.
STRELIŠKA 32
1000 LJUBLJANA
SLOVENIA
TEL. +386 (0) 61 / 314-227
TEL. +386 (0) 61 / 13-14-149
FAX: +386 (0) 61 / 13-14-149

For More Information Contact:
Buehler Ltd. • 41 Waukegan Road
P.O. Box One • Lake Bluff, IL 60044-1699
Sales: 1-800-BUEHLER (1-800-283-4537)
Fax: (847) 295-7929

FN01003